Failure Monitoring in Small Permanent-Magnet Synchronous Motors

by

Peyman Milanfar

B.S., Engineering Mathematics
University of California at Berkeley
(1988)

SUBMITTED TO THE DEPARTMENT OF
ELECTRICAL ENGINEERING AND COMPUTER SCIENCE
IN PARTIAL FULFILLMENT OF THE
REQUIREMENTS FOR THE
DEGREE OF
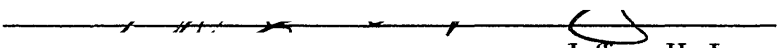MASTER OF SCIENCE IN ELECTRICAL ENGINEERING

at the

MASSACHUSETTS INSTITUTE OF TECHNOLOGY

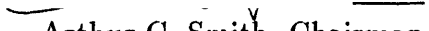October 1990

© 1990 Massachusetts Institute of Technology

Signature of Author: _____
Department of Electrical Engineering and Computer Science
October 3, 1990

Certified by: _____
Jeffrey II. Lang
Associate Professor, Department of Electrical Engineering and Computer Science
Thesis Supervisor

Accepted by: _____
Arthur C. Smith, Chairman
Departmental Graduate Committee

1

Failure Monitoring in Small Permanent-Magnet Synchronous Motors

by

Peyman Milanfar

Submitted to the Department of Electrical Engineering and Computer Science
on October 3, 1990 in partial fulfillment of the
requirements for the Degree of
Master of Science in Electrical Engineering

ABSTRACT

This thesis develops a real-time failure monitoring system for small permanent-magnet synchronous motors. Although its focus is on thermally-related failures, the approach taken here is more general. The failure monitoring system has three major applications. Firstly, it can be used to test a motor as it is manufactured to ensure that the motor functions properly. Secondly, it can be used to monitor the operation of a motor so as to prevent, predict, and detect failures. Thirdly, since the monitoring system involves estimation of the temperature-varying parameters of a motor, it can also be used simultaneously as an integral part of an adaptive controller for the motor.

To effect the real-time failure monitoring system, the thermally-varying parameters in the electromechanical model of the motor are identified, and their temperature dependencies are calibrated. In this way, through measurements of electrical line variables, the thermally-dependent parameters can be estimated and hence estimates of temperature rises in the motor can be obtained. In addition, a dynamic model for the thermal behavior of the motor is developed; its inputs are the sources of heat loss in the motor, and its outputs are estimates of temperature rises in the windings and the case of the motor. The electrically estimated temperature rises are then combined with the thermally estimated temperature rises in a closed-loop stable observer that is a Kalman filter. Experimental evidence indicates that this observer can follow the average winding temperature to within $2°C$. Finally, by an appropriate modification to the Kalman gain, the observer structure is tuned to make use of the geometric properties of the innovations for the purpose of failure detection. To accomplish this, the innovations are monitored and compared against appropriate thresholds to indicate failures.

Thesis Advisor: Jeffrey H. Lang
Associate Professor, Department of Electrical Engineering and Computer Science

2

Acknowledgements

This is the part of the thesis that is the most fun to write. Its also the most difficult since there are so many people to thank. First, big thanks go to my advisor Jeff Lang. I've learned a great deal from him and I admire his sense of intuition about practical matters. I especially want to thank him for allowing me to define my own general directions in pursuing the results in this thesis, while making sure I stayed on track.

I also want to thank Professor George Verghese for his help with some of the theoretical questions and for teaching me linear systems. He has had a very positive influence on my way of thinking.

Everyone in LEES has been great to me in the past year and a half and I want to thank them all. Carlos, Larry, Miguel, Kris, and everyone else in the lab that I haven't mentioned, thanks. The hardware used in this thesis would not have worked without the help of Ray and Clem. The technical help from Clem in both theory and practice during the course of this thesis have been instrumental. He's also been a great friend and colleague to me. Thanks Clem!

Sheila deserves more thanks than can be put into words, for her patience, support, and love. And especially for typing in the bibliography! She's been my friend and companion, and life would be just plain dull without her.

I want to thank the best mom and dad in the world for all that they've given me throughout the years. I also want to thank my brother Shahrad for being my brother.

This thesis is dedicated to my family. My dad, Mohammad Ali Milanfar, my mom, Malehe Milanfar, my brother Shahrad Milanfar, and all the rest of my family in Iran. I also dedicate this thesis to the memory of Haji.

Contents

List of Figures

9

List of Tables

Chapter 1

Introduction

1.1   Overview

The advent of low-cost digital electronics has resulted in the ability to inexpensively and quickly perform complex data processing. As a result, it is now possible to collect an extended sequence of measurements from a motor and process them in real-time to monitor the condition of the motor. In general, a variety of sensors can be used to collect measurements from an electric motor for the purpose of failure monitoring. It is apparent then that the failure monitoring system should be capable of extracting, in a consistent manner, the evidence of many possible failures from measurements of many physically different sensors. The failure monitoring system here does so by combining physical models of the motor with the estimation of the temperature-dependent parameters of these models. Variations of the states and parameters from their norms will be used to detect thermally-related failures. Furthermore, it is conceivable that failures can be prevented by avoiding stressful motor operation indicated by these variations.

We have chosen motor voltages, currents, and shaft position measurements as our sensed variables. Using an electromechanical model of the permanent-magnet synchronous motor, it is possible in turn to estimate the winding resistance and magnet strength in the motor from a sequence of these sensed variables. Since the temperature dependencies of the winding resistance and magnet strength can be accurately characterized, it is possible to estimate at least average temperatures inside the motor. As these temperatures are observed to rise dangerously high, winding insulation and magnet failures can be prevented by reducing the currents in the motor. If this is unacceptable, the operator can at least be notified of the possibility

of failure. Further, the thermal stress on the windings can be integrated over time to predict long-term damage to the winding insulation and the probability of insulation failure.

We will consider two important directions in our failure monitoring system. The first involves thermal modeling. The winding and magnet temperatures are interdependent, and this dependence can be modeled. Their variations in time are driven by losses in the motor, for example in the windings and laminations. This dissipation can also be modeled. Together, this new information constitutes a thermal model of the motor that can be used to improve the temperature estimates based on measured electrical variables. These estimates can be further improved with measurements of motor internal, or case, temperatures. Indirect thermal measurements taken from electrical variables, and estimates of the temperatures taken from the thermal model are two fundamentally different methods which can be combined to produce a single estimate. It is the thermal model that dictates how this combination must take place. This emphasizes the need for physical models in failure monitoring. The second direction involves consistency checking and failure detection. In estimating motor temperatures, it may become apparent that the cumulative measurements and estimated temperatures are not physically self-consistent. For example, the estimation of temperatures using the electromechanical and thermal models independently might yield very different temperatures. This could be a sign of a failure in the motor or the sensors. Such consistency checking forms the basis for failure detection.

Figure 1.1 outlines the basic approach to thermal estimation and failure detection employed in this thesis. The temperature rises in the motor are estimated by two independent methods. The first method makes use of the electromechanical properties of the motor, while the second relies on the thermal properties of the motor. Since we do not have direct access to measurements of the temperature of the windings and the magnet, the estimation of parameters that change with these temperatures provides a way of indirectly sensing these temperatures. So as illustrated in Figure 1.1, if we consider the thermal system, the estimation of the winding resistance R and the measurement of the case temperatures is effectively equivalent to sensing the outputs of this plant. To be more specific, the motor is electromechanically excited so as to make available the currents i, the voltages v, and the speed ω. These measured values are then combined to estimate the thermally-varying parameters R and K. These parameters are then converted to temperatures. These temperatures, combined with the direct sensing of the motor case temperature, provide the measurements of the

13

outputs of the thermal system. On the other hand, the thermal model is a model of this physical dynamic system in the absence of failures. The current and speed also drive the thermal model which produces estimates of the desired temperature rises T_R and T_C. By comparing the electrically estimated temperature rises and the thermally estimated temperature rises, innovations are obtained that are used to drive a closed-loop observer. Failure detection is then performed by choosing an appropriate observer gain to exploit the geometric contents of the innovations in the presence of a failure.

1.2   Background and Thesis Layout

Monitoring the condition of a motor is of interest for several reasons. Firstly, in the manufacturing process, a monitoring system can be used to assure compliance with standards of operational quality. Secondly, an online failure monitoring system can be used to prevent stressful operation, and guard against or detect the failure that may occur as a result. Much work has been done on detecting mechanically induced failures in electric motors. For instance, [4] has investigated the possibility of detecting broken rotor bars in induction motors through the use of various sensors. There has also been $c_{\ell_{r'}} \cdot j_{r'} \quad r_{r'} \gamma_{r'}$ work done on monitoring the thermal conditions under which a motor is operating [30]. However, such research efforts have either concentrated on static thermal models for motors or have not used the dynamic information formally to detect and/or prevent failures. The use of a dynamic thermal model along with parameter estimation techniques, as presented in this thesis, is a novel approach that constitutes a significant contribution to the area of failure monitoring for motors in general.

In Chapter 2, a detailed model of the electromechanical dynamics of a permanent-magnet synchronous motor are presented. Several sources including [19] can be referenced for a more detailed account of how this model is derived. In this same chapter, several techniques will be presented for estimating the values of temperature dependent parameters through the use of the electromechanical model. The parameter estimation is done through a least-squares error formulation as described in [35]. The remainder of the thesis is organized as indicated in Figure 1.1. Each chapter which follows addresses one or more of the blocks in the figure on a theoretical basis. A final chapter presents experiments which demonstrate the operation of the complete failure monitoring system.
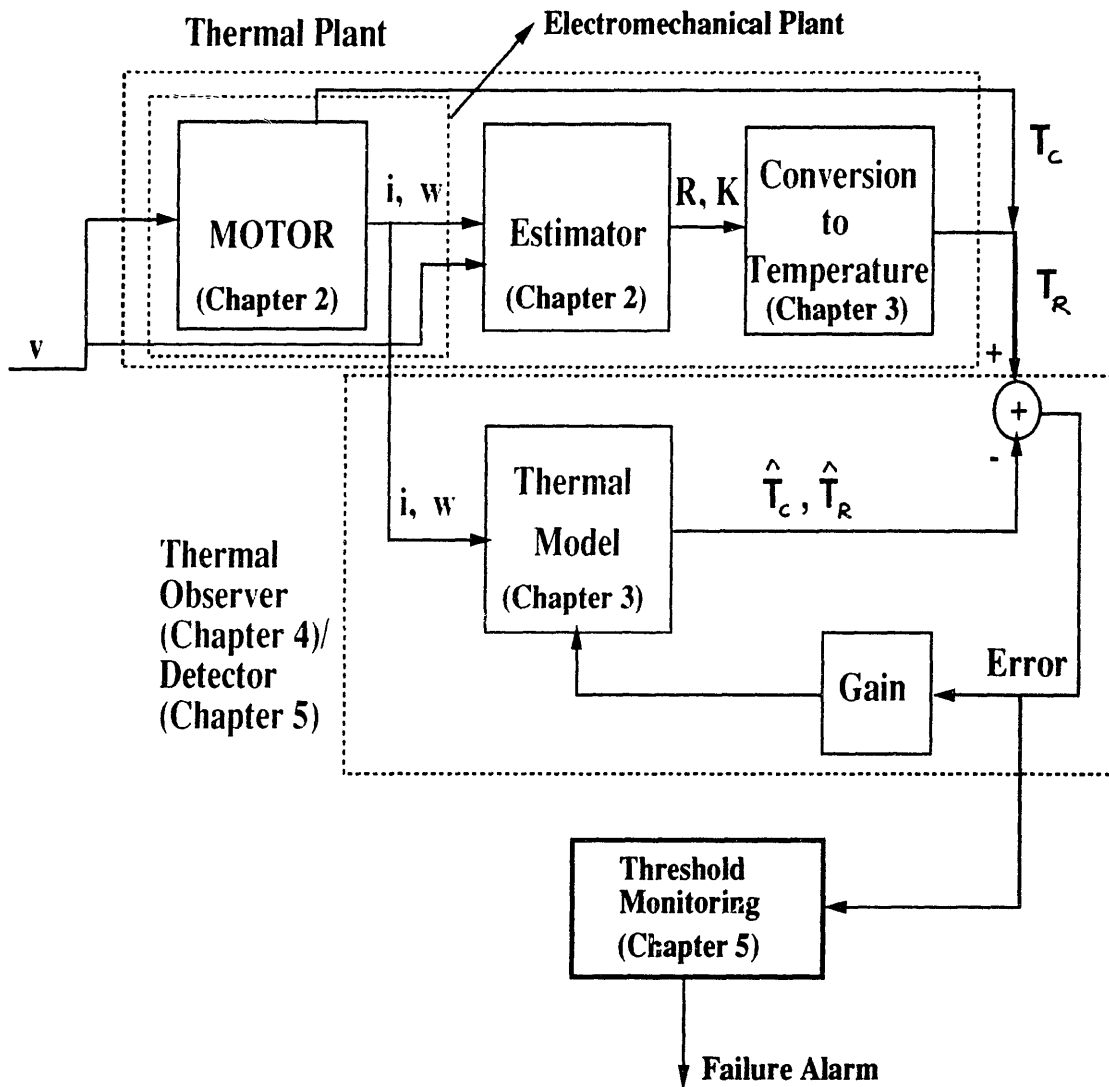
Figure 1.1: Overview of the observer/detector system

In Chapter 3, a dynamic thermal model of the motor is developed by way of identifying the parameters in a time-varying model that relates the sources of heat-loss to temperature rises in the motor. This model uses the temperature dependence of the winding resistance and the magnet constant as described in [28, 27] and [1]. The model is validated by assuring that it complies with physically imposed constraints, such as exponential stability [10, 41], and theoretically imposed constraints that are implied by these, [31, 32].

Chapter 4 undertakes the problem of designing stable, optimal observers for the thermal system using a Kalman filter, [17, 8, 16, 23]. A novel approach is presented for obtaining identity observers for a class of time-varying systems that display linear and time-invariant error dynamics.

In Chapter 5 a geometrically motivated technique introduced in [13] is employed to solve the failure detection problem. It is shown that failure detection in the thermal system can be effectively used to prevent/detect physical breakdowns in the motor. Some extensions to sampled-data systems of the concepts in [13] are arrived at. Although many techniques for failure detection have been investigated, as summarized in [40, 11], the approach taken in our work was concentrated on the geometrically inspired one since it provides a simple detection law, and is also implemented rather trivially, given an underlying observer structure.

Chapter 6 contains the results of experiments that illustrate the effectiveness and limitations of the failure detection techniques studied in this thesis, as applied to the failure detection problem in permanent-magnet synchronous motors. It is demonstrated that the proposed detection system is capable of indicating a cooling failure due to insulation. It is also shown that in the absence of failures, the observer structure is capable of tracking temperature rises in the windings to within 2°C, and the temperature rises on the surface of the motor to within 0.5°C.

Chapter 7 contains the conclusions arrived at in this thesis. This chapter also presents a summary of the work done in this thesis and provides some recommendations for future work on the topic of failure monitoring for motors.

In Appendix A some theoretical results are presented to support assertions made throughout the rest of the thesis. Appendix B contains listings of the computer simulations in MATLAB referred to in Chapters 3, 4, and 5. This appendix also contains listings of assembly code used to control the data acquisition system referred to in Chapter 6.

Chapter 2

Electromechanical Modeling and Parameter Estimation

2.1 Introduction

In this chapter we introduce the electromechanical model for the experimental motor, and develop an effective way to estimate thermally dependent parameters on the basis of this model. The electromechanical model is for a permanent-magnet synchronous motor with magnets mounted on the rotor, and phases connected in a delta configuration. The electromechanical model of the motor, initially developed in the stator frame, is simplified by a transformation that removes the nonlinearities due to the parameter dependencies on the rotor position. This transformation, known widely as the Blondel-Park transformation [22], [19], expresses the electromechanical equations of the model in the rotor frame. For convenience, the thermal estimation problem is then undertaken in this frame using a steady-state model simplification.

The steady-state electrical model, transformed to the rotor frame is used to estimate two thermally varying parameters R and K, where R is the resistance of the stator windings, and K is the permanent-magnet constant. The remaining parameters of the electromechanical model of the motor are assumed to be constant. Due to the nonlinear nature of the electromechanical model, even in the rotor frame, the estimation problem is a nonlinear one. Two least-squares error estimation schemes are developed based on the steady-state electrical model of the motor and their relative performance is evaluated. This evaluation is done both by way of sensitivity analysis and direct numerical simulations.

The parameter estimation results presented here have two fundamental uses.

Firstly, these parameters can be integrated into a closed-loop adaptive controller for the motor. In a realistic setting, the parameters R and K can change enough under thermal stress so as to require a control loop to be redesigned. Failure to take into account these parameter variations may result in inappropriate control action and hence inadequate operation of the motor. Since these parameters tend to change slowly relative to the electromechanical dynamics, the parameter estimates can be computed in the background and fed to the controller in an asynchronous fashion. In this way, the controller is updated every several seconds, or minutes, hence yielding optimal performance while keeping the computational complexity of the control algorithm to a minimum. Secondly, these parameter estimates can be used as indicators of temperature inside the motor. The average temperatures in the magnet and the windings can be inferred by characterizing the thermal dependence of these parameters. Since the parameter estimates are obtained by observing only the line currents, voltages, and speed, the thermal dependence of these parameters provides a completely non-invasive way of monitoring temperatures inside the motor. One can alternatciy construct a dynamic model for the thermal behavior of the motor and predict these same temperatures. On the basis of comparison of the predicted temperature and the estimated temperature one can form a basis for failure detection due to thermal overload.

2.2   Electromechanical Model

The model presented here for the permanent-magnet synchronous motor provides the basis for the work presented in this thesis. The motor is assumed to have three balanced phases wound with a single harmonic. These phases are assumed to be connected in a delta configuration. The mechanical load is assumed to be an inertia retarded by viscous drag, and the motor and mechanical parameters are assumed to vary slowly.

Given the assumptions, the dynamics of the permanent-magnet synchronous motor and its load are given by

$$\tilde{\lambda} = \begin{bmatrix} \tilde{L} + \tilde{P}\cos(2N\theta) & -\tilde{M} - \tilde{P}\cos(2N\theta + \frac{\pi}{3}) & -\tilde{M} - \tilde{P}\cos(2N\theta - \frac{\pi}{3}) \\ -\tilde{M} - \tilde{P}\cos(2N\theta + \frac{\pi}{3}) & \tilde{L} + \tilde{P}\cos(2N\theta + \frac{2\pi}{3}) & -\tilde{M} - \tilde{P}\cos(2N\theta - \pi) \\ -\tilde{M} - \tilde{P}\cos(2N\theta - \frac{\pi}{3}) & -\tilde{M} - \tilde{P}\cos(2N\theta - \pi) & \tilde{L} + \tilde{P}\cos(2N\theta - \frac{2\pi}{3}) \end{bmatrix} \tilde{i}$$

$$+ \tilde{K} \begin{bmatrix} \cos(N\theta) \\ \cos(N\theta - \frac{2\pi}{3}) \\ \cos(N\theta + \frac{2\pi}{3}) \end{bmatrix} \tag{2.1}$$

$$\frac{d\omega}{dt} = -\frac{N\tilde{P}}{H}\tilde{i}^T \begin{bmatrix} \sin(2N\theta) & -\sin(2N\theta + \frac{\pi}{3}) & -\sin(2N\theta - \frac{\pi}{3}) \\ -\sin(2N\theta + \frac{\pi}{3}) & \sin(2N\theta + \frac{2\pi}{3}) & -\sin(2N\theta - \pi) \\ -\sin(2N\theta - \frac{\pi}{3}) & -\sin(2N\theta - \pi) & -\sin(2N\theta - \frac{2\pi}{3}) \end{bmatrix} \tilde{i}$$

$$-\frac{N\tilde{K}}{H} \begin{bmatrix} \sin(N\theta) & \sin(N\theta - \frac{2\pi}{3}) & \sin(N\theta + \frac{2\pi}{3}) \end{bmatrix} \tilde{i} - \frac{B}{H}\omega - \frac{1}{H}\tau \tag{2.2}$$

$$\frac{d\tilde{\lambda}}{dt} = -\tilde{R}\tilde{i} + \tilde{v} \tag{2.3}$$

$$\frac{d\theta}{dt} = \omega \tag{2.4}$$

where $\tilde{v}$, $\tilde{\lambda}$, and $\tilde{i}$ are vectors of the three-phase stator voltages, flux linkages, and currents, respectively, ω and θ are the rotor velocity and position respectively, τ is a disturbance torque, $\tilde{R}$, $\tilde{L}$, and $\tilde{M}$ are the stator phase resistance, self inductance and mutual inductance respectively, $\tilde{K}$ is the permanent-magnet constant, N is the number of rotor magnet pole pairs, H is the rotor inertia, and B is the coefficient of viscous rotor friction. The motor magnets align with the first phase at $\theta = 0$, and positive rotor motion is then in the direction of the second phase.

Note that the currents referred to above are the phase currents. Actual measurements, however, are made only of the line currents in the delta connection. The transformation between phase currents and line currents is determined by using the fact that the sum of all line currents is zero; see Figure 2.1. Let the vector containing the line currents be denoted by $\tilde{I}$, then the transformation from line to phase currents is given by

$$\tilde{I} = \begin{bmatrix} 1 & 0 & -1 \\ 1 & -1 & 0 \\ 0 & -1 & 1 \end{bmatrix} \tilde{i} \tag{2.5}$$

The matrix in (2.5) is not invertible, so we can not obtain $\tilde{i}$ from $\tilde{I}$, which is desired for experimental purposes. To allow inversion, the bottom row of (2.5) is replaced by
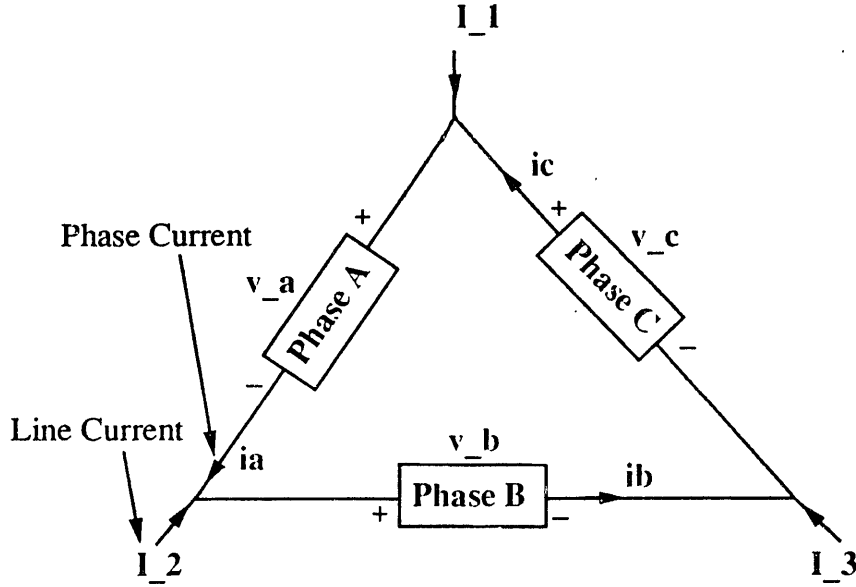
Figure 2.1: Delta connection in the motor

the assumption that $[1\ 1\ 1]\tilde{i}=0$. This yields

$$
\begin{bmatrix} \tilde{I}_A \\ \tilde{I}_B \\ 0 \end{bmatrix} = \begin{bmatrix} 1 & 0 & -1 \\ 1 & 1 & 0 \\ 1 & 1 & 1 \end{bmatrix} \tilde{i}
$$

The above relation is now invertible so that $\tilde{i}$ can be obtained from two line-current measurements. The assumption $[1\ 1\ 1]tilde i=0$ is equivalent to assuming a null zero-sequence current, as discussed below.

In anticipation of delta connection, model 2.1-4 is transformed according to

$$\bar{\lambda} = S\tilde{\lambda} \tag{2.6}$$

$$\bar{v} = S\tilde{v} \tag{2.7}$$

$$\tilde{i} = S\tilde{i} \tag{2.8}$$

20

where

$$S = \begin{bmatrix} \sqrt{2/3} & -\sqrt{1/6} & -\sqrt{1/6} \\ 0 & \sqrt{1/2} & -\sqrt{1/2} \\ \sqrt{1/3} & \sqrt{1/3} & \sqrt{1/3} \end{bmatrix} \qquad (2.9)$$

Here, S is a unitary matrix so that the transformation is power invariant. When the motor is delta-connected, the zero-sequence voltage is identically zero. This voltage is the sum of the three original stator phase voltages, and is the third component of $\tilde{v}$. It can be seen that the corresponding zero-sequence flux linkage and current evolve independently from the other two flux linkages and currents, and that their evolution is stable so that they too eventually vanish given any nonzero initial conditions. Also, it can be seen that the zero-sequence current does not contribute to torque. Given these characteristics of the zero-sequence variables, they can be omitted from 2.6-8, resulting in the following simplified model

$$\lambda^* = \begin{bmatrix} \tilde{L} + \tilde{M} + \frac{3}{2}\tilde{P}\cos(2N\theta) & \frac{3}{2}\tilde{P}\sin(2N\theta) \\ \frac{3}{2}\tilde{P}\sin(2N\theta) & \tilde{L} + \tilde{M} - \frac{3}{2}\tilde{P}\cos(2N\theta) \end{bmatrix} i^*$$

$$+ \sqrt{\frac{3}{2}}\tilde{K} \begin{bmatrix} \cos(N\theta) \\ \sin(N\theta) \end{bmatrix} \qquad (2.10)$$

$$\frac{d\omega}{dt} = -\frac{3N\tilde{P}}{2H} i^{*T} \begin{bmatrix} \sin(2N\theta) & -\cos(2N\theta) \\ -\cos(2N\theta) & -\sin(2N\theta) \end{bmatrix} i^*$$

$$- \sqrt{\frac{3}{2}}\frac{N\tilde{K}}{H} \begin{bmatrix} \sin(N\theta) & -\cos(N\theta) \end{bmatrix} i^* - \frac{B}{H}\omega - \frac{1}{H}\tau \qquad (2.11)$$

$$\frac{d\lambda^*}{dt} = -\tilde{R}i^* + v^* \qquad (2.12)$$

$$\frac{d\theta}{dt} = \omega \qquad (2.13)$$

where v^*, λ^*, and i^* are vectors which include only the first two components of $\tilde{v}$, $\bar{\lambda}$, and $\bar{i}$ respectively.

One prominent nonlinearity of the simplified model are the trigonometric functions. These terms can be eliminated using the Blondel-Park transformation

$$\lambda = T\lambda^* \qquad (2.14)$$

$$v = Tv^* \qquad (2.15)$$

$$i = Ti^* \qquad (2.16)$$

where

$$T = \begin{bmatrix} \cos(N\theta) & \sin(N\theta) \\ -\sin(N\theta) & \cos(N\theta) \end{bmatrix} \tag{2.17}$$

Here, T is also a unitary matrix so that it too is a power invariant transformation. This yields

$$\bar{L}\frac{di}{dt} = -Ri + N\omega \begin{bmatrix} 0 & L_q \\ -L_d & 0 \end{bmatrix} i - NK\omega \begin{bmatrix} 0 \\ 1 \end{bmatrix} + v \tag{2.18}$$

$$\frac{d\omega}{dt} = \frac{PN}{H} i^T \begin{bmatrix} 0 & 1 \\ 1 & 0 \end{bmatrix} i + \frac{KN}{H} \begin{bmatrix} 0 & 1 \end{bmatrix} i - \frac{B}{H}\omega - \frac{1}{H}\tau \tag{2.19}$$

$$\frac{d\theta}{dt} = \omega \tag{2.20}$$

where

$$\bar{L} = \begin{bmatrix} L_d & 0 \\ 0 & L_q \end{bmatrix} \tag{2.21}$$

$$L_d = \tilde{L} + \tilde{M} + \frac{3}{2}\tilde{P} \tag{2.22}$$

$$L_q = \tilde{L} + \tilde{M} - \frac{3}{2}\tilde{P} \tag{2.23}$$

$$P = \frac{3}{2}\tilde{P} \tag{2.24}$$

$$K = \sqrt{3/2}\tilde{K} \tag{2.25}$$

$$R = \tilde{R} \tag{2.26}$$

which is the final form of the model used throughout this thesis. The set of equations 2.18-20 is also referred to here as the model of the motor in the *rotor-frame* or *dq-frame*. The transformation T maps the voltages and currents to the frame of the rotor. In this way, the dependence on the rotor position is eliminated. In this frame, the currents and voltages can be thought of as being aligned along the direction parallel to the magnets (represented by subscript $_d$) and along the direction orthogonal to the magnets (represented by the subscript $_q$). Hence, in the rotor frame we have

$$i = \begin{bmatrix} i_d & i_q \end{bmatrix}' \tag{2.27}$$

$$v = \begin{bmatrix} v_d & v_q \end{bmatrix}' \tag{2.28}$$

22

2.3 Parameter Estimation

In this section, we use the equations describing the electrical dynamics of the motor to estimate the parameters R and K. These dynamics are described by Equation 2 18. As we can see, the parameter K also appears in the equation describing the mechanical dynamics of the motor (2.19). This relation, however, is not suitable for the estimation of K since the load torque τ is in general unknown. Hence we concentrate only on estimation through the electrical equations. The estimation problem is best solved using data from the steady-state operation of the motor. There are two reasons for this. Firstly, due to the short response-time of the electrical dynamics, and the typical operation of the motor, a random sampling of the line voltages and currents most probably yields the steady-state values of those quantities. Secondly, the computation of the derivatives on the left-hand-side of Equation 2.18 is both computationally burdensome and numerically unsound. Computing the time derivative of the variables from their noisy measurements is bound to accentuate the noise, thereby yielding poor estimates of the parameters of interest. In contrast, steady-state values of the currents and voltages in the rotor frame can be directly used to setup a least-squares estimation problem in a more noise-immune manner. Equation 2.18 in steady-state operation of the motor can be written as

$$-Ri_d + N\omega L_q i_q + v_d = 0 \qquad (2.29)$$

$$-Ri_q - N\omega L_d i_d - NK\omega + v_q = 0 \qquad (2.30)$$

These relations can be rewritten to contain the parameters R and K on one side only. This yields

$$Ri_d = N\omega L_q i_q + v_d \qquad (2.31)$$

$$Ri_q + NK\omega = -N\omega L_d i_d + v_q \qquad (2.32)$$

This set of equation can now be used directly to estimate R and K. Let us rearrange these relations so that the parameters of interest are placed in a single vector. We have that

$$\begin{bmatrix} i_d & 0 \\ i_q & N\omega \end{bmatrix} \begin{bmatrix} R \\ K \end{bmatrix} = \begin{bmatrix} N\omega L_q i_q + v_d \\ -N\omega L_d i_d + v_q \end{bmatrix} \qquad (2.33)$$

We may now measure the speed, line currents, and line voltages, use these quantities to find the corresponding values in the dq-frame, and use these values to estimate the

desired parameters. We present two different approaches to the estimation problem and discuss their relative performance.

2.3.1 Estimator I : The Use of Both Electrical Equations With No Prior Information

Having no prior information regarding the values of the parameters of interest, and given Equations 2.29-30, we may use both equations to incorporate all the information available to estimate R and K. Assume that n measurements of the speed, and the currents, and voltages in the dq-frame are available, then we can use Equation 2.33 to write

$$
\begin{bmatrix}
i_{d_1} & 0 \\
i_{q_1} & N\omega_1 \\
i_{d_2} & 0 \\
i_{q_2} & N\omega_2 \\
\vdots & \vdots \\
i_{d_n} & 0 \\
i_{q_n} & N\omega_n
\end{bmatrix}
\begin{bmatrix}
R \\
K
\end{bmatrix}
=
\begin{bmatrix}
N\omega_1 L_q i_{q_1} + v_{d_1} \\
-N\omega_1 L_d i_{d_1} + v_{q_1} \\
N\omega_2 L_q i_{q_2} + v_{d_2} \\
-N\omega_2 L_d i_{d_2} + v_{q_2} \\
\vdots \\
N\omega_n L_q i_{q_n} + v_{d_n} \\
-N\omega_n L_d i_{d_n} + v_{q_n}
\end{bmatrix}
+ noise
\tag{2.34}
$$

Note here that *noise* refers to the collective measurement noise on the right and left hand sides of Equation 2.33. This noise is actually not completely additive due to the appearance of multiplicative terms between measured speed and currents. However, this is ignored.

In more compact notation, Equation 2.34 becomes

$$
A(n)x = B(n) + e
\tag{2.35}
$$

where x is the 2×1 unknown vector of parameters R and K, and with reference to Equation 2.33, the matrices A and B are defined in the obvious way using the n available data points. An estimate of x can now be obtained through a linear least-squares-error estimation problem, the solution to which is easily obtained by multiplying both sides of 2.35 on the left by the right-inverse of $A(n)$ [37]. Hence, denoting the estimate by $\hat{x}$ we have

$$
\hat{x}(n) = A^{+r}(n)B(n)
\tag{2.36}
$$

24

where the right-inverse of $A(n)$ is given by

$$A^{+r}(n) = (A^T(n)A(n))^{-1}A(n)^T \tag{2.37}$$

Note, however, that the matrix A in our estimation problem is not noise-free due to the multiplicative terms, as is the case in the standard setup for a least-squares error problem. Hence, the quantity e in Equation 2.35 is a convenient approximation of the actual uncertainties. This simplifying assumption allows the application of the standard least squares error solution given by Equation 2.36, as derived in [37]. This solution minimizes the norm of the estimation error over all choices of $\hat{x}$. In other words,

$$\hat{x}(n) = \text{argmin}_x \|A(n) - xB(n)\|^2 = \text{argmin}_x e^T e. \tag{2.38}$$

Due to the noise in A, however, this estimate can not be assumed to be unbiased, as is the case in a standard least-squares setup.

If any information is available regarding the relative confidence in the measured variables, this information may be integrated into the estimation process approximately using a weighting matrix Q. Q may be chosen as a positive definite diagonal matrix with each diagonal element being the reciprocal of the variance of e. The solution to the *weighted* least-squares error problem may be obtained in a similar way as before. The solution [37] is given by

$$\hat{x} = (A^T(n)QA(n))^{-1}A^T(n)QB(n) \tag{2.39}$$

This solution minimizes the weighted sum of the squares of the estimation error. i.e. the quantity $e^T Q e$ where

$$e = A(n)x - B(n) \tag{2.40}$$

In order for the solution to either problem (weighted or not) to exist, the right-inverse of $A(n)$ must exist. From the definition of the right-inverse, it is seen that $A^{+r}(n)$ exists if and only if $A(n)$ has full column rank. This is the case if and only if the direct current i_d is nonzero in the steady-state operation of the motor. However, since i_d does not contribute to significant torque production in the motor, any desirable controller for the motor will aim to drive i_d to zero in the steady-state. This further complicates the estimation problem. As i_d approaches zero, the condition number of the (square) matrix $A^T(n)A(n)$ approaches infinity. Thus, small measurement errors will result in parameter estimates that are unacceptably corrupt.

We can explore the aforementioned sensitivity to i_d by studying the relative sensitivities of Equation 2.33. Assume that measurements of the currents, voltages, and the speed are corrupt. We seek to relate the relative sensitivities of the estimates to those of the measured currents, voltages, and speeds. Define the normalized change in a scalar variable x at $x = x_o$ as the ratio between a differential perturbation in x and the reference value x_o. More precisely, if we define δ_x to denote the normalized change in x, we have

$$\delta_{x_o} = \frac{dx}{x}|_{x_o} \tag{2.41}$$

where dx denotes the differential of x. An alternate way to define the sensitivity function δ_x is as the differential of the natural logarithm of $|x|$. i.e.

$$\delta_{x_o} = d(ln|x|)|_{x_o} \tag{2.42}$$

We seek to find a relationship between the normalized errors in the variables i_d, i_q, v_d, v_q, and w and those of the parameters R and K. This relationship is obtained by taking differentials of both sides of 2.33 and normalizing the respective variables. This gives

$$\delta_{R.K} = \Delta_{i,v,w}\delta_{i,v,w} \tag{2.43}$$

where

$$\delta_{(R,K)} = \begin{bmatrix} \delta_R & \delta_K \end{bmatrix}^T$$

$$\Delta_{(i,v,w)} = \begin{bmatrix} \frac{R^2}{i_d^2} & \frac{NL_q\omega R}{i_d i_q} & \frac{R}{v_d i_d} & 0 & \frac{NL_q i_q R}{i_d v_d} \\ \frac{K}{i_d}(\frac{i_q R}{N\omega i_d} - L_d) & -\frac{K}{i_q}(\frac{i_q}{i_d} - \frac{R}{N\omega i_q}) & -\frac{i_q K}{N\omega i_d v_d} & \frac{K}{N\omega v_q} & -\frac{K}{\omega^2 i_d}(L_q i_q^2 + L_d i_d^2 + K i_d) \end{bmatrix}$$

$$\delta_{(i,v,w)} = \begin{bmatrix} \delta_{i_d} & \delta_{i_q} & \delta_{v_d} & \delta_{v_q} & \delta_w \end{bmatrix}^T$$

where the matrix Δ is evaluated at a given operating point of the motor. The respective magnitudes of the elements of the matrix Δ now show how sensitive each parameter is to measurement noise in the speed or each of the voltage and current channels. For instance, the magnitudes of the elements of the first column of Δ show the relative contribution of the measurement noise in i_d to the error in the estimate of R. It is then seen that as i_d approaches zero, the contribution of measurement noise in i_d is the largest source of error in the estimates of the parameters.

By carefully examining the nature of the variables that appear on either side of 2.33, we can see that the there exist multiplicative terms (ωi_d and ωi_q) on the right

26

hand side with both multiplicands containing noise. Hence, the noise characteristics of the variables that appear in the matrices $A(n)$ and $B(n)$ do not coincide with those assumed in a standard least-squares error problem; the noise in $B(n)$ is not accurately modeled as additive noise. In a standard least squares problem, the matrix $A(n)$ is assumed to be noise free, and the noise in the matrix $B(n)$ is assumed to be additive. Neither of these conditions holds in our formulation. Thus, we can not generally expect the proposed estimator for R and K to be unbiased. We will see, through simulations, that the estimator is in fact biased. In summary, we have identified two potential problems with the use of the estimator given by (2.36). The first is the sensitivity of the solution to the size of the current i_d and consequently to the noise associated to it, and the second problem is that the estimator may be biased. Simulations were performed to investigate the potential problems with the estimator. The results of these simulations will be discussed in Section 2.4 where numerical results are presented.

2.3.2 Estimator II : The Use of Both Electrical Equations And Knowledge of K

In the above formulation, we ignored the fact that there exists prior information on the values of the parameters being sought. This prior information is in fact obtained by simply measuring the values of R and K at room temperature. The value of K in the particular experimental motor under study tends to vary very little with changing temperature. (It is shown in Chapter 3 that an increase of $55°C$ in temperature yields a change of less than 4 percent in K.) Hence, if one is willing to compromise, it may be possible to obtain a more reliable estimate of the winding resistance R by considering the value of K fixed. Of course, it is only natural that the accuracy of this estimate of R should depend upon how closely the fixed value of K approximates the actual value of K. Given a fixed value of K, and the confidence in its accuracy, we can rewrite 2.31 and 2.32 as

$$i_d R = N L_q \omega i_q + v_d \qquad (2.44)$$
$$i_q R = -N L_d \omega i_d + v_q - N \omega K \qquad (2.45)$$

Given a set of n measurements of the currents and voltages in the rotor frame, the estimation problem may now be set up as

$$
\begin{bmatrix} i_{d_1} \\ i_{q_1} \\ i_{d_2} \\ i_{q_2} \\ \vdots \\ i_{d_n} \\ i_{q_n} \end{bmatrix} R = \begin{bmatrix} NL_q\omega_1 i_{q_1} + v_{d_1} \\ -NL_d\omega_1 i_{d_1} + v_{q_1} - N\omega_1 K \\ NL_q\omega_2 i_{q_2} + v_{d_2} \\ -NL_d\omega_2 i_{d_2} + v_{q_2} - N\omega_2 K \\ \vdots \\ NL_q\omega_n i_{q_n} + v_{d_n} \\ -NL_d\omega_n i_{d_n} + v_{q_n} - N\omega_n K \end{bmatrix} + noise \qquad (2.46)
$$

or more conveniently as before

$$
A(n)x = B(n) + \epsilon \qquad (2.47)
$$

As in Estimator I, the estimation problem here again is not a standard least-squares-error (LSE) problem due to the fact that the matrix A is noisy. However, we simplify the problem into a standard LSE problem by collecting (approximately) all of the noise present in the problem into the noise vector ϵ. We may now solve for the unknown parameter x by minimizing the weighted square sum of the estimation error. This solution again is

$$
\hat{x} = (A^T(n)QA(n))^{-1}A^T(n)QB(n) \qquad (2.48)
$$

Notice now that in 2.48, the least squares problem is not ill conditioned as a result of the nearness of i_d to zero. Simulation results presented in the next section show the performances of the proposed estimators.

2.4   Numerical Results

In this section we present the results of simulations performed to investigate the relative performances of the estimator structures proposed in Section 2.3. Comparisons are made between the errors for each estimator. These comparisons are made on the basis of ensemble averages of the respective estimator errors where the average is taken over 200 runs of simulations. In each run, the same set of noisy data is used by both estimators to produce values of R and K, while each run uses a different set of random noise values to produce the data set used by all estimators. A set of 200

28

ω   τ   Id

Steady-State
Electrical Equations
(2.29-30)

Vd Vq Iq

Inverse Blondel-Park
Transformations
(2.17)

I1 I2 V1 V2

Add Gaussian Noise

Noise
Variances

I1 I2 V1 V2

Blondel-Park
Transformation
(2.17)

Id Iq Vd Vq

ESTIMATOR
(2.36, 2.48)

R

K
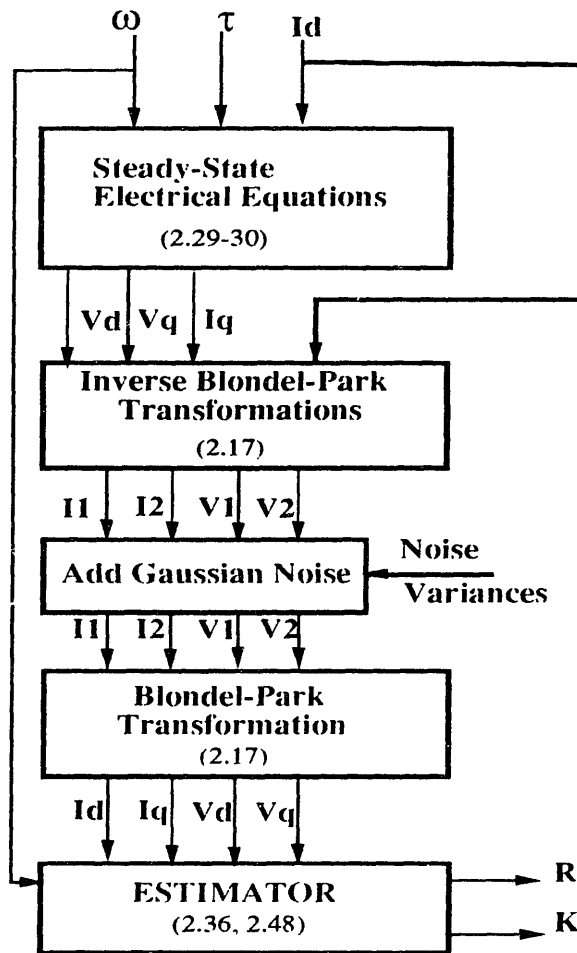
Figure 2.2: Structure of Estimator Simulations

estimator errors are generated for each algorithm, and the average of these results are compared below. Results are presented below in terms of the number of data points available (n). This is to illustrate the minimum number of data points necessary to obtain an estimate which has some desired accuracy.

In the following simulations, a fixed ω and τ were chosen along with a desired value for i_d. These values were then used to generate ideal values for the line currents and voltages which were then measured. The line measurements were then corrupted by gaussian noise and passed through the line-to-phase transformations, the three-to-two phase transformations, and the Blondel-Park transformations to yield corrupted values of i_d, i_q, v_d, and v_q These values were in turn used to generate the matrices $A(n)$ and $B(n)$ and hence produce estimates of R and K. Figure 2.2 shows the structure of these simulations.

Variance of voltage measurement errors	0.00004	volts
Variance of current measurement errors	0.00004	amps
Variance of speed measurement errors	0.00004	rad/sec
Variance of angle measurement errors	0.000004	radians
Winding Resistance (R)	1.7479	ohms
Permanent-Magnet Constant (K)	0.0917	V-sec/rad
Nominal i_d	1	amps
i_q	3.02	amps
v_d	-22.15	volts
v_q	100.34	volts
Load Torque	0.636	N-m
Speed	3000	rpm

Table 2.1: Experiment 1

Experiment 1:   In the following simulation, the speed and load torque were kept constant, and the values in Table 2.1 were used to produce the measurement noises. Figure 2.3 shows a typical set of data composed of 200 points. Figure 2.4 shows the estimated values of R along with the actual R for comparison. Figures 2.5 and 2.6 show the estimated values of K and their error.

The performance of Estimator II which includes knowledge of K is clearly superior in estimating R to that of Estimator I.

Experiment 2:   In Figures 2.7-9 we present the results of a simulation that assumes the parameters in Table 2.2 below. In this experiment, the commanded value of i_d is reduced to 0.1, i.e. to 10 percent of its value in Experiment 1. We wish to see the effect of this change on the performance of the estimators.

By comparing the estimated parameter values to those of Experiment 1, we can see that as a result of reduction of the value of i_d, the error of Estimator I suffers an increase in size. However, the accuracy of Estimator II is not fundamentally affected, as expected.

Experiment 3:   In this experiment we keep the commanded current i_d at 0.1 Amps but decrease the speed to see whether the accuracy of the estimators are improved or not. Figures 2.10 to 2.12 illustrate the results. The parameters shown in Table 2.3 were used in this simulation.

Comparing the estimated parameters to those of Experiment 2 we observe that
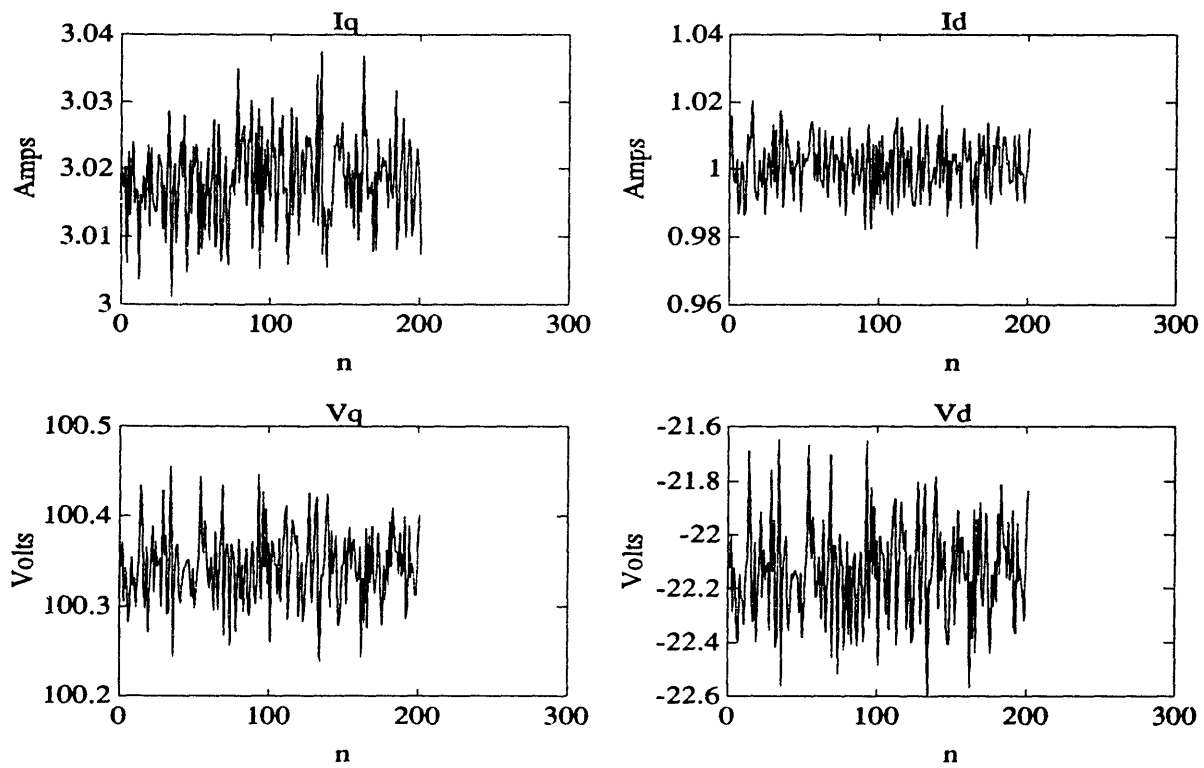
Figure 2.3: A typical Data Set
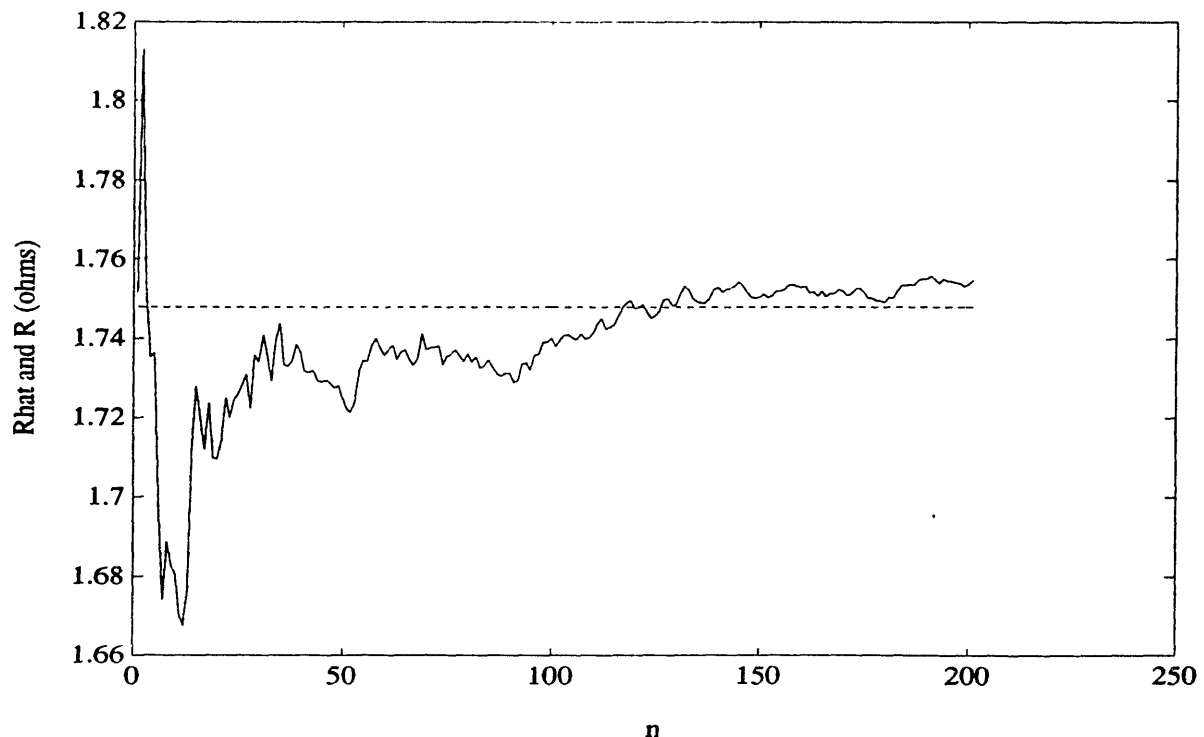
Figure 2.4: (Experiment 1) Estimates of R : Estimator I
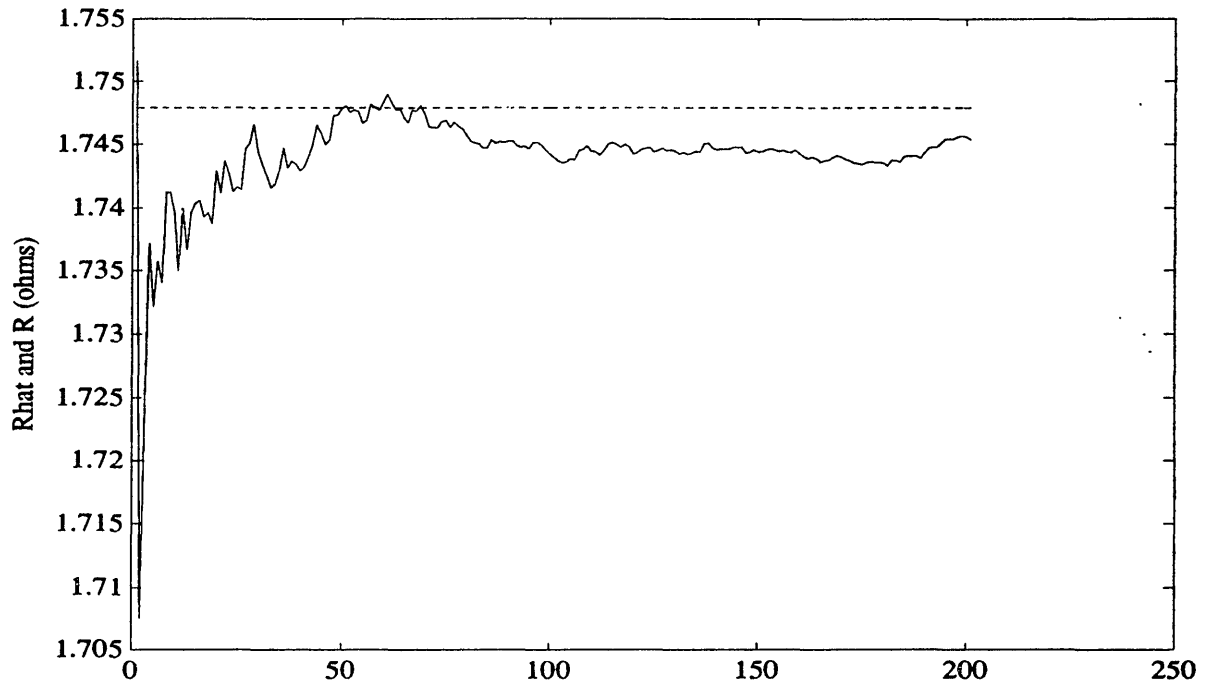
Figure 2.5: (Experiment 1) Estimates of R : Estimator II
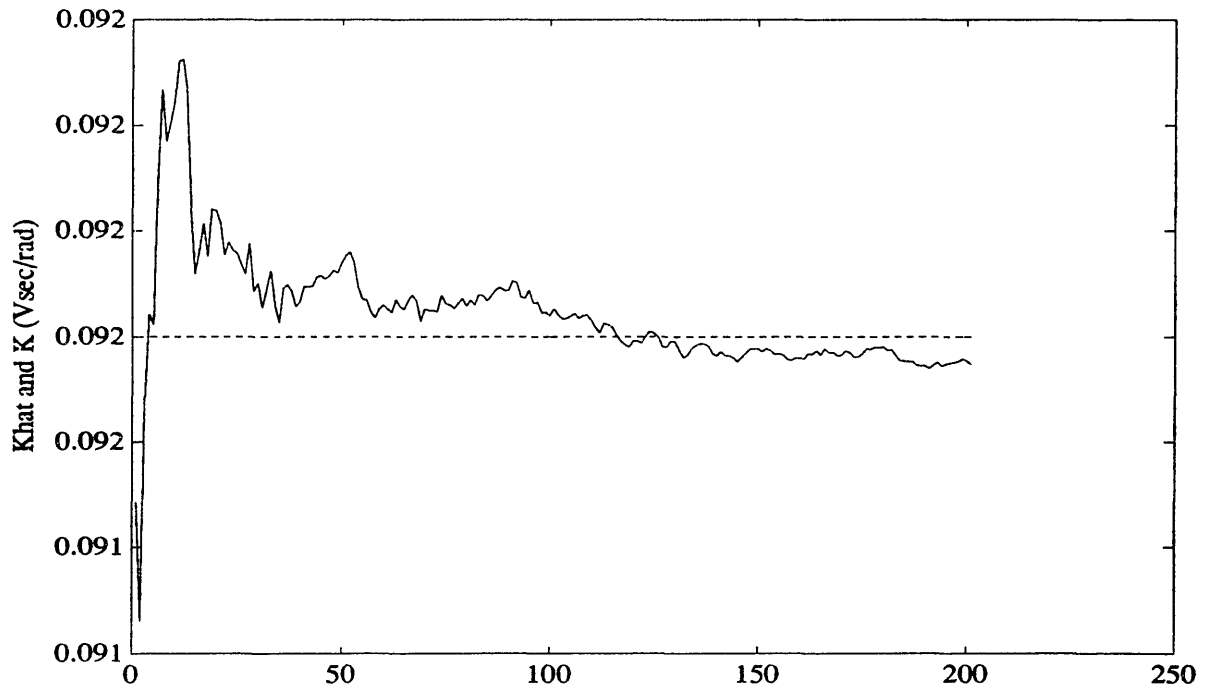
Figure 2.6: (Experiment 1) Estimates of K : Estimator I

Variance of voltage measurement errors	0.00004	volts
Variance of current measurement errors	0.00004	amps
Variance of speed measurement errors	0.00004	rad/sec
Variance of angle measurement errors	0.000004	radians
Winding Resistance (R)	1.7479	ohms
Permanent-Magnet Constant (K)	0.0917	V-sec/rad
Nominal i_d	0.1	amps
i_q	3.04	amps
v_d	-23.9	volts
v_q	92.6	volts
Load Torque	0.636	N-m
Speed	3000	rpm

Table 2.2: Experiment 2
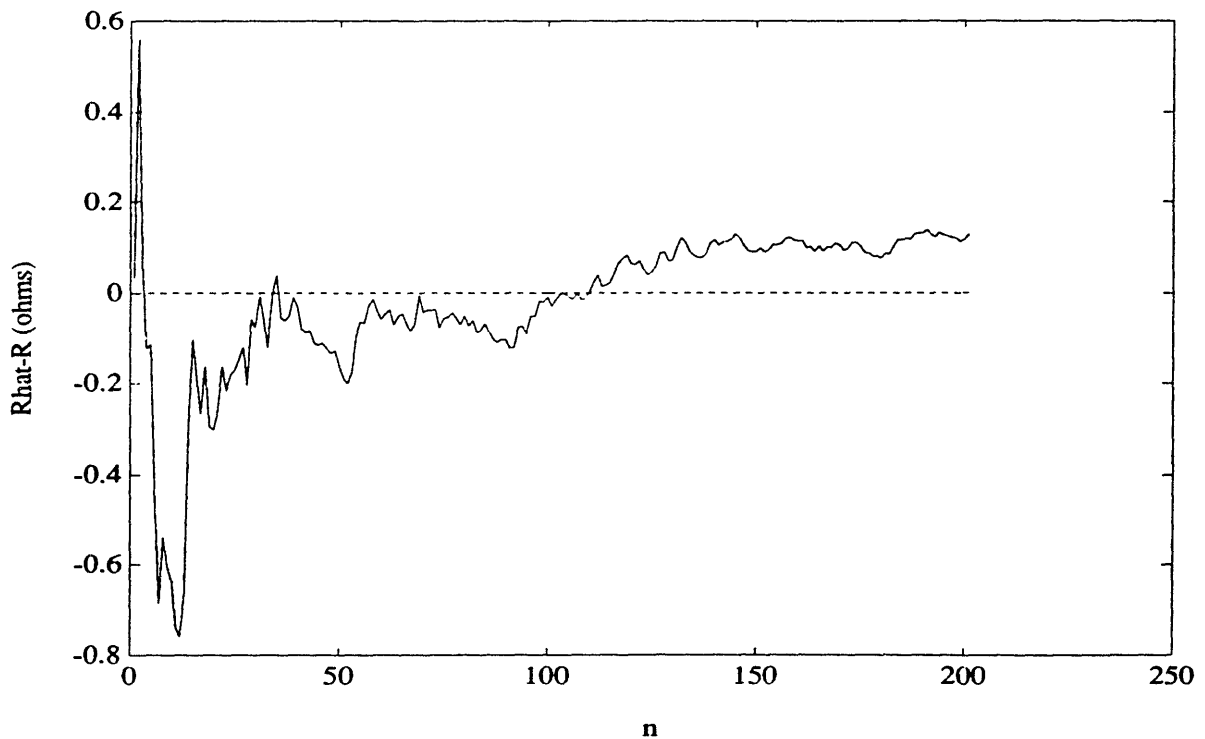
Figure 2.7: (Experiment 2) Estimator I error in R vs. n

33
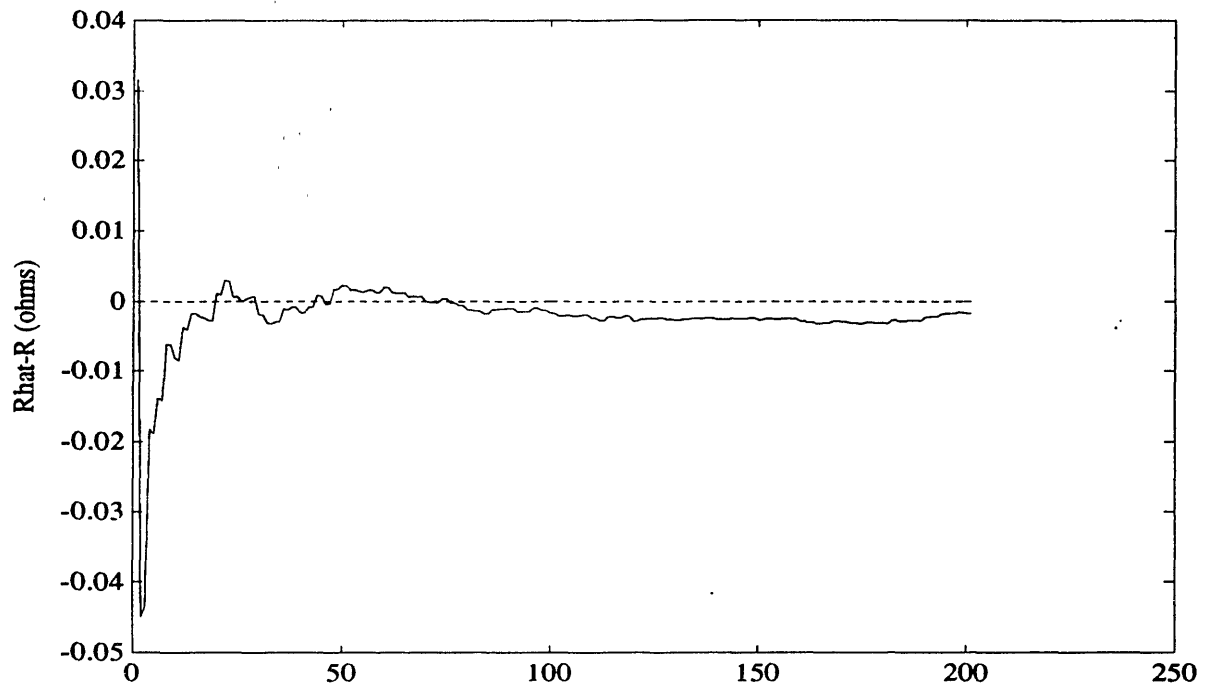
Figure 2.8: (Experiment 2) Estimator II error in R vs. n
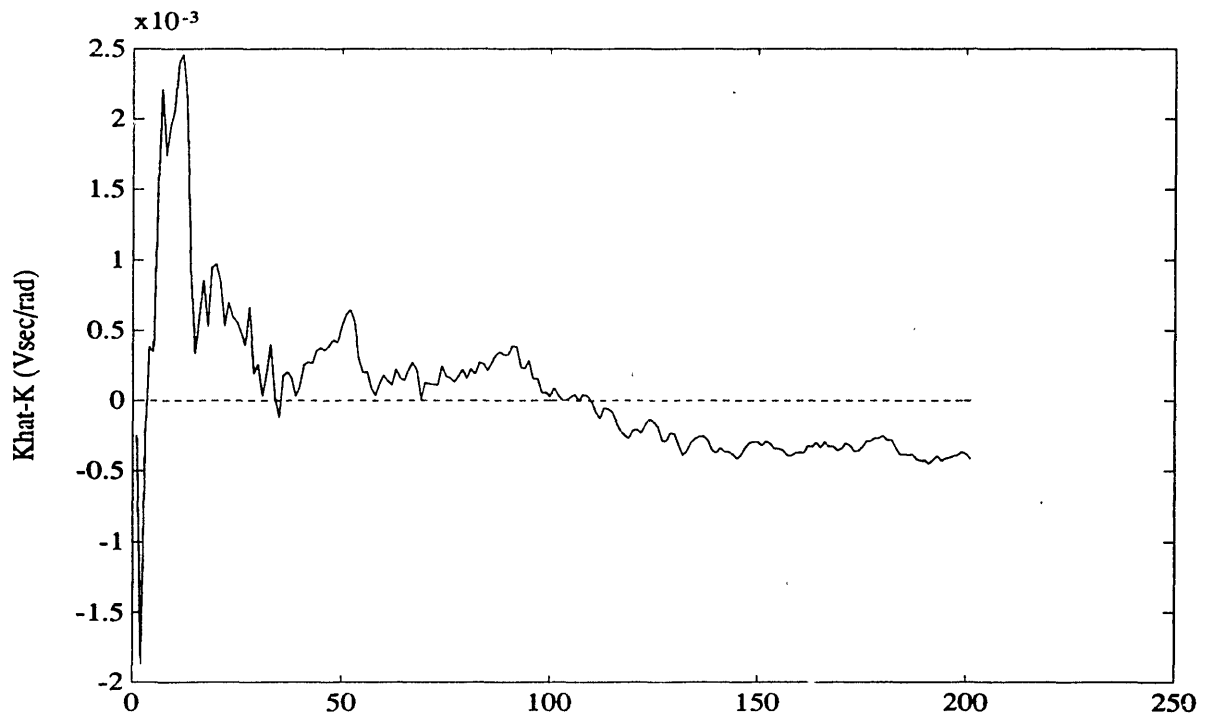
Figure 2.9: (Experiment 2) Estimator I error in K vs n

34

Variance of voltage measurement errors	0.00004	volts
Variance of current measurement errors	0.00004	amps
Variance of speed measurement errors	0.00004	rad/sec
Variance of angle measurement errors	0.000004	radians
Winding Resistance (R)	1.7479	ohms
Permanent-Magnet Constant (K)	0.0917	V-sec/rad
Nominal i_d	0.1	amps
i_q	2.6	amps
v_d	-6.7	volts
v_q	33.6	volts
Load Torque	0.636	N-m
Speed	1000	rpm

Table 2.3: Experiment 3
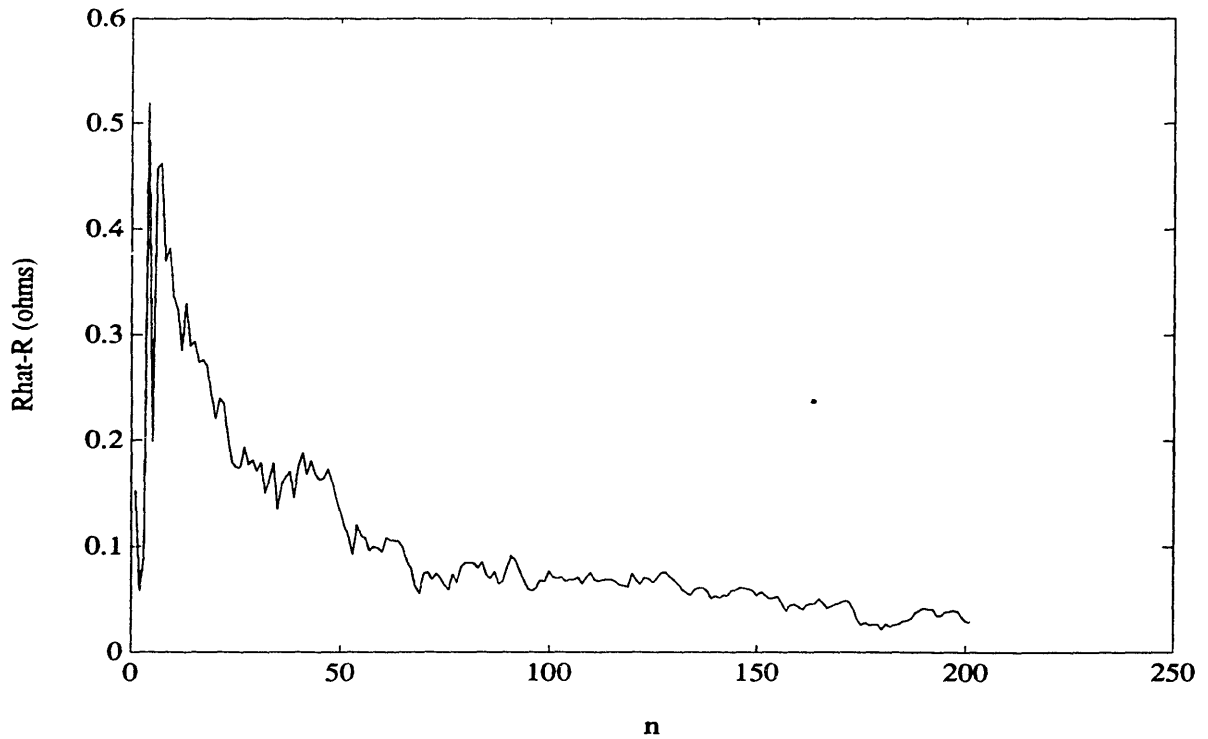
Figure 2.10: (Experiment 3) Estimator I error in R vs n

35
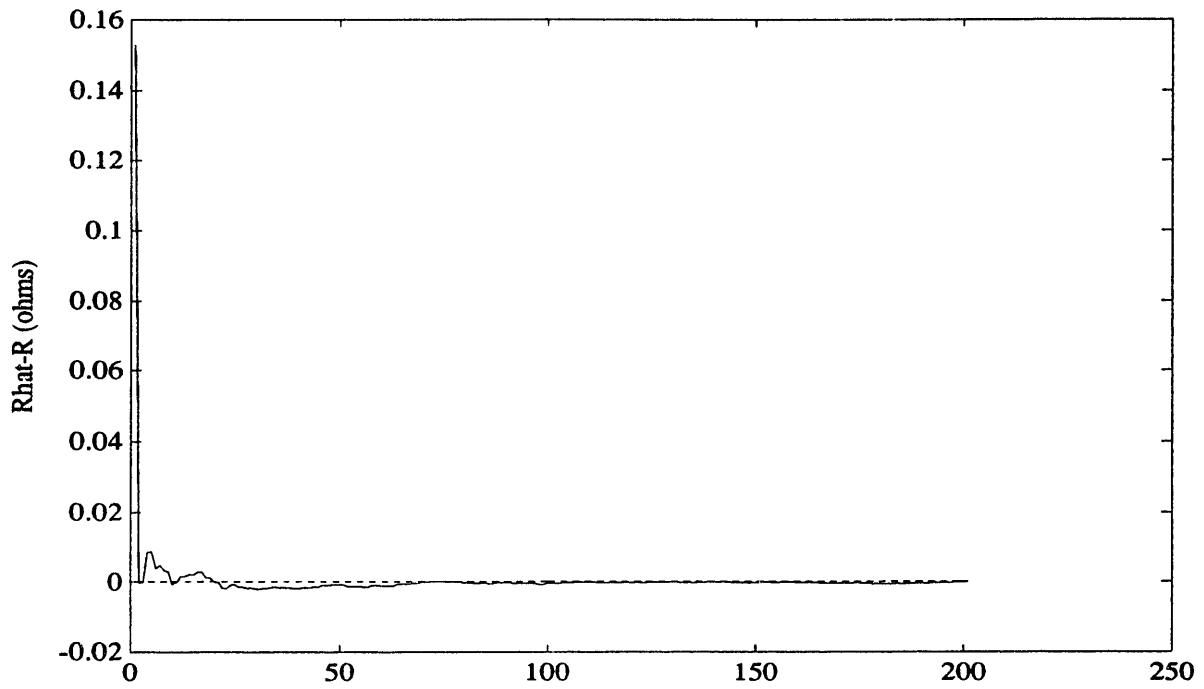
Figure 2.11: (Experiment 3) Estimator II error in R vs n

Figure 2.12: (Experiment 3) Estimator I error in K vs n

36

the magnitudes and biases in the estimation errors for both estimators I and II have reduced. This is somewhat counter-intuitive since one would expect that at higher speeds the data set may provide richer information for the estimation problem. The case, however seems to be the opposite. The explanation is that on the right-hand side of Equation 2.33, there exist the multiplicative terms ωi_q and ωi_d. Let the subscript $_o$ represent a nominal quantity, or equivalently, a perfect measurement. Then, a corrupt measurement of ω and i_q enters the right-hand-side of 2.33 as

$$(\omega_o + \delta\omega)(i_{q_o} + \delta i_q) = \omega_o i_{q_o} + \omega_o \delta i_q + i_{q_o}\delta\omega + \delta\omega\delta i_q \qquad (2.49)$$

The second, third, and fourth terms on the right-hand-side of 2.49 are noisy but the dominant noise term is the second term. It is seen that this term is made larger as the speed is increased. In fact, the noise in this term is amplified linearly with speed. Hence if the noise variances are kept constant, and the speed is increased, we should expect the estimation algorithms to perform more poorly. This is the case observed in Experiments 2 and 3. However, a case can be made for the fact that one can not decreases the speed to arbitrarily small values and consistently obtain better results since the conditioning of the estimation problem will get worse with decreasing speed. The fact is, one can see through the steady-state equations of the motor that the critical speed at which the conditioning of the problem would become noticeably problematic is very small.

2.5   Summary

In this chapter we have presented the electromechanical model of the permanent-magnet synchronous motor in the rotor frame. We have used this model in steady-state to develop methods of estimating the winding resistance R, and the magnet strength K. We have observed that given a priori knowledge of the parameter K, a more accurate estimate of the parameter R can be obtained. In light of the fact that the experimental motor under study in this thesis has hard magnets, i.e. ones whose strength changes very little under thermal stress, it is feasible to assume that the value of K is constant and only estimate R by way of Estimator II. In what follows we will only deal with the problem of estimation of R alone.

Chapter 3

The Thermal Model

3.1 Introduction

In this chapter, we discuss the thermal behavior of the experimental motor. We first identify those parameters of the electromechanical model of the motor that vary with temperature. We then calibrate these parameters as thermometers by determining analytic expressions for their temperature dependencies. The next step is to determine the sources of heat which give rise to temperature increases within the motor, consequently affecting the thermally varying parameters. By measuring the effects of those heat sources on the parameters, we can track the input and the output of the thermal system shown in Figure 3.1. We then use these input-output measurements to establish a dynamic model for the thermal behavior of the motor.

In the final section of this chapter, we present some ways to confirm the correctness and accuracy of the thermal model. We also derive thermally-limited torque-speed curves for the motor using the steady-state version of the thermal model. These curves assist in determining limits on speed and torque production for the motor
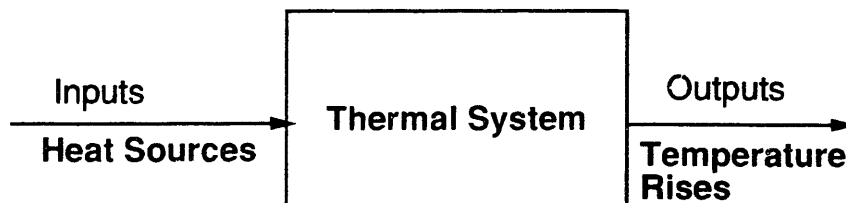
Figure 3.1: Input-output measurement for the thermal system

under various thermal conditions.

3.2 Calibration of Parameters

There exist two parameters in the electromechanical model of the motor that are known to vary with temperature. They are, the resistance of the stator windings R, and the strength of the permanent magnet, K. The resistivity of copper, from which the stator windings are constructed, is known to increase with temperature. In contrast, the strength of most permanent magnets decreases with increasing temperature.

We have limited our study to the thermal dependencies of only these two parameters for the following reasons. Firstly, the only other parameters that might vary with temperature are the inductances L_d and L_q. From experience, we know that these quantities are very weakly sensitive to changes in temperature and are, therefore, not very good thermometers. Furthermore, it is extremely difficult to detect any changes in these quantities. Secondly, some of the most common failures in small permanent-magnet synchronous motors occur as a result of thermally weakened insulation on the stator windings, and the thermal demagnetization of the permanent magnets. Therefore, it is valuable to study R and K as indicators for failure prevention and/or detection purposes.

3.2.1 The Thermal Dependence of R

Here, we seek to establish a relationship between the average winding resistance, R, and the aveage temperature, T_R^*, at or sufficiently nearby the windings. We know [1] that the resistance of copper increases approximately linearly with temperature over a large temperature range. Assume that at a reference temperature, T_{ref}, the winding resistance equals R_{ref}. Hence, we have

$$R(T_R^*) = R_{ref} + C(T_R^* - T_{ref}) \tag{3.1}$$

where C is a constant. So for two distict temperatures $T_{r_1}^*$ and $T_{r_2}^*$, we have

$$R_1(T_{R_1}^*) = R_{ref} + C(T_{R_1}^* - T_{ref}) \tag{3.2}$$

$$R_2(T_{R_2}^*) = R_{ref} + C(T_{R_2}^* - T_{ref}) \tag{3.3}$$
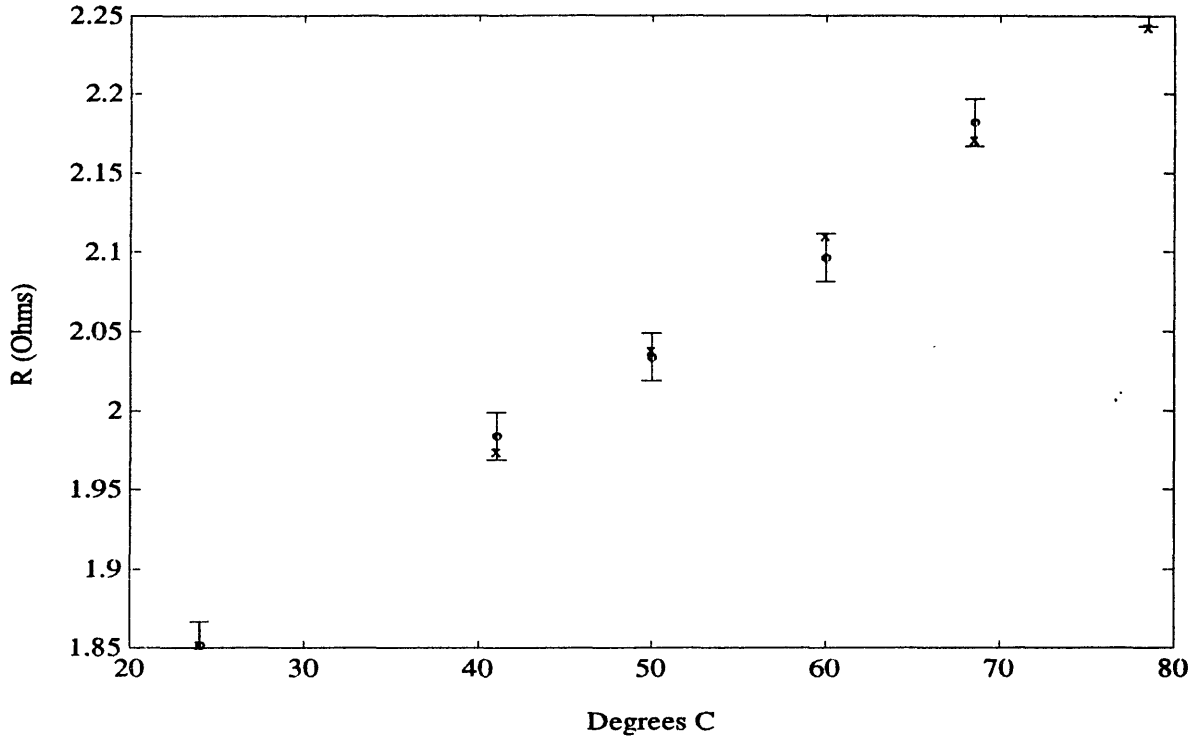
Figure 3.2: Measured (o) and Theoretical (x) R vs. Temperature

We know from [1] that the quantity $\frac{C}{R_{ref}}$ is known as the temperature coefficient of a metal and at $T_{ref} = 20$ °C this quantity equals 0.00393 ohms/°C for copper. Noting this, we divide Equations 3.2 and 3.3, and substitute for T_{ref} and C above to obtain

$$\frac{R_1(T^*_{R_1})}{R_2(T^*_{R_2})} = \frac{234.5 + T^*_{R_1}}{234.5 + T^*_{R_2}} \tag{3.4}$$

This expression represents the incremental model of the thermal dependence of the winding resistances.

Experiments were performed to establish that the average resistance of the windings is accurately predicted by Equation 3.4. In these experiments, the motor was placed in an oven and heated to a specific temperature. The winding resistances were then measured. The experiment was then repeated over a range of temperatures. The results are shown in Figure 3.2, where the error bars represent the accuracy of the measured resistance. Note the good agreement between the measured temperatures and those predicted by Equation 3.4.

3.2.2   The Thermal Dependence of K

The permanent-magnets used in the experimental motor are Samariun-Cobalt magnets. It is shown in [28, 27] that the strength of such a magnet decreases monotonically

with temperature. We performed experiments where K was measured as a function of the magnet temperature T_K^*. In these experiments, the motor was again placed inside an oven and heated to a specific temperature. Then a second motor was used to spin the experimental motor briefly, and K was measured through the measurement of its terminal voltage. These experiments confirmed the result in [28, 27] in that the magnet strength does indeed decrease monotonically. However, it was seen that the magnet stength does not decrease substantially under thermal stress. In particular, we noticed a 4 percent decrease in K over a 55°C increase in temperature as shown in Figure 3.3. This indicates that we can infer a reliable estimate of T_K^* from K only if we have a very accurate measurement of K.

Despite the insensitivity of K to T_K^*, we obtained a model for the data relating K to T_K^*. At the time when this was done, no exact functional form for this relationship was available in the literature. Hence, we chose a function that best fit the data and the monotonicity criterion. Using a simplex algorithm for fitting nonlinear functions, we obtained the following model

$$K(T_K^*) = \alpha (\frac{T_K^*}{T_{ref}})^{-n} \tag{3.5}$$

where $\alpha = 7.476e - 2$, and $n = 2.973e - 2$, and T_{ref} is the reference ambient temperature taken to be 20°C. This model proved to be an effective fit to the data as shown in Figure 3.3. It is worth noting that taking differentials of both sides of 3.5 gives

$$\|\frac{dT_K^*}{T_K^*}\| = \frac{1}{n}\|\frac{dK}{K}\| \tag{3.6}$$

We can see in Equation 3.6 that since n is small, as T_K^* increases, if there is any error in the measurement of K, it becomes increasingly more difficult to infer the value of T_K^* from the measurement of K. In other other words, a small error in the measurement of K will produce a very large error in the value of T_K^* that is produced through Equation 3.5. This is an inherent property of the samarium-cobalt permanent magnet over which we have no control. In summary, we have learned that samarium-cobalt magnets make very poor thermometers.

3.2.3 Direct Thermocouple Measurements

Given the difficulty in measuring T_K^* through K, we sought a third temperature sensor for the experimental motor. A thermocouple that measures the temperature of
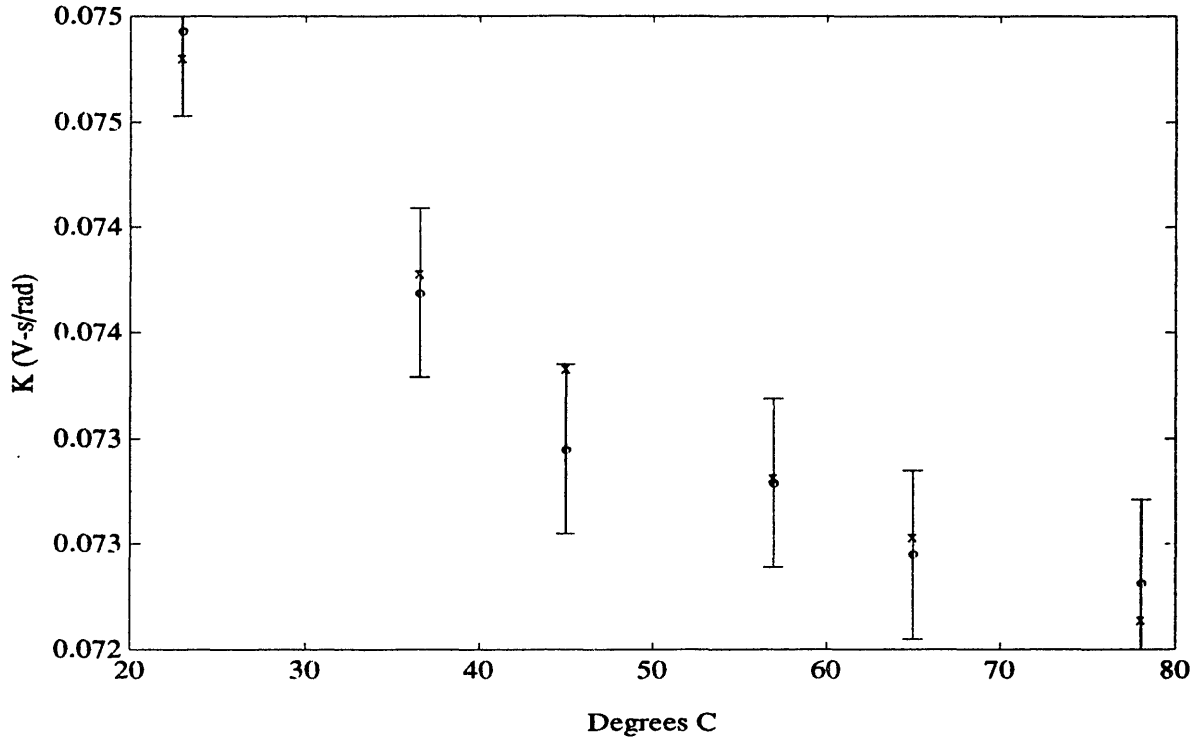
Figure 3.3: Measured(o) and theoretical(x) K vs. temperature

the surface of the motor was introduced as shown in Figure 3.4. A type-K thermocouple was electrically insulated and attached to the stand where the experimental motor is supported. A side view of the motor as shown in Figure 3.5 shows the actual location of the thermocouple. The thermocouple was then connected to an amplifier which incorporates the appropriate cold-junction compensation and provides an analog voltage of 1 mV/°C as output. The output of this device was filtered with an analog low-pass filter for noise suppression.

3.3 Heat Sources

From experience, we know of three major sources of heat within a permanent-magnet motor while it is in operation. Most obvious is the dissipation caused by currents in the stator windings. The heat dissipated in the winding is given by $i^2 R$, where i is the winding current and R is the winding resistance. For our purposes, it is more convenient to express this dissipation in terms of currents in the d-q frame. As discussed in Chapter 2, the desired expression for the winding dissipation is

$$P_W = (i_d^2 + i_q^2)R \qquad (3.7)$$

42
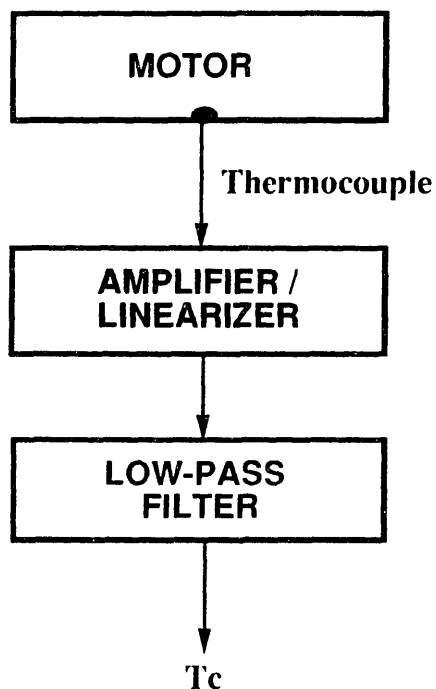
Figure 3.4: Thermocouple Measurements

where P_W is the winding dissipation, and R is the average resistance of all three phase windings.

The second source of heat is the power dissipated in the core due to eddy currents. Assuming linear magnetic properties for the steel in the motor, the power dissipated due to eddy currents is proportional to $w^2 B^2$ where w denotes the speed of the rotor in radians per second, and B denotes the magnitude of the magnetic flux density in the airgap. B is proportional to the airgap flux, which is in turn proportional to the total flux linkage. Let the quantity $\lambda_d^2 + \lambda_q^2$ denote the square of the total flux linkage expressed in the d-q frame. So in the d-q frame we have

$$P_E \propto w^2(\lambda_d^2 + \lambda_q^2) \qquad (3.8)$$

where

$$\lambda_d = L_d i_d + K \qquad (3.9)$$

$$\lambda_q = L_q i_q \qquad (3.10)$$

THERMOCOUPLE

MOTOR

STATOR

ROTOR

ALUMINUM
STAND

SIDE VIEW
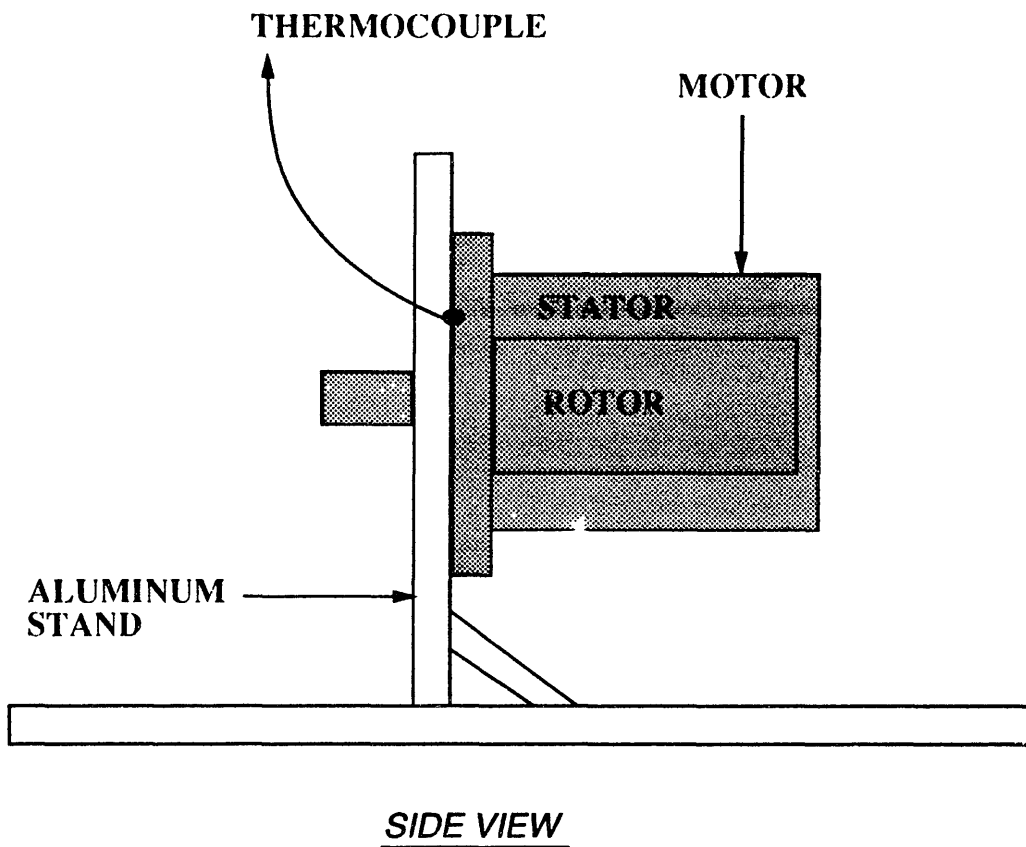
Figure 3.5: Thermocouple Location

and P_E is the dissipation due to eddy currents.

The third source of heat is the combined friction loss in the bearings and hysteresis loss in the core. In both cases, the heat generated is proportional to the rotor speed, w. Thus,

$$P_{F/H} \propto w \qquad (3.11)$$

where $P_{F/H}$ denotes the dissipation due to friction and hysteresis.

Experiments discussed below confirm that P_W, P_E, and $P_{F/H}$ are the only significant sources of heat in the experimental motor. Therefore, the thermal system of the motor has three inputs u_1, u_2, and u_3, given by

$$u_1 = (i_d^2 + i_q^2)R \qquad (3.12)$$

$$u_2 = w^2(\lambda_d^2 + \lambda_q^2) \qquad (3.13)$$

$$u_3 = w \qquad (3.14)$$

An important observation from the experiments is that the largest source of heat dissipation is the winding losses. The second largest is the combined hysteresis and friction losses, and the third is the eddy-current losses. This result is compatible with our intuitive sense of these effects. The model that we build should reflect this property accordingly.

3.4   Dynamic Thermal Model

We wish to obtain a state-space representation for the thermal system with inputs as described in Section 3.3, and outputs being the temperature rises in the motor. To do so, we must first choose the quantities which will be the thermal states. In the interest of simplicity, we develop our state-space model based on temperature *rises* within the motor. Assume that initially, all points in the motor are at the same reference temperature T_{ref}. Then at any future point in time, if any of the inputs u_i ($i = 1, 2, 3$) is nonzero, the temperature rises in the motor will be denoted by T_R, T_C(thermocouple), and T_K. Thus,

$$T_R^* = T_{ref} + T_R \qquad (3.15)$$

$$T_C^* = T_{ref} + T_C \qquad (3.16)$$

$$T_K^* = T_{ref} + T_K \qquad (3.17)$$
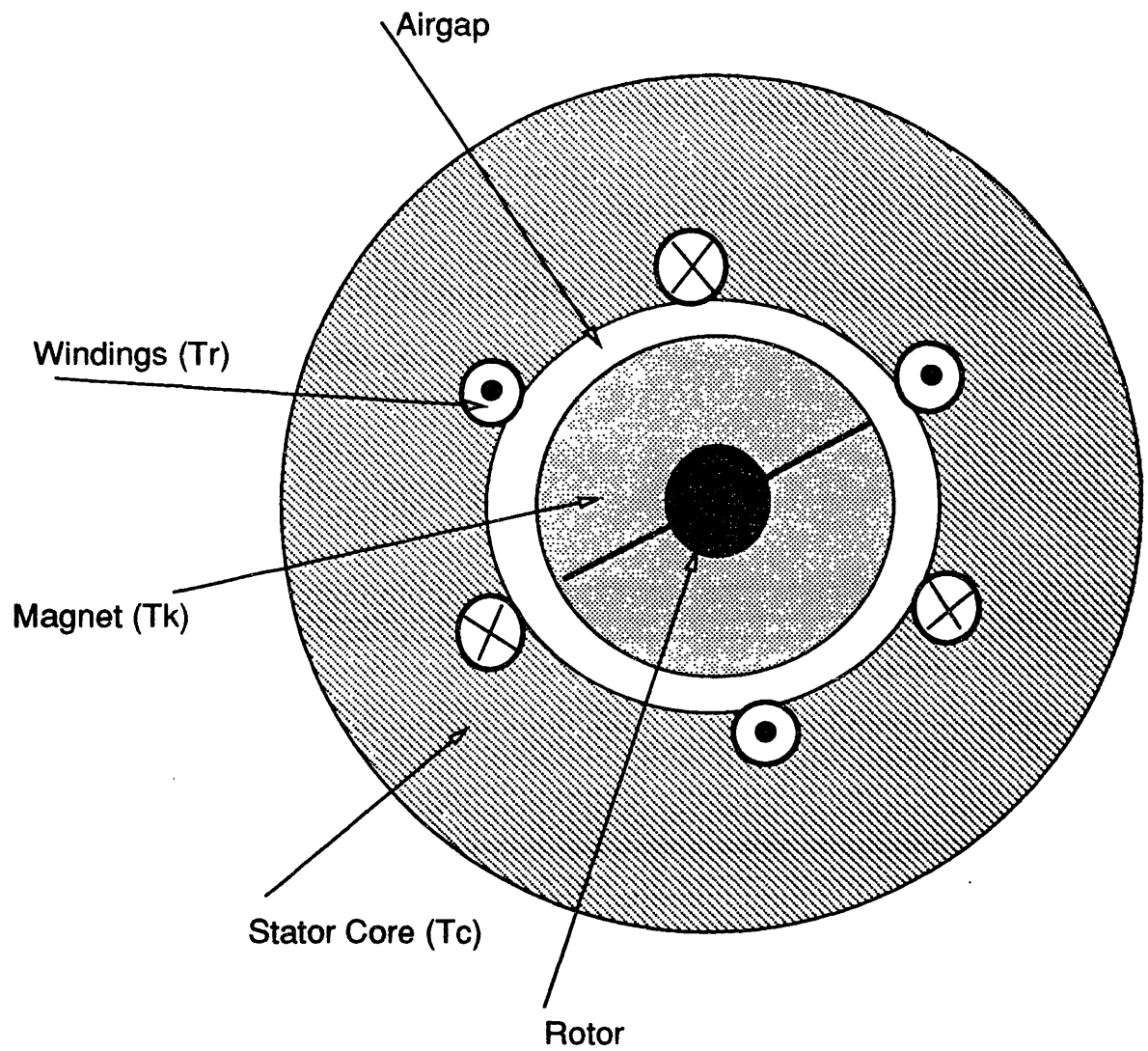
Figure 3.6: Thermal State Variables

We should like to designate T_R, T_C, and T_K as our state variables. However, as discussed in Section 3.2, while performing the experiments to characterize the input-output map for the thermal system, we were confronted with the difficulty of measuring T_K accurately. This is because the slightest error in the measurement of K yields a T_K that is far from accurate. Therefore, it is not sensible to include T_K as a state variables since the input-output map for this variable could not be accurately characterized. This is to say that the inclusion of T_K as a state variable introduces a nearly unobservable mode in the model, a situation that is not desirable. It should be underscored, however, that the difficulty with T_K is dependant on the type of magnet used in the motor. If a sufficiently thermally sensitive magnet is used in a permanent-magnet synchronous motor, then it may be possible to charactrize the dynamics of T_K accurately enough so as to include this temperature as a state variable.

3.4.1   Modeling

By construction, we know that for our purposes, the permanent magnet synchronous motor is made up of two distinct thermal masses. The first being the stator windings and the second the collective mass of the core and the magnets. Hence, it seems appropriate to propose a second order dynamic model for the thermal system. We denote the vector $T = [T_C \ T_R]'$ as our state vector, and the vector $u = [u_1 \ u_2 \ u_3]'$ as our input vector. We measure the state directly so our observation matrix is the identity. Hence we have:

$$\dot{T} = AT + Bu \qquad (3.18)$$

$$Y = IT \qquad (3.19)$$

where A and B are 2×2 and 2×3 matrices, respectively, while I denotes the 2×2 identity matrix. In proposing this model, we have assumed that the motor has linear thermal properties. So that the thermal masses in the motor (rotor, magnet, etc.) behave as dictated by the thermal properties of the metals that constitute them. This allows us to draw parallels between our thermal system and passive, linear resistive-capacitive networks [10].

As discussed in [10], any linear thermal system can be thought of as a linear RC network with all capacitors sharing a common ground. See Figure 3.7. This analogy holds if the electrical and thermal capacitance and resistances are taken to be equivalent quantities. Given this analogy, we wish to characterize the structure of

47
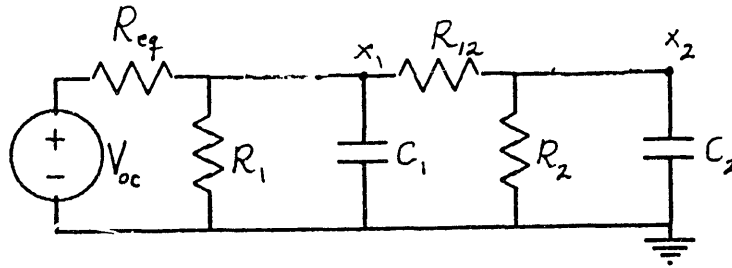
Figure 3.7: The electrical equivalent of a second order linear thermal system

the matrices A and B in 3.18. We will first need some definitions and notations.

Notation 1 *Following [31], let $Z^{(n,n)}$ denote the set of all real $n \times n$ matrices $A = [a_{ij}]$ such that $a_{ij} \leq 0$ for all $i \neq j$, $1 \leq i, j \leq n$.*

Notation 2 $\rho(Q)$ *denotes the maximum of the moduli of the eigenvalues of Q.*

Definition 1 *An $n \times n$ matrix A that can be expressed in the form $A = sI - Q$, where $-Q \in Z^{(n,n)}$ and $\rho(Q) \leq s$, is called an $M - matrix$.*

We now present a theorem that establishes the relationship between M-matrices and linear thermal systems.

Theorem 1 *Any linear thermal system has a minimal state-space representation which has a dynamic matrix A, the negative of which is an M-matrix.*

Proof: As mentioned before, a linear thermal system can be described by a linear RC network with all capacitors sharing a common ground. In Thévenin equivalent form we can describe this circuit as shown in Figure 3.7. Pick the voltage across capacitor C_j to be the state variable x_j. Then, for each state variable we can write

$$\dot{x}_j = a_{j,j-1} x_{j-1} + a_{j,j} x_j + a_{j,j+1} x_{j+1} \tag{3.20}$$

48
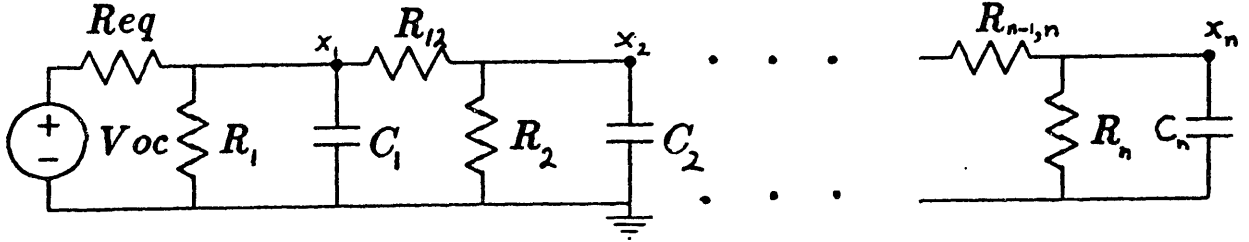
Figure 3.8: The Thévenin equivalent circuit describing a general linear thermal system

where

$$a_{j,j-1} = \frac{1}{C'_j R_{j-1,j}} \tag{3.21}$$

$$a_{j,j} = -\left(\frac{R_{j-1,j} \| R_j \| R_{j,j+1}}{C'_j}\right) \tag{3.22}$$

$$a_{j,j+1} = \frac{1}{C'_j R_{j,j+1}} \tag{3.23}$$

Let $x = [x_1\ x_2\ ...\ x_n]'$, and the output be $y = x$. Note that the superscript $'$ denotes algebraic transposition. We obtain a minimal state-space representation of the form

$$\dot{x} = Ax + Bu \tag{3.24}$$

$$y = x \tag{3.25}$$

By construction, we see that the matrix $A = (a_{pq})$ is an $n \times n$ tridiagonal matrix such that $a_{pq} \geq 0$ for all $p \neq q$. So it follows that $-A \in Z^{(n,n)}$. We also know that any linear RC network is necessarily strictly exponentially stable. Hence, all the eigenvalues of $-A$ are positive real numbers. Therefore, by Definition 1, $-A$ is an M−matrix.

We can also show that we can arrive at the result of Theorem 1 regardless of the order in which we assign the state variables. In other words, we can assign the state

variable x_j to the voltage across the capacitor C_i for **any** pair of integers (i,j) with $1 \leq i,j \leq n$, and still prove Theorem 1. Reordering the state variables corresponds to the linear tranformation $V = PX$ where P is a permutation matrix. Under this transformation, the system 3.28 becomes

$$\dot{V} = PAP^{-1}V + PBU \qquad (3.26)$$

We can write P as $P = [e_{p_1} \ e_{p_2} \ ... \ e_{p_n}]'$ where $\epsilon_{p_i} = [0...0..1..0]'$ with the 1 in the p_i^{th} location. Then, we can see that $PAP' = [a_{p_i p_j}]$. This shows that the diagonal elements of A are mapped to diagonal elements of PAP'. i.e. PAP' is a rearrangement of the elements of A in such a way that diagonal elements are swapped with other diagonal elements and off-diagonal elements with other off-diagonal elements. Furthermore, PAP' is strictly exponentially stable since it has the same eigenvalues as A. Hence, $-PAP'$ is also an $M-$matrix.

As for the matrix B in 3.18, we know from experience that all the inputs to the thermal system are "active" in the sense that none of them ever slows down the heating of the motor, or introduces a cooling effect. So all the elements of the matrix B must be positive.

3.4.2 Stability

In our experiments we observed that given bounded thermal inputs, the outputs (and hence the states) remained bounded. This fact is consistent with the structure of the matrix A as discussed in section 3.4.1. However, a more careful consideration of Equation 3.18 reveals that the input u is not exogenous. In fact, u is a function of the states T_R and T_C since by definition, u_1 and u_2 are functions of R and K. These parameters, being temperature-dependent, vary with the thermal states. So the question of the stability of the system described by Equations 3.18 and 3.19 is non-trivial. We are most interested in the stability of our model for thermal inputs that result from steady-state electromechanical operation of the motor. This is because so far as the task of failure analysis is concerned, we typically deal with the electromechanical system in steady-state operation, resulting in constant electrical inputs to the thermal system. Let us assume that the motor is in electromechanical steady state. Hence, the quantities i_d, i_q, and w are constant. The average resistance of the stator windings can be written as $R = R_{ref} + \delta R$ where R_{ref} is the resistance due to the reference temperature and δR is the incremental resistance due to the local

temperature rise T_R. So we have

$$R = R_{ref} + \delta R = R_{ref} + \beta T_R \qquad (3.27)$$

where δR is obtained from taking differentials of both sides of Equation 3.1. Theoretically, we should consider the effect of the coupling between the two parameters R and K and the thermal states. Yet, as we have seen before for our motor, the effect of T_K on the value of K is extremely small, effectively allowing us to ignore the dependence of u_2 on the thermal states. So we consider only the coupling between the input u_1 and the state T_R.

The thermal system can be written as

$$\dot{T} = AT + Bu_{ref} + B[\beta(i_d^2 + i_q^2)T_R \quad 0 \quad 0]' \qquad (3.28)$$

where $u_{ref} = [R_{ref}(i_d^2 + i_q^2) \quad u_2 \quad u_3]'$. We note that given $B = [b_{ij}]$, the third term of the right hand side of 3.32 can be written as

$$B \begin{bmatrix} \beta(i_d^2 + i_q^2)T_R \\ 0 \\ 0 \end{bmatrix} = \beta(i_d^2 + i_q^2)T_R \begin{bmatrix} b_{11} \\ b_{21} \end{bmatrix} = \begin{bmatrix} 0 & \beta(i_d^2 + i_q^2)b_{11} \\ 0 & \beta(i_d^2 + i_q^2)b_{21} \end{bmatrix} \begin{bmatrix} T_C \\ T_R \end{bmatrix} = JT$$

Hence, 3.18 can be written as

$$\dot{T} = (A + J(i_d, i_q))T + Bu_{ref} \qquad (3.29)$$

For constant currents i_d and i_q, the above system is linear and time-invariant. Hence, for stability we must have

$$Tr(A + J) < 0 \qquad (3.30)$$
$$Det(A + J) > 0 \qquad (3.31)$$

The above conditions translate into

$$\begin{aligned} (i_d^2 + i_q^2) &< -\frac{Tr(A)}{\beta b_{21}} = l_1 \\ (i_d^2 + i_q^2) &< -\frac{Det(A)}{\beta Det([a_1|b_1])} = l_2 \end{aligned} \qquad (3.32)$$

where a_1 and b_1 are the first columns of A and B, respectively. So stability is guaranteed for $(i_d^2 + i_q^2) < \min(l_1, l_2)$. Furthermore, we expect 3.29 to be *exponentially* stable

51

(no oscillatory behavior), in keeping with the RC-network analogy and our intuition for dissipative thermal systems. To verify this, we must have

$$(Tr(A + J))^2 - 4Det(A + J) \geq 0 \qquad (3.33)$$

It is possible to check that the latter condition is satisfied for any value of $(i_d^2 + i_q^2)$, as desired. It is also possible to check that for all $(i_d^2 + i_q^2) < \min(l_1, l_2)$, $A + J$ is an M−matrix. Note that the above stability condition is only a sufficient condition. However, it should be mentioned that several simulations showed that stability is lost if the root-mean-square value of $i_d^2 + i_q^2$ exceeds $\min(l_1, l_2)$. This instability phenomenon is known as a thermal runaway.

3.4.3   Torque-Speed Characterization

It is possible to characterize torque-speed curves for the motor under study from the thermal model. This is useful because it provides the manufacturer with guidelines on the limits of safe operation of the motor under various thermal conditions. These guidelines are, in turn, passed on to the consumer. Let us consider the thermal system in steady-state. We can write

$$AT + Bu = 0 \Rightarrow T = -A^{-1}Bu \Rightarrow T = Gu \qquad (3.34)$$

Given that we are interested in torque-speed (τ-w) relationships, it is only relevant to study the local temperature rise in the windings, T_R. It is the current in these windings that produces a desired torque at a specified speed. Furthermore, τ-w curves obtained by studying the steady-state behavior of T_R give rise to safe operating limits that prevent the windings from getting too hot, hence avoiding failures due to burned insulation. So from equation 3.34 we obtain

$$T_R = g_{21}R(i_d^2 + i_q^2) + g_{22}w^2(\lambda_d^2 + \lambda_q^2) + g_{23}w \qquad (3.35)$$

Without significant loss of generality, we can assume that in electromechanical steady state, the current i_d is kept at zero. This is reasonable since this current does not contribute to torque production at all. It does, however, contribute to heat production, so it is often driven to zero. An exception is in the case of field weakening control

[12]. Given this, in electromechanical steady-state we have

$$
\begin{aligned}
i_d &= 0 \\
i_q &= \frac{Bw + \tau}{3K} \\
\lambda_d &= K \\
\lambda_q &= L_q i_q
\end{aligned}
$$

Substituting these values in Equation 3.39 yields a quadratic equation in τ which is solved in terms of w to give

$$
\tau = 3K \sqrt{\frac{T_R - g_{22} w^2 K^2 - g_{23} w}{g_{21} R + g_{22} L_q^2 w^2}} - Bw \tag{3.36}
$$

This equation relates the torque τ to the speed w while the windings are at a local temperature of $T_R^* = T_R + T_{ref}$. Note that R and K in the Equation 3.40 are both evaluated at T_R^*. This represents a worst-case scenario in the sense that T_K is assumed to be equal to T_R. In the next section we obtain explicit values for g_{2i}, $1 \le i \le 3$, and display τ-w curves for various temperatures T_R^*.

3.4.4 Experimental Results

So far, we have only considered a continuous-time model of the thermal system. Yet, our input-output measurements were made at discrete instances in time. Hence, it is only natural that we fit a discrete-time model to our data. The discrete-time model will, in turn, provide us with a continuous-time model as demonstrated below.

We have the system $\dot{T} = AT + Bu$. The input vector u can be explicitly measured at discrete instants in time. Since the sampling period of the electrical variables in u is far smaller than the smallest time-constant of the thermal system, the input u is effectively piecewise constant. In other words, it is appropriate to represent the vector u at each discrete point in time by its average value during the preceeding t_o units of time, provided that the sampling time t_o is sufficiently small. In our case we know that the sampling interval t_o is sufficiently small since it is far smaller than the fastest time-constant of the thermal system. It is well known [7] that the corresponding discrete-time system with a sampling period of t_o seconds is given by:

$$
T(n+1) = \Phi T(n) + \Gamma u(n) \tag{3.37}
$$

where $\Phi = e^{At_o}$ and $\Gamma = \int_0^{t_o} e^{A\sigma} d\sigma B$. Given Γ and Φ, we can write $A = \frac{\log(\Phi)}{L}$ where the log function is defined by the Taylor series:

$$\log(\Phi) = \sum_{j=1}^{\infty} \frac{(I - \Phi)^j}{j} \tag{3.38}$$

Note that this power series converges if and only if all the eigenvalues of $I - \Phi$ have magnitude strictly less than 1. By truncating this series we can find a good approximation to A and therefore compute B from Γ. We can write the discrete-time system as follows

$$T'(n + 1) = [T'(n) \quad u'(n)] \begin{bmatrix} \Phi \\ \Gamma \end{bmatrix} \tag{3.39}$$

We measure $T(n + 1)$, $T(n)$, and $u(n)$ at $i + 1$ instants in time and obtain

$$\begin{bmatrix} T'(1) \\ T'(2) \\ \vdots \\ T'(i + 1) \end{bmatrix} = \begin{bmatrix} T'(0) & U'(0) \\ T'(1) & U'(1) \\ \vdots & \vdots \\ T'(i) & U'(i) \end{bmatrix} \begin{bmatrix} \Phi \\ \Gamma \end{bmatrix} \tag{3.40}$$

or equivalently, $P = Q[\Phi \ \Gamma]'$. Hence, using an ordinary least squares fit [35] yields the minimum-square-norm-error solution as

$$\begin{bmatrix} \Phi \\ \Gamma \end{bmatrix} = (Q'Q)^{-1}Q'P \tag{3.41}$$

Experiments were performed in which the motor was allowed to spin at several speeds with different loads to produced thermal rises. Meanwhile, the currents, the magnet constant, the winding resistance, and the case temperature were mesured at discrete instants in time. The above estimation procedure was then used to yield the following estimates of the desired unknown parameters of the thermal system.

$$\Phi = \begin{bmatrix} 6.70 & .47 \\ 3.45 & 3.06 \end{bmatrix} \times 10^{-1}; \ \Gamma = \begin{bmatrix} 207.2 & 1.84 & 7.27 \\ 870.0 & 4.48 & 4.83 \end{bmatrix} \times 10^{-3}$$

$$A = \begin{bmatrix} -4.8 & 1.17 \\ 8.6 & -14 \end{bmatrix} \times 10^{-4}(1/\text{sec});$$

$$B = \begin{bmatrix} 0.2212 \text{J}^{-1} & 0.0022(\text{s}(\text{Vrad})^2)^{-1} & 0.0097\text{rad}^{-1} \\ 1.5781 \text{J}^{-1} & 0.0076(\text{s}(\text{Vrad})^2)^{-1} & 0.0055\text{rad}^{-1} \end{bmatrix} \times^{\circ} C 10^{-3}$$

$$G = \begin{bmatrix} 0.8709 & 0.0070 & 0.0249 \\ 1.6888 & 0.0099 & 0.0195 \end{bmatrix}$$

Now given these estimates, we compare the predicted results as given by the estimated model against the measured data. Figures 3.9 and 3.10 show these results for various excitations. Furthermore, given the estimated value of G, we can now explicitly find $\tau - w$ curves for the motor at various values of T_R^* as shown in Figure 3.11. In Figure 3.9 shows the temperature rises while the experimental (AC) motor was spun using a DC motor drive at the speed of 230 rpm while the three phases of the AC motor were tied together. In this experiment, a large torque is being overcome at a slow speed. All three elements of the input vector u are active in this experiment. Figure 3.9 also shows these same temperatures under no excitation. This is to say that the motor was stopped and allowed to cool down while this data was taken. Figure 3.10 shows the temperature rises and the subsequent cooling of the motor as a result of excitation that consisted of spinning the experimental motor with again the same DC motor, but at a higher speed of 3000 rpm while leaving the three phases of the motor open. The temperature rises are not as high as in Figure 3.9 due to the fact that in this experiment, only the bearing friction and some hysteresis loss contribute to the temperature rises. There are no currents flowing in the motor in this experiment.

3.4.5 Consistency Checks

In this section we wish to validate the thermal model described by Equation 3.18 with parameters as estimated by 3.41. Each of the following observations presents a fact that supports the accuracy and correctness of our estimated model.

1: Accuracy We can see that the estimated values for the matrices A and B give rise to a model that closely approximates the data as demonstrated by the graphs in Figures 3.9 and 3.10. This is perhaps the most important test of the validity of the model. Note that the typical measurement error in the measurement of T_R was about 1.4 °C while the measurement error in T_C was typically about 1 °C. Both of these standard errors were obtained from the measurement apparatus.
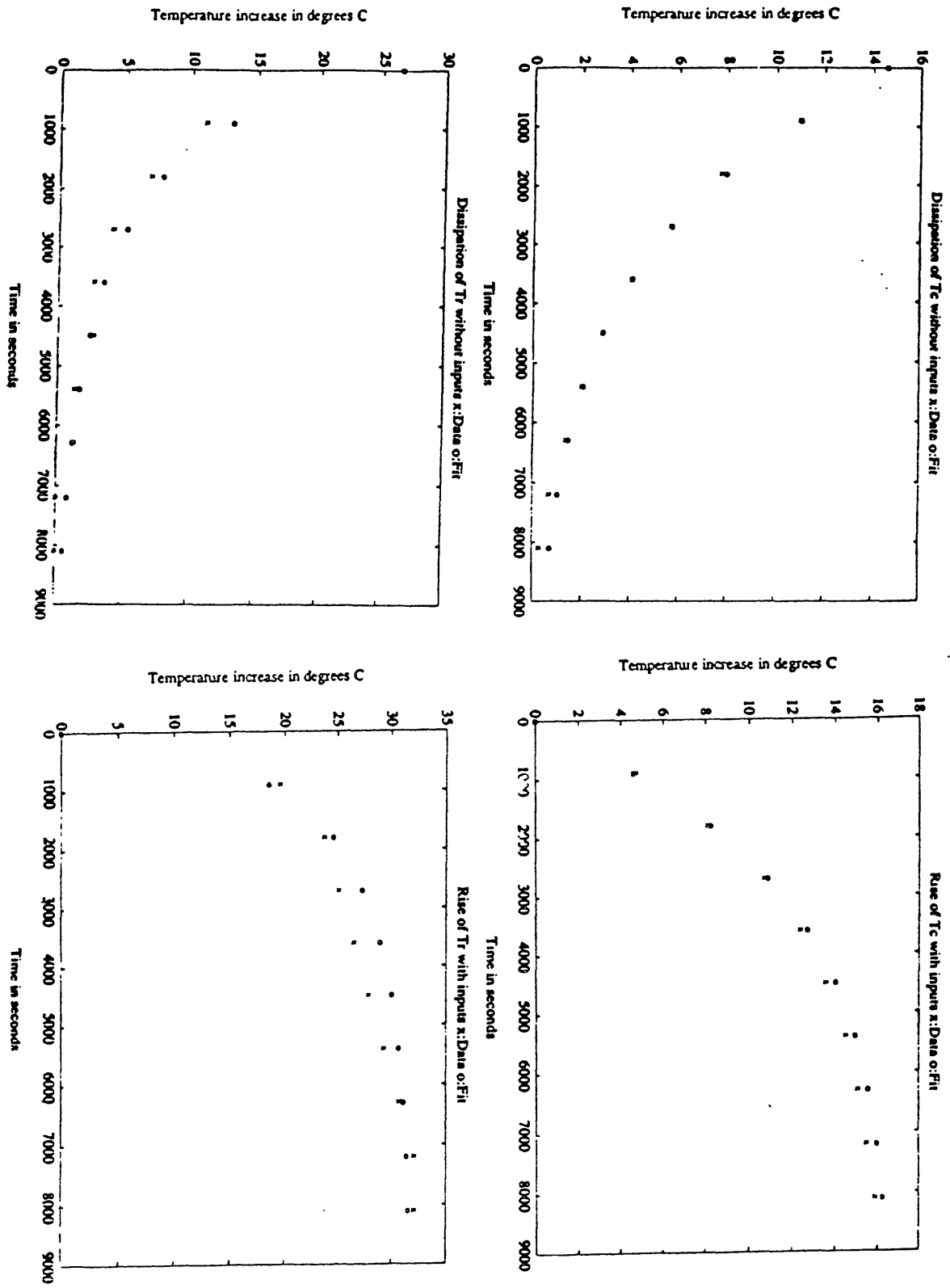
Figure 3.9: Data vs. Fit
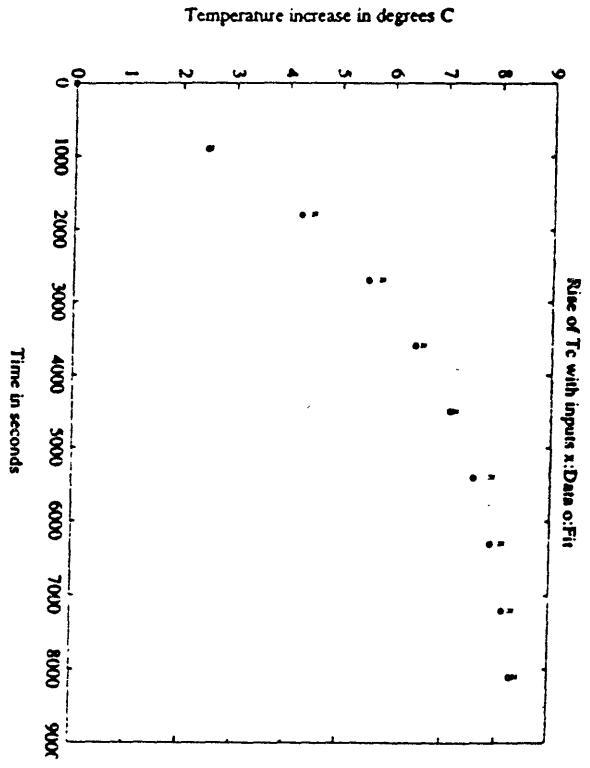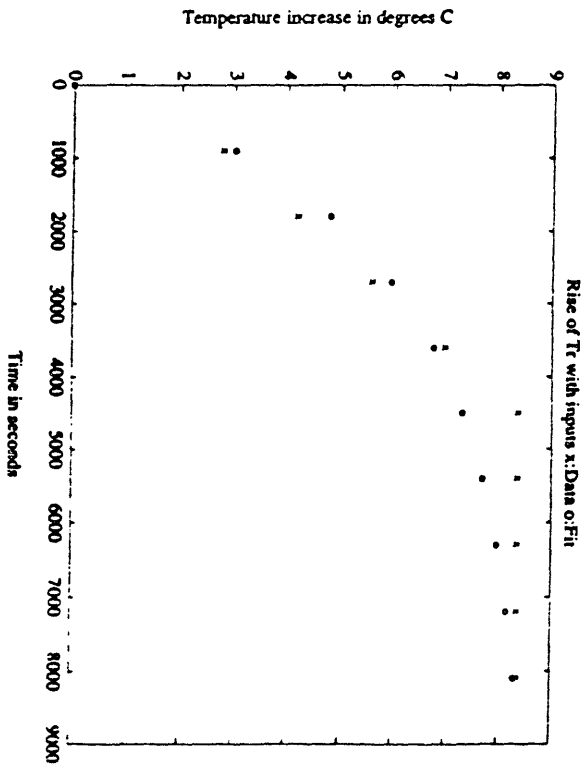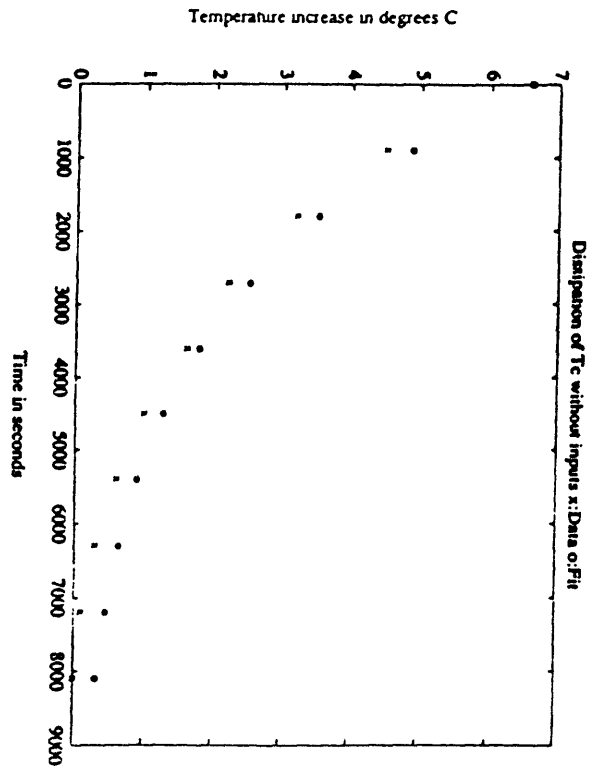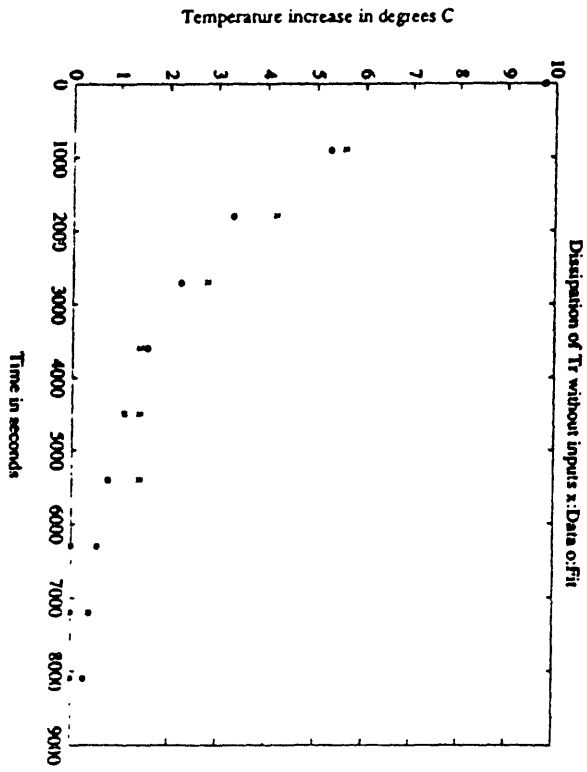
Figure 3.10: Data vs. Fit
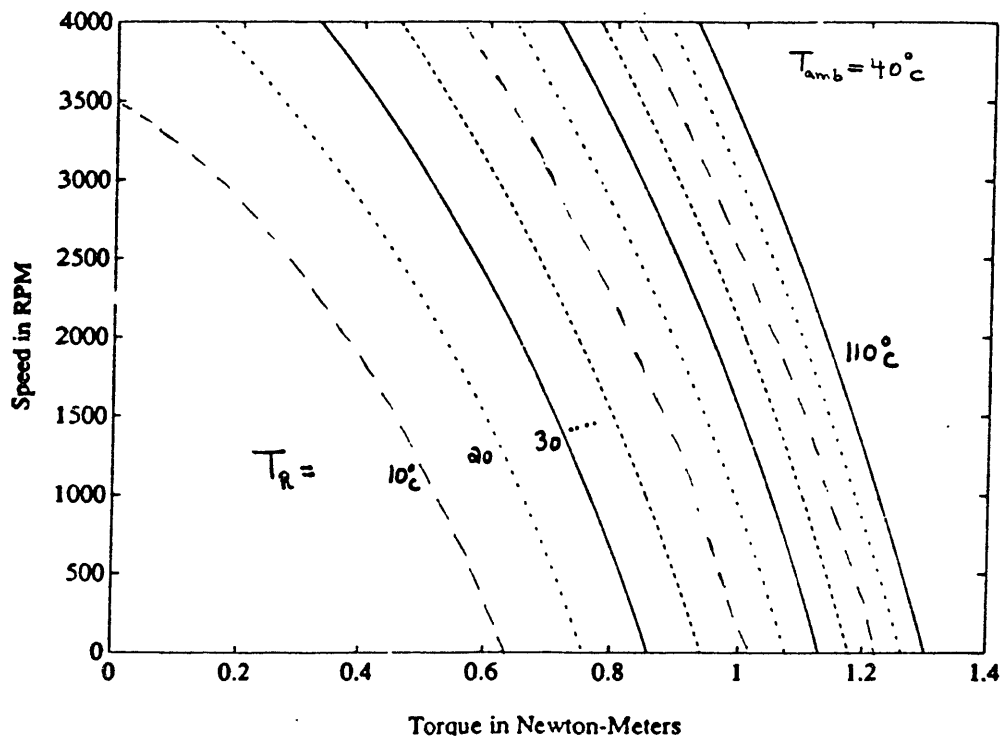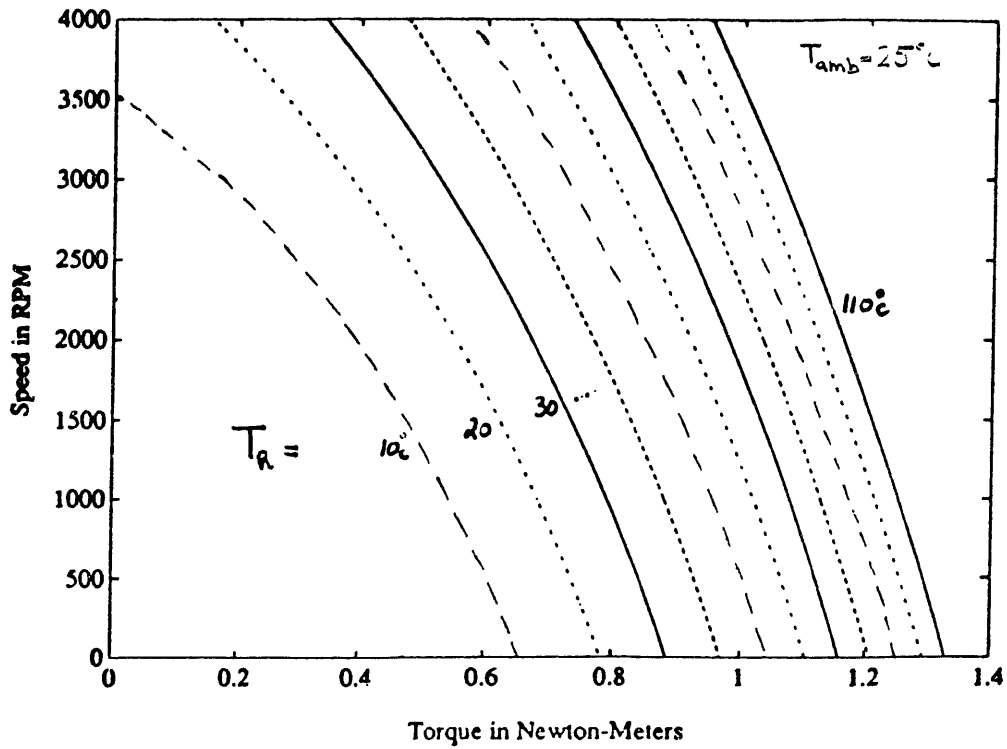
Figure 3.11: $\tau\text{-}w$ curves at various temperatures T_R^*

2: Structural Consistency The eigenvalues of the matrix A are -0.0004 and -0.0015 (1/sec). It is also clear that $A \in Z^{(2,2)}$. Hence, A is an M-matrix, as expected. Futhermore, all the elements of the matrix B are strictly positive, a fact which is consistent with our expectations as discussed in section 3.4.1.

3: Thermal inputs By looking at the estimated matrix B we can see that the column corresponding to the input u_1 (the first column) contains the largest elements of B. Similar observations can be made regarding the other two columns of B, confirming that the input due to the winding dissipations is the largest source of heat loss, followed by the frictional effects and the eddy-current losses respectively. This is to be expected.

4: Stability limits We know that the stability of the thermal model is guaranteed for $(i_d^2 + i_q^2) < \min(l_1, l_2)$. Given the estimated A and B, we can compute the quantities l_1 and l_2 as $l_1 = 164.36$ A^2, and $l_2 = 82.66$ A^2. This insures that the thermal model will remain stable for $(i_d^2 + i_q^2) < 82.66$ A^2. If the model is an accurate representation of the thermal system, the current of $\sqrt{82.66} = 9.1$ A, should agree with the quantity provided by the manufacturer in the data sheet as the maximum output current deliverable by the servo driver to the motor. The data specifiec a maximum current of 10 A. We have arrived at a figure that is within 10 % of the specification. This consistency further confirms the validity of our model.

5: Thermal response The estimated value of A gives two eigenvalues. It is seen that the faster eigenvalue -0.0015(1/sec) corresponds to the state variable T_R. This fact can be seen by observing that the eigenvector corresponding to s_2 points approximately in the direction $[0 \ 1]'$, as shown in Figure 3.12. This direction corresponds to the state variable T_R. This is consistent with the fact that the windings have a relatively small thermal mass as compared to the thermal mass of the core of the motor. Consequently, the dynamics of T_R should evolve faster than the dynamics of T_C. Our model reflects this property accordingly.

6: Physical interpretation As one last cross-check, we wish to calculate the time-constant of the thermal system by considering the motor to be a simple cylinder of steel, and verifying that this number is close to the time-constant obtained from the
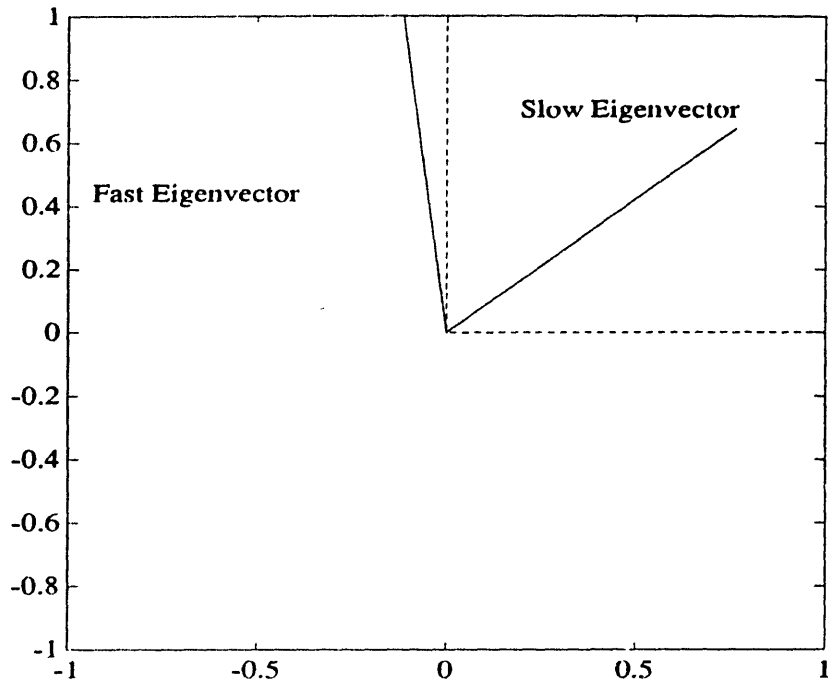
Figure 3.12: Eigenvectors of A

estimated model. It is well known [10] that the time constant τ for this object is

$$\tau = \frac{c\rho V}{hA} \qquad (3.42)$$

where for our motor we have

$$
\begin{aligned}
c &= .2175 && KJ/Kg^\circ C \\
A &= .0395 && m^2 \\
V &= 5.5e - 4 && m^3 \\
\rho &= 7.8e + 6 && Kg/m^3 \\
h &= 6.5 && W/^\circ C m^2
\end{aligned}
$$

where c denotes the thermal capacity, A represents the surface area, V denotes the volume of the cylinder, and ρ denotes the density of steel. Given these quantities, τ is approximately 3650 seconds, or about one hour. The time constant of the estimated model is approximately 1/0.0004, or 42 minutes. Although the cylinder is a very rough approximation to the real motor, these two quantities seem to be relatively close. This confirms that the model is realistic.

60

3.4.6 Failure Modeling

It is possible to quantify the effects of a thermally related failure in terms of parameter variations in the thermal model obtained in this chapter. To this end, we will concentrate our efforts on two common situations that could lead to a thermal failure. First, we wish to understand how the dynamics of our model would be affected if there should arise a situation where the motor would have trouble cooling down while in operation. A simple, and common, way in which this may take place is if the motor were to be covered with some material that would obstruct the exchange of thermal energy with the cooler ambient air. For instance, if the motor happened to be covered by a blanket, dirt, or some other thermally insulating material. We will demonstrate that this will affect the dynamic matrix A in form of an additive perturbation. The second type of common situation that may lead to undesirable operating conditions is if the ambient temperature in which the motor resides would rise dangerously high. As far as the thermal model is concerned, this represents a bias in the measurement of the states of the thermal system. Both of the situations described above are common in applications where small permanent-magnet synchronous motors are used. In industrial robotic applications such as welding, parts manipulation, and handling of toxic substances, the ambient temperature within the plant must be controlled so as to, among other factors, prevent damage to the robots which are, in many cases, actuated by permanent-magnet motors.

Cooling Obstruction   We performed a series of experiments to determine the effect of cooling obstruction on the dynamics of the thermal model. It is clear that while the motor is in electromechanical steady-state operation, the electrical contribution to the heat sources identified in the previous section will remain constant regardless of whether there is a cooling problem. Hence it is natural to expect that a cooling obstruction would alter only the parameters in the dynamic matrix A. Our experiments showed that this effect can be adequetly modelled by an additive perturbation matrix E to the matrix A. Given constant thermal inputs, the dynamics of the unfailed thermal system can be described by

$$\dot{T} = (A_1 + J(i_d, i_q))T + Bu_{ref} \qquad (3.43)$$

while the dynamics of the failed sytem can be modelled as

$$\dot{T} = (A_2 + J(i_d, i_q))T + Bu_{ref} \qquad (3.44)$$

where $A_2 = A_1 + E$. For convenience, let us drop the subscript $_{ref}$ from the input to the thermal system below. In thermal steady-state, for a constant input u_i we can write the equations 3.44 and 3.45 as

$$(A_1 + J_i)T_1 + Bu_i = 0 \qquad (3.45)$$

$$(A_2 + J_i)T_2 + Bu_i = 0 \qquad (3.46)$$

Subtracting the above two identities we obtain

$$(A_1 + J_i)T_1 = (A_2 + J_i)T_2 \qquad (3.47)$$

or equivalently,

$$(A_1 + J_i)T_1 = (A_1 + E + J_i)T_2 \qquad (3.48)$$

Now we may perform N experiments for distinct inputs $u_1, ..., u_N$ to obtain

$$
\begin{bmatrix} T'_{21} \\ \vdots \\ T'_{2N} \end{bmatrix} E' =
\begin{bmatrix} (T_{11} - T_{21})'(A_1 + J_i)' \\ \vdots \\ (T_{1N} - T_{2N})'(A_1 + J_N)' \end{bmatrix}
$$

The matrix E may now be estimated as follows using a linear least squares fitting scheme

$$E' = (C'QC)^{-1}C'QY \qquad (3.49)$$

where

$$
C = \begin{bmatrix} T'_{21} \\ \vdots \\ T'_{2N} \end{bmatrix} ; \quad Y =
\begin{bmatrix} (T_{11} - T_{21})'(A_1 + J_i)' \\ \vdots \\ (T_{1N} - T_{2N})'(A_1 + J_N)' \end{bmatrix}
$$

and Q is a diagonal, strictly positive-definite weighting matrix of appropriate dimension.

Our experiments indicated that if the motor is covered with insulating material,

the 2x2 matrix E perturbs the elements of the second row of A_1 the most. The experiments consisted of first allowing the motor to reach thermal steady-state while under thermal input. The inputs chosen were speeds of 100 and 200 rpm driven by a DC motor drive while the three phases of the motor were shorted to each other. After the motor had reached thermal steady-state, it was covered in 3 inches of styrofoam and air-cushioned insulation which caused the temperatures in the motor to increase to new steady-state values which were subsequently recorded. This data was then used to form the matrices C and Y. Examples of these transients due to this type of failure are presented in Chapters 5 and 6. It is important to note that the we do not seek to characterize the matrix E explicitly on a term-by-term basis. This is because firstly, E may be time-varying. Secondly, so far as geometric failure detection is concerned, only the structure of E in the sense of the span of its range space is of interest since geometric detection theory deals with directions in the output space. In our case, using the aforementioned experiments, we have established that a cooling obstruction failure is adequately represented by a matrix E with rank 1, whose range space is spanned by the unit vector $[0\ 1]'$. This is all the information needed to formulate the detection problem for this failure.

Raised Ambient Temperatures   Keeping in mind the RC circuit corresponding to a linear thermal model, it is clear that a rising ambient temperature is equivalent to placing a voltage source $v(t)$ "at ground". This is to say that all the outputs (state variables) will be biased by an amount proportional to $v(t)$. Hence this type of failure is equivalent to having biased sensors, a situation that is modelled in Chapter 5.

Chapter 4

Thermal Observer: Theory and Design

4.1 Introduction

Having identified a dynamic model for the thermal behavior of the motor, we can now proceed toward the design of a complete failure detection system. We accomplish this by designing an observer for the thermal model, and then tuning this observer to accentuate the effects of failures. The observer structure presented here is a non-invasive way of predicting the temperature rises in the motor through observation of the currents and the speed of the motor. As alluded to in the introduction, this method makes use of only the thermal characteristics of the motor for the prediction of temperatures and is hence fundamentally different from the method of observing temperatures through the estimation of thermally-dependent parameters. Thus, discrepancies in the temperature estimates produced by these two methods can form a basis for failure detection.

The process of designing the observer is of great importance, independently of whether a failure detection system is derived from it or not. The fact that the observation matrix in our plant is the identity matrix makes the design of an observer somewhat redundant on its own. However, the designs presented in this chapter are equally applicable to systems whose state vectors are not completely measurable.

The path taken in this thesis is to design a failure detection system by first designing an associated observer, and then deriving the failure detection filter from this in the simplest possible way. This route was taken in the interest of simplicity of design and ease of implementation. The continuous-time dynamics of the plant are

discretized and the observer design problem is undertaken in the discrete-time domain. To this end, we will show that given the fact that the time-constants of the thermal system are on the order of 1 hour, through an appropriate choice of a sampling period, we may assume that the (electrical) inputs to the thermal system are piecewise-constant between each pair of consecutive samples in time. This will allow us to deal with a simple, discrete, nonlinear, time-varying plant. Given this discrete-time plant, we propose two different observer structures. The first is an extended Kalman filter (observer) for the time-varying system and the second relies upon an approximation that is developed in Appendix A whereby the time-varying plant is approximated by a time-invariant part and a time-varying part. Then an "optimal" observer is designed around this approximate plant. The first of these observers is an optimal filter in the presence of gaussian noise dynamics in the sense of the Kalman filter in that it provides the minimum-variance estimate of the state of the model. The latter observer is also optimal, but in the sense that it provides the minimum-variance estimate of the state of an approximate model. We will compare the relative performance of these two observers in this chapter and design failure detection filters based on both of these observers in the next chapter.

4.2   Sampled-Data Dynamics

Recall from the previous chapter that the dynamics of the thermal system are described by the following:

$$\dot{T} = (A + J(i_d, i_q))T + Bu_{ref} \qquad (4.1)$$

$$y = T \qquad (4.2)$$

We have observed that the above system has very slow time-constants and that it is by far "low-pass" with respect to variations in the input u. This is to say that the thermal system is very insensitive to fast changes in its input u. These fast changes maybe due either to electromechanical load variations or some commanded transients. However, the system is clearly sensitive to the amplitudes of the input variations, but responds to them quiet slowly. Hence, it is reasonable to assume that if the sampling interval t_0 is chosen to be sufficiently small, the input may be adequetly represented at each sampling time $t_0 k$ by its average value during the previous t_0 units of time. (i.e. during $t_0(k-1) \leq t \leq t_0 k$.)

65

We may now apply standard discretization techniques to derive a sampled-data model of the plant. Given that

$$u(t) = u_k, \qquad t_0(k-1) \le t \le t_0 k, \qquad (4.3)$$

we have that $J(i_d, i_q)$ is also piece-wise constant across the same time periods. For convenience, we denote $J(i_{d_k}, i_{q_k})$ by J_k. Hence, the associated sampled-data model becomes

$$T_{k+1} = \Phi_k T_k + \Gamma_k u_k \qquad (4.4)$$

$$\Phi_k = \epsilon^{(A+J_k)t_0} \qquad (4.5)$$

$$\Gamma_k = \int_0^{t_0} \epsilon^{(A+J_k)\sigma} d\sigma B \qquad (4.6)$$

The above system describes the sampled-data dynamics of the thermal system.

4.3 'Exact Optimal' Design

Given the time-varying nature of the plant described above, and given that the statistics of the noise sources can be characterized, a natural choice for an observer seems to be the discrete Kalman filter. This approach takes advantage of the fact that we can assign probability distributions to the various sources of noise. This property is used to design a filter that provides an estimate of the state of the system in such a way as to minimize the variance of the estimation error; see Appendix A for details. This filter has several desirable properties. First, and foremost, it can be shown [8] that if the measurement and plant noise sources are normally distributed, this filter provides the *best* possible unbiased state estimator. Secondly, the recursive structure of this filter allows for simple implementation and avoids the problem of storage of multiple past measurements which one encounters in deterministic or maximum-likelihood based approaches. A further important feature of this filter is that it accommodates, in a natural way, situations where the noise sources may not be stationary random processes. This is to say when the noise sources have time-varying statistics. As we will see, this is a situation that we may have to deal with.

To start, let us describe the dynamics of the discrete-time plant with the noise sources included. We can categorize the noise sources in two major classes. Those arising from process disturbance in the physical system, and those arising from im-

perfect measurements. Without loss of generality, we can assume that the statistics of the temperature measurement errors are stationary. Recall that the states of the thermal system were measured directly. T_C^* is measured from a thermocouple attachment, while T_R^* is measured by estimating the winding resistance R and converting to temperature via a linear relation. Then, T_R and T_C are calculated by subtracting the ambient temperature from T_R^* and T_C^*, respectively. Assuming that the estimate of R has stationary statistics (variance), and that the thermocouple performance does not degrade or improve over time, we can adequately model these measurement errors as normally distributed random variables with constant variances. On the other hand, the process noise can not be dismissed as having time-invariant statistics. In the previous chapter we undertook the modeling of the physical system. There, we found, through a least-squares fitting scheme, a model that approximately represented the observed behavior of the physical plant. However, we must bare in mind that certain effects were ignored in the interest of simplicity. For instance, we know that the input varies as K, the magnet constant, is varied. This quantity is, in turn, a function of the state variables. Hence the input is coupled to the state through the presence of K. We conveniently ignored this effect due to the fact that this coupling was extremely weak since the variations in K over large temperature increases were very small. Now, we may absorb this effect into the process noise as a random variable with time-varying statistics. Another effect which was ignored is that of heat flow through the shaft of the motor due to coupling with a hot object. This situation may arise in some realistic settings. We choose to absorb this effect as part of the process disturbance as well.

We can now formulate the stochastic time-varying model of the thermal system as

$$
\begin{aligned}
T_{k+1} &= \Phi_k T_k + \Gamma_k u_k + m_k \\
Y_k &= T_k + n_k
\end{aligned}
$$

where m_k and n_k are normally distributed, uncorrelated random vectors with zero mean and covariances Q_k and S, respectively. Let us denote the estimated state just before the measurement at sampling instant k by $\hat{T}_k^-$ and the updated estimate just after the measurement by $\hat{T}_k^+$. So the structure of the observer is determined by the fact that given a *prior* estimate of the state at time kt_0 denoted by $\hat{T}_k^-$, we seek an updated estimate, $\hat{T}_k^+$, based on the measurement Y_k of the state T_k. This estimate is sought in a linear, recursive form. Let ϵ_k^+ denote the difference between the estimated

state and the observed state. i.e.

$$e_k^+ = \hat{T}_k^+ - T_k \tag{4.7}$$

and let P_k^+ denote the covariance of this estimation error. i.e.

$$P_k^+ = E[e_k^+ e_k^{+'}] \tag{4.8}$$

where $E[\cdot]$ denotes the expected value of its argument. The Kalman filter minimizes the trace of the matrix P_k^+. In Appendix A, we derive the equations that describe this algorithm. Figure 4.1 depicts the time-evolution of the different quantities involved in this algorithm. The algorithm is as follows.

Algorithm I

1. Initialize the error covariance matrix P_0^- and hence the gain H_0. Also Initialize the original estimate $\hat{T}_0^-$.

2. Compute Q_k.

3. Update the estimate of the state
$$\hat{T}_k^+ = \hat{T}_k^- + H_k(Y_k - \hat{T}_k^-)$$

4. Update the error covariance matrix
$$P_k^+ = (I - H_k)P_k^-(I - H_k)' + H_k S H_k'$$

5. Simulate the observer
$$\hat{T}_{k+1}^- = \Phi_k \hat{T}_k^+ + \Gamma_k u_k$$

6. Extrapolate the error covariance matrix
$$P_{k+1}^- = \Phi_k P_k^+ \Phi_k' + Q_k$$

7. Make the measurement
$$Y_{k+1} = T_{k+1} + n_{k+1}$$

8. Compute the new gain
$$H_{k+1} = P_{k+1}^-(P_{k+1}^- + S)^{-1}$$

9. Return to step 2 with updated k.
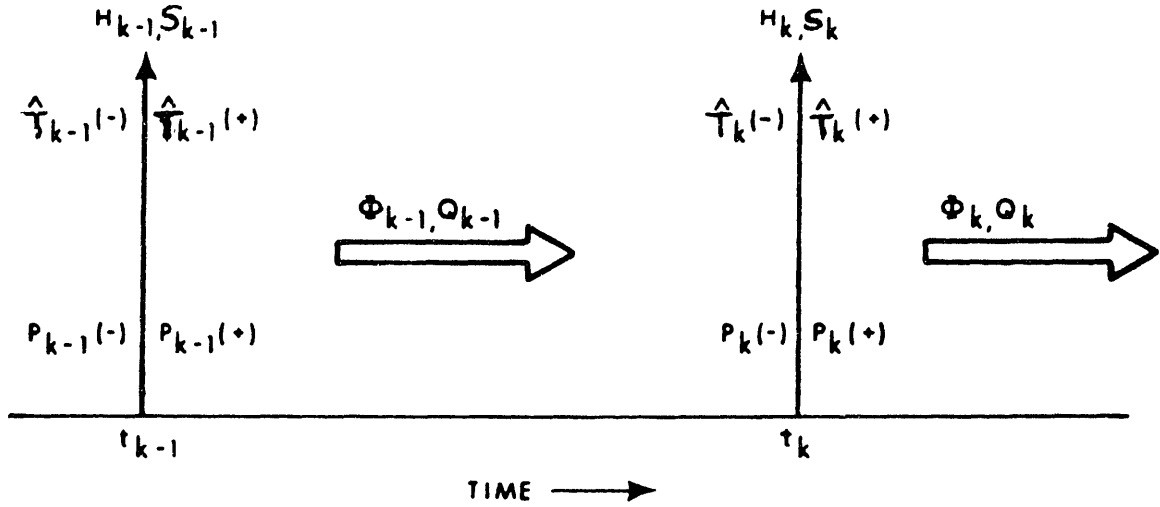
Figure 4.1: Time-evolution of the filter parameters (taken from [8])

4.4 Approximate Suboptimal Design

In this section we propose an observer in which the dynamics of the plant are approximated by a time-varying part and a time-invariant part. Then the observer is constructed using this approximate model and a gain is chosen so as to adaptively cancel out the time-varying part of the dynamics. The major advantage of this approach is that, at the expense of performance, it provides us with an observer structure for a time-varying nonlinear system such that the error dynamics are linear and time-invariant. This turns out to be useful in the design of detection filters. We will also show in Appendix A that based on this approximation, the same technique can be developed to design locally stable linear time-invariant observers for a general class of nonlinear time-varying systems.

Consider the time-varying plant described by 4.4. It is shown in Appendix A that given a sufficiently fast sampling time t_0, we may make the following approximation.

$$\Phi_k \approx e^{At_0} + J_k t_0 = \Phi_0 + J_k t_0 \tag{4.9}$$

An identity observer for the original plant (4.4) yields the error dynamics

$$e_{k+1} = (\Phi_k - H_k)e_k - m_k + H_k n_k \tag{4.10}$$

69

Using the approximation to Φ_k presented above, we may rewrite this equation as

$$e_{k+1} = (\Phi_0 + J_k t_0 - H_k)e_k - m_k + H_k n_k \qquad (4.11)$$

Now, we pick the gain H_k so as to cancel the term $J_k t_0$ from the error dynamics. Let

$$H_k = h_k + J_k t_0 \qquad (4.12)$$

This gives

$$e_{k+1} = (\Phi_0 - h_k)e_k - m_k + (h_k + J_k t_0)n_k \qquad (4.13)$$

We now wish to choose h_k so as to produce an unbiased state estimate with minimum error variance. The following algorithm describes this process in the context of the Kalman filter. The details of this algorithm and its optimality will be discussed in the next section.

Algorithm II

1. Initialize the error covariance matrix P_0^- and hence the gain h_0. Also Initialize the original estimate $\hat{T}_0^-$.

2. Compute Q_k.

3. Compute S_k. (*See below.*)

4. Update the estimate of the state
$$\hat{T}_k^+ = \hat{T}_k^- + H_k(Y_k - \hat{T}_k^-)$$

5. Update the error covariance matrix
$$P_k^+ = (I - h_k)P_k^-(I - h_k)' + h_k S_k h_k'$$

6. Simulate the observer
$$\hat{T}_{k+1}^- = \Phi_k \hat{T}_k^+ + \Gamma_k u_k$$

7. Extrapolate the error covariance matrix
$$P_{k+1}^- = \Phi_k P_k^+ \Phi_k' + Q_k$$

8. Make the measurement
$$Y_{k+1} = T_{k+1} + n_{k+1}^*$$

70

9. Compute the new gain.

$$h_{k+1} = P_{k+1}^{-}(P_{k+1}^{-} + S_k)^{-1} \quad (See \; below.)$$

10. Include the cancellation term

$$H_{k+1} = h_{k+1} + J_{k+1}t_0$$

11. Return to step 2 with updated k.

Note that in this algorithm, $S_k = N_k S N_k'$.

4.5 Optimality

It is important to consider the relative performance of the two proposed observer designs. From a theoretical viewpoint, we can investigate the optimality of each of these observers. The first observer, as we have discussed, offers an estimate of the state of the system described by 4.4 directly, minimizing the variance of observer error. So given normally distributed noise sources m_k and n_k, this observer provides optimal estimates (in the sense of the Kalman filter) of the desired states. However, the question of how well the second observer performs under the same disturbances must be analyzed more carefully.

As we can see, the observation noise in the algorithm of the second observer is different. This arises from the fact that due to the approximation of Φ_k, and the cancellation term, the proposed observer is optimal only in the sense that it produces a minimum-variance, unbiased estimate of the state of an approximation of 4.4. More concretely, we have the following claim.

Claim The second observer produces optimal estimates of the states of the following approximate version of the original plant (4.4) described by

$$T_{k+1} = \Phi_0 T_k + \Gamma_k u_k + m_k \qquad (4.14)$$

$$Y_k = T_k + n_k^* \qquad (4.15)$$

where n_k^* is given by

$$n_k^* = (I + h_k^{-1} J_k t_0) n_k = N_k n_k \qquad (4.16)$$

71

Proof: It can be seen that an identity observer for the above system with the "optimal" gain h_k gives the error dynamics

$$e_{k+1} = (\Phi_0 - h_k)e_k - m_k + h_k n_k^* \qquad (4.17)$$

Substituting the right hand side of the expression for n_k^* in 4.17 gives exactly 4.13; verifying the claim. Note that the noise vector n_k is comprised of two elements that are statistically uncorrelated. i.e. The matrix S is diagonal. In contrast, the elements of the new noise vector n_k^* are statistically correlated since N_k is not necessarily diagonal. However, given the expression for N_k (4.16), we can see that N_k is almost diagonal in the sense that the term $h_k^{-1}J_k t_0$ is a 2×2 matrix of rank 1 with the first column identically zero and the second column comprised of elements that are small relative to 1. Hence, in the interest of simplicity, we may proceed with the assumption that the noise vector n_k^* has statistically uncorrelated elements. One may interpret the system 4.14-15 as an approximation of 4.4-5 in that the time-varying part of the dynamic matrix Φ_k has been ignored, yet compensated for in (or absorbed into) the measurement noise.

In comparison, given Gaussian noise, the first design provides a minimum-variance estimator for the exact plant (4.4) while the second design provides a minimum-variance estimator for an approximate version of the plant. Hence, we would expect that the original time-varying design would perform better than the second design under the same noise conditions. We shall verify this in the next section.

4.6 Numerical Results

In this section we present the results of our simulations of the observers discussed in the previous sections. We will compare their relative performances under the same noise characteristics. We will refer to the first observer as Observer I and the second as Observer II. All of the following simulations were performed using $t_0 = 60$ seconds and the error characteristics shown in Table 4.1, where t_o denotes the time between each cycle of the observer.

The following graphs show the performance of the two observers with the given parameters. The dotted lines on the observer error graphs define the 99 percent confidence interval of the error. This is to say that 99 percent of the observer error due to noise lies within the indicated limits. These values are obtained directly from

Variance of voltage measurement errors	0.00004	volts
Variance of current measurement errors	0.00004	amps
Variance of speed measurement errors	0.00004	rad/sec
Variance of angle measurement errors	0.000004	radians
Variance of the measurement of T_C	0.1	$^\circ C$

Table 4.1: Noise characteristics for the simulations

the Kalman filter equations as $\pm 3\sqrt{p_{ii}}$ where p_{ii} are the diagonal elements of the observer error covariance matrix P.

Observer I In the following simulated experiment, the speed and torque of the motor were kept constant. Simulated values for the temperature rises in the motor were then produced using the given electromechanical operating condition. These operating conditions (currents, voltages, shaft angle) were corrupted by gaussian noise before the temperature rises were deduced from them. The 'measurements' of these temperature rises were then passed on to the Kalman filter which produced estimates of these temperatures. The results were then compared. The initial condition of the observer is $\hat{T}_0^+$ ($^\circ C$) which is given below while P_o denotes the initial guess of the observer error covariance matrix, and P_∞ denotes the final value of the observer error covariance matrix. The elements of P_o and P_∞ have units of $(^\circ C)^2$.

$$P_0 = \begin{bmatrix} 0.5 & 0 \\ 0 & 0.75 \end{bmatrix}$$

$$\hat{T}_0^+ = [1 \quad 2]$$

$$P_\infty = \begin{bmatrix} 0.0479 & 0.0127 \\ 0.0127 & 0.3772 \end{bmatrix}$$

Observer II This simulated experiment was performed in the same way as the one described above. Given the parameters

$$P_0 = \begin{bmatrix} 0.5 & 0 \\ 0 & 0.75 \end{bmatrix}$$

$$\hat{T}_0^+ = [1 \quad 2]$$
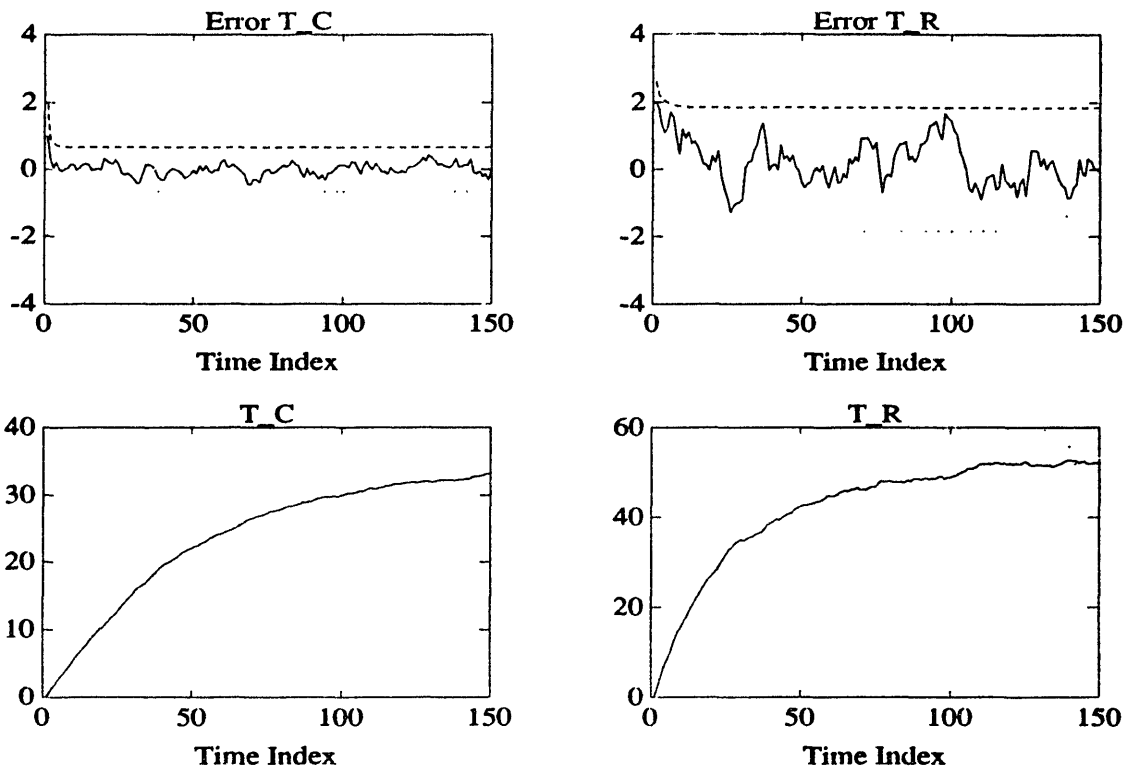
Figure 4.2: (Observer I) States and observer errors

the infinite-horizon error covariance matrix is

$$
P_\infty = \begin{bmatrix} 0.0480 & 0.0141 \\ 0.0141 & 0.3922 \end{bmatrix}
$$

It is worth noting the respective values of P_∞ for the two observers. The first observer, being the exact Kalman filter, converges to the smaller value of P_∞ as expected. This fact holds true for all levels of noise, but the margin of difference between the performance of the two observers widens as the level of noise is increased. However, the second observer displays excellent tracking behavior as well, even though it is sub-optimal with respect to the first observer.
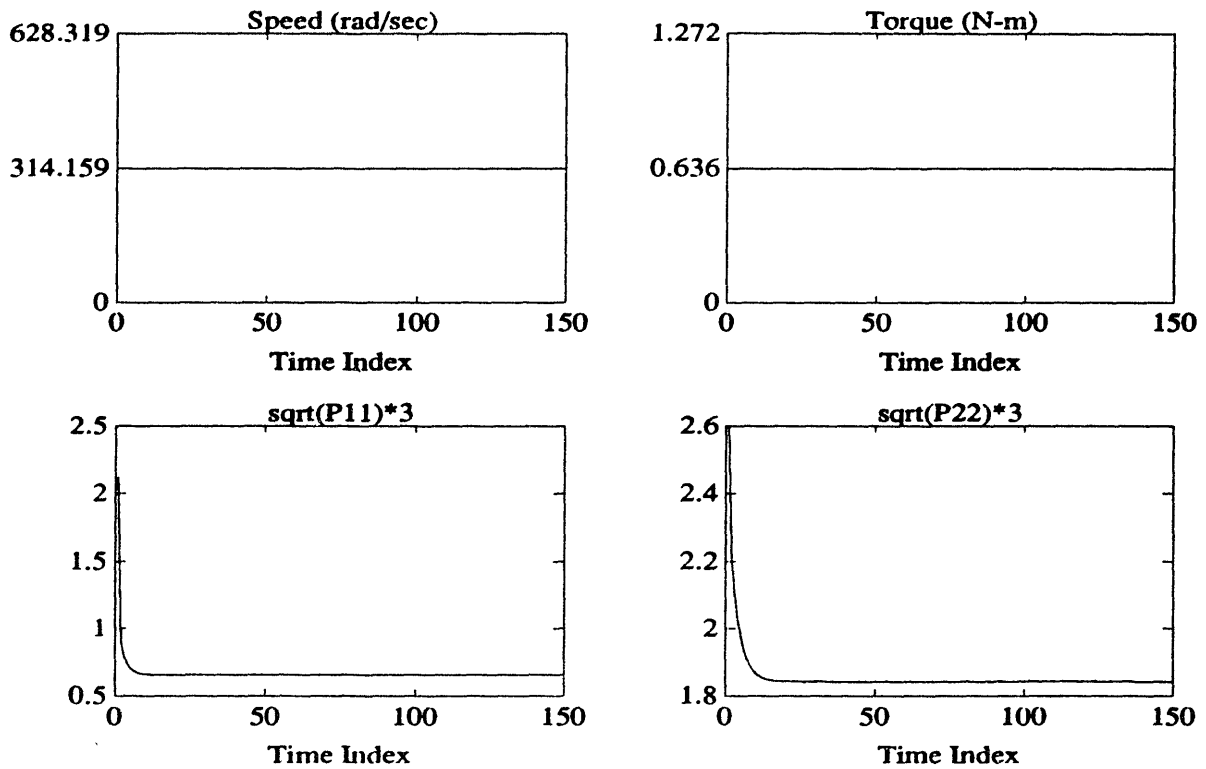
Figure 4.3: (Observer I) Speed, torque and confidence Region
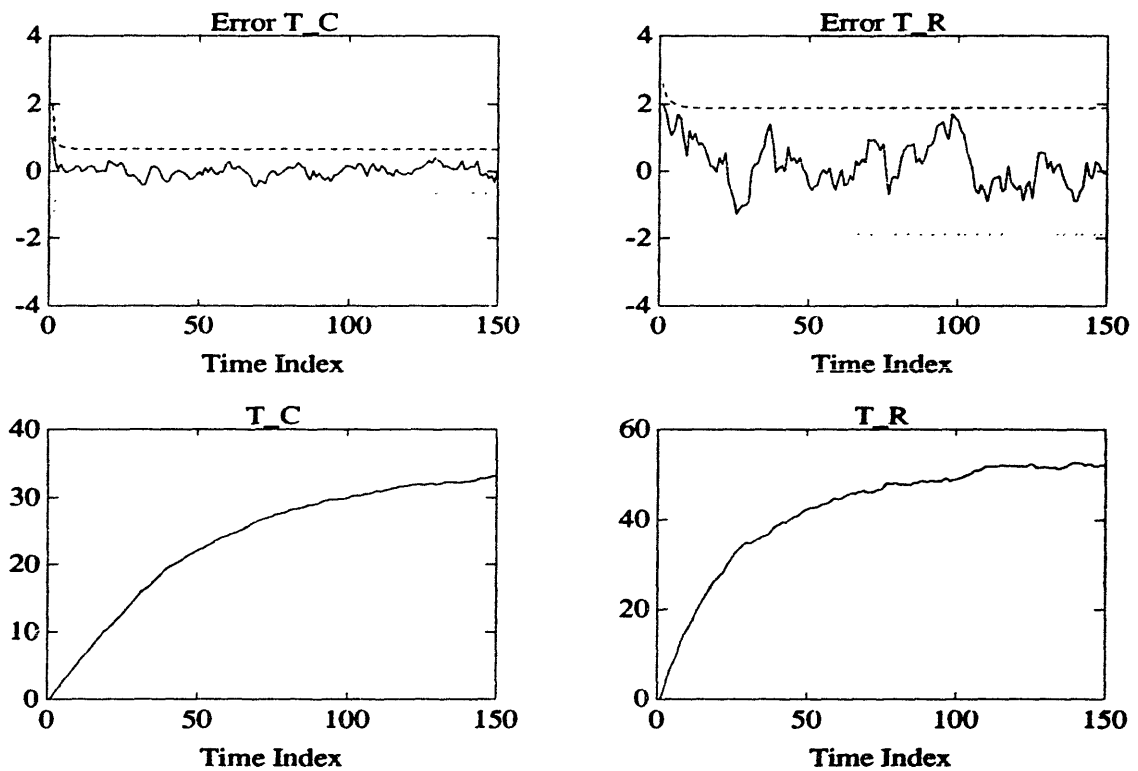
Figure 4.4: (Observer II) States and observer Errors
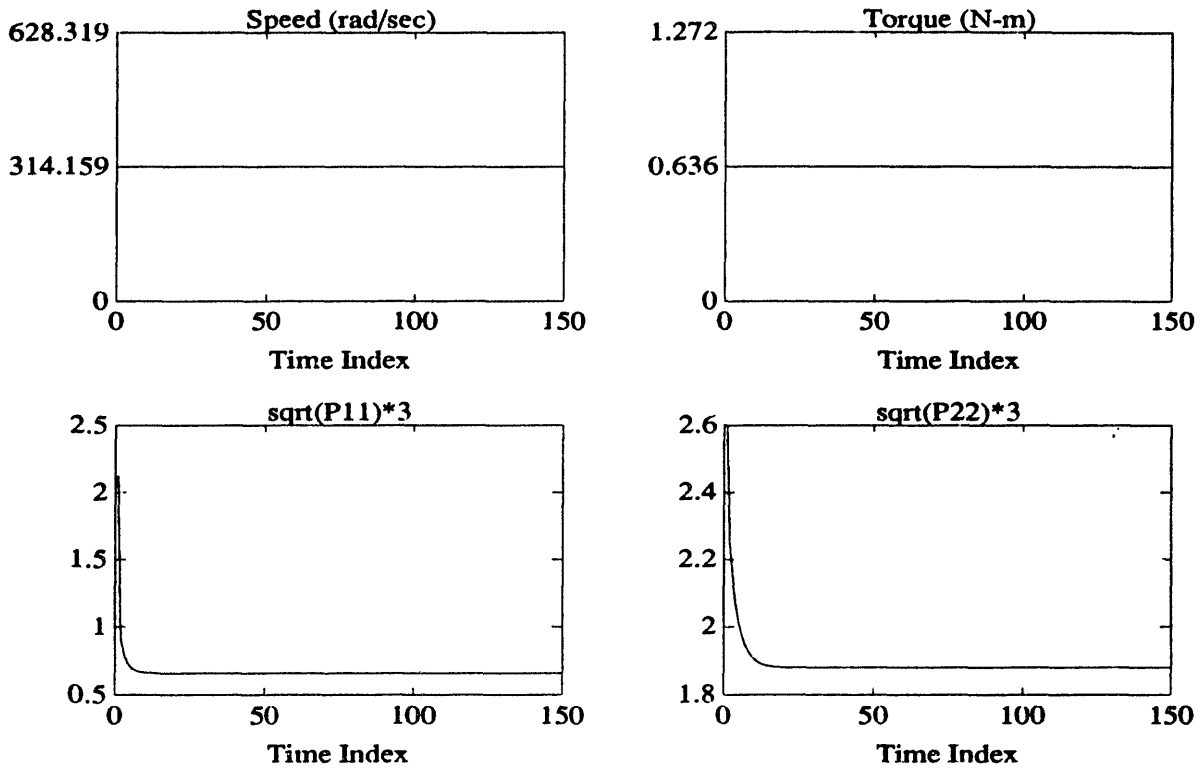
Figure 4.5: (Observer II) Speed, torque and confidence region

In the next set of graphs, Figures 4.6-9, we introduce steps in the commanded speed and torque as shown, and observe the response of the system and the observer. As an illustrative exercise, the variance of the plant noise is taken to be proportional to the magnitude of the input. Hence, the error covariance matrix responds to the step changes in the input, reducing the size of the confidence interval, as expected. This shows that if the statistics of the noises are time-varying, but deterministic, and if this relation can be accurately modeled, the confidence interval may be adaptively adjusted. This is a useful feature as we will see in Chapter 5.

Observer I Given the parameters

$$P_0 = \begin{bmatrix} 0.5 & 0 \\ 0 & 0.75 \end{bmatrix}$$

$$\hat{T}_0^+ = \begin{bmatrix} 1 & 2 \end{bmatrix}$$

the infinite-horizon error covariance matrix is

$$P_\infty = \begin{bmatrix} 0.0479 & 0.0127 \\ 0.0127 & 0.3772 \end{bmatrix}$$

76
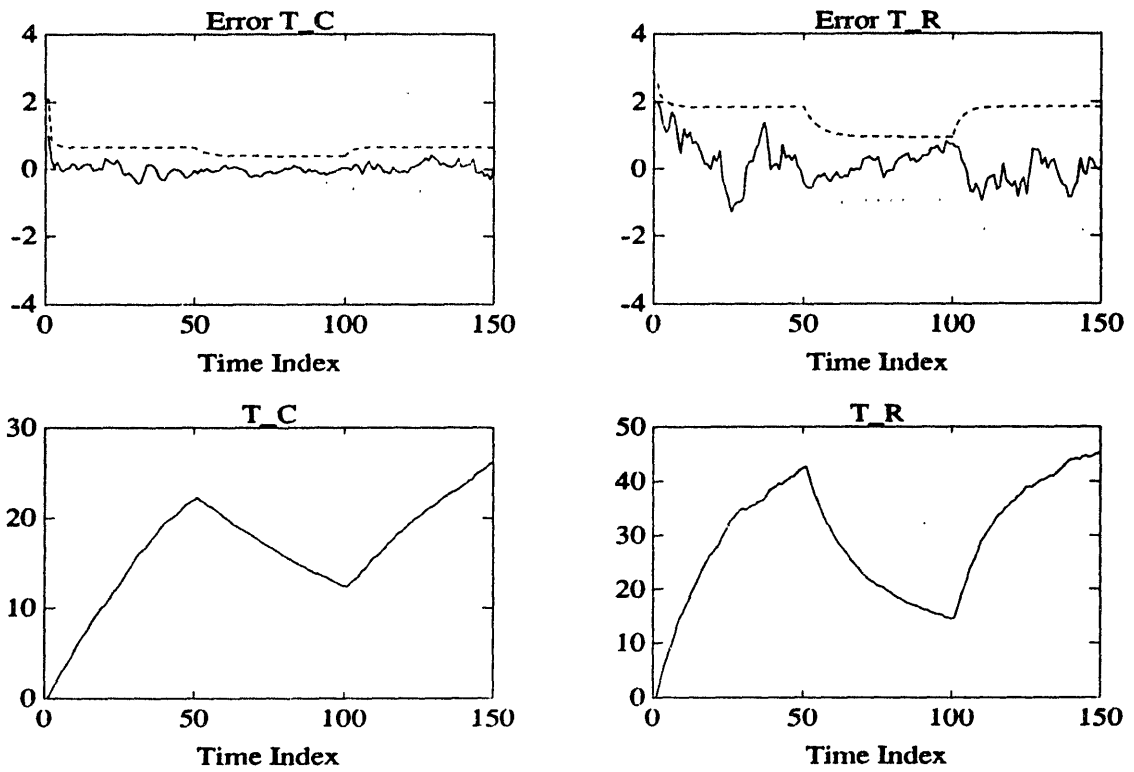
Figure 4.6: (Observer I) States and observer errors

Observer II Given the parameters

$$P_0 = \begin{bmatrix} 0.5 & 0 \\ 0 & 0.75 \end{bmatrix}$$

$$\hat{T}_0^+ = \begin{bmatrix} 1 & 2 \end{bmatrix}$$

the infinite-horizon error covariance matrix is

$$\Gamma_\infty = \begin{bmatrix} 0.0480 & 0.0141 \\ 0.0141 & 0.3922 \end{bmatrix}$$
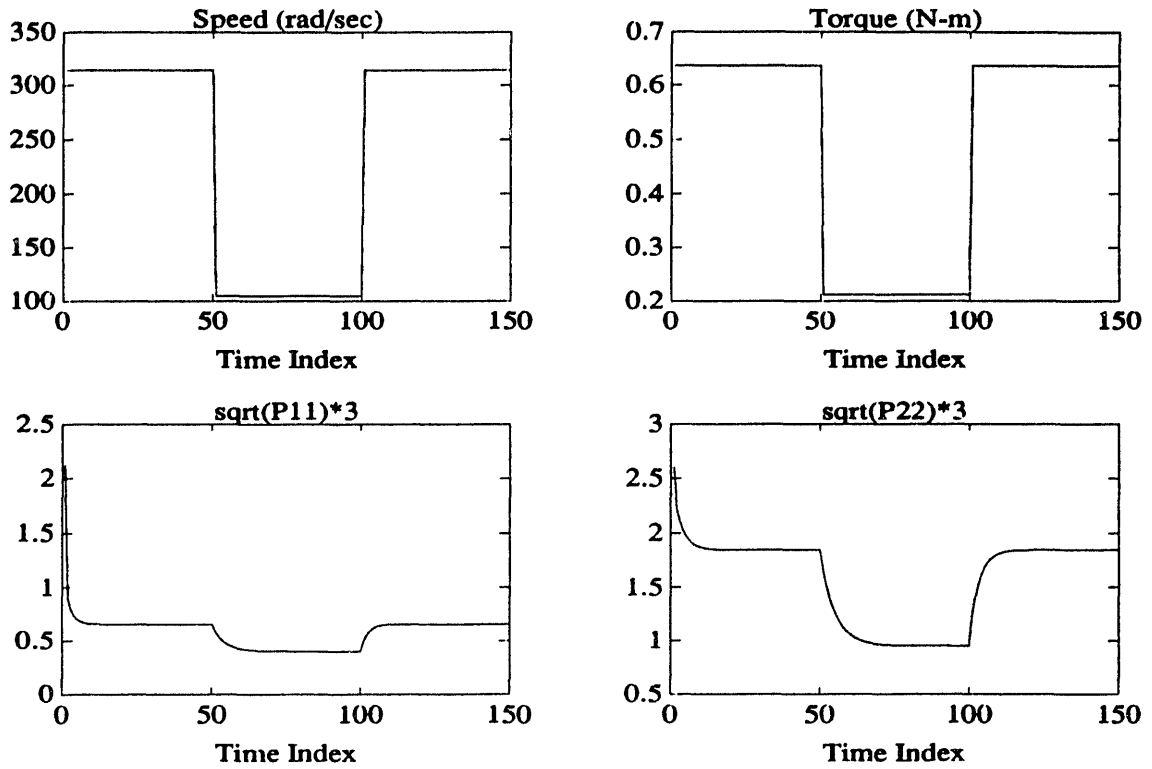
Figure 4.7: (Observer I) Speed, torque and confidence region
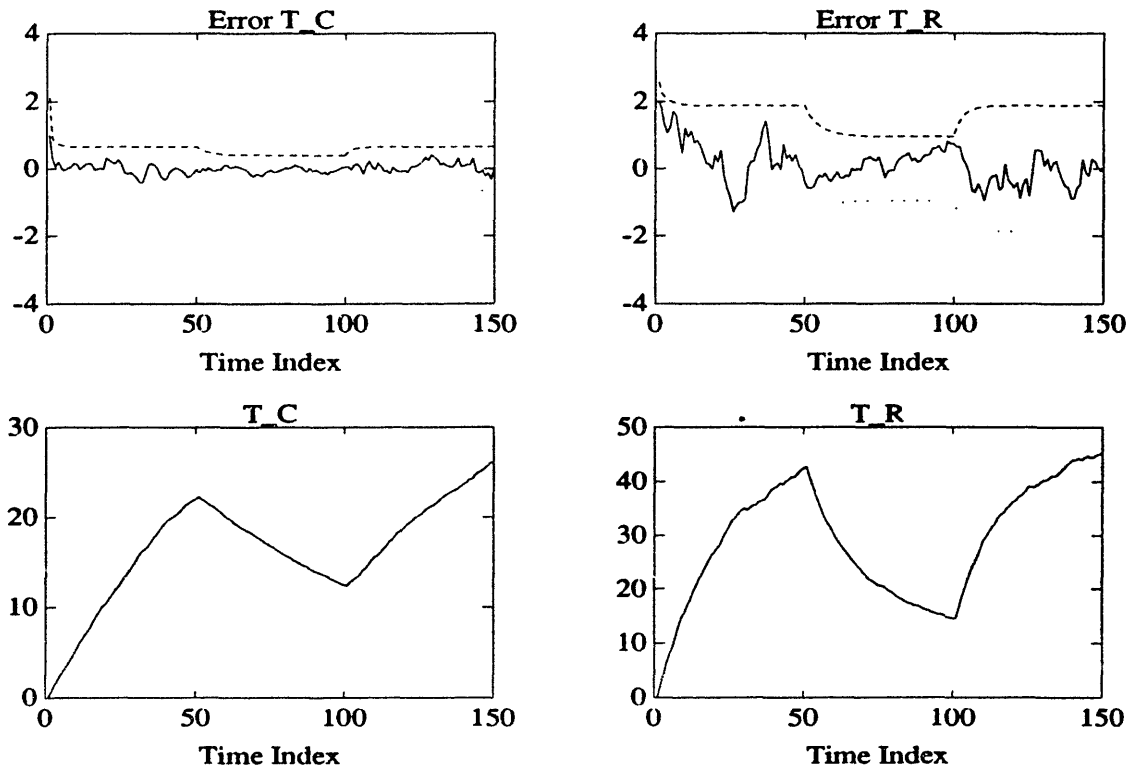
Figure 4.8: (Observer II) States and observer errors
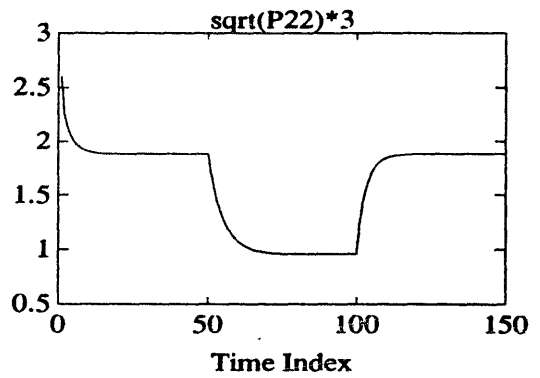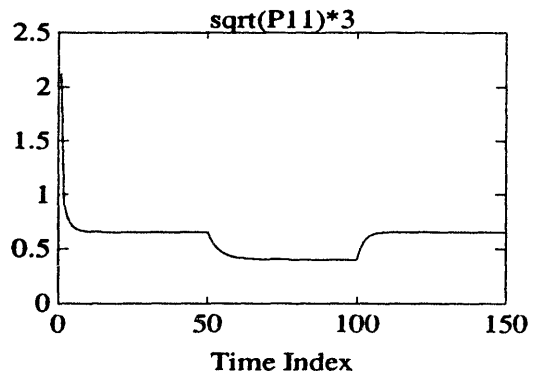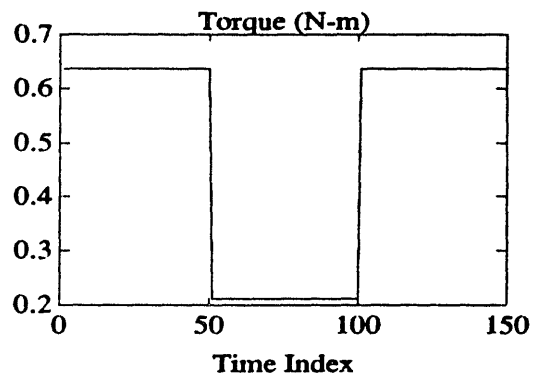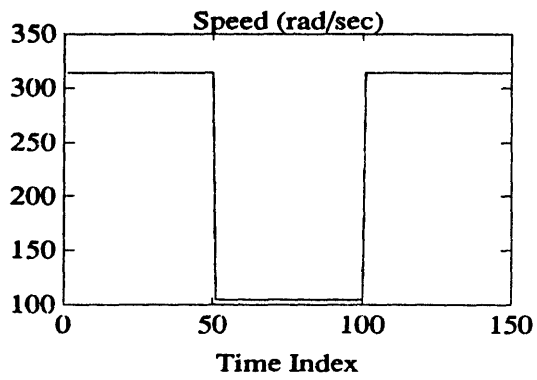
Figure 4.9: (Observer II) Speed, torque and confidence region

Chapter 5

Detection Filter: Theory and Design

5.1 Introduction

Observers provide estimates of the states of a dynamical system based on an input-output model of the system and measurements of the corresponding quantities. In this chapter we use an observer to develop a model-based method of predicting temperature rises inside the motor based on measurements of line currents, speed and shaft angle. This model-based approach uses the measured electromechanical variables to generate the inputs to the thermal model of the motor as developed in Chapter 4. These inputs are then fed into the model and estimates of the temperature rises are produced in this way. These estimates are then compared with the estimated temperatures as obtained in Chapter 2. Discrepency between the values obtained from the two methods forms the basis for failure detection.

The goal of failure detection is to identify any unexpected phenomenon that may occur within the dynamic system or its associated sensor arrays, and if possible, indicate precisely what type of failure has occured. In this section we discuss some basic results of geometric detection theory and apply them the problem of designing a failure detection filter based on the observers designed in the previous chapter. In his thesis, Jones [13] developed a design whereby in the absence of failures, the failure detection system acts as a suboptimal state estimator. A detection system that provides near-optimal estimates of the states in the absence of failures is important from an economic viewpoint in that the designer can provide a single compact product that will estimate the states of the system in near-optimal fashion, and at the same
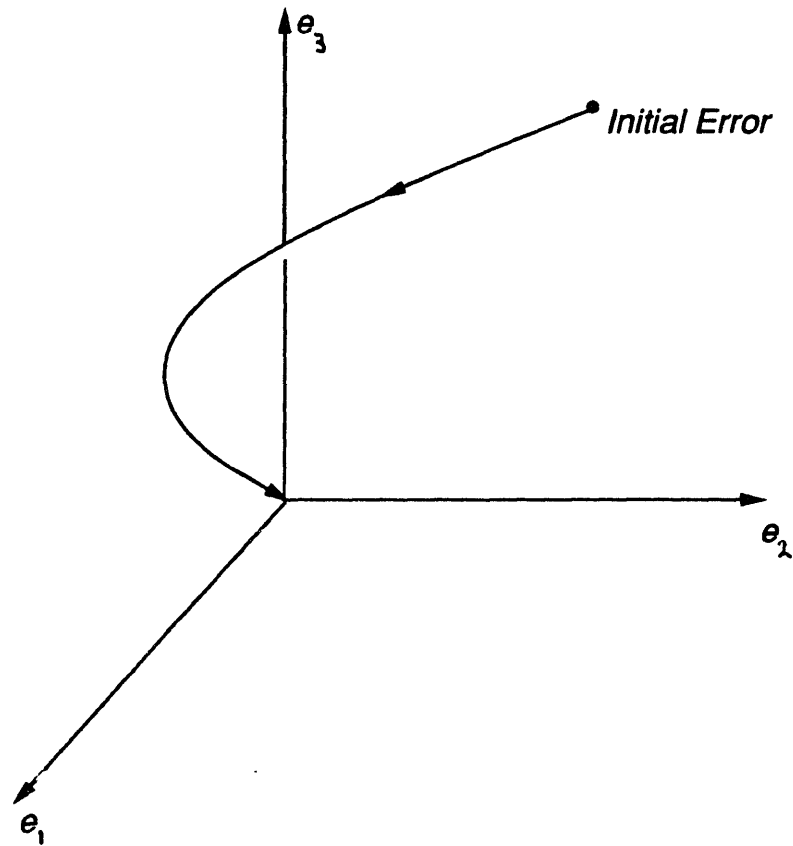
Figure 5.1: Untuned observer: Error decaying to zero.

time, alarm the user of the system against failures within it. As we will see, this approach leads to a very simple detection law, according to which an error signal due to a failure may be distinguished from noise.

In general terms, observer-based failure detection, or geometric failure detection, is based on the notion that it may be possible to *tune* an observer so that its associated error dynamics evolve in a given subspace of the output-space. This subspace is found from a model of the particular failure of interest. If one can establish that a given failure in the dynamic system will result in the evolution of observer errors only within a subspace of the output-space (the detection space of the failure), then one can hope to detect the failure by monitoring the observer error in this subspace. Figures 5.1-3 illustrate this idea.

It is possible that two distinct failures may correspond to two subspaces that are not disjoint. Hence, if there is an error vector growing away from the origin in the intersection of these two subspaces, one can declare that at least one, or perhaps
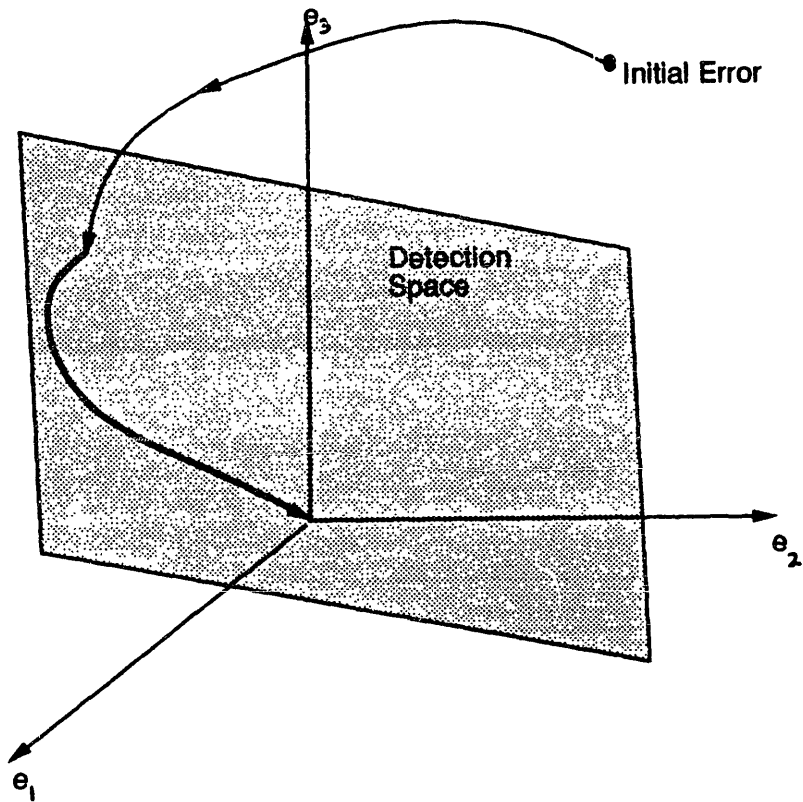
Figure 5.2: Tuned observer: Error converging to detection space, then decaying to zero.
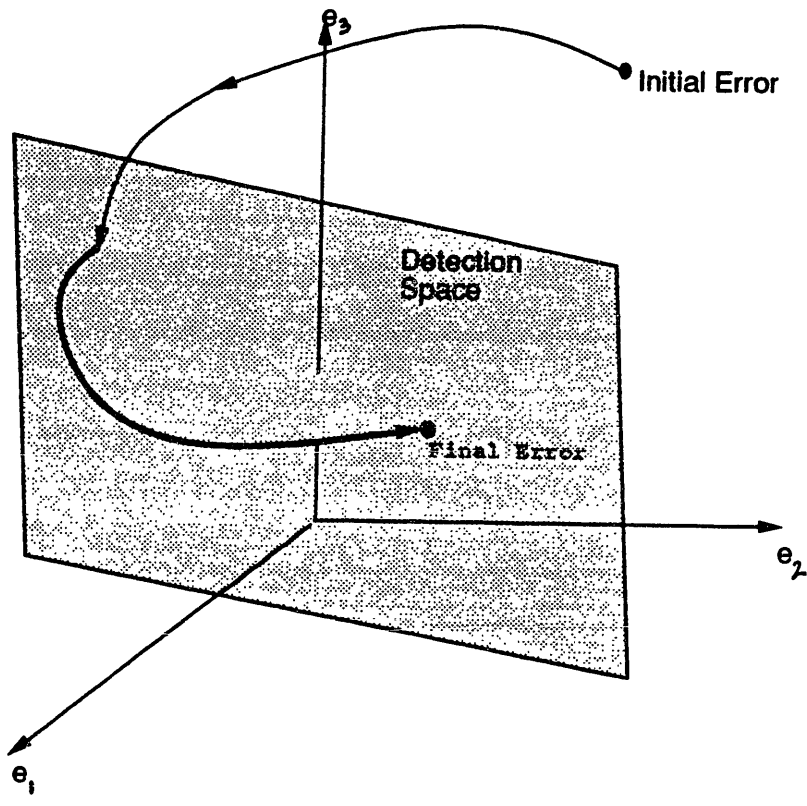
Figure 5.3: Tuned Observer error with failure : Error converging to detection space but not decaying to zero.
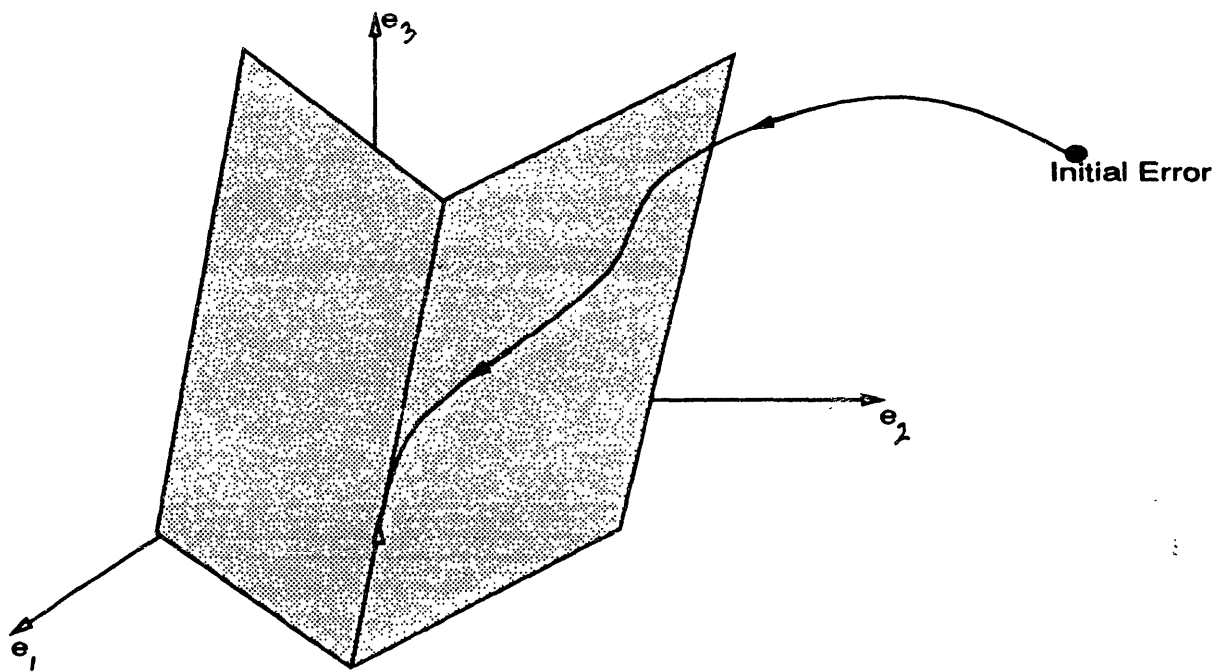
Figure 5.4: Intersecting detection spaces with failure: Error converging to intersection, then moving away from zero.

both of the failures in question have occured. Yet, one can not decide, on the basis of such error direction alone, which of the two failures has occured; see Figure 5.4. However, if the dimension of the subspace corresponding to a particular failure is one, i.e. its detection space is spanned by a single vector, then the difficulty depicted in Figure 5.4 does not exist. This is to say that if we restrict our work to the detection of failures with one-dimensional detection spaces, we can detect any one of such failures unambiguously by using appropriate detection filters. As we will show, under certain circumstances, it may even be possible to detect several distinct failures simultaneously.

In this thesis, we restrict our attention to simple failures whose detection spaces are one dimensional, and base our work on that of Jones [13] in which the detection problem for linear time-invariant systems is solved. In [13] an explicit solution to the problem is derived in the sense that exact expressions are given for the gain of an identity observer for a linear time-invariant(LTI) system. This observer is, by construction, capable of detecting a particular set of failures. Furthermore, the detection problem is solved for stochastic LTI systems as well, and a detailed algorithm is provided for finding an observer gain that is suboptimal and that also has the desired failure detection properties. In our work, we seek to apply these techniques to the particular problem of failure detection in permanent-magnet synchronous motors. A specific algorithm is provided for the motor detection problem given discrete samples of certain outputs of the motor. We establish a Kalman filter as the underlying stable observer, as discussed in the previous chapter. In each iteration of the observer we adjust the eigenvectors of the error dynamics to the desired directions. This method is slightly different than the method presented in [13]. The difference being that in [13] a static gain is precomputed so as to give an observer that is optimal in the absence of failures only in certain directions. The techniques in [13] are not directly applicable to the motor failure detection problem at hand since here we deal with a sampled-data, nonlinear model for the thermal behavior of the model. Thus, although the concepts in [13] serve as the basic building blocks for our approach, they have been modified to accomodate the situation at hand. Some general results regarding the applicability of these techniques to time-varying systems are presented in appendix A.
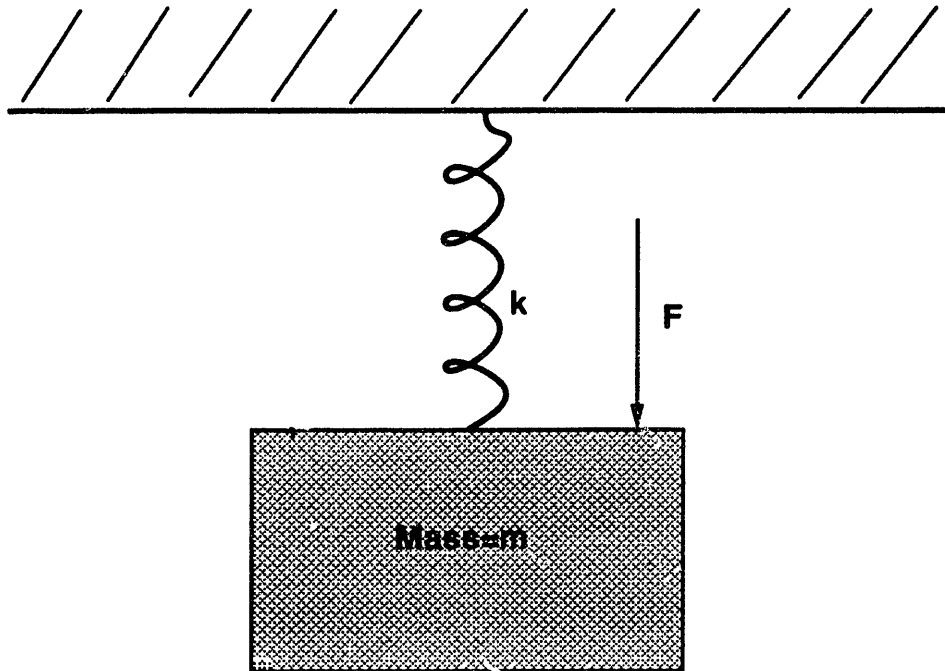
Figure 5.5: Spring-Mass System

5.2 Detection Theory Basics

5.2.1 Motivation

Perhaps the best way to motivate the basic results of geometric detection theory is by presenting an example. Let us analyze the case where we are interested in detecting a failure in the dynamics of an LTI system of the form

$$\dot{x} = Ax + Bu \tag{5.1}$$

$$y = Cx \tag{5.2}$$

where x is the stat$\smile$ vector, u is the input vector, and y is the output vector. Systems where the rank of C is equal to the length of x are referred to in [13] as fully measurable systems.

As an example, consider a lossless spring-mass system with a forcing function as shown in Figure 5.5. This system can be modeled by the second order single-input,

86

two-output LTI system

$$\dot{x}(t) = \begin{bmatrix} 0 & 1 \\ \frac{-k}{m} & 0 \end{bmatrix} x(t) + \begin{bmatrix} 0 \\ \frac{-1}{m} \end{bmatrix} u(t) \tag{5.3}$$

$$y(t) = x(t) \tag{5.4}$$

where k represents the spring constant, m represents the mass of the object, and $u(t)$ is the forcing function F. In the above model, the state x is a 2×1 vector with elements x_1 and x_2 where x_1 is the position (the height of the mass relative to ground reference level), and x_2 the velocity of the mass. With $y = x$, this is clearly a fully measurable system. Now suppose that we are interested in detecting changes in the spring constant k perhaps for the purpose of failure detection. A change in the spring constant from its nominal value of k can be modelled as a bias $E(t)$ in the dynamic matrix A of our model. More specifically, we have

$$E(t) = \begin{bmatrix} 0 & 0 \\ \epsilon(t) & 0 \end{bmatrix}$$

where ϵ is the bias. So, the failed model can be written as

$$\dot{x} = (A + E(t))x + Bu \tag{5.5}$$

$$y = Cx \tag{5.6}$$

with A, B, and C as given in the spring-mass system. The above failed model can be rewritten as

$$\dot{x} = Ax + Bu + E(t)x = Ax + Bu + f_1 \eta_1(t) \tag{5.7}$$

$$y = Cx \tag{5.8}$$

where we have

$$f_1 = [0 \quad 1]'$$

$$\eta_1(t) = \epsilon(t)x_1(t)$$

The vector f_1 is called the event vector of the failure in question and $\eta_1(t)$ is a scalar function of time.

Now, let us design an identity observer for the unfailed system as follows

$$\dot{\hat{x}} = A\hat{x} + Bu + D(y - \hat{y}) \tag{5.9}$$

$$\hat{y} = C\hat{x} \tag{5.10}$$

Defining the observer error to be $e = \hat{x} - x$, we obtain the following error dynamics

$$\dot{e} = (A - DC)e \tag{5.11}$$

If the failure in question occurs, the error dynamics then become

$$\dot{e} = (A - DC)e + f_1 \eta_1 \tag{5.12}$$

Let $D = [d_{ij}]$ and suppose that we would like the eigenvalues of the observer to be at λ_1 and λ_2 respectively. Naturally, we would like to have eigenvalues with negative real parts to ensure exponential stability. For the purpose of detecting the failure represented by f_1, we also need to pick D so that the matrix $A - DC$ has f_1 as an eigenvector. In this way, the effects of the failure represented by $f_1 \eta_1(t)$ is seen only in the direction of f_1 in the output space. We can now pick the second eigenvector of $A - DC$ to be orthogonal to f_1. So we would like to find the gain matrix D such that

$$A - DC = W \Sigma W^{-1} \tag{5.13}$$

where W is the matrix whose columns are the desired eigenvectors of $A - DC$ and Σ is the diagonal matrix of the desired eigenvalues. Note that the second eigenvector of $A - DC$ is arbitrarily taken but so as to make W invertible. It is convenient to pick this eigenvector so as to make W an orthogonal transformation.

The solution to 5.13 is easily obtained as

$$D = (A - W \Sigma W^{-1})C^{-1} = \begin{bmatrix} -\lambda_1 & 1 \\ \frac{-k}{m} & -\lambda_2 \end{bmatrix} \tag{5.14}$$

Note that if C is not square and invertible, then 5.13 may not have a solution for the desired W and Σ. It it this seemingly small detail that makes algebraic failure detection a challenging problem. In our work, however, we will focus our discussion on fully measurable systems. Given D, the observer error, including the failure, can

88

be written as

$$\epsilon(t) = v_1 e^{\lambda_1 t} + v_2 e^{\lambda_2 t} + f_1 \eta_1(t) \tag{5.15}$$

where the v_i denote the eigenvectors of $A - DC$. We have chosen the eigenvectors such that $v_1 = f_1 = [0 \quad 1]'$ and $v_2 = [1 \quad 0]'$. So we have

$$\epsilon(t) = f_1(e^{\lambda_1 t} + \eta_1(t)) + v_2 e^{\lambda_2 t} \tag{5.16}$$

In the output space we have

$$\bar{\epsilon} = C\epsilon(t) = Cf_1(e^{\lambda_1 t} + \eta_1(t)) + Cv_2 e^{\lambda_2 t} \tag{5.17}$$

In the absence of the failure we have that $\eta_1(t) = 0$ and hence we get

$$\lim_{t \to \infty} \bar{\epsilon}(t) = [0 \quad 0]'$$

However, if the failure occurs, then the observer error does not collapse to the origin, rather it evolves in the direction of f_1 with a magnitude given by $\eta_1(t)$.

It is clear that the output produced by $f_1\eta_1(t)$ maintains a fixed direction in the output space. So, if in the steady state operation of the observer we detect the error growing in the direction of Cf_1, we can declare that the strength of the spring has changed from its nominal value. Even if the failure occurs before the error reaches the steady state, the error is clearly accentuated in the direction of Cf_1 so that the error is not decaying asymptotically to zero in this direction. However, the failure detection techniques described here assume that a given failure occurs after the observer error has reached steady-state. By monitoring each component of the output error $\bar{\epsilon}(t)$, in the steady-state, against a threshold (to be quantified later), the failure in question can be detected. A failure is declared when the output error vector crosses the threshold in the direction of f_1.

5.2.2 Definitions

In this section we define the basic concepts of geometric detection theory. First, we need to quantify what is meant by a failure. Let us denote (possibly time-varying) biases in the matrices A, B, C, or u, as failures in the dynamic system described by 5.1-2. Following Jones [13], we will call a bias in A a dynamics failure, a bias in B, a controller failure, a bias in u a control-element failure, and a bias in C, a sensor

failure. In specific, a control-element failure is one in which the commanded input is not the actual input that is received by the system. In other words, it is an actuator failure. It can be shown [13] that all of theses failures can be categorized into two classes. The first class is the controller failure model given by

$$\dot{x}(t) = Ax(t) + Bu(t) + f_1\eta_1(t) \tag{5.18}$$

$$y(t) = Cx(t) \tag{5.19}$$

and the second class is the sensor failure model, given by

$$\dot{x}(t) = Ax(t) + Bu(t) \tag{5.20}$$

$$y(t) = Cx(t) + v_i m_i(t) \tag{5.21}$$

where v_i is the ith vector in the standard orthonormal basis for the state-space. The manner in which the observer estimates approaches the model can be given for the unfailed system as

$$\dot{e} = (A - DC)e \tag{5.22}$$

$$\bar{e} = Ce \tag{5.23}$$

In the context of detection theory, it is important to define the error $\bar{e}$ since this quantity represents the errors that are physically measurable quantities. Note that for fully measurable systems, the output space coincides with the state-space, and therefore, e and $\bar{e}$ evolve in the same space.

Now with the failure occurring at t^*, the error equations corresponding to 5.18-19 and 5.20-21 respectively are

$$\dot{e} = (A - DC)e + f_1 n_1 \quad t^* \leq t \tag{5.24}$$

$$\bar{e} = Ce \tag{5.25}$$

and

$$\dot{e} = (A - DC)e - d_i m_i(t) \quad t^* \leq t \tag{5.26}$$

$$\bar{e} = Ce + v_i m_i(t) \tag{5.27}$$

where d_i represents the ith column of the observer gain matrix D. So the ith column of

D is the event vector associated with any failure of the ith sensor. Roughly speaking, subject to some conditions to be discussed later, constraining the error $\bar{e}$ to lie in the output direction Cf_1 allows the error to be uniquely associated with the event vector f_1 and hence with the failure modelled by $f_1\eta_1(t)$.

Definition 2 *Detectability: Given the error equations 5.24-25, the failure associated with the event vector f_1 is* detectable *if and only if*

- *the output generated by $f_1\eta_1(t)$ maintains a fixed direction in the output space, and*

- *arbitrary, self-conjugate eigenvalues can be specified for $A - DC$ through appropriate choice of D.*

For example, in the spring-mass example presented above, the event vector f_1 is detectable since both requirements of the above definition are satisfied. Furthemore, f_1 is detectable even if only measurements of the position of the mass are available. i.e. if $C = [1 \ 0]$. In this case, the gain D is a 2×1 column vector $D = [d_i]$. So we have

$$A - DC' = \begin{bmatrix} -d_1 & 1 \\ \frac{-k}{m} - d_2 & 0 \end{bmatrix}$$

It is easy to check that given this observation matrix C, the pair (A,C) is observable. Hence, by the eigenvalue placement theorem [23], arbitrary self-conjugate eigenvalues can be assigned to $A - DC$ through the appropriate choice of D. Also, the output space is one-dimensional, so the first condition in the definition of detectability is trivially satisfied. Hence, f_1 is again detectable.

Definition 3 *Detection Equivalence: Let f_1 and f_2 be the event vectors associated with two failures in an LTI system given by 5.1-2. The event vector f_2 is said to be detection equivalent to f_1 if*

1. *Every Detection filter for f_1 is a detection filter for f_2, and*

2. *The output error generated by f_1 is in the same direction as the output error generated by f_2.*

So clearly, if two event vectors are detection equivalent, then a failure detection system can not discriminate between them on the basis of the output error direction alone.

91

Definition 4 *Detection Space: The detection space of an event vector f_1 is the set of all vectors that are detection equivalent to f_1.*

It is worth noting that in the case of fully measurable systems, the detection space of an event vector f_1 is the set of all vectors αf_1 where α is any nonzero real number.

Definition 5 *Mutual Detectability: The failures associated with the event vectors f_i, $i = 1,...,r$, are mutually detectable if they are all detectable via the same detection filter.*

5.2.3 Results

In this section we present some basic results derived in [13] regarding failure detection in linear time-invariant systems. The main result regarding detectability relates this concept to the observability of the dynamic system under scrutiny, and is as follows.

Theorem 2 *Detection Theorem: The failure associated with the event vector f_1 is detectable if and only if the LTI system 5.1-2 is observable.*

This result follows from the fact that the pair (A, C) is observable if and only if the pair $(A - DC', C')$ is observable. Roughly speaking, the observability of (A, C) will allow us to arbitrarily assign self-conjugate eigenvalues to $A - DC$, and the observability of $(A - DC', C')$ allows for the output due to the failure to remain unidirectional. As an example, we can see that in the spring-mass problem, the pair (A, C) is observable.

The following is a corollary of a general result (for arbitrary C) proved in [13].

Theorem 3 *Mutual Detectability: If the elements of a set of event vectors $\{f_i\}$ are linearly independent, then they are mutually detectable for any fully measurable LTI system.*

Consider that a second failure is to be detected in the spring-mass system. For instance the appearance of increased damping; whose event vector is also $[0\ 1]'$. Then these two failures are not mutually detectable since their corresponding event vectors are not linearly independant. For a given n-dimensional fully-measurable system, it is then easy to see that if we are given a set of r, $r \leq n$, mutually detectable event vectors and a set of desirable, self-conjugate (or more conveniently, negative and real) eigenvalues for the error dynamics of the observer, then the detection problem is that of finding a gain D such that the identity

$$A - DC' = W\Sigma W^{-1} \tag{5.28}$$

92

is satisfied. In other words, we seek a gain D such that $A - DC$ is diagonalizable by W, with the prespecified eigenvalues in Σ. Here, the first r columns of W are the event vectors f_1 through f_r and the remaining $n - r$ columns are chosen freely, but to make W invertible. The matrix Σ is a diagonal matrix of desired eigenvalues λ_i, $i = 1$ to n which are freely assigned. If the rows of $A - W\Sigma W^{-1}$ are in the row space of C, and C has full row rank, the solution is given by

$$D = (A - W\Sigma W^{-1})C'(CC')^{-1} \tag{5.29}$$

which reduces to

$$D = (A - W\Sigma W^{-1})C'^{-1} \tag{5.30}$$

for square C. This solution appears deceivingly simple due to the fact that C has full row rank, or in the square case, is invertible. The solution to the general problem is much more involved and in the interest of keeping focus on our motor failure detection problem, we choose not to elaborate further upon it. The interested reader may find thorough treatments of this material at several levels of depth in [13], [39], and [24].

5.3 Failure Detection in Sampled-Data Systems

In this section we show that the results presented in the previous section are directly applicable to the case of sampled-data systems if certain provisions are satisfied. However, the analytic results of the previous section are only approximate for sampled-data systems. Hence, one must make certain simplifying assumptions in order to put the detection problem for sampled-data systems in tractable form. An important issue which arises in passing from continuous to discrete models is that of the corresponding mapping of the event vectors. It is usually advantageous to model failures in the continuous-time domain since one has a better intuitive handle on which failures cause what types of perturbations in the system parameters. So it is important to investigate how a given event vector maps from the continuous-time model to the corresponding sampled-data model.

93

5.3.1 Mapping Failures from the Continuous to the Sampled-Data Model

Dynamics Failures Consider the LTI dynamic system given by 5.1-2. A failure in the dynamic matrix A can be represented as follows

$$\dot{x} = (A + E^{(A)}(t))x + Bu \tag{5.31}$$

$$y = Cx \tag{5.32}$$

As we have mentioned, we shall concentrate our efforts on "simple" failures, i.e. ones with a single event vector associated to them. These failures have 1-dimensional detection spaces since the range of E is spanned by the single vector f. For convenience, let us drop the superscript (A). So we can write

$$E(t)x(t) = f\eta(t) \tag{5.33}$$

where f is the fixed event vector and n is a scalar function of time. Now assume that both the input $u(t)$ and the bias matrix $E(t)$ are piecewise constant. i.e.

$$u(t) = u_k, \quad t_0(k-1) \le t < t_0 k \tag{5.34}$$

$$E(t) = E_k, \quad t_0(k-1) \le t < t_0 k \tag{5.35}$$

where t_0 is the sampling period. Then, the sampled-data representation of the failed system maybe written as

$$x_{k+1} = e^{(A+E_k)t_0}x_k + \int_0^{t_0} e^{(A+E_k)s} ds B u_k \tag{5.36}$$

$$y_k = Cx_k \tag{5.37}$$

If the size of the perturbation E_k is sufficiently small, and the sampling rate is sufficiently fast, we may use the result proved in the Appendix A to approximate the quantity $e^{(A+E_k)t_0}$. Given this approximation, the above sampled-data system becomes

$$x_{k+1} = (e^{At_0} + E_k t_0)x_k + \int_0^{t_0} (e^{As} + E_k s) ds B u_k \tag{5.38}$$

$$y_k = Cx_k \tag{5.39}$$

If the sampled-data version of the unfailed system 5.1-2 is

$$x_{k+1} = \Phi x_k + \Gamma u_k \qquad (5.40)$$

$$y_k = C x_k \qquad (5.41)$$

then the failed sampled-data system can be approximately written as

$$x_{k+1} = \Phi x_k + \Gamma u_k + t_0 E_k x_k + \frac{1}{2} t_0^2 E_k B u_k \qquad (5.42)$$

$$y_k = C x_k \qquad (5.43)$$

Given that E_k has a 1-dimensional range space spanned by f, the above failed system can be written as

$$x_{k+1} = \Phi x_k + \Gamma u_k + f(t_0 n_k + m_k) = \Phi x_k + \Gamma u_k + f q_k \qquad (5.44)$$

$$y_k = C x_k \qquad (5.45)$$

where

$$f m_k = \frac{1}{2} t_0^2 E_k B u_k \qquad (5.46)$$

Hence, the dynamics failure represented by $f \eta(t)$ in the continuous-time is mapped, approximately, to a failure that is represented by $f q_k$ in the sampled-data system, leaving the event *vector* unchanged.

Controller Failures   As we have discussed previously, a controller failure is represented as a bias in the input matrix B in the LTI system described by 5.1-2. Hence, a controller failure is given as

$$\dot{x} = A x + (B + E^{(B)}(t)) u(t) \qquad (5.47)$$

$$y = C x \qquad (5.48)$$

Again, we make the assumptions that both the input and the bias matrix are piecewise-constant between every consecutive pair of sample points. We also make the assumption that the controller failure is simple so that $E^{(B)}(t)$ has rank 1 for all time. Now suppose that the ith controller channel has failed, then the only nonzero column of $E^{(B)}(t)$ is the ith column. Hence one can write

$$E^{(B)}(t) u(t) = \delta b_i(t) u_i(t) \qquad (5.49)$$

95

where $\delta b_i(t)$ is the ith column of $E^{(B)}$, and $u_i(t)$ is the ith element of $u(t)$. To simplify matters, let us assume that the event vector $\delta b_i(t)$ is used to indicate a change in the effectiveness of the control element. In this case

$$\delta b_i(t) = k(t)\delta b_i \tag{5.50}$$

where δb_i is now a fixed event vector, and $k(t)$ is a scalar function of time. For example, $k(t) = -1$ indicates a control channel that is completely disfunctional. Given this, we can write the failed system as

$$\dot{x} = Ax + Bu(t) + h(t)g \tag{5.51}$$

$$y = Cx \tag{5.52}$$

where $h(t) = k(t)u_i(t)$, and $g = \delta b_i$. The sampled-data model of the failed system becomes

$$x_{k+1} = \Phi x_k + \int_0^{t_0} e^{As}ds(B + E_k^{(B)})u_k = \Phi x_k + \Gamma u_k + G(t_0)gh_k \tag{5.53}$$

$$y_k = Cx_k \tag{5.54}$$

where

$$G(t_0) = \int_0^{t_0} e^{As}ds \tag{5.55}$$

and h_k is well defined since both the input and the failure bias matrix $E^{(B)}$ are piecewise-constant. Hence, the controller failure represented by $h(t)g$ in the continuous-time has been mapped to the failure represented by $h_k G(t_0)g$ in the sampled-data failed system.

Control Element Failures   A failure of the ith control element of the continuous-time model can be described as

$$\dot{x} = Ax + B(u(t) + \delta u(t)) = Ax + Bu + b_i\delta u_i(t) \tag{5.56}$$

$$y = Cx \tag{5.57}$$

where b_i is the ith column of B, and δu_i is the ith element of δu. Given the same assumptions as above regarding the input and the simplicity of the failure, we can

96

write the sampled-data failed system

$$x_{k+1} \;\; = \;\; \Phi x_k + \int_0^{t_0} \epsilon^{As} ds B(u_k + \delta u_k) = \Phi x_k + \Gamma u(k) + \Gamma \delta u_i(k) \qquad (5.58)$$

$$y_k \;\; = \;\; C x_k \qquad (5.59)$$

Equivalently, the above system can be rewritten as

$$x_{k+1} \;\; = \;\; \Phi x_k + \Gamma u_k + \gamma_i \delta u_i(k) \qquad (5.60)$$

$$y_k \;\; = \;\; C x_k \qquad (5.61)$$

where γ_i denotes the ith column of Γ. So the control element failure represented by $b_i \delta u_i(t)$ in continuous-time is mapped to the failure represented by $\gamma_i \delta u_i(k)$.

Sensor Failures If the ith sensor fails, the continuous-time failed model can be given as

$$\dot{x} \;\; = \;\; Ax + Bu \qquad (5.62)$$

$$y \;\; = \;\; (C + E^{(C)}(t))x = C x + v_i l(t) \qquad (5.63)$$

where $l(t)$ is the scalar function $l(t) = \delta c_i(t) x_i(t)$, $\delta c_i(t)$ is the only nonzero element of $E^{(C)}$, and v_i is the ith vector in the standard orthonormal basis for the n-dimensional euclidean space. Respectively, the sampled-data failed model is give as

$$x_{k+1} \;\; = \;\; \Phi x_k + \Gamma u_k \qquad (5.64)$$

$$y_k \;\; = \;\; (C + E_k^{(C)}) x_k = C x_k + v_i l_k \qquad (5.65)$$

Where l_k is the (well-defined) piecewise-constant representation of $l(t)$. Hence, the sensor failure represented by $v_i l(t)$ is mapped to the sensor failure represented by $v_i l_k$ in the sampled-data system, leaving the event vector unchanged. The important assumption that makes the detection problem for sampled-data systems directly solvable using the same technique as in the continuous-time case, is the assumption of piecewise continuity of the input and the failure modes. This assumption allows the failure to be isolated from the dynamics of the sampled-data sytem and hence treated as a bias. Without this assumption, the discretization process, given by the variation of constants formula would yield a system where a failure would appear nonlinearly in the dynamics. An example is an exponent in the case of a dynamics failure.

5.4 Detection Filter Design for Stochastic Systems

In a realistic setting, one can not hope to find an exact model of any physical system, nor to make exact measurements of the true inputs and outputs of any given physical system. The major difficulty in failure detection arising from the presence of the corresponding uncertainties is that in order to have an effective detector, we must design a scheme that allows us to differentiate between the output error produced by a failure and that produced by measurement and dynamic uncertainties. To this end, we must use all the degrees of freedom provided by the deterministic design to optimize the filter for a dynamic system with stochastic disturbances. It is clear that one must try to minimize the effects of these disturbances in order to effectively detect failures. The principal freedom in the design of the deterministic detection system is the ability to arbitrarily assign eigenvalues to the error dynamics of the underlying observer. This property is exploited in the stochastic design.

5.4.1 The Base Normal Canonical Form

In order to motivate the design approach and also as another theme of theoretical interest, we describe the transformations to the base normal canonical form. In this form, the choice of the gain for the observer, given an LTI plant, is simple. The algorithms to follow, however, have been stated without reference to this canonical form so as to emphesize the fact that these algorithms are obtained by incorporating simple modifications in the underlying observer algorithms. In this discussion, we maintain focus only on fully measurable systems and define the base normal canonical form only for these systems. The transformation to this canonical form has the advantage that it permits the reference model to be decoupled into a set of lower-dimensional subsystems. Consider the fully measurable, n-dimensional, LTI system defined by 5.1-2, and its associated identity observer. Assume that we are given a set of r ($r \leq n$) mutually detectable event vectors f_i and are asked to design a failure detection system to detect the corresponding failures. Define two transformations T and T_m as follows.

$$T = [f_1 \quad f_2....f_r \quad w_{r+1}....w_n] \tag{5.66}$$

$$T_m = [Cf_1 \quad Cf_2....Cf_r \quad Cw_{r+1}....Cw_n] = CT \tag{5.67}$$

$$(5.68)$$

where w_i are chosen to make T invertible. Now define the transformed observer by the following relations.

$$\bar{A} = T^{-1}AT \qquad (5.69)$$

$$\bar{B} = T^{-1}B \qquad (5.70)$$

$$\bar{C} = T_m^{-1}CT \qquad (5.71)$$

$$\bar{D} = T^{-1}DT_m \qquad (5.72)$$

In this domain, the system $(\bar{A}, \bar{B}, \bar{C})$ is input-output equivalent to $(A, B, T_m^{-1}C)$. So in the base normal canonical form, the r given event vectors are the first r basis vectors in the standard orthonormal basis of the new state-space. If we now pick a gain $\bar{D}$ such that

$$\bar{A} - \bar{D}\bar{C} = \Sigma \qquad (5.73)$$

where Σ is a diagonal matrix with the desired eigenvalues as its elements, we would ensure that the matrix $\bar{A} - \bar{D}\bar{C}$ has as eigenvectors the standard orthonormal basis vectors v_i for the state space. As we know, the first r of these vectors are the r event vectors of interest in the base normal canonical form. Hence, the solution for square C is obtained as

$$\bar{D} = (\bar{A} - \Sigma)\bar{C}^{-1}. \qquad (5.74)$$

But now note that according to the definition of $\bar{C}$, we have that in the base normal coordiantes

$$\bar{C} = I \qquad (5.75)$$

Hence, a simple solution to the problem is obtained as

$$\bar{D} = \bar{A} - \Sigma \qquad (5.76)$$

The gain D can now be recovered by inverting the transformations.

It is easy to show that this solution is the same as one obtained without transforming the reference model to base normal form. We can write

$$\bar{A} - \bar{D}\bar{C} = T^{-1}AT - T^{-1}DT_mT_m^{-1}CT = T(A - DC)T^{-1} = \Sigma \qquad (5.77)$$

Transfering the T's to the right hand side of the equation, the problem becomes that

of finding a D such that

$$A - DC = T\Sigma T^{-1}. \tag{5.78}$$

Note that if we set $T = W$, this relation becomes identical to Equation 5.28 where the problem was posed without reference to the base normal form.

5.4.2 Theory and Design

At this point, it should be clear that the detection problem for stochastic systems is directly that of the choice of appropriate eigenvalues for the error decay equations of the underlying observer. The liberty in choosing these eigenvalues is a distinctive feature that makes geometric detection theory an attractive approach to the failure detection problem. We use this flexibility to deal with stochastic settings.

Stochastic sources of noise can be categorized as plant disturbances and measurement errors represented by the random vectors $\mu(t)$ and $\nu(t)$ respectively. These disturbances enter the model as

$$\dot{x} \;\; = \;\; Ax + Bu + \mu(t) \tag{5.79}$$

$$y \;\; = \;\; Cx + \nu(t) \tag{5.80}$$

We assume that the two random vectors μ and ν are uncorrelated, normally distributed variables with covariance matrices $Q(t)$ and $S(t)$ respectively. These disturbances, in turn, appear in the observer error dynamics as

$$\dot{e} \;\; = \;\; (A - DC)e + \mu(t) - K(t)\nu(t) \tag{5.81}$$

$$\bar{e} \;\; = \;\; Ce + \nu(t) \tag{5.82}$$

As discussed in the previous chapter, the Kalman filter structure can be used to find an optimal gain which minimizes the expected value of the norm of the observer error. Given this gain $K(t)$, if a failure represented by $f\eta(t)$ occurs, the error equations become

$$\dot{e} \;\; = \;\; (A - K(t)C)e + \mu(t) - K(t)\nu(t) + f\eta(t) \tag{5.83}$$

$$\bar{e} \;\; = \;\; Ce + \nu(t) \tag{5.84}$$

Using the Kalman gain, the matrix $A - K(t)C$ may not have the desired eigenvectors required for the purpose of failure detection, eventhough the observer is optimal. This

100

problem can be circumvented, however, by finding a suboptimal observer that has the desired properties of a detection filter as well.

In Appendix A it is proved that if a time-varying matrix $F(t)$ has eigenvalues with negative real parts for all time, then the system

$$\dot{x} = W\Sigma(t)W^{-1}x + v(t) \tag{5.85}$$

is uniformly, asymptotically stable; where $\Sigma(t)$ is the diagonal matrix of the eigenvalues of $F(t)$, $v(t)$ is a bounded input, and W is an invertible matrix with the desirable eigenvectors (for failure detection) as its columns. Now let $F(t)$ denote the dynamic matrix of the error decay equations $A - K(t)C$, and assume that it has eigenvalues with negative real parts for all time. Hence, according to the aforementioned theorem, the new error dynamics given by

$$\dot{e} = W\Sigma(t)W^{-1}e + \mu(t) - D\nu(t) \tag{5.86}$$
$$\bar{e} = Ce + \nu(t) \tag{5.87}$$

are uniformly, asymptotically stable since the noise is assumed to be bounded. This approach provides a suboptimal observer that also possesses the desired failure detection characteristics. The question of which of the eigenvalues to assign to which of the eigenvectors is addressed by considering that the failure detection system essentially works after the error dynamics have come sufficiently close to their steady-state value of zero. Hence, it is desirable to assign the fastest eigenvalues to the eigenvectors corresponding to the failure directions of interest. In this way, the effect of the filter's initial error dies out quickly in these directions and the corresponding failure are detected more readily.

It is worth mentioning in passing that through our simulations of the motor failure detection system, we found that with reasonable noise covariances, the above detection-filter/state-observer is very nearly optimal in that the minimum value of the cost function associated to the optimal observer is raised only by a few percent as a result of the adjustment of the eigenvectors. This will be illustrated in Section 5.7.

The same analysis can be repeated with minor modifications to include the case of sampled-data dynamics. In this setting, the statement that the eigenvalues of $A - K(t)C$ have negative real parts translates to one where the eigenvalues in the corresponding sampled-data matrix ($\Phi - H_kC$) have magnitude strictly less than

one. Given this, the observer algorithms presented in the previous chapter can be modified slightly to accomodate for the failure detection properties. The reason for this direct applicability of the method introduced here to the motor problem is the structure of the thermal model. The model of the thermal system under study is given by the dynamics matrix $A + J(i_d, i_q)$ as discussed in Chapter 3. This matrix is an M-matrix for all values of (i_d, i_q). Using this property, one can demonstrate that given stochastic complete observability and stochastic complete controllability, the Kalman filter is not only uniformly asymptotically stable, but that the error dynamics satisfy the desired condition of negativity of the real part of the eigenvalues (or $|\lambda_i| < 1$ for sampled systems). Furthermore, in our case, the eigenvalues of the error dynamics are, in fact, real for all time. This discussion is quite theoretically involved and we shall omit it from our work. The interested reader may find excellent treatments of the stability problems of the Kalman filter in [17, 16]. For our practical purposes, we have *observed* that the discrete filter designs developed in Chapter 4 lead, quite conveniently, to error dynamics with eigenvalues which are always real and have magnitude less than one for all time.

5.5 Algorithms For Sampled-Data Optimal Detection Filters

In this section we present algorithms based on the ideas presented above for the design of sampled-data optimal, and suboptimal detection filters for the motor detection problem. The algorithms presented here are directly modified versions of the algorithms for the corresponding underlying observers presented in Chapter 4. First, we present the design based on Algorithm I of Chapter 4. In this approach an identity observer in the form of a recursive optimal Kalman filter is designed. The modifications necessary in this case are inserted after the steps where the gain is computed, as follows.

Algorithm I'

1. Initialize the error covariance matrix P_0^- and hence the gain H_0. Also Initialize the original estimate $\hat{T}_0^-$.

2. Compute Q_k.

3. Update the estimate of the state

$$\hat{T}_k^+ = \hat{T}_k^- + H_k(Y_k^- - \hat{T}_k^-)$$

4. Update the error covariance matrix

$$P_k^+ = (I - H_k)P_k^-(I - H_k)' + H_k S H_k'$$

5. Simulate the observer

$$\hat{T}_{k+1}^- = \Phi_k \hat{T}_k^+ + \Gamma_k u_k$$

6. Extrapolate the error covariance matrix

$$P_{k+1}^- = \Phi_k P_k^+ \Phi_k' + Q_k$$

7. Make the measurement

$$Y_{k+1}^- = T_{k+1} + n_{k+1}$$

8. Compute the new gain

$$\bar{H}_{k+1} = P_{k+1}^-(P_{k+1}^- + S)^{-1}$$

9. Find the eigenvalues of $\Phi_{k+1} - \bar{H}_{k+1}$, verify their negativity, and form Σ_{k+1} according to

$$\Sigma_{k+1} = diag[\lambda(\Phi_{k+1} - \bar{H}_{k+1})]$$

10. Form the corrected gain with the desired eigenvectors according to

$$H_{k+1} = \Phi_{k+1} - W\Sigma_{k+1}W^{-1}$$

11. Return to step 2 with updated k.

The quantities referred to in the above algorithm are defined in Algorithm I of Chapter 4.

Next, we present the design based on the approximate suboptimal observer design as described in Algorithm II of Chapter 4. In this algorithm, the time-varying contribution of the system dynamics to the error equation is cancelled, and then, the gain is readjusted to have ideal eigenvectors.

Algorithm II'

1. Initialize the error covariance matrix P_0^- and hence the gain H_0. Also Initialize the original estimate $\hat{T}_0^-$.

2. Compute Q_k as in Algorithm II.

3. Compute S_k as in Algorithm II.

4. Update the estimate of the state
$$\hat{T}_k^+ = \hat{T}_k^- + H_k(Y_k - \hat{T}_k^-)$$

5. Update the error covariance matrix
$$P_k^+ = (I - H_k)P_k^-(I - H_k)' + H_k S_k H_k'$$

6. Simulate the observer
$$\hat{T}_{k+1}^- = \Phi_k \hat{T}_k^+ + \Gamma_k u_k$$

7. Extrapolate the error covariance matrix
$$P_{k+1}^- = \Phi_k P_k^+ \Phi_k' + Q_k$$

8. Make the measurement
$$Y_{k+1} = T_{k+1} + n_{k+1}^*$$

9. Compute the new gain
$$h_{k+1} = P_{k+1}^-(P_{k+1}^- + S_k)^{-1}$$

10. Include the cancellation term
$$\bar{H}_{k+i} = h_{k+1} + J_{k+1}t_0$$

11. Find the eigenvalues of $\Phi_{k+1} - \bar{H}_{k+1}$, verify their negativity, and form Σ_{k+1} according to
$$\Sigma_{k+1} = diag[\lambda(\Phi_{k+1} - \bar{H}_{k+1})]$$

12. Form the corrected gain with the desired eigenvectors
$$H_{k+1} = \Phi_{k+1} - W\Sigma_{k+1}W^{-1}$$

13. Return to step 2 with updated k.

Of the two proposed detection filters, one expects the design based on the exact model of the system (Algorithm I') to perform better than the latter under identical noise conditions. This assertion is verified in Section 5.7 where numerical results on the detection filters are presented. The equations that define the extrapolation and update of the error covariance matrix are based only on the *structure* of the Kalman filter and not on any assumption of optimality. Hence, they can be used to analyze the filter error covariance for any arbitrary gain. This property is desirable in the context of the failure detection problem since it provides a simple detection law which discriminates between stochastic noise and the effect of a failure. We describe this detection law and some generalizations to it in the next section.

5.6 The Detection Law

In this section we quantify some concepts regarding the manner in which the effects of the observer error produced by a failure can be distinguished from those errors due to noise. One reason why the Kalman filter design is useful in failure detection is that the structure produces values of the quantity P_k during its operation. As we have seen, this quantity is the covariance matrix of the observer/detector error. The diagonal elements of this matrix are then the squares of the standard deviations of the elements of the error vector. More specifically, we have

$$P = [p_{ij}] \tag{5.88}$$

where the dependence on k is suppressed for convenience. Hence, we have

$$\sigma_i = \sqrt{p_{ii}} \tag{5.89}$$

where σ_i is the standard deviation of the ith element $\bar{e}_i$ of the error vector $\bar{e}$.

Assuming that the noise in $\bar{e}_i$ behaves as a Gaussian random variable with mean zero, Figure 5.6 shows the probability distribution function of $\bar{e}_i$. Note that this probability distribution is in general a function of time. Given this information, the simplest way to differentiate between stochastic noise and failures is a *threshold criterion*. This criterion defines a likelihood error ellipsoid centered at the origin of R^N, where N is the dimension of the error vector $\bar{e}$. The lengths of the semi-axes of this ellipoid are determined directly from the filter error covariance matrix. By observing the behavior of the error vector with respect to this likelihood region, we
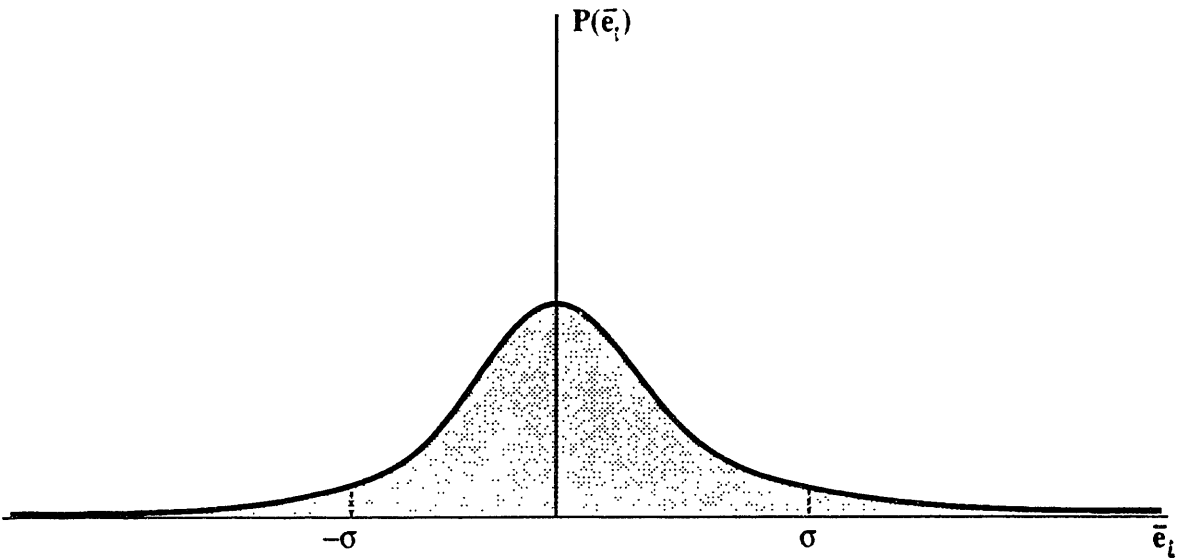
Figure 5.6: Probability distribution of $\bar{e}_i$

may make decisions as to whether a failure has taken place or not. In the absence of a failure, the filter error lies within this ellipsoid for almost all time (Figure 5.7). Unfortunately, the threshold criterion makes a decision regarding the presence of a failure on the basis of the magnitude of the residuals alone. For example, one may pick the likelihood region as the 99 percent confidence interval by letting the length of the ith semi-axis of the ellipsoid to be $3\sigma_i$. In this way, in the absence of failures, the error vector remains inside the ellipsoid 99 percent of the time. So upon observing an error vector that lies outside the ellipse, a failure is immediately declared. This may prove problematic if the crossing is due to noise that is either not in the 99 percent likelihood region or that has not been accounted for. Hence, it seems clear that it is necessary to smooth the data so as to increase the signal to noise ratio and thereby decrease the probability of false alarms.

There exist several ways to reduce the probability of false alarms, all of which can be expressed in terms of a symmetric moving window across the residuals produced by the filter. As shown in Figure 5.8, the height of this window determines the size of the likelihood ellipse while the width of the window holds the number of data points that are to be smoothed across the window. A window is then assigned to each channel of the filter error (i.e. each element of the vector of residuals), and threshold crossings are monitored across each channel. A set of threshold crossings defines a signature that is then associated uniquely (up to detection equivalence)

106
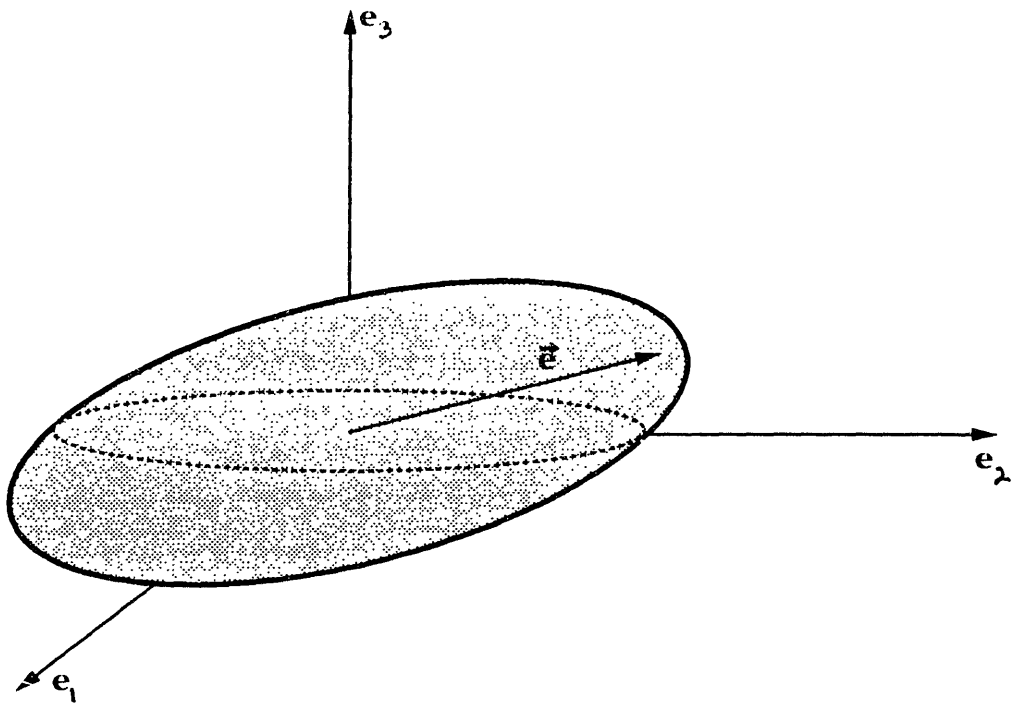
Figure 5.7: The Error Vector and the Confidence Region
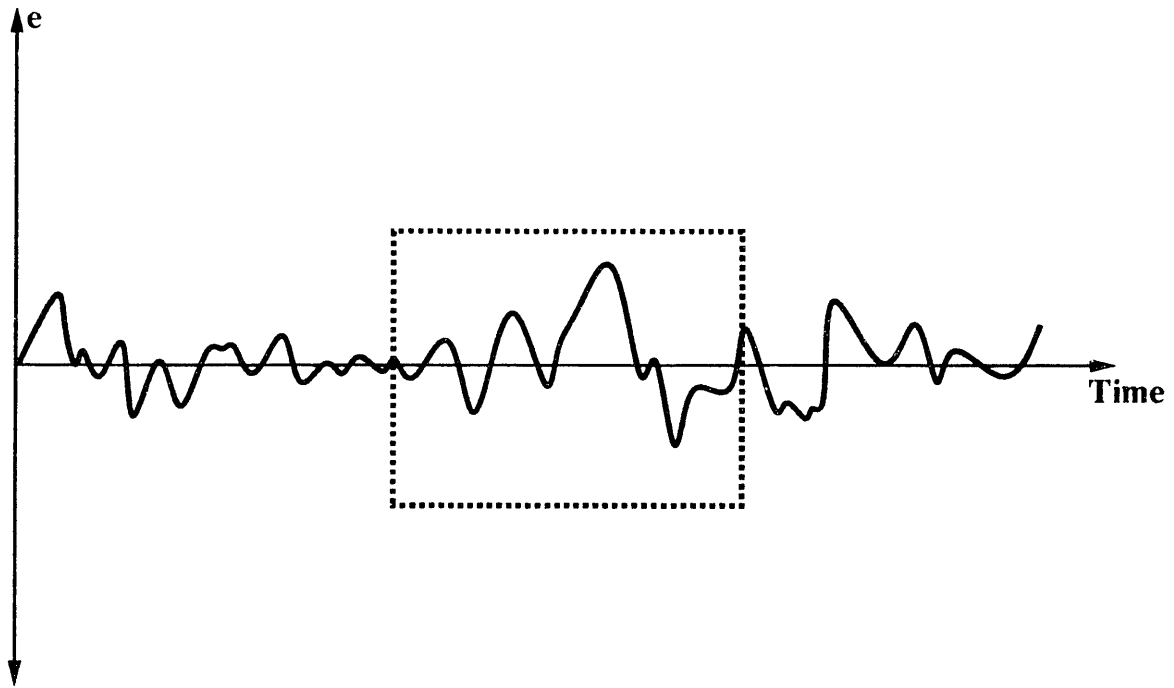
Figure 5.8: Moving Window and the Residuals

to a given failure. For example, in the spring-mass example presented before, with measurements of speed and position, a change in the spring constant is represented by a failure in the direction $[0 , 1]'$. This correspods to finding a threshold-crossing in the second channel of the filter and none in the first. Figure 5.9 illustrates this idea for a general situation.

5.6.1   Choice of Window Height

The height of the window can be chosen to give a likelihood ellipsoid of any desired size by letting this length be equal to $2a_i\sigma_i$, where a_i is a positive, real number. The numbers a_i need not coincide for different channels, hence the subscript i. From a practical standpoint, a reasonable value for each a_i must be chosen so as to make the detection system sensitive enough to failures, yet not so sensitive as to produce false alarms. Given Gaussian noise characteristics a reasonable value is given by

$$a_i = 3 \tag{5.90}$$
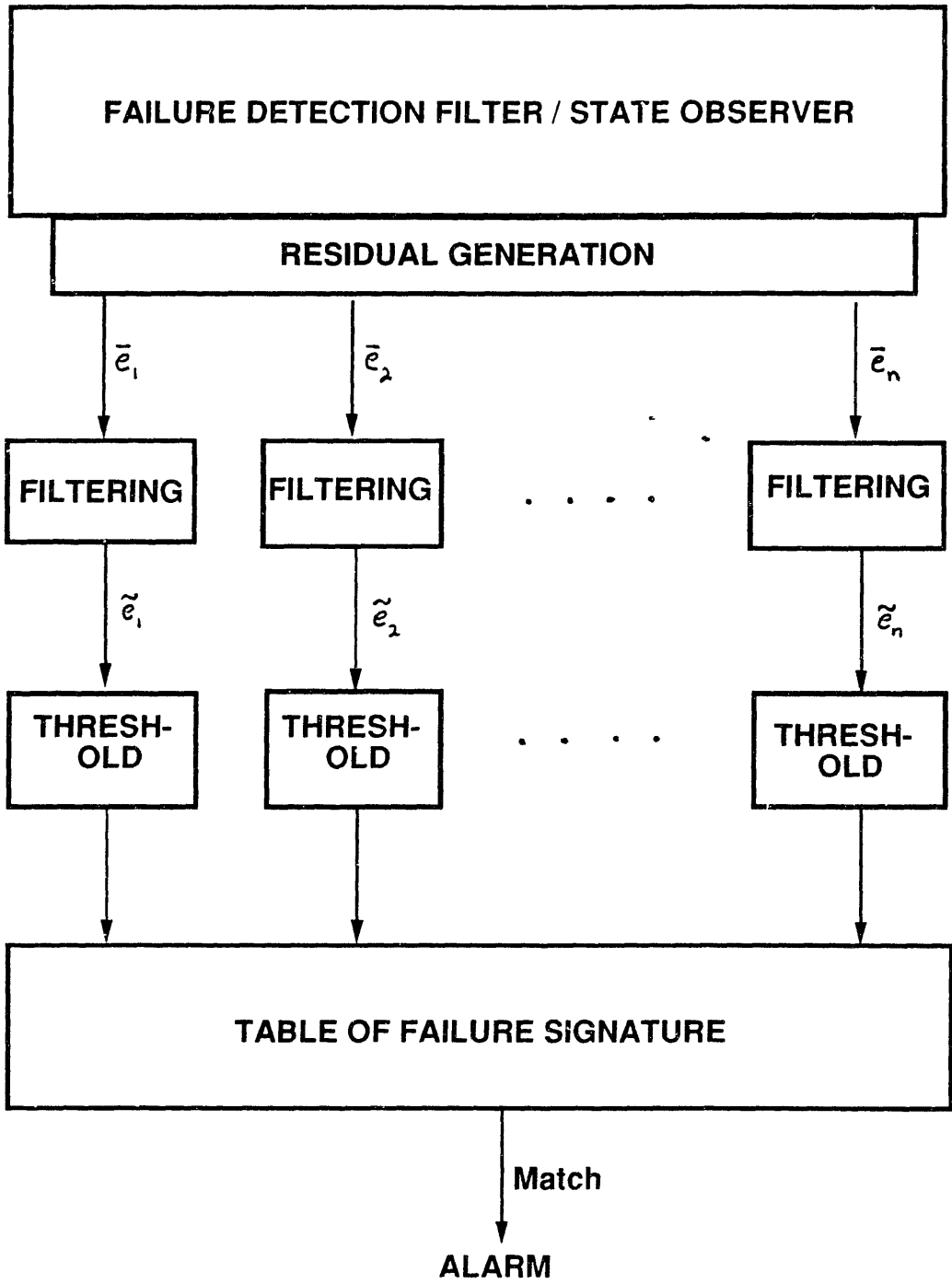
Figure 5.9: Detection of failures by monitoring threshold crossings

For Gaussian noise, a value of 3 for a_i gives the 99 percent confidence interval for the ith channel. This value was employed in our simulations. The only objective way to decide on what particular values of a_i to use is the knowledge of the type of error that is being dealt with. The easiest case is clearly that of Gaussian noise. However, if the noise in the residuals is distributed, say, uniformly, exponentially, or perhaps by a Cauchy distribution, as is the case with corrupt measurements that contain large spikes, different criteria must be applied to ensure the effectiveness of the detection system. In these situations, the performance of the Kalman filter itself may be questionable.

5.6.2 Choice of Window and the Smoothing Filter Width

The choice of the width for the window is dependent on the degree of filtering needed to ensure the least number of false alarms, while increasing the probability of capturing a failure in the shortest possible time. Depending on the type of noise being dealt with, several possibilities exist for the choice of the smoothing filter. Depending on the choice of the filter, the length of the window must be picked appropriately. We briefly elaborate on several filtering methods that may be applied.

Moving Average Given a window of width equal to L, where L is an integer, the output of this window at instant k is the average of the previous L data points. Let $\bar{e}_k$ denote the output of this filter at instant k and recall that $\bar{e}_k$ is the filter error in the output space at instant k. Then this filter gives

$$\bar{e}_k = \frac{\sum_{i=0}^{L-1} \bar{e}_{k-i}}{L} \qquad (5.91)$$

For Gaussian noise, this is the simplest effective way to smooth the data, however, the appropriate length L (an integer) to be used must be determined by considering the size of the disturbances involved and also by considering the speed with which the transient due to the failure settles down. This filter can be implemented on-line quite easily and does not present a major computational burden. Variants of this approach include a weighted moving average, and a moving average with a forgetting factor.

Median Filter Another approach to the smoothing problem is to consider the use of a median filter. A causal median filter with a window size of L (L and odd integer)

has an output, $\tilde{e}_k$, that is given by

$$\tilde{e}_k = M_{i=0}^{L-1}(\bar{e}_{k-i}) \tag{5.92}$$

where M_0^L denotes the operator that evaluates the median of a sequence indexed by the corresponding integers. This filter is well suited for situations where the residuals contain "spikes" that may not be due to any failure. If a moving average is employed in such a case, a sufficiently large spike can cause the average to cross the threshold, thereby producing a false alarm. A disturbance of this kind is readily suppressed by the median operation, hence guarding against false alarms. Although median filters work best on noise that is distributed according to Cauchy-type distributions, they represent an attractive alternative that is easily implemented using analog or digital circuitry, with the major computaional burden being the sorting operation of the elements in the window.

Trimmed Moving Average   This technique represents a compromise between median filtering and averaging. The output of a trimmed moving average filter with a window of length L is obtained by taking the elements within the window and sorting them, discarding the α (even integer) largest and smallest elements of the window, and then averaging the remaining elements. This filter may be called an α-trimmed moving average, where α is an adjustable parameter. Note that if $\alpha = (L-1)/2$, then the median filter is obtained, and if $\alpha = 0$ the moving average is obtained. This is the most versatile approach, however, for arbitrary α the most computationally burdensome.

The above methods work well in detecting failures where the event vector moves away from the origin in a monotonic fashion. However, they tend to suppress valid failure alarms, if as a result of the failure, the residual vector tends to oscillate symmatrically about zero. This is the case in the detection problem for the spring-mass system discussed previously. In such cases, rather than dealing with the residual in each channel, one may use the absolute value of the residual and apply the above techniques by redefining the threshold above zero.

Examples

1. In Figure 5.10 we present an error channel, from the spring-mass problem, and its associated 99 percent confidence intereval. The confidence interval spans

111
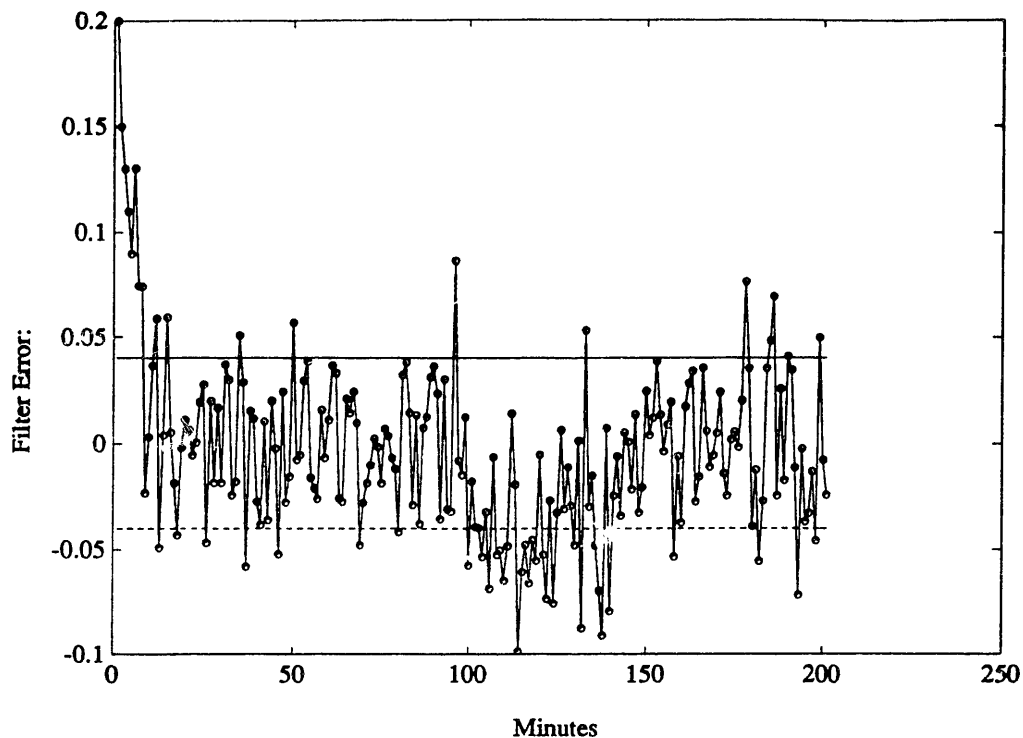
Figure 5.10: Error Channel

the region between 0.04 and -0.04. A failure (20 percent increase in spring constant) has occured at 100 minutes and repaired at 140 minutes. However, many instances of threshold crossings are observed where no failures exist. In Figure 5.11 we have shown the filtered versions of the error using a moving average, and a median filter of window lengths 20 and 40 points respectively. We can see that the 20-point moving average declares a failure at 108 minutes while the 20-point median filter declares a failure at 105 minutes, 3 minutes earlier than the moving average. In contrast, the 40-point moving average fails to declare a failure at all while the 40-point median filter declares a failure at 120 minutes.

2. Figure 5.12 shows a spring failure in the spring-mass system discussed before. The spring constant increase by 20 percent. The failure occurs at 100 minutes and the result is that the second error channel shows oscillatory behavior at this point. Direct filtering of this error signal will most likely suppress the failure, yet by considering the absolute value of the error signal, a stronger change in the size of the residual is detected as shown in Figure 5.13, thereby declaring a failure. Note that when considering the absolute value of the residual in the particular channel, the confidence intervals must be recomputed. A simple way

112
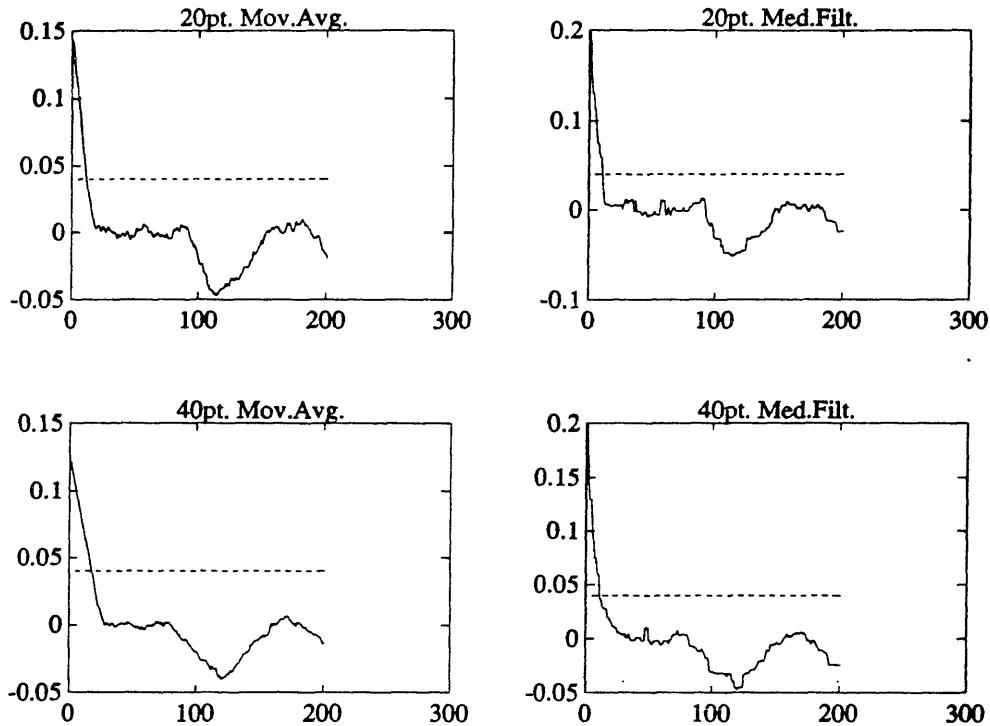
Figure 5.11: Filtered Error

to do this is by setting the new upper bound of the confidence interval to the height of the old confidence interval, and setting its lower bound to zero. It should be pointed out that this type of oscillatory behavior as a result of a failure can never take place in a thermal system such as ours. This is due to the physical characteristics of the system. Thermal systems are by nature monotonic whether stable or unstable.

5.7 Numerical Results

In this section we present the results of our simulations of the detection filters discussed in the previous sections, and we will compare their relative performances under the same noise characteristics. We will refer to the first filter (Algorithm I') as Detection Filter I and the second as Detection Filter II. All of the following simulations were performed using $t_o = 60$ seconds sampling period and the same error characteristics as shown in Table 3.1.

Detection Filter I   In the graphs to follow, the motor is operating under constant load at a constant speed, and at cycle 50 of the operation (i.e. 50x60 seconds = 50

113
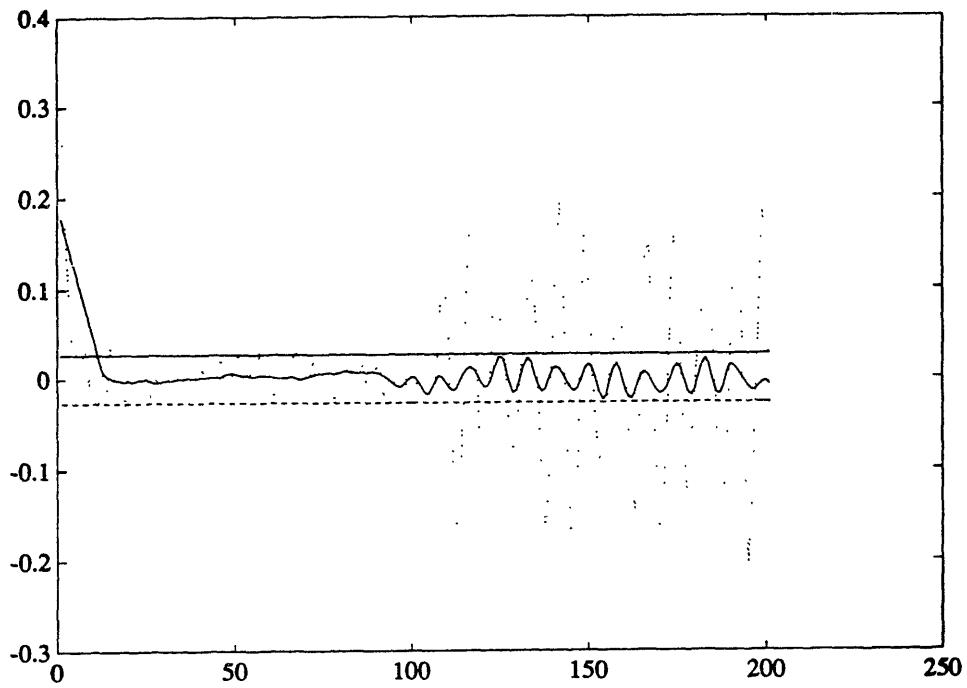
Figure 5.12: Spring Failure
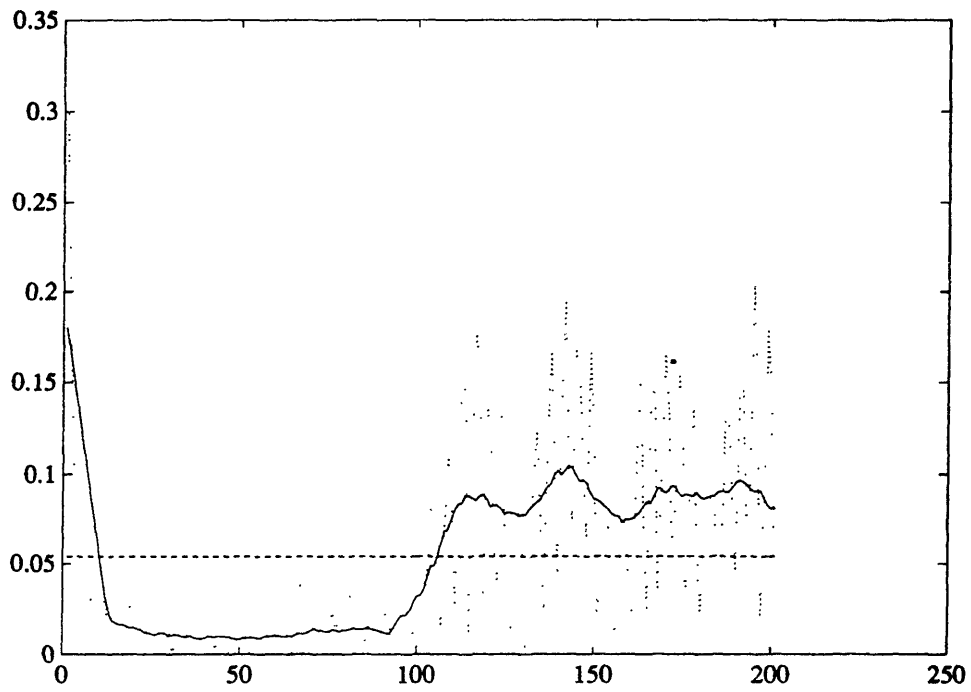
Figure 5.13: Absolute Error

114

minutes) a failure occurs in the thermal system. This failure is one in which the motor is insulated and has difficulty dissipating heat to the ambient environment. Figures 5.14-15 show the performance of the Detection Filter I with the given parameters. The dotted lines on the filter error graphs define the 99 percent confidence interval of the error. A failure is then recognized by observing which elements of the error vector have remained in their respective confidence regions, and which have not. This fact will indicate a particular direction in the state-space which corresponds to the direction of the event vector associated with the failure of interest. As we have shown in Chapter 3 (failure identification), this failure can be accurately modelled as a bias E in the matrix A where E is a 2×2 matrix with nonzero elements in the second row. From our failure identification exercises, we found that a reasonable value for E is

$$E = \begin{bmatrix} 0 & 0 \\ 0.002 & 0.0015 \end{bmatrix} \tag{5.93}$$

Corrective action is taken at cycle 100 and the filter error begins to return to its 99 percent confidence region. For this simulation we have

$$P_0 = \begin{bmatrix} 0.5 & 0 \\ 0 & 0.75 \end{bmatrix} ; \qquad P_\infty = \begin{bmatrix} 0.0482 & 0.0127 \\ 0.0127 & 0.3772 \end{bmatrix}$$

$$\hat{T}_0^+ = \begin{bmatrix} 1 & 2 \end{bmatrix}$$

Comparing the value of P_∞ for this detector to the value of the same variable for the underlying Kalman filter, which does not include eigenvector tuning, one can see that the respective traces of these matrices, which are the minima of the associated cost functions, differ by only about 1 percent. This shows that adjusting the eigenvectors of the error equation in the Kalman filter takes little away from the optimality of the filter in the motor detection problem.

Detection Filter II In the next set of simulations, the performance of the second detection filter (Algorithm II') is analyzed. The same initial and operating conditions were employed in this simulation. Thus,

$$P_0 = \begin{bmatrix} 0.5 & 0 \\ 0 & 0.75 \end{bmatrix} ; \qquad P_\infty = \begin{bmatrix} 0.0483 & 0.0142 \\ 0.0142 & 0.03922 \end{bmatrix}$$

115
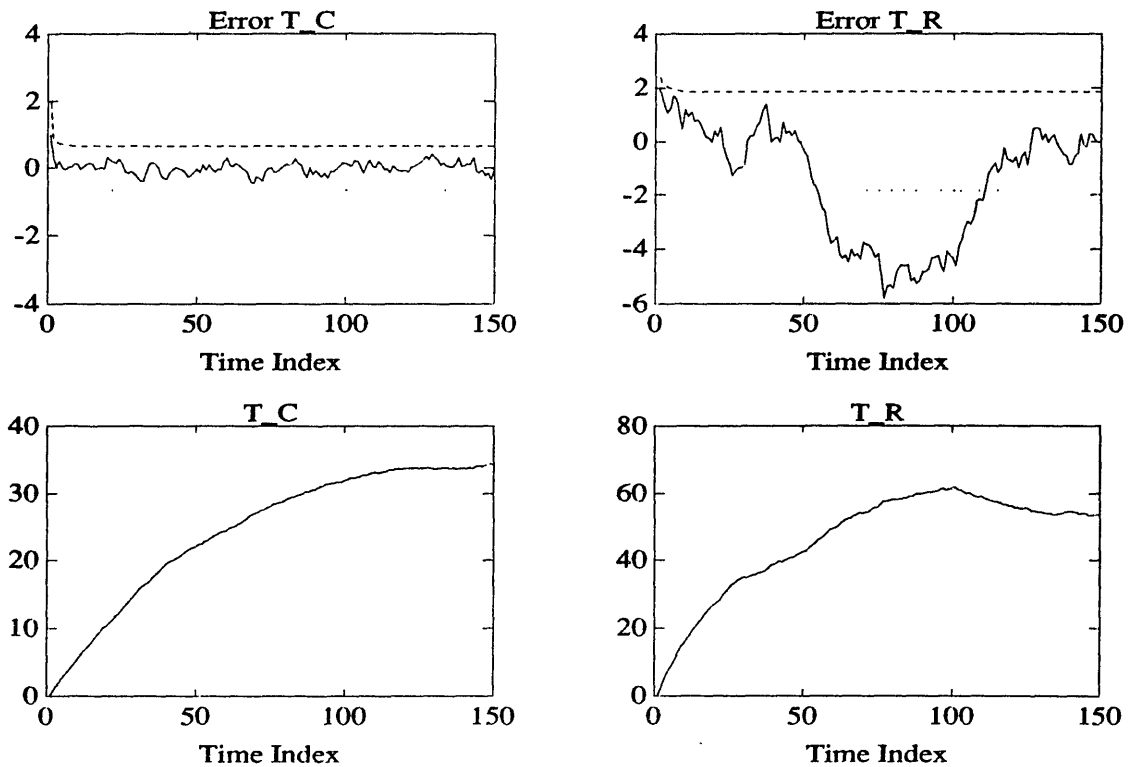
Figure 5.14: (Detector I) States and Observer Errors

$$\hat{T}_0^+ = [1 \quad 2]$$

Figures 5.16-17 show the responses of the thermal system and detection filter II to the commanded inputs. It is worth comparing the respective values of P_∞ for the two detection filters. The first filter, based on the optimal Kalman filter, converges to a smaller value of P_∞ as expected. However, the second filter displays excellent tracking behavior as well, even though it is based on the sub-optimal observer structure.

In the next experiment, we introduce steps in the commanded speed and torque as shown in Figures 5.18-21, and observe the response of the system and the detection filters. Again, the same failure as in the previous exercise is introduced at cycle 50 and corrected at cycle 100. We have chosen the starting times of the steps in speed and torque to coincide with the time of the occurance of the failure. This is to simulate the worst-case scenario. Note that since the variance of the plant noise is proportional to the magnitude of the input, the error covariance matrix responds to the step changes in the input, reducing the size of the confidence interval, as expected.

Detection Filter I In this experiment, steps in the torque and the speed have been commanded as seen in Figure . The following show the initial and final values of the
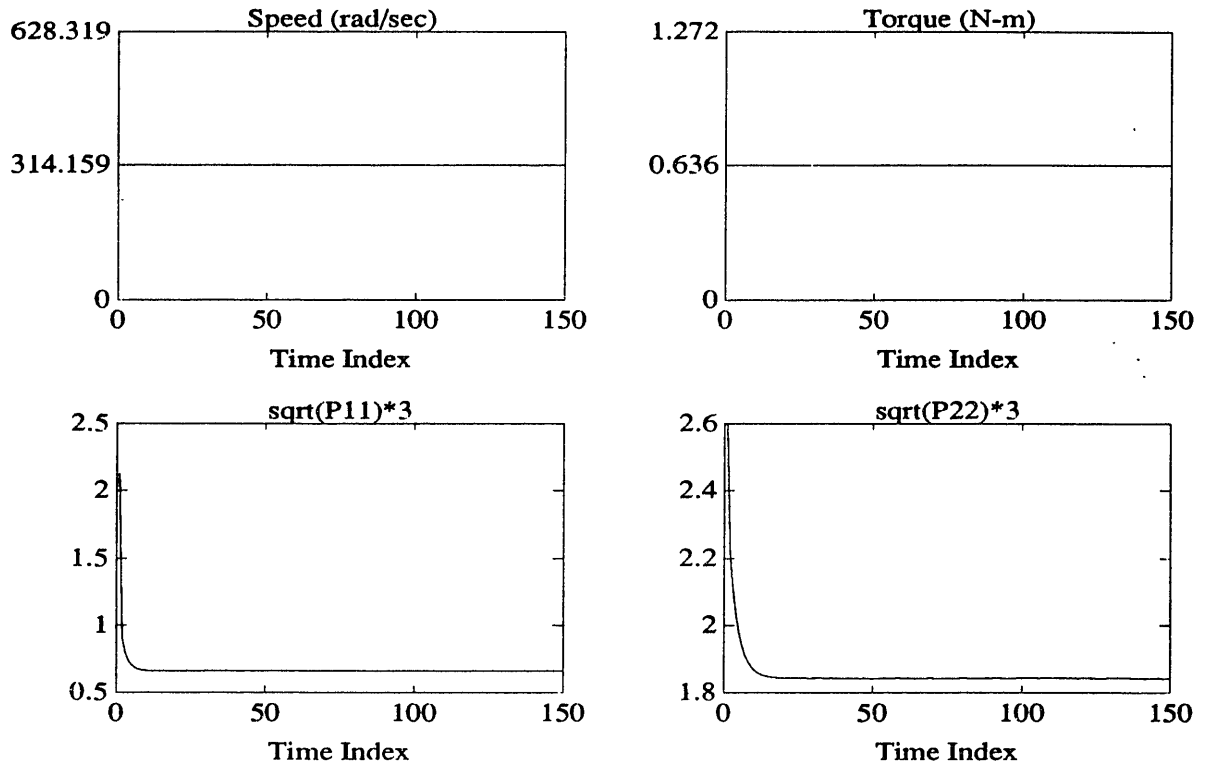
Figure 5.15: (Detector I) Speed, Torque and Confidence Region
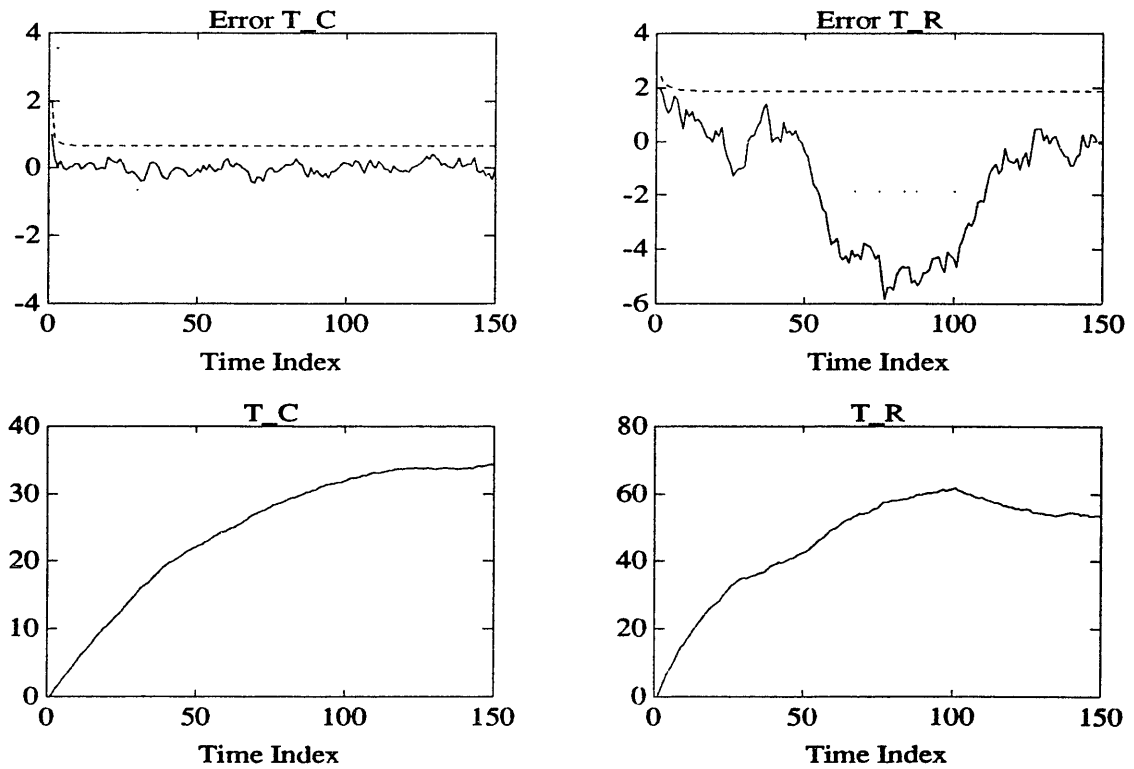
Figure 5.16: (Detector II) States and Observer Errors
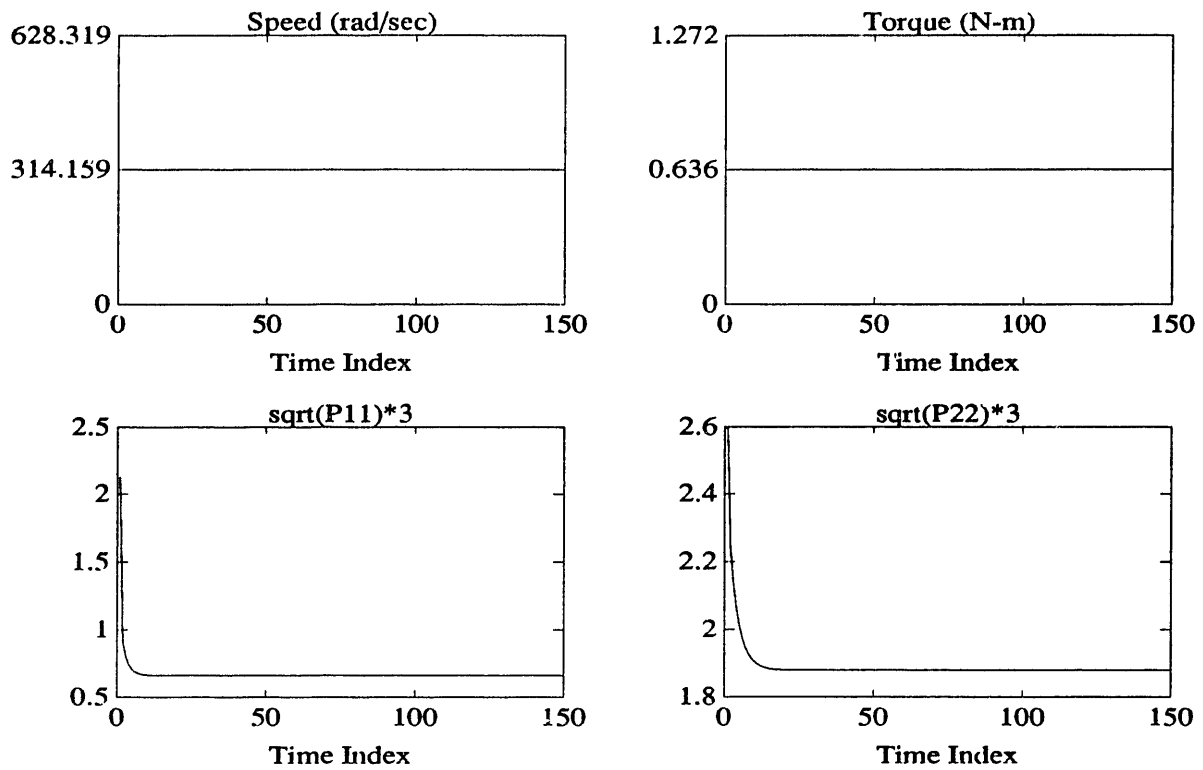
Figure 5.17: (Detector II) Speed, Torque and Confidence Region

filter error covariance matrix and the initial value of the thermal state estimate.

$$P_0 = \begin{bmatrix} 0.5 & 0 \\ 0 & 0.75 \end{bmatrix} ; \qquad P_\infty = \begin{bmatrix} 0.0482 & 0.0127 \\ 0.0127 & 0.3772 \end{bmatrix}$$

$$\hat{T}_0^+ = [1 \quad 2]$$

Detection Filter II In this experiment, steps in the torque and the speed have been commanded as seen in Figure 5.21. The following show the initial and final values of the filter error covariance matrix and the initial value of the thermal state estimate.

$$P_0 = \begin{bmatrix} 0.5 & 0 \\ 0 & 0.75 \end{bmatrix} ; \qquad P_\infty = \begin{bmatrix} 0.0483 & 0.0142 \\ 0.0142 & 0.3922 \end{bmatrix}$$

$$\hat{T}_0^+ = [1 \quad 2]$$

118
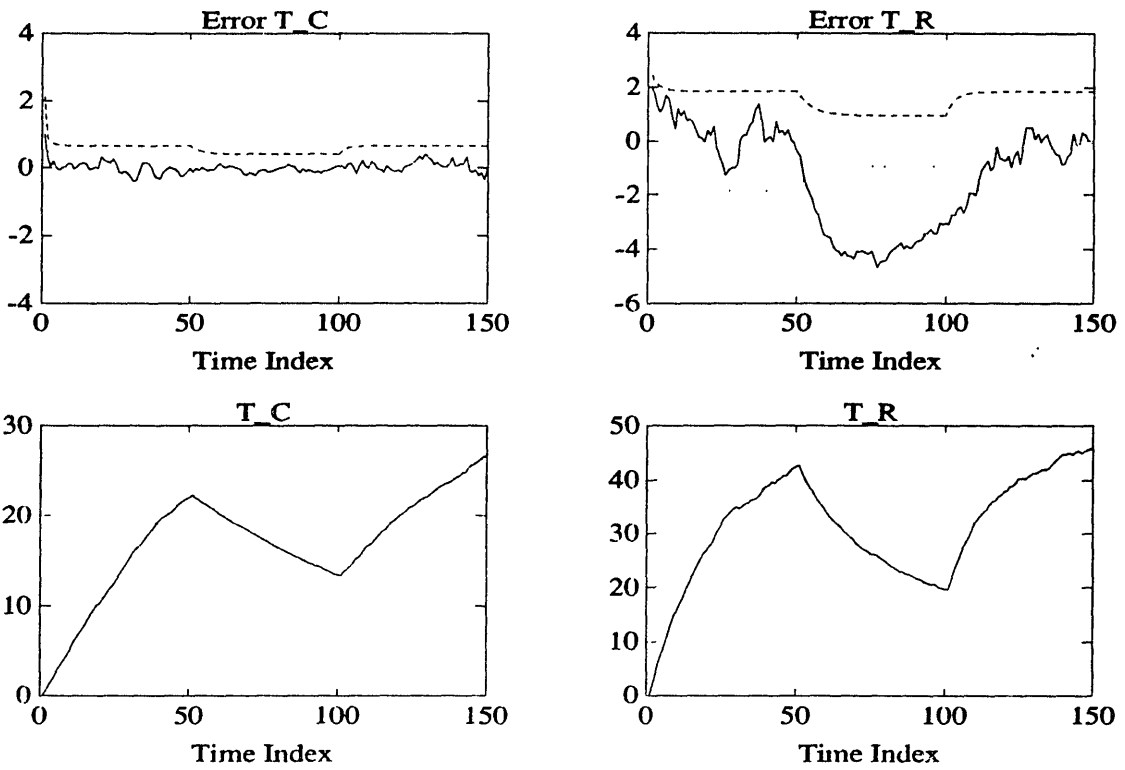
Figure 5.18: (Detector I) States and Observer Errors
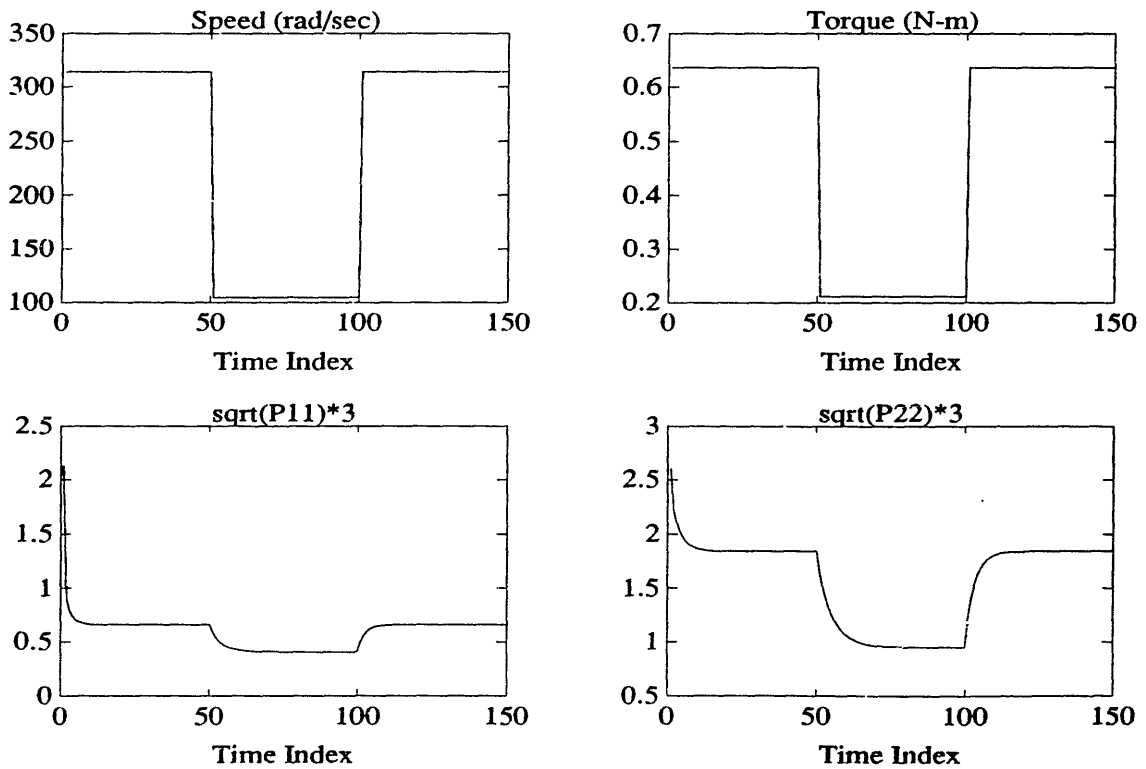
Figure 5.19: (Detector I) Speed, Torque and Confidence Region

119
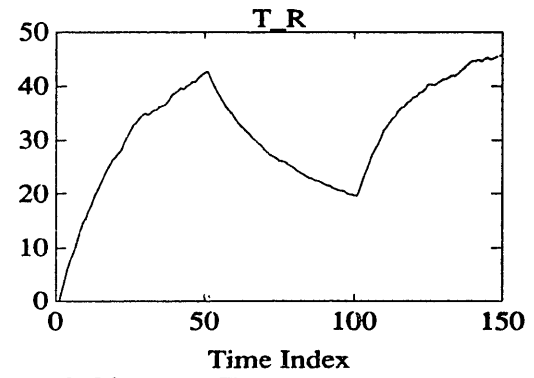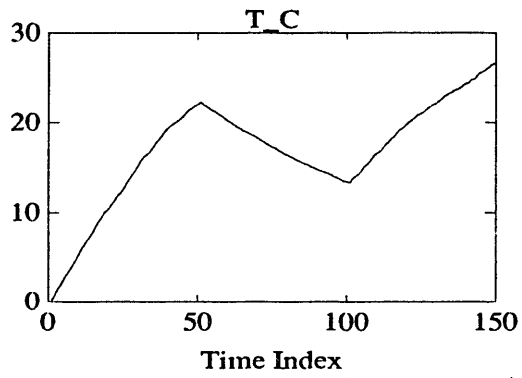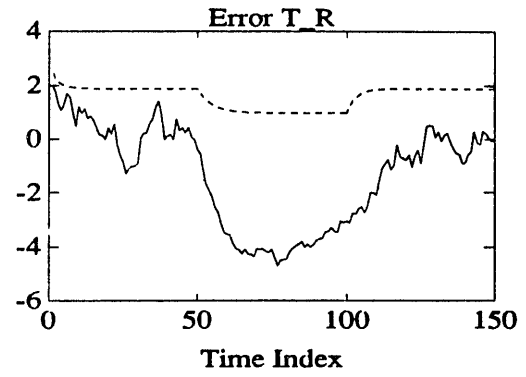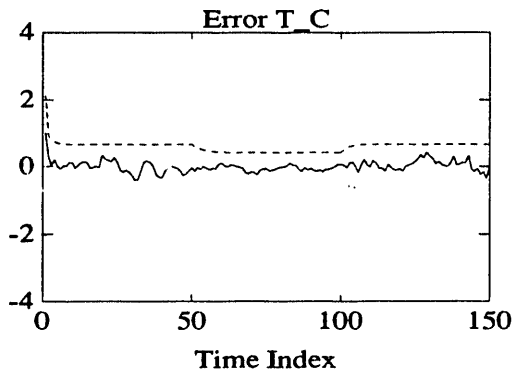
Figure 5.20: (Detector II) States and Observer Errors
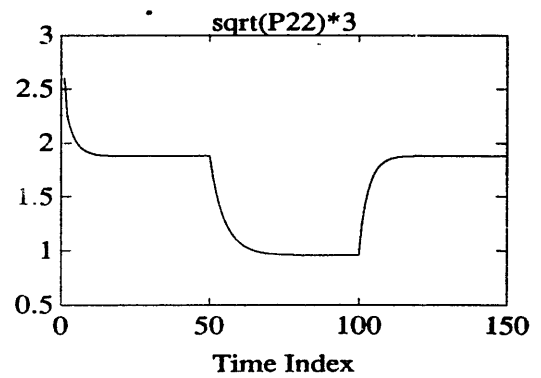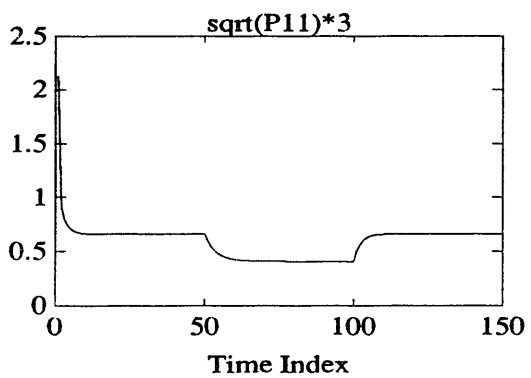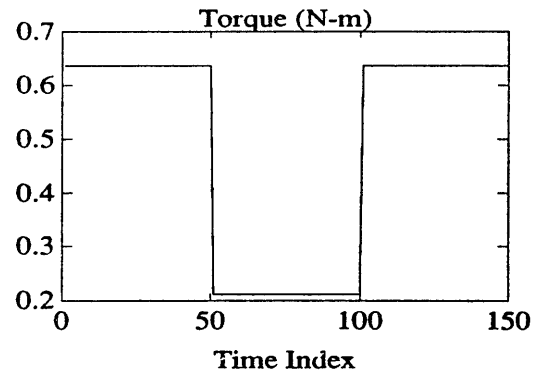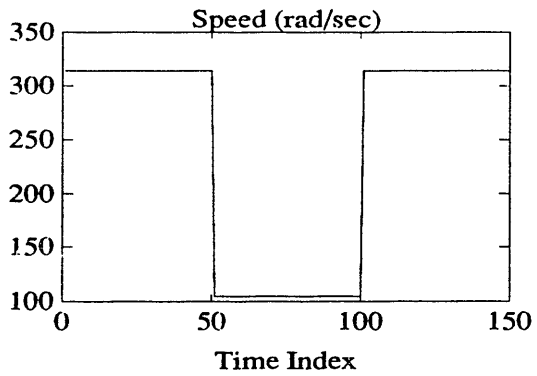
Figure 5.21: (Detector II) Speed, Torque and Confidence Region

120

5.8 Summary

In this chapter we have presented the basic concepts of geometric failure detection theory. We have applied these concepts to the problem of detecting thermally related failures in small permanenet- magnet synchronous motors. Two designs were presented based on the two observer designs discussed in Chapter 4. It is shown that the design based on the Kalman filter without the cancellation of time-varying dynamics is the best approach. In Chapter 6, we perform some physical experiments to establish that the preferred observer design (Algorithm I, Chapter 4) and the preferred Detection Filter design (Algorithm I', Chapter 5) work well under actual physical circumstances.

Chapter 6

Experimental Results

6.1 Introduction

In this chapter we describe the results of experiments performed to confirm the validity of the concepts presented in the previous chapters, and also to demonstrate the success of our proposed failure detection system. Experiments were performed with a permanent-magnet synchronous motor manufactured by Omron with characteristics as given in Table 6.1. The experiments included two tests to explore the performance of Thermal Observer I and the performance of the failure detection system based on this observer design. The performance of the thermal observer II was not studied experimentally because the simulations demonstrated its performance to be inferior.

The experiments were performed under external load torque produced by a direct-current motor that acted as a brake. Both motors were mounted on an aluminum stand and their rotors were coupled together. Figure 6.1 shows the experimental setup, while Figure 6.2 illustrates the data-acquisition process. The line voltages and currents, and the shaft angle, along with the thermocouple reading, were sampled with a sampling period of 3 ms. 100 samples were collected beginning every minute while the motor was in electromechanical steady-state. The sampling rate was chosen to be slow since, due to the fact that the thermal time-constants were large, data must be collected over a long time period. This experimental time period was chosen to be 135 minutes, three times the slowest time constant of the thermal model. However, the sampling rate was chosen to be fast enough so as to avoid aliasing when sampling the line voltages and currents. The maximum speed of the experimental motor was 3000 rpm or approximately 300 radians per second. Since the motor has three phases, the electrical line variables then have a maximum frequency of 300×3 radians

Output Power	200	watts
Continuous Torque	0.636	Nm
Peak Torque	1.908	Nm
Continuous Speed	3000	rpm
Maximum Speed	4000	rpm
K	0.092	Vs/rad
R (at 24°C)	1.82	ohms
L_d	0.00917	mH
L_q	0.0084	mH
N	3	-
P	0.00039	mH
B	5.8e-4	$\text{Nm-rad}^{-1}\text{sec}$
C	1.91e-2	Nm
Weight	2.0	kg

Table 6.1: Physical characteristics of the experimental motor

per second, or 143 Hertz. So the slowest sampling frequency that avoids aliasing is roughly 290 Hertz. As mentioned above, the sampling frequency used in the experiments was about 330 Hertz. Thus, aliasing was avoided for all speeds. The data sets were then used to produce the electrical variables in the dq-frame. As shown in Figure 6.3, averaging is then performed to produce a single value of the electrical variables, and the thermocouple readings, to represent the sample taken each minute. These values are then used to drive the observer/detection filter. As shown in Figure 6.3, the rotor frame electrical variables are used to compute the inputs to the thermal observer/detector and also to directly produce electrically based estimates of the temperature rises in the motor. These estimates are then compared against those temperature rises estimated by the thermal observer and the residual is used as feedback to the observer. This residual is compared against appropriately chosen thresholds for purposes of failure detection.

A VMEBUS Motorola processor was used as the computer. The analog-to-digital conversion was performed with a 12-bit multichannel, synchronous A/D converter supplied by Analog Devices. It is important to mention that due to varying propagation delays in the analog input boards that condition the signals received by the A/D converters, the sampler does not receive the voltages, currents and the shaft angle in an exactly synchronous fashion. This is an important technical matter that must be studied carefully. If these signals are not received synchronously by the A/D converter, the Blondel-Park Transformations produce rotor frame variables that
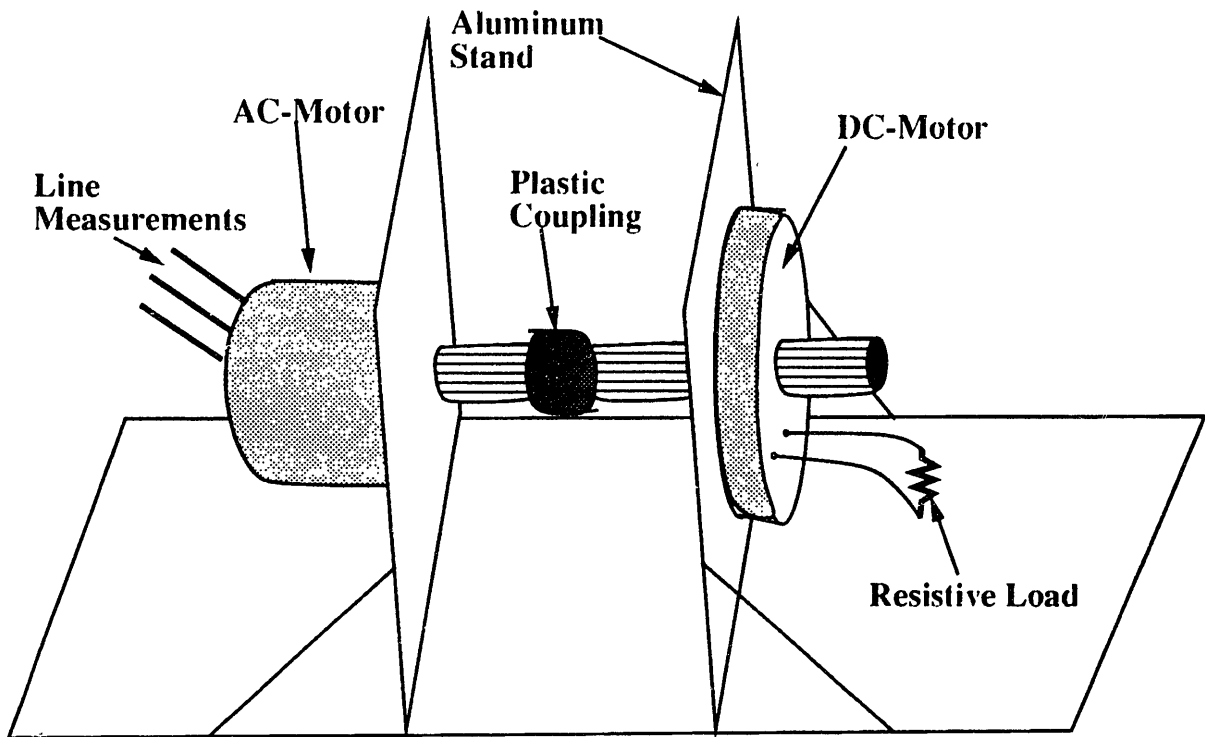
Figure 6.1: The Experimental Setup

are incorrect. We carefully measured the respective delays in these channels and compensated for them accordingly.

6.2   Characterization of the DC Load

In order to carry out accurate experiments, it is important to characterize the load torque produced by the DC-motor shown in Figure 6.1. A simple model for a DC-motor in steady-state can be described as an RL circuit with a voltage source that is linearly dependent on the speed, as shown in Figure 6.4. A series of stand-still tests and steady-state measurements were performed and the parameters shown in the circuit of Figure 6.4 were identified as shown in Table 6.2.

Figure 6.5 shows the short-circuit current versus the speed for the DC-motor in question. The slope of these measurements is the ratio $\frac{K_{dc}}{R_{dc}}$. Next, the open circuit voltage of the DC-motor as a function of velocity is shown in Figure 6.6. The slope of the measurements is K_{dc}. The value of K_{dc} and that of the ratio $\frac{K_{dc}}{R_{dc}}$ yield the value of R_{dc}. If i_{dc} denotes the short-circuit current in the DC-motor, then the quantity $K_{dc}i_{dc}$ denotes the bearing torque in the motor. The bearing torque was measured

124
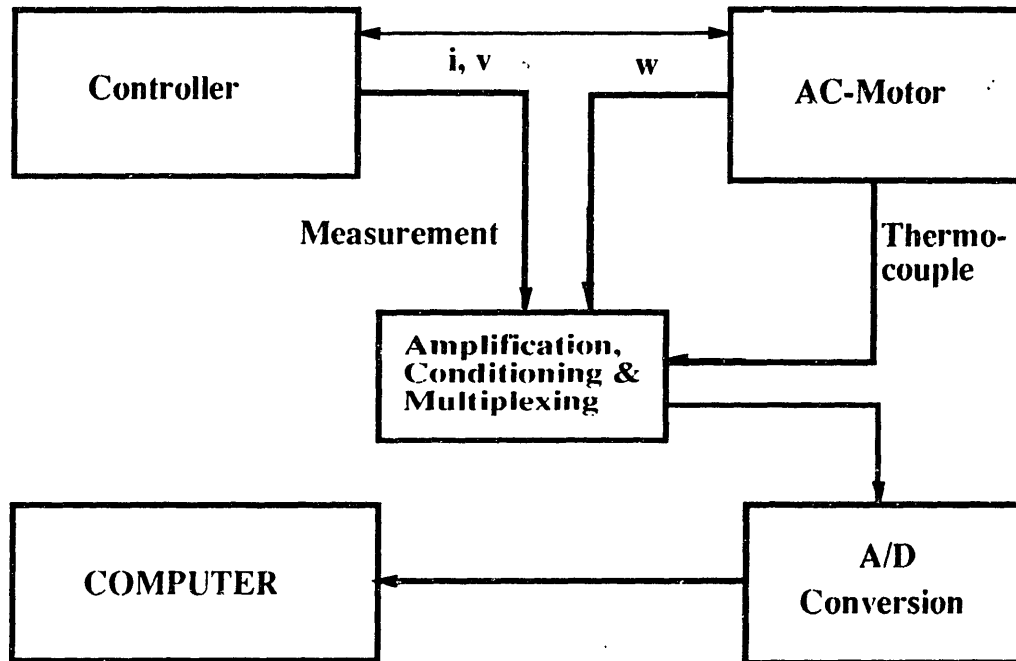
Figure 6.2: The Data Acquisition System

R_{dc}	0.4579 ohms
K_{dc}	0.1028 Vs/rad
L_{dc}	0.082 mH
Bearing Torque (τ_b)	$\alpha tan^{-1}(\frac{\omega}{\beta}) + \gamma\omega$
α	3.972e-2 Nm
β	6.745 rad/s
γ	1.56e-4 Nms

Table 6.2: DC Motor Parameters
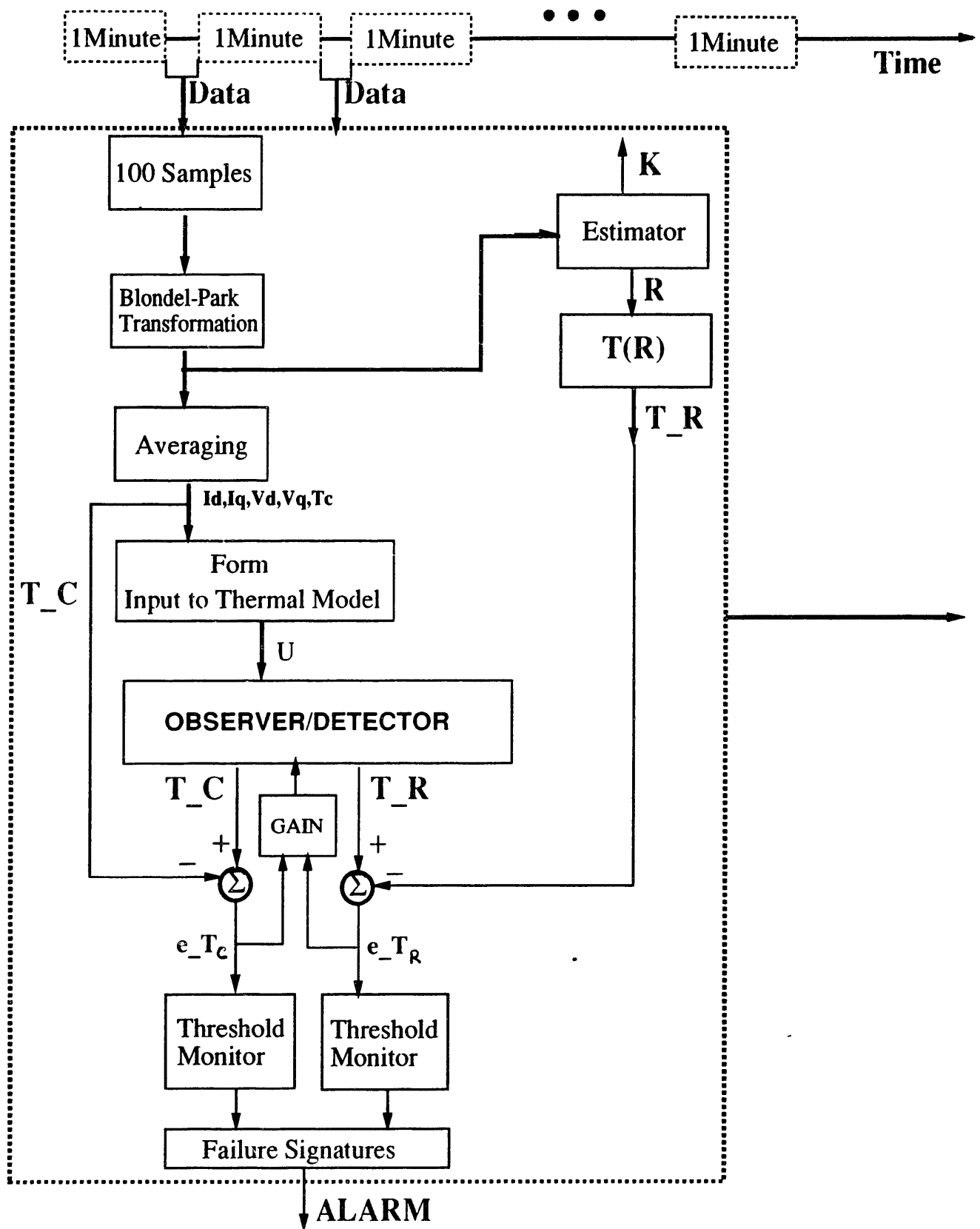
Figure 6.3: Real-Time Operation Of the Filter
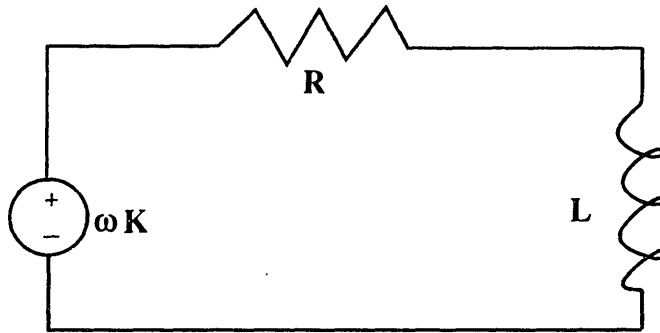
Figure 6.4: Simple Model of DC-Motor in Steady-State

versus the speed, and a nonlinear function was fitted to the data as shown in Figure 6.7. The inductance L_{dc} was measured directly using a bridge.

6.3 Observer Performance and Failure Detection

In this section we present three sets of experiments to confirm the results of Chapters 4 and 5 in a realistic situation. In the first two experiments, the performance of Observer 1 is studied. In the first experiment, the motor is operating at a constant speed of 1000 rpm with a constant load torque throughout the experiment, while in the second experiment, the speed of the motor is stepped up from 1500 rpm after 45 minutes to 2500 rpm, and then stepped back down after another 45 minutes to the original speed. No failure is introduced in these two experiments. In the third experiment, the speed is fixed at 2500 rpm and a failure is introduced at 45 minutes, and the failure is then corrected at 90 minutes

6.3.1 Experiment I

In this experiment, the speed of the motor is controlled at a constant level of 1000 rpm while a load torque of 0.39 Nm is applied to the rotor using the DC motor. The motor is maintained in this condition for 135 minutes while once every minute, 100 samples of the line currents, voltages, thermocouple, and shaft angle are taken and stored. The corresponding values in the dq-frame are then computed as shown in Figure 6.3. Figure 6.8 shows the dq-frame voltages and currents versus time into the experiment.
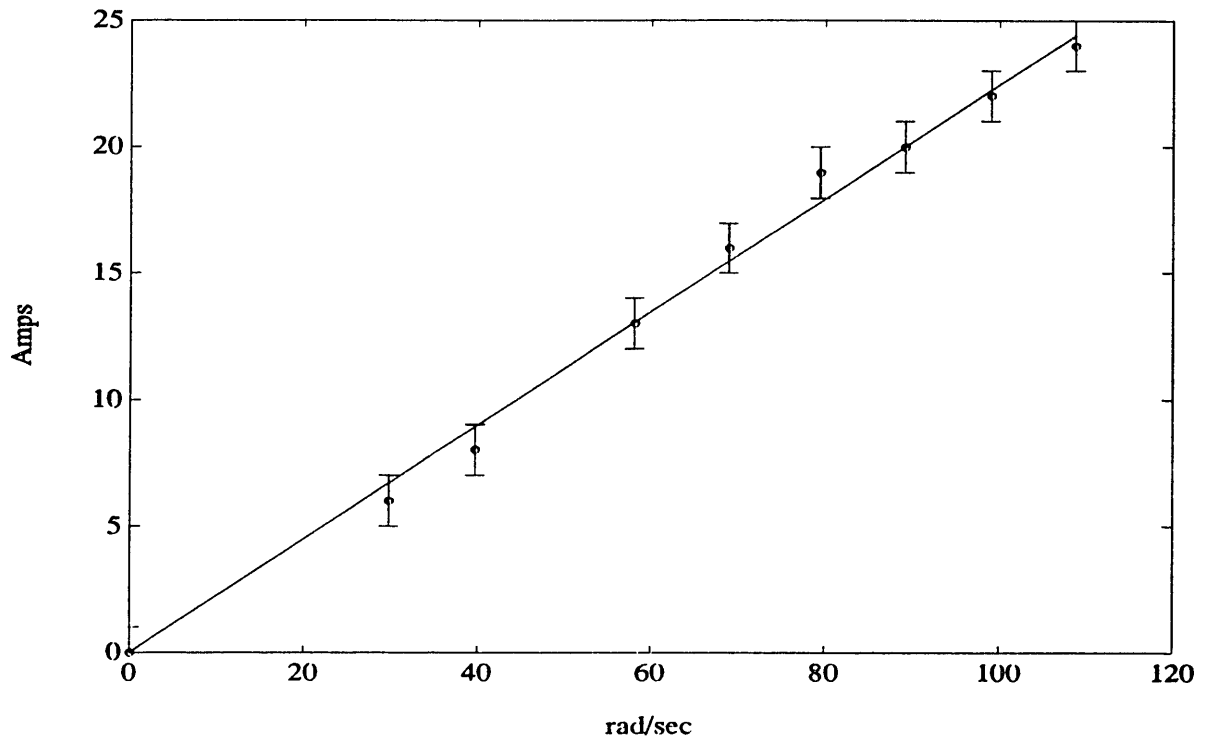
Figure 6.5: Short-Circuit Current vs Speed
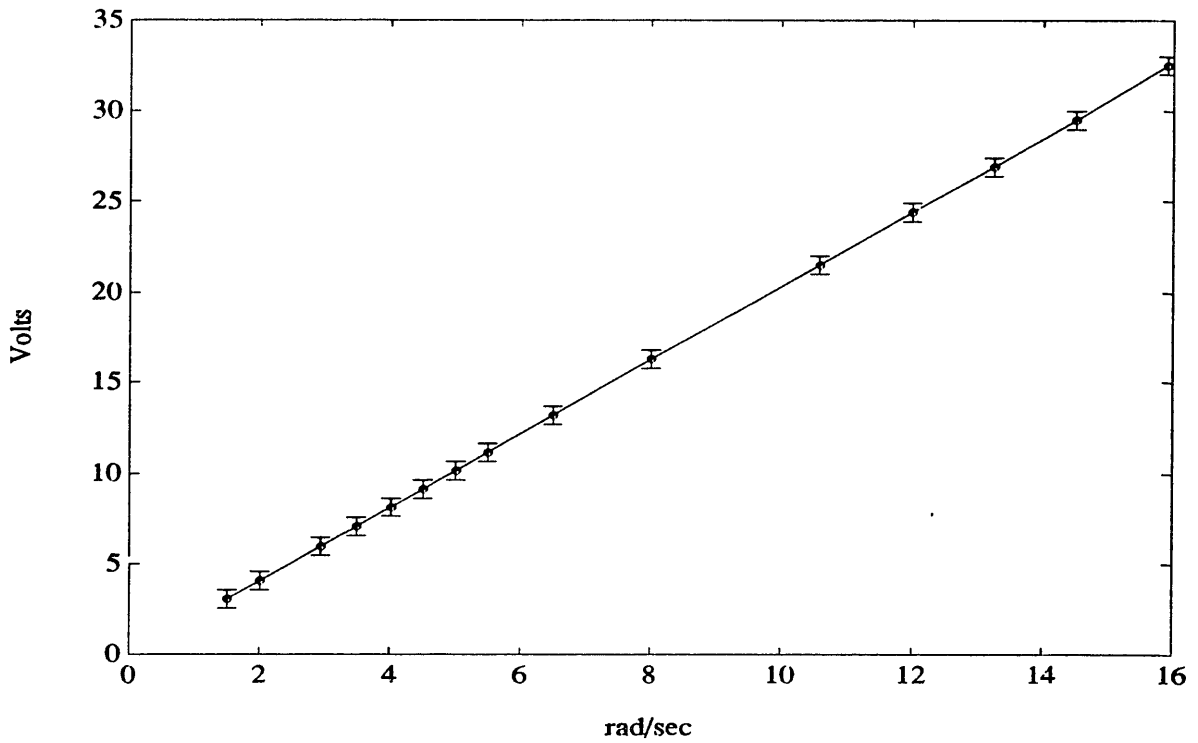
Figure 6.6: Open Circuit Voltage vs Speed
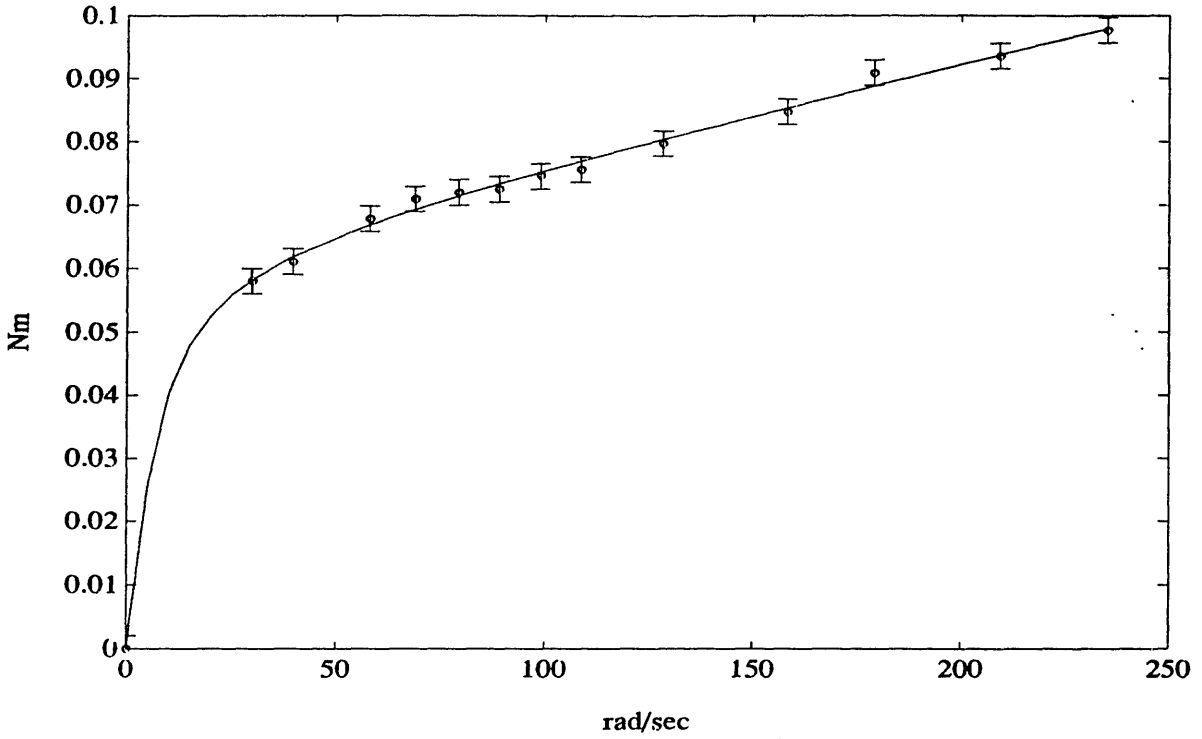
Figure 6.7: Bearing Torque vs Speed
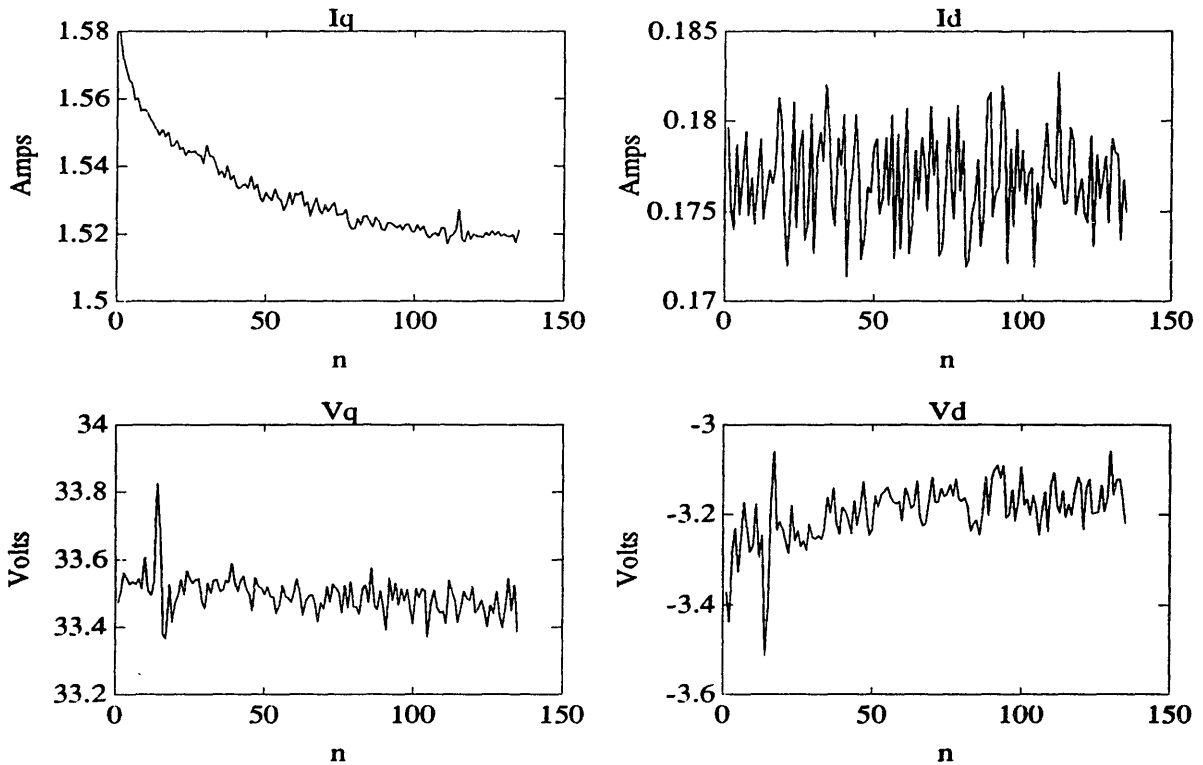
Figure 6.8: (Experiment I) Measured Rotor Frame Variables
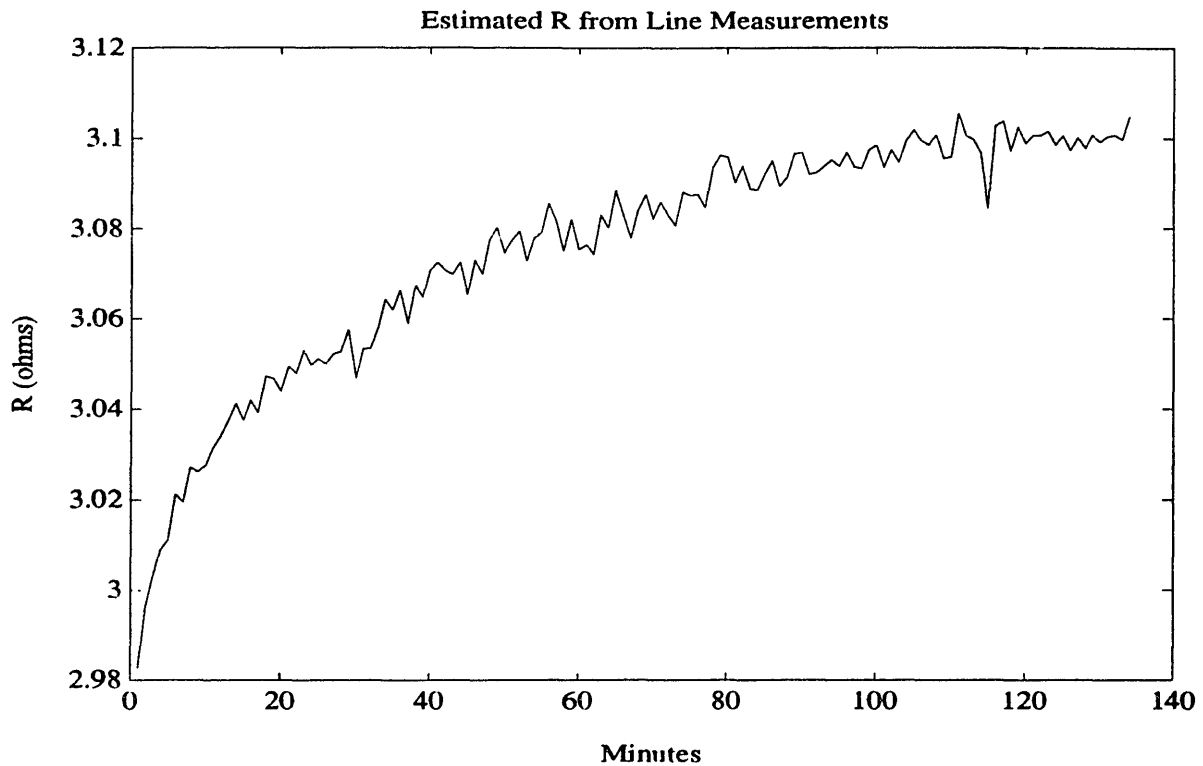
Figure 6.9: (Experiment I) Estimated Values of R From Line Measurements

Figure 6.9 shows the estimated values of R from line measurements only, for every minute. These estimates were obtained by assuming a known constant value of $K = .092V - s/rad$ since this quantity is effectively constant for this motor due to the use of samarium-cobalt magnets in the rotor. Note that all the estimated values are biased above the value of R at room temperature, which is known to be approximately 1.82. However, we are only interested in the relative rises in the values of R since the thermal model is constructed in terms of the relative temperature rises in the motor. Figure 6.10 shows the estimated temperature rise implied by the electrically estimated values of R after the removal of the bias, while Figure 6.11 compares this estimated temperature rise to the actual temperature rises. The actual temperature rises were obtained by interrupting the experiment every 15 minutes and directly measuring R. The period of interruption was so small relative to the time-constants of the thermal system that no noticeable thermal transients were introduced as a result of these interruptions. We observe reasonable agreement within 2 °C between the estimated and the measured temperature rises in the windings. Next, Figure 6.12 shows the performance of the optimal observer in tracking the winding and case temperatures. The initial condition for the observer is $\hat{T} = [3\ 5]^T$, while the initial value of the state is $[0\ 0]^T$; i.e. the motor is initially at room temperature.

The process noise covariance matrix, Q, and the measurement noise covariance matrix, S, were chosen according the observed noise in the respective quantities, to

130
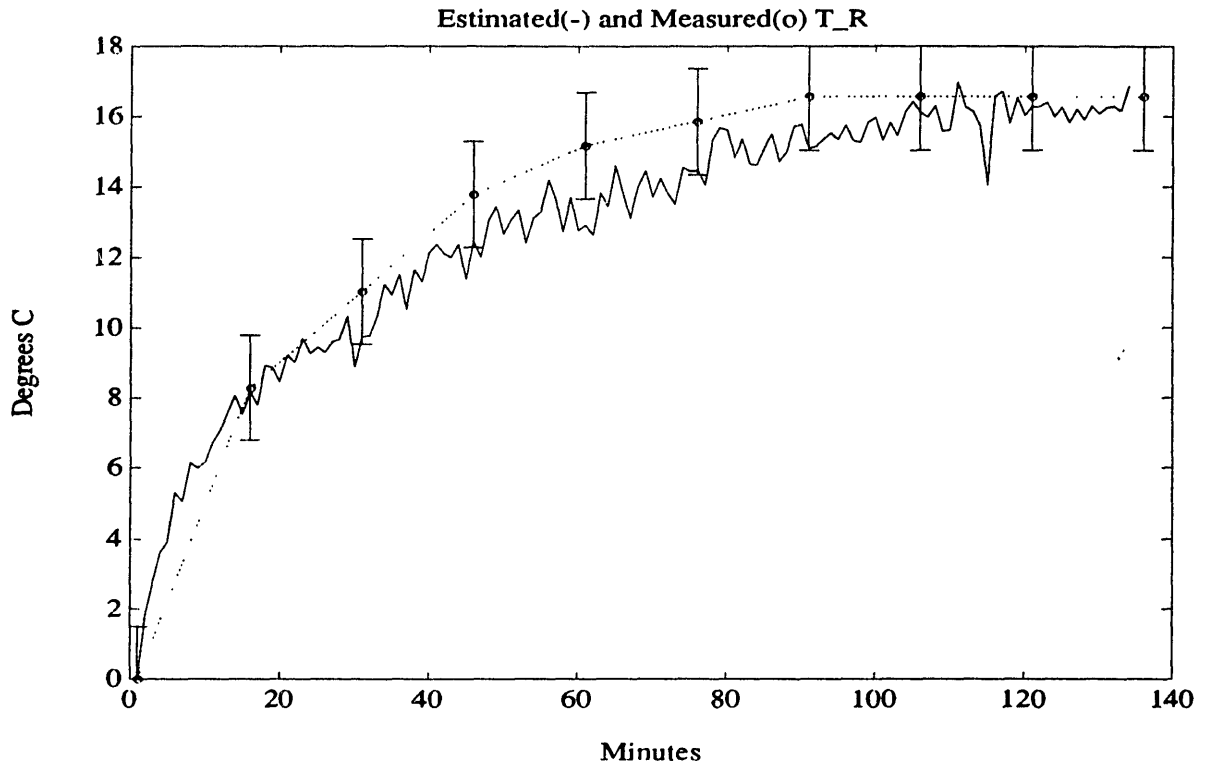
Figure 6.10: (Experiment I) Electrically estimated (-) and actual (o) T_R
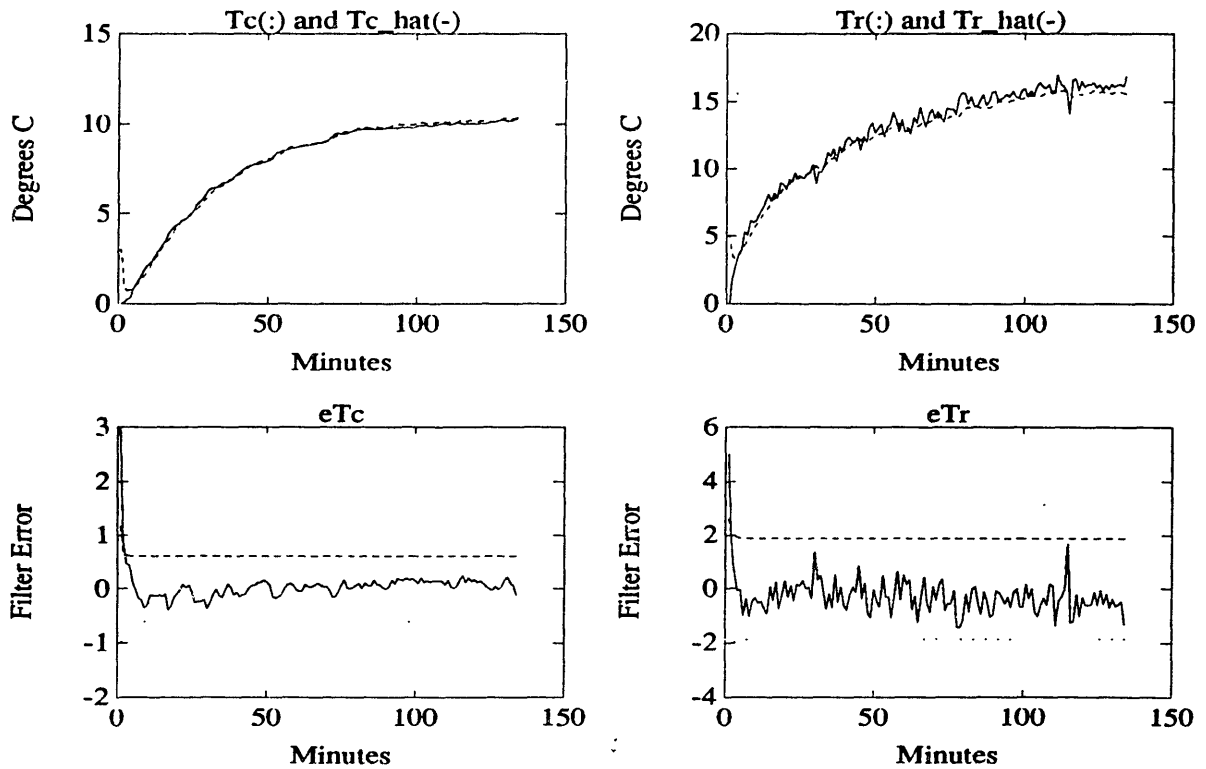
Figure 6.11: Performance of the Kalman filter during Experiment I

131

be

$$S = \begin{bmatrix} 0.2 & 0 \\ 0 & 1.4 \end{bmatrix} (^{\circ}C)^2$$

$$Q = \begin{bmatrix} 0.044 & 0 \\ 0 & 0.121 \end{bmatrix} (^{\circ}C)^2$$

The values for the covariances of the measurement errors in Q were determined by using the degrees of accuracy provided by the measurement equipment while the process noise covariances were empirically derived based on our intuition regarding the size of the unmodeled thermal phenomena in the motor.

From Figure 6.11, we can see that the Kalman filter tracks the (electrically) measured temperature rises quite accurately. The error dynamics of the filter appear to converge to near zero in about 2 cycles, or two minutes. Considering the fact that the slowest time-constant of the thermal system is nearly 40 minutes, this shows excellent convergence. Note that the filter error shows that it is possible to predict the temperatures in the windings and the core to an accuracy of about 2 and 0.5 degrees Centigrade, respectively, at the given speed and torque. This can be seen by observing the 99 percent confidence intervals given by the dotted lines in the two lower graphs of Figure 6.11.

Experiment II This experiment is similar to Experiment I in that no failures are present. However, in contrast to the first experiment, in Experiment II, both the speed and the torque are fixed only for the first 45 minutes at 1500 rpm and 0.18 Nm, respectively. After 45 minutes, they are stepped to 2500 rpm and 0.275 Nm for another 45 minutes, and then finally stepped back down to their original values, as shown in Figure 6.12. The same initial conditions were employed in the observer as in Experiment I. This experiments was performed to establish the fact that the Kalman filter still operates well in tracking more complicated transients.

Figure 6.13 illustrates the measured rotor-frame variables versus time in minutes. These quantities reflect the step changes in the speed and torque appropriately. Figure 6.14 shows the estimated values of R from line measurements while Figure 6.15 compares the estimated temperature rises from these values to the actual measured temperature rises obtained by direct measurement of the average line resistance. Again, good agreement between the two curves is observed. The error bars that appear in this figure reflect the resolution of the ohm-meter used to measure the line

132
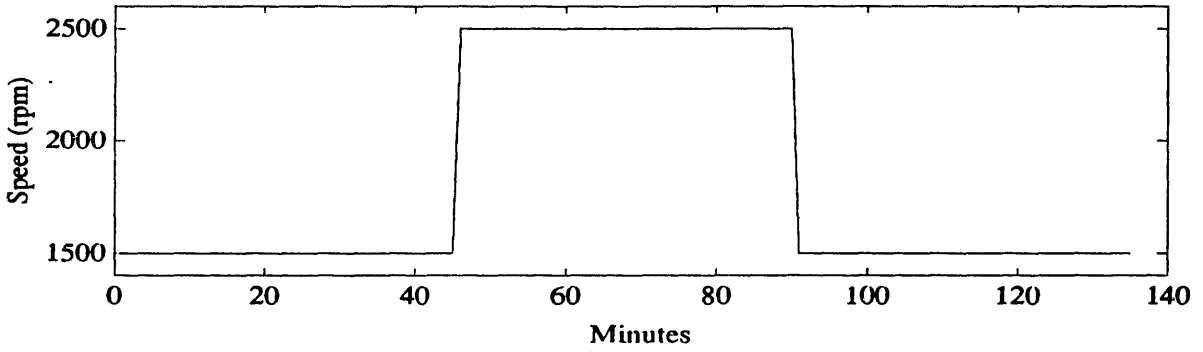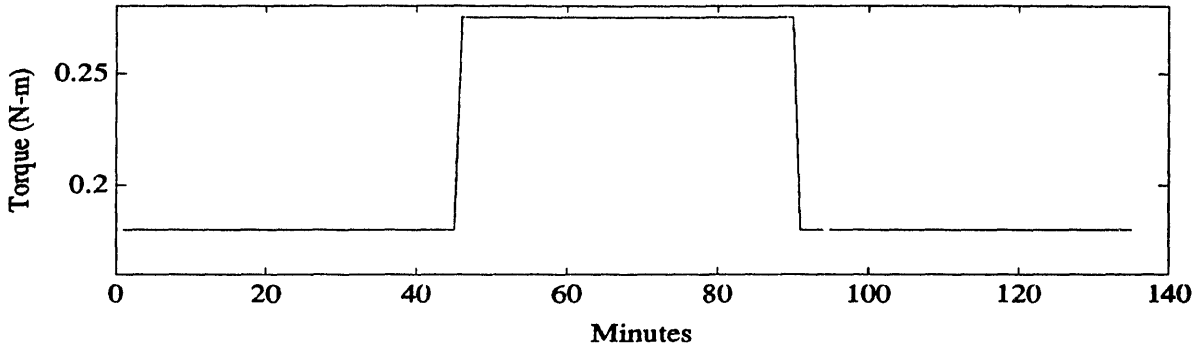
Figure 6.12: (Experiment II) Speed and Torque Transients versus Time
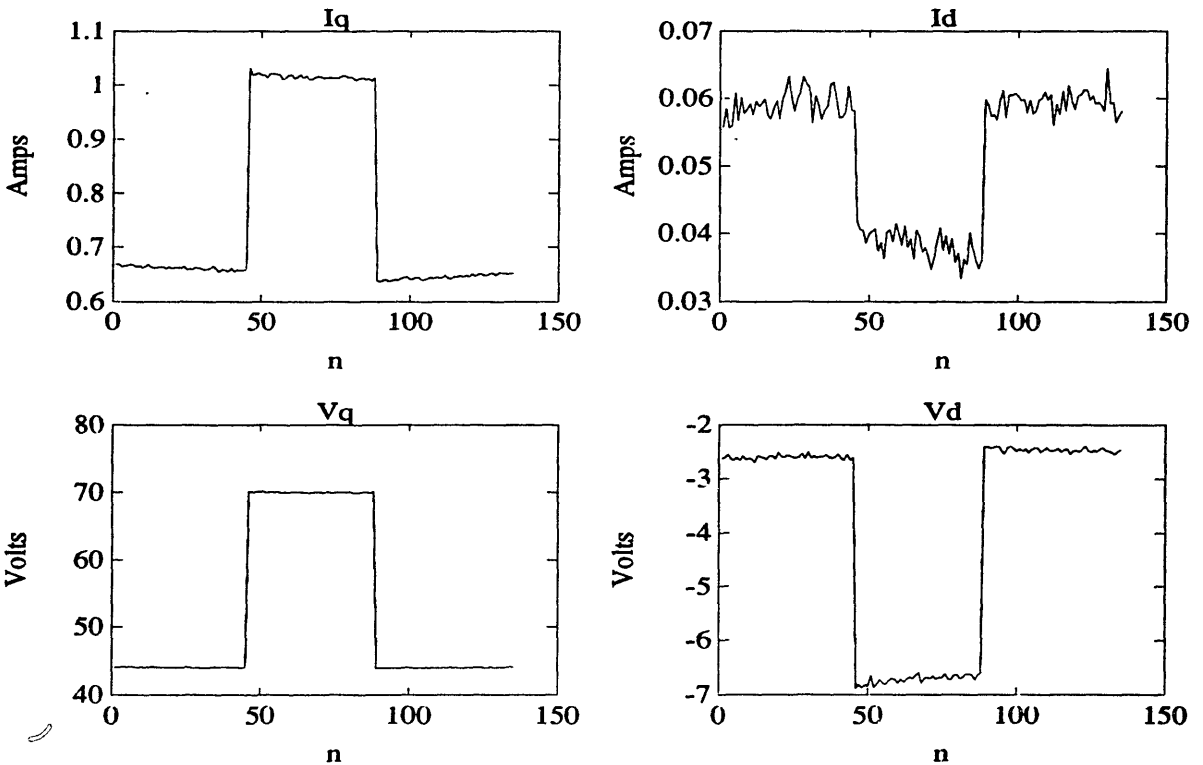
Figure 6.13: (Experiment II) Rotor-frame Variables

133
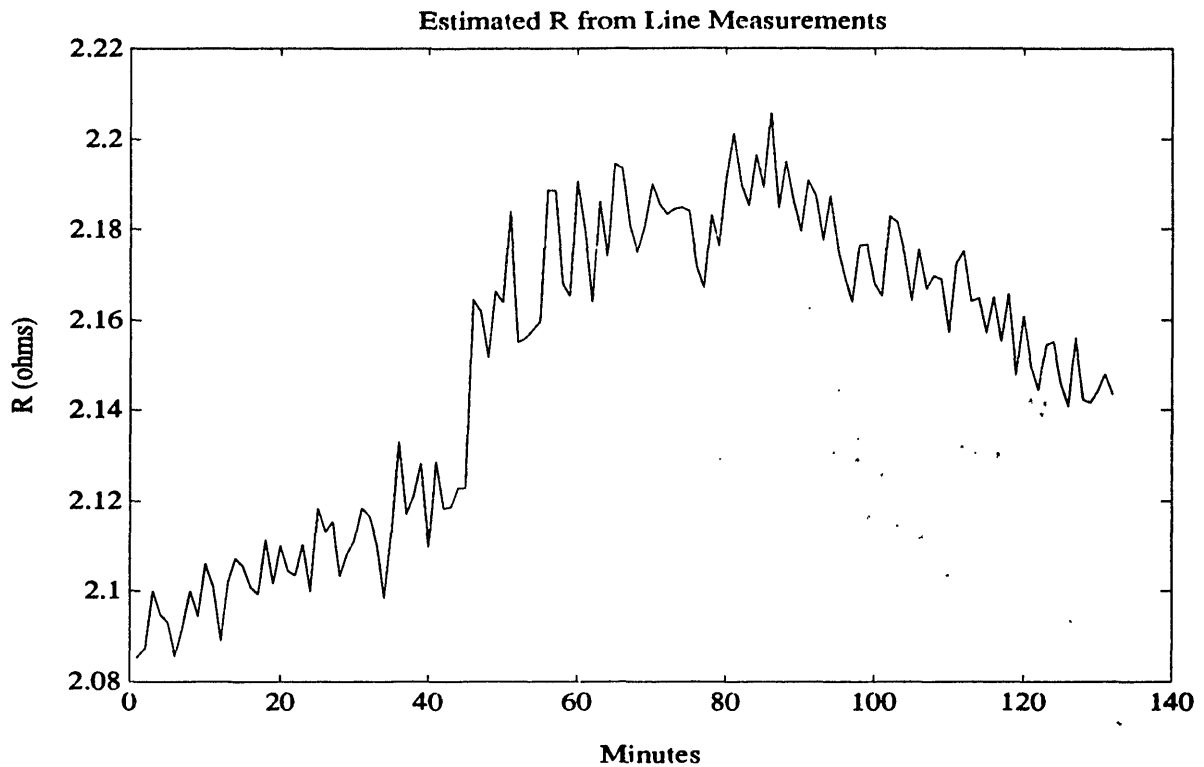
Figure 6.14: (Experiment II) Estimated R From Line Measurements

resistances directly. This resolution is 0.01 Ohms, which translates to about 1.4 °C.

Figure 6.16 illustrates the performance of the Kalman filter in tracking the temperature transients. We can see excellent tracking while it appears that filter noise e_{T_R} is somewhat larger between 45 and 90 minutes. This indicates that the variance of the noise in the measurement of R is larger at higher speeds. We have already described this situation in Chapter 2 where parameter estimation is studied. At higher speeds, the noise in the measurements of the currents and voltages is amplified in the estimation problem due to the existence of multiplicative terms between the currents i_d, i_q, and the speed ω. Hence, an accurate representation of the disturbances would relate the measurement noise covariance matrix to the operating speed of the motor, as we have done in simulations in Chapter 4. In the interest of simplicity, constant values for the process noise covariance matrix Q and the measurement noise covariance matrix S were employed. These values were

$$S = \begin{bmatrix} 0.2 & 0 \\ 0 & 3.5 \end{bmatrix}$$

$$Q = \begin{bmatrix} 0.078 & 0 \\ 0 & 0.2925 \end{bmatrix}$$
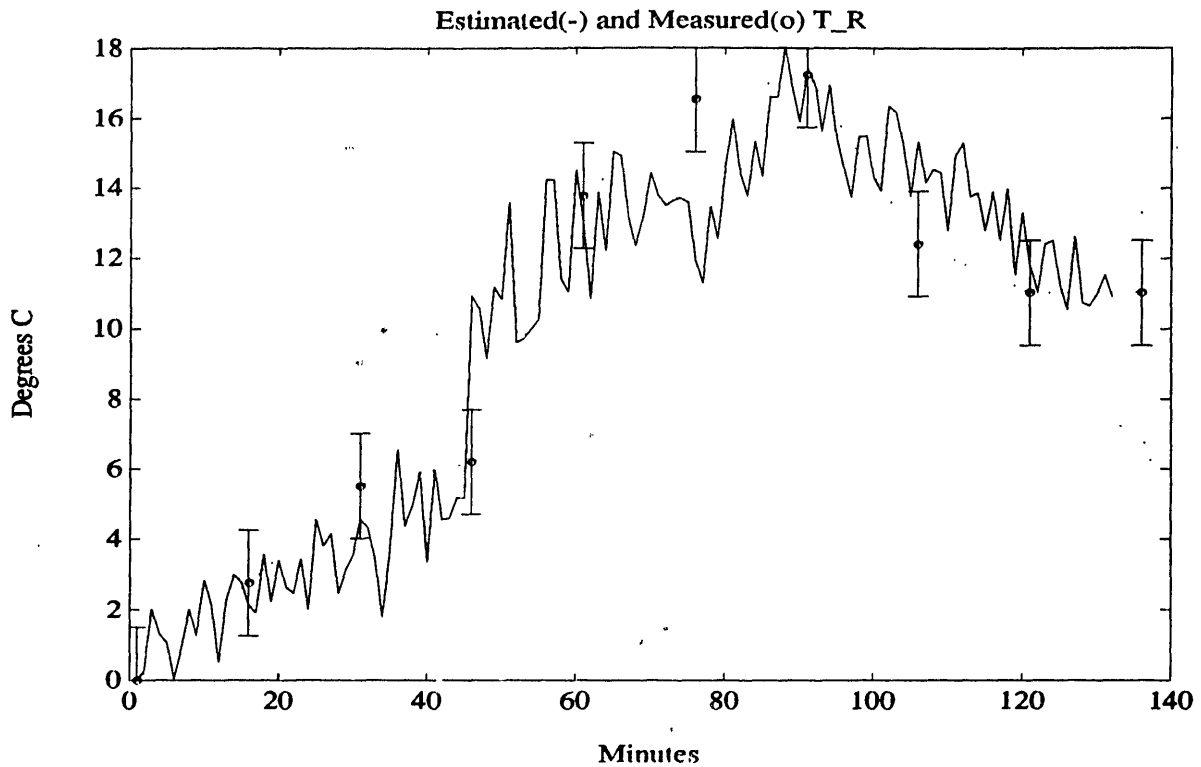
Figure 6.15: (Experiment II) Estimated(-) and Measured(o) T_R

As a result of the exclusion of the speed dependence of the measurement noise, several threshold crossings in the error channel e_{T_R} are observed, which could result in false alarms. To avoid this problem, a filtered version of the error must be monitored rather than the error itself, as described in Chapter 5. Figure 6.17 shows the 20-point median-filtered error e_{T_R}. This figure shows that there are no failures present in this experiments, as is the case.

By carefully choosing the noise covariance matrices, we can see from the observer error covariances that it is again possible to track the temperature of the windings to within approximately 2 °C and the temperature of the core to within 0.5 °C using the Kalman filter.

Experiment III In this experiment, the speed is maintained at a constant level of 2500 rpm, while the load torque is fixed at 0.27 N-m. After 45 minutes of operation, the motor is insulated using multiple with 1 inch of styrofoam and 2 inches of air-cushioned insulating sheets. This induces a thermal failure whose associated event vector is the vector $[0 \ 1]'$, as discussed in Chapter 5. We wish to detect this failure using the techniques described in Chapter 5.

As before, we first present the dq-frame voltages and currents in Figure 6.18. Figure 6.19 shows the estimated values of R from these variables. In Figure 6.20 we present the electrically estimated temperature rises and the actual measured temper-

135
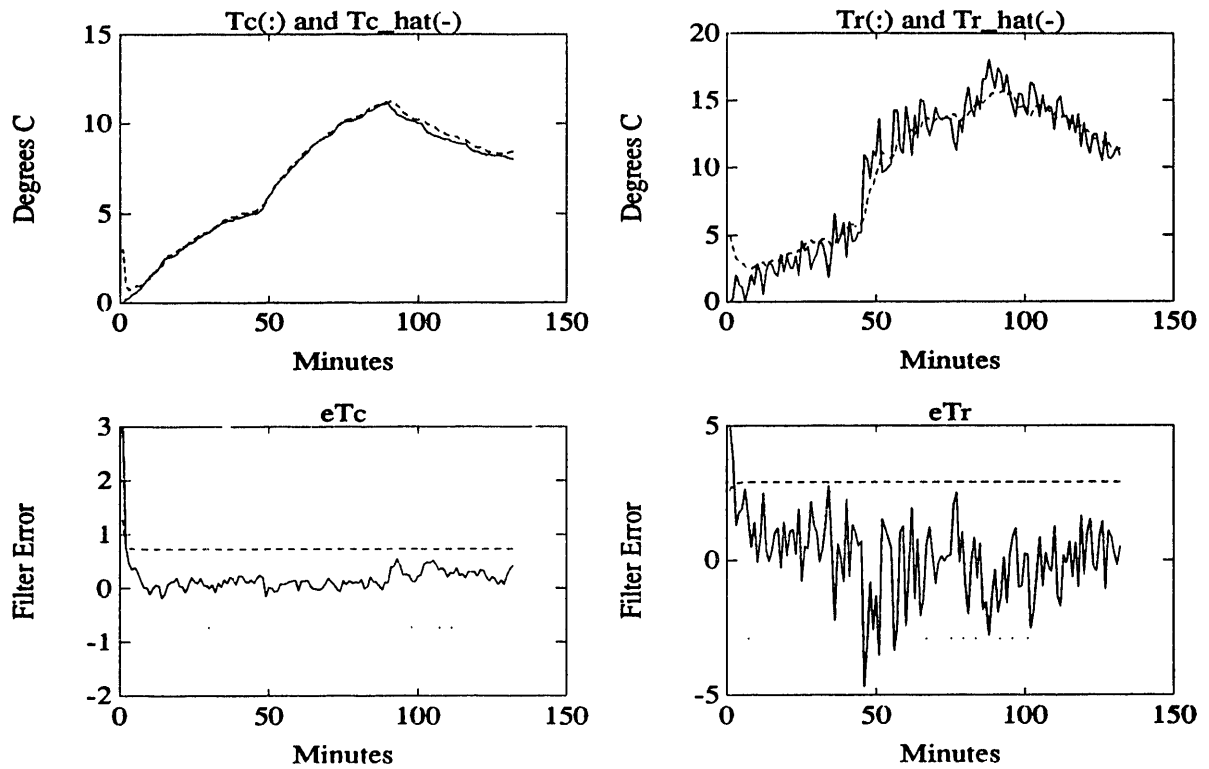
Figure 6.16: (Experiment II) Performance of the Kalman Filter
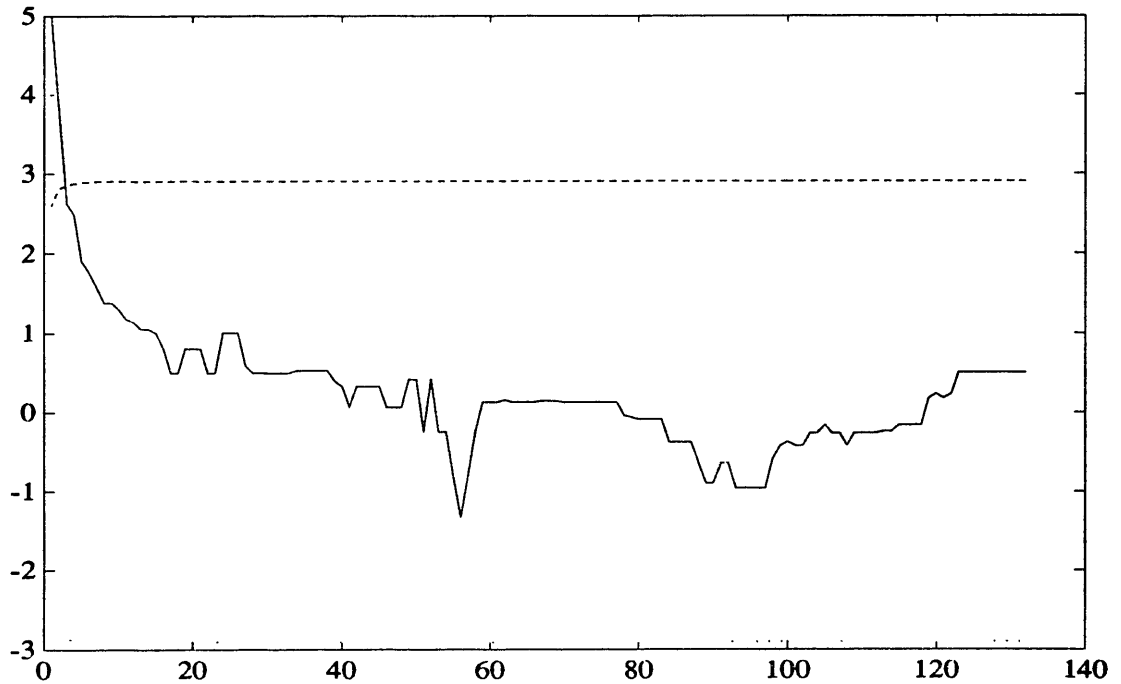
Figure 6.17: (Experiment II) 20-point Median Filtered e_{T_R}
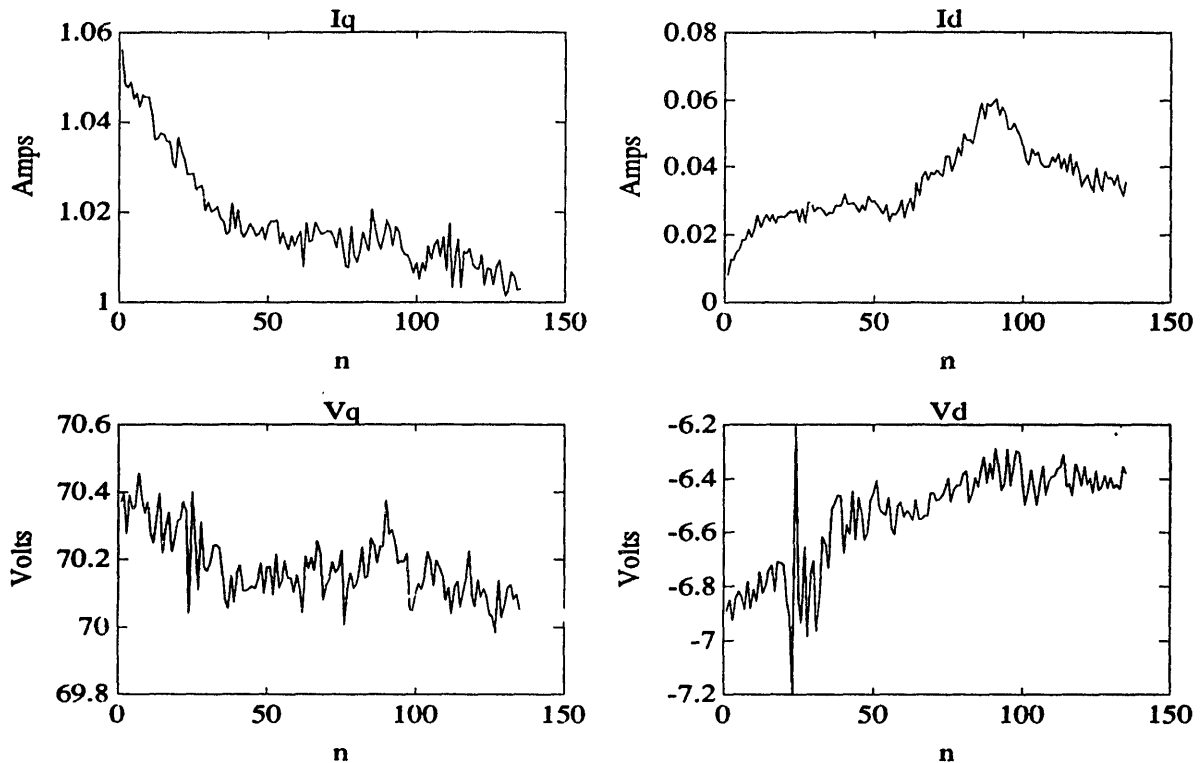
Figure 6.18: (Experiment III) Rotor-frame Measured Voltages and Currents

ature rises in the windings. Good agreement is again observed in this set of data.

Figure 6.21 shows the performance of the failure detection filter, Detector I. The failure is seen to affect the e_{T_R} channel rather noticably as it should. However, the failure appears to also affect the e_{T_C} channel. Eventhough no threshold crossings are observed in this channel, the sudden change in the shape of the error due to the failure must be explained. Theoretically, this error channel is not supposed to be affected at all under a failure that occurs in the direction $[0\ 1]'$, yet a distinct change in the error signal is observed. Two explanations are possible. Firstly, the model of the failure in continuous-time is not perfect. This is to say that the vector $[0\ 1]'$ is an approximation to the actual event vector that describes this failure. Therefore there may be a weak coupling of the event vector into e_{T_C}. Secondly, any event vector associated with a *dynamics failure* (as is the case here) in continuous-time, is mapped to itself in the discrete-time, sampled-data model as discussed in Chapter 5. However, this mapping is only an approximation to what really happens as a result of sampling. Despite the apparent movement, e_{T_C} does not cross the 3σ lines (99 % confidence interval). Hence, the failure detection filter works as advertised. At any rate, the only channel that exhibits a consistent set of points that remain outside the confidence region of the channel is e_{T_R}. To be more precise, one can apply a median filter to the error in this channel, as we have shown in Figure 6.22. The 20-point median filtered error shows the failure, and it is detected at approximately 65 minutes, 20 minutes after

137

Estimated R from Line Measurements
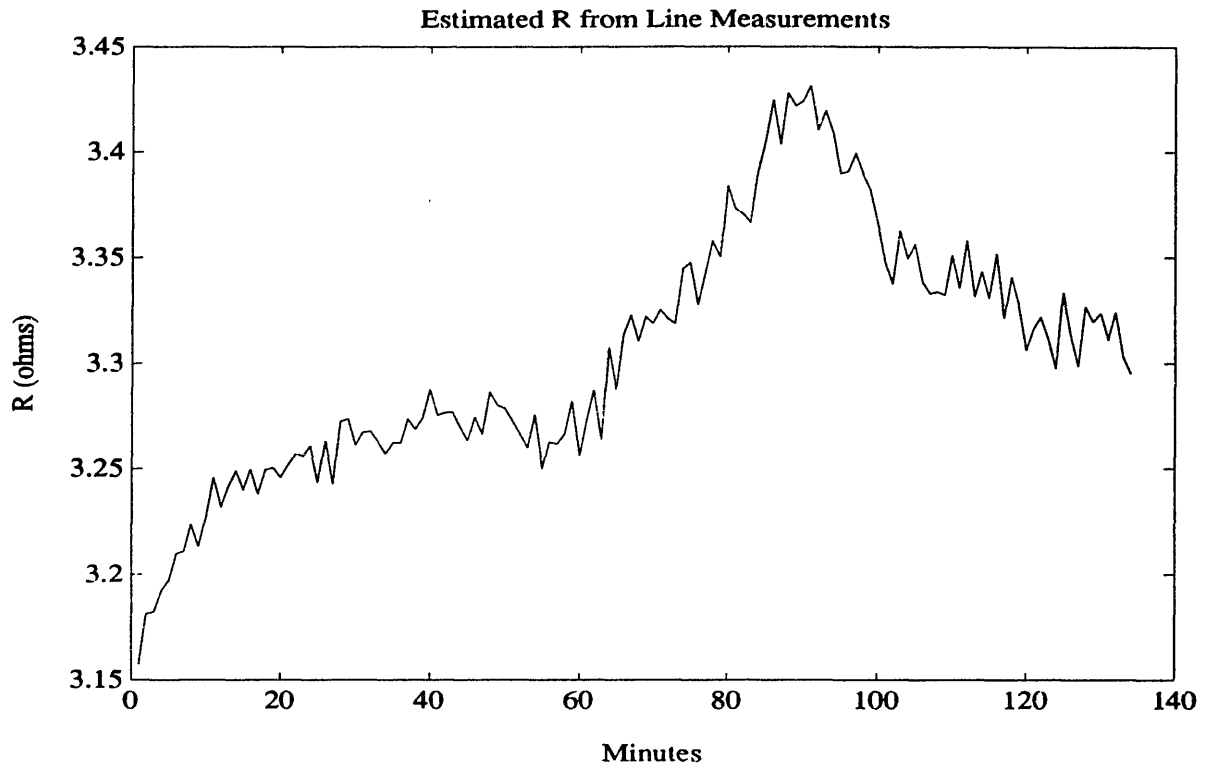
Figure 6.19: (Experiment III) Estimated R from Line Measurements

Estimated(-) and Measured(o) T_R
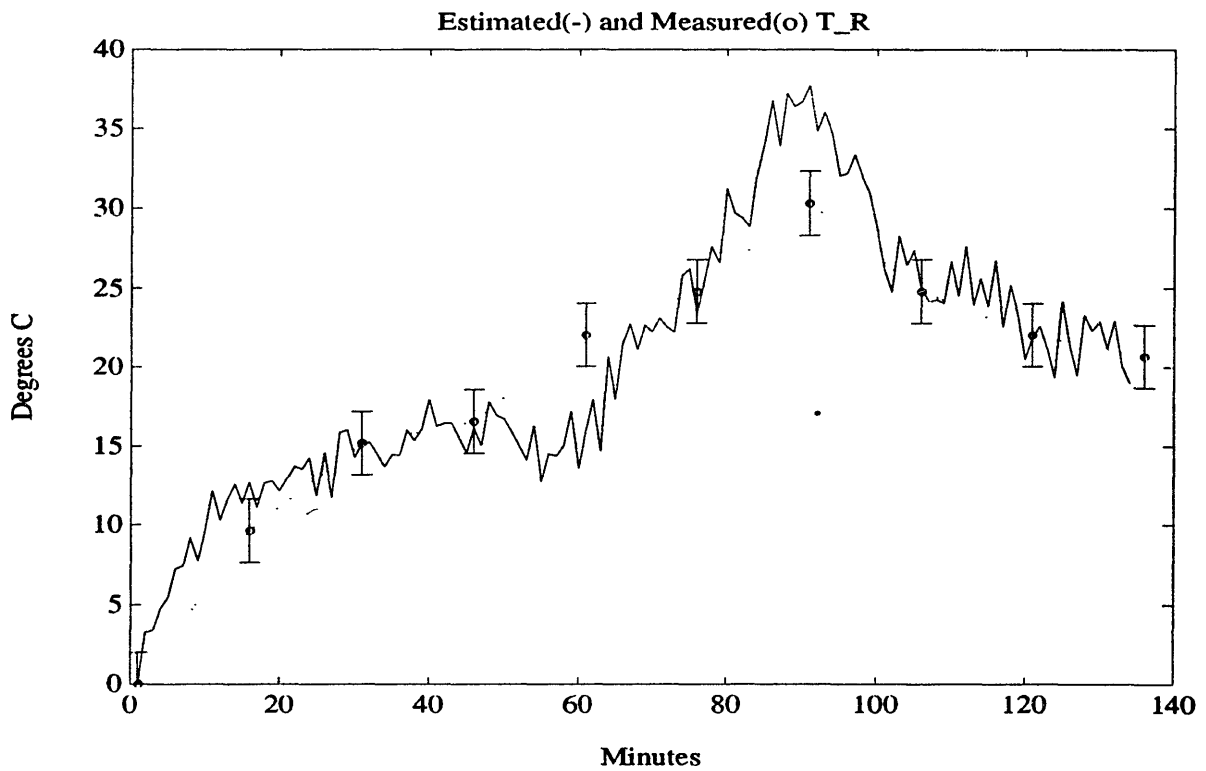
Figure 6.20: (Experiment III) Estimated(-) and Measured(o) T_R
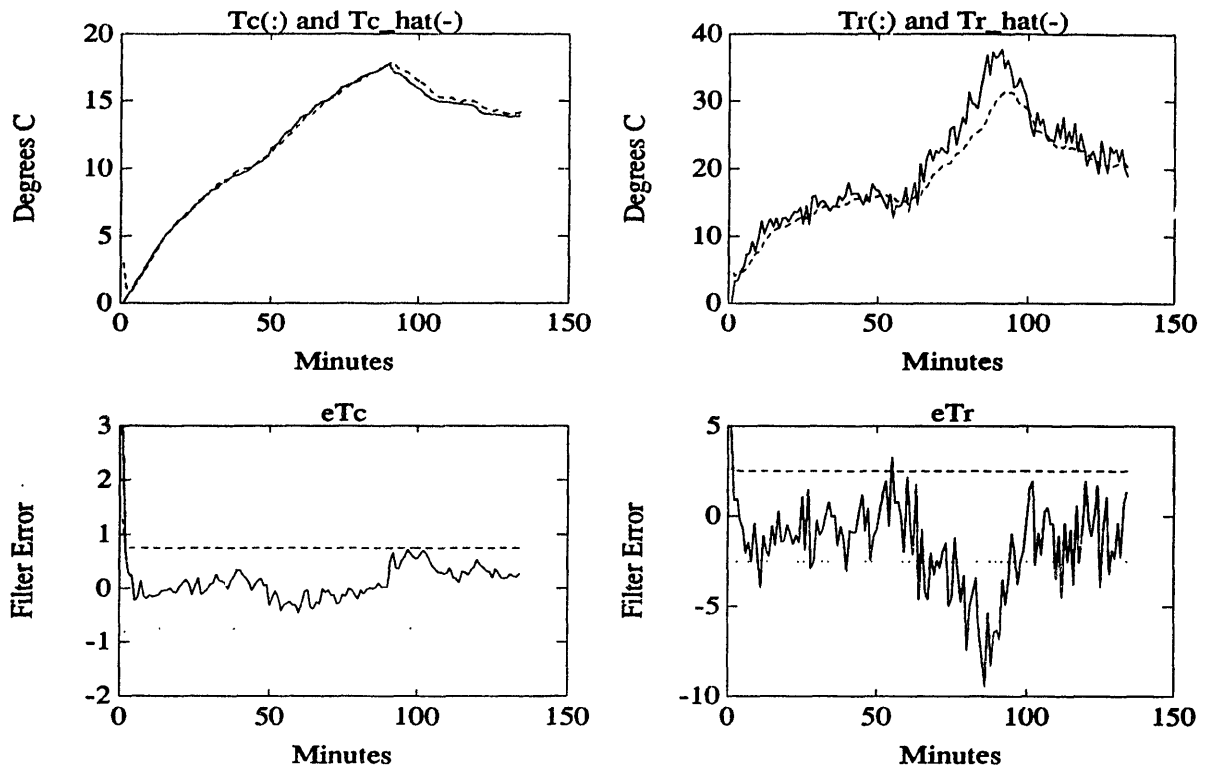
Figure 6.21: Performance of the detection filter/state observer during Experiment III

the introduction of the failure. As discussed in Chapter 5, the failure can be detected earlier (but with less confidence) if the width of the filtering window is reduced. The median filtering applied to e_{T_C} is not shown here since no threshold crossings were observed in this channel.

6.4 Summary

We have shown, through the above experiments, that the average temperature rise in the motor windings can be estimated within 2 °C by way of estimating the winding resistance using noninvasive measurements of the line currents, voltages, speed, and the shaft position of the motor. We have further seen that in the absence of failures, the temperature rises in the windings and the case can be predicted to within 2 and 0.5 °C respectively, using a dynamic thermal model. Most importantly, we have shown that in the presence of a thermal cooling failure, the electrically estimated temperature rises and the thermally estimated temperature rises can be subtracted to produce residuals that drive the proposed failure detection system. This failure detection system is shown to have successfully captured an induced insulation failure.
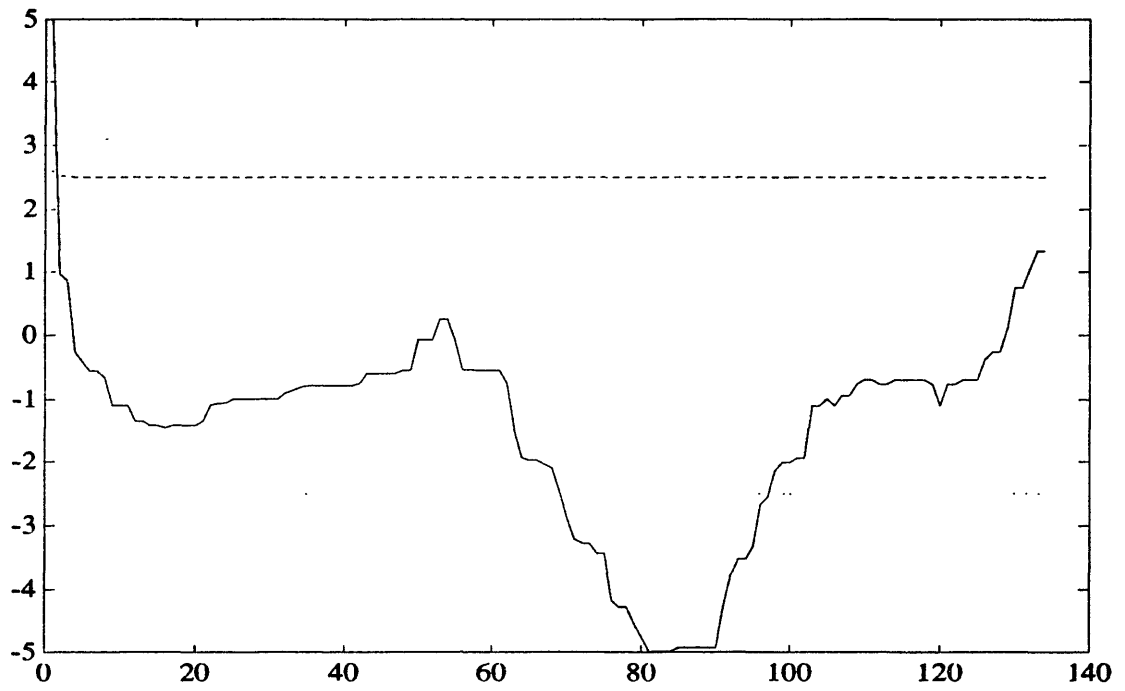
Figure 6.22: (Experiment III) 20-point Median Filtered e_{T_R}

Chapter 7

Conclusion

7.1 Summary

In this thesis, we investigated the problem of monitoring failures in small permanent-magnet synchronous motors. Detecting a failure of the physical makeup of the motor after one has occurred has been only a secondary goal in our work. Instead, we have concentrated on detecting anomalies in those conditions that may cause an actual failure in the motor. Specifically, we have concentrated on monitoring the behavior of the thermal dynamics of the motor since many physical failures in these motors arise from thermal overload. By developing a model of the thermal behavior of the motor, we have designed a system that monitors the progress of these thermal dynamics and declares any anomalies in the development of these dynamics as *failures*. Thus, failures of the thermal system are indicative of abnormal thermal behavior that may lead to physical breakdown in the motor if appropriate actions are not taken to correct these anomalies. Hence a failure detection filter for the thermal system of the motor is in actuality a failure prevention system for the physical parts of the motor that are affected by heat. These parts include the stator windings, the permanent-magnets, and the bearings.

The failure monitoring system developed here combines physical models of the motor, which include failure mechanisms and symptoms, with the estimation of parameters within the models. Variations of the parameters are used as means of measuring temperature rises within the motor. These temperature rises are also estimated independently using a thermal model of the system. Combining these two methods in a closed-loop observer forms the basis for a thermal observer which guides failure prevention and detection.

Invasive methods of measuring temperatures inside a motor are not desirable since they not only complicate the motors' manufacturing process, but are, in many instances, impossible due to the geometry and size of the motor in question. Hence, alternative ways need to be developed for monitoring these temperatures. Using the electromechanical model of the motor, as developed in Chapter 2, we have developed algorithms to estimate the average winding resistance and the magnet strength from a sequence of voltage, current, and shaft position measurements (Chapter 2). The temperature dependencies of winding resistances and the magnet strength were then studied (Chapter 3), and hence average temperatures inside the motor were estimated noninvasively through a sequence of current, voltage, and position measurements alone.

As an alternative method of estimating temperatures inside the motor, in Chapter 4, a dynamic thermal model was developed for the experimental motor in question. This model is general enough that it may be employed for many permanent-magnet synchronous motors. The model takes into account the major sources of heat-loss in the motor as inputs, and has the temperature of the windings and that of the case of the motor as state variables. Given an initial condition, this model produces estimates of these temperatures given a set measurements of the speed and currents in the motor alone.

By combining the electrically and thermally estimated parameters in a closed-loop observer that is a Kalman filter, we have designed an observer that is capable of tracking the average temperature in the windings to within 2°C. This observer is also capable of tracking the average temperature of the surface of the motor to within 0.5°C.

Another contribution of this thesis and the intended goal of this thesis was to combine the above two methods (Chapter 4) for estimating the temperatures inside the motor and use the difference between the respective estimated temperatures as a basis for detecting anomalous behavior in the thermal dynamics of the motor (Chapter 5). In Chapter 5, a geometric approach to failure detection was studied based on the work of Jones [13]. In this approach, residuals are generated by subtracting the electrically estimated temperatures (state observations) from those produced by the thermal model (state estimates). These residuals are then used to drive a close-loop observer which is based on the thermal model of the motor, and which is, by design, capable of amplifying residuals due to failures and suppressing those due to stochastic sources such as measurement and process noise. Failures are then detected

by observing the magnitude of the residuals and the directions in which they develop.

7.2 Conclusions

7.2.1 General Conclusions

Both general conclusions regarding the problem of failure detection for motors and specific conclusions regarding monitoring thermally related failures in permanent-magnet motors can be derived from the work presented in this thesis. So far as general conclusions are concerned, the following categorization is useful.

1. Failure detection systems are classically designed around those components of a system that are most likely to suffer breakdowns. Philosophically, it seems reasonable that, if possible, one should also invest in the design of failure *prevention* systems that monitor the progress of those factors that are most likely to *cause* a failure. Interestingly enough, the design problem is almost identical to that of a failure detection system, except that an alarm in a failure monitoring system serves as an indicator that a physical failure will take place and that appropriate corrective measures should be employed. In specific, so far as motors in general are concerned, a detection system built around the thermal model of the motor may, in fact, be capable of both prevention <u>and</u> detection of failures induced by thermal overload. The detection systems proposed in this thesis are capable of detecting "hard" failures such as winding shorts and opens, demagnetized magnets, and bearing failures. If the speed of the response of these systems is not acceptably fast for detecting failures after the fact, the line voltages and currents can be used directly to monitor these failures via simple hypothesis testing techniques.

2. Thermal models provide an efficient way to monitor the operation of any motor. Using these models is beneficial not only to the consumer, but also to the manufacturer in the design process. These models can be used to test a prototype motor to assure that it is compliant with the manufacturer's standards. Steady-state thermal models provide a direct way to produce thermally dependent torque-speed curves that characterize the limits of safe operation for a motor. Limits of stability of the thermal model of a motor can also be used to indicate upper bounds on the magnitudes of the currents and voltages that the motor is capable of operating under without damage.

7.2.2 Specific Conclusions

So far as specific conclusions regarding small permanent-magnet motors, and, in specific, our experimental motor, are concerned, the following points are worth underscoring.

1. In Chapter 2 of this thesis, we have established algorithms for estimating the average winding resistance and the permanent magnet strength. As we have seen, for small permanent-magnet motors that use hard magnets such as samarium-cobalt, which are very insensitive to variations in temperature, it is difficult to detect thermally significant variation. In this case, it is useful to assume a constant value for the magnet strength, and estimate the winding resistance only. This improves the accuracy of the estimation process and yields more realistic temperature values. If a different type of magnet is used or if it is imperative that both parameters be estimated simultaneously, special care must be taken to ensure that the estimation problem is not ill-conditioned. This situation arises when the motor is under closed-loop control action which tries to drive the direct axis current (i_d) to zero. The condition number of the least-squares problems worsens as the direct-axis current is driven to zero. A possible solution to this problem may be to inject enough i_d, for a short period of time to improve the condition of the estimation problem, and then drive i_d back to zero once sufficient data has been collected to support accurate estimates of the desired parameters. This approach has the clear disadvantage that the temperatures in the motor rise as a result of increased i_d. However, this effect can be kept to a minimum by injecting a sufficiently small i_d only when new estimates of the parameters are desired.

   We have also observed that the estimation problem is more sensitive to noise in the current channels rather than the voltage channels. This is fortunate since the voltage channels are usually more noisy than the current channels. However, special care must be taken so as to minimize the noise in the current channels, especially if i_d happens to be small. Careful modeling of any delays in the analog input channels for the currents and voltages must be done since small delays in these channels can result in severely biased values for the currents and voltages in the rotor frame. This follows from the fact that the Blondel-Park transformations will yield correct results only if the samples of currents, voltages, and shaft position are taken synchronously.

The estimation problem worsens at higher speeds as we have shown in Chapter 2 due to the existence of nonlinear terms in the electrical equations of the motor that involve the currents in the rotor frame, and the speed. Any noise in the values of i_d and i_q is amplified proportionally to the speed of the rotor ω. Hence, if at all possible, the estimation problem should be performed at lower speeds. At higher speeds, worse estimates of the parameters of interest can be expected. Clearly, one does not want to perform the estimation problem using data from the operation of the motor at very low speeds since this data may not be sufficiently rich to support an accurate estimate of the parameters of interest. The optimal situation seems to be one where the speed of the motor is in its intermediate range (between 1000 and 2000 rpm) while a fairly large load torque is applied to the rotor. In this case, fairly large quadrature currents are produced while the speed does not amplify the noise in these currents significantly.

2. A thermal model of the motor was constructed constructed in Chapter 4 by measuring the input-output characteristics of the thermal system. The thermal model was developed in terms of temperature *rises* rather than absolute temperatures. This has the advantage that the descriptions of the input to the system are simpler, and that only relative values of the estimates of R are necessary to identify the model, hence a biased sensor (estimator) is not a problem. The states of the thermal system were chosen to be the average temperature rise of the windings and the temperature rise of the case of the motor. The input-output map for the temperature rises in the magnet was not accurately measurable due to the insensitivity of the magnet strength to temperature. Hence, this quantity was not included as a state variable. The outputs of the plant describing the thermal system were the same as the state variables.

The inputs and the outputs of the thermal system were directly measured in experiments and the plant was identified through a constrained least-squares technique. The system identification problem was constrained since the dynamics of the thermal system were known to be described by a stable, non-oscillating dynamic system. These dynamics would necessary imply that the dynamic matrix A obtained in the identification process must be an *M-Matrix* for any stable operating conditions of the motor. Furthermore, an additional constraint must be imposed on the input matrix B since all the inputs (heat sources) have a positive action on the dynamics of the thermal system. That is, no source of heat in the motor ever contributes to the cooling of the motor. Using the

steady-state description of the thermal system, this constraint effectively translates to the fact that the matrix $-A^{-1}B$ must have all positive elements. The identification process here yielded a plant that complied with both of the above constraints. It is interesting to note that the general form of the thermal model introduced in this work assumes only knowledge of the values of the average winding resistance and the magnet constant at a reference temperature which can be conveniently taken to be the ambient room temperature in which the motor resides. Using the thermal model developed for the experimental motor, we determined limits for the safe operation of the motor that agreed closely to those provided by the manufacturer. The steady-state model of the thermal system was then used to identify thermally dependent torque-speed curves for the motor. These assist the manufacturer in determining more realistic limits for the safe operation of the motor. Finally, the identified thermal model was cross-checked against several consistency arguments to assure that it is both realistic and accurate.

3. As shown in Chapter 4, to incorporate the measurements of temperatures in the motor and those obtained from the thermal model, a closed-loop identity observer was designed using a Kalman filter based on the thermal model. Two designs were presented for the observer. In the first design, a Kalman filter was designed to track the states of the thermal system. In the second approach, the design was modified so as to adaptively cancel the time-varying nonlinearities from the observer error dynamics. In this way, an identity observer was designed for the nonlinear thermal system such that the error dynamics were linear and time-invariant. The performance of these two designs was compared via simulations and it was established that the first design worked best, as expected. However, it was noted that the second design is very nearly optimal in the particular case of the motor under study. These observers served as building blocks for the failure detection systems to be designed.

4. The solution to the failure detection problem, as discussed in Chapter 5, was obtained using a geometric approach where the output error due to a failure is forced to move in a fixed direction in the output space by appropriate choice of gain for the underlying observer. This approach exploits the structure of the Kalman filter and provides for a very simple detection law for declaring failures. The advantages of the geometric approach over more stochastically

oriented ones is the ease of implementation and the ability to isolate failures rather than declaring that *some* failure has taken place. A model is constructed for every failure of interest and then a failure detection system is designed for each particular failure. It is shown that in some instances, it is possible to detect several failures simultaneously. By construction, it is seen that the proposed failure detection scheme is incapable of distinguishing failures whose associated event vectors lie in the same direction. However, if the "size" of the two failures are sufficiently different (i.e. the two failures give rise to errors with significantly different magnitude in the output space), these failures may be distinguished on the basis of their associated magnitudes in the output space. In this thesis, we have not concentrated on this aspect of failure detection.

Two designs were developed for detection filters based on the two observer designs presented in Chapter 4. According to simulations, both performed well while the detection filter based on the exact optimal Kalman filter displayed better state tracking in the absence of failures, as expected. Both detection filter designs were implemented in discrete time using sampled-data models of the thermal system. The concepts of geometric detection theory were shown to be applicable to sampled-data systems, given some simplifying assumptions. Explicit expressions were derived for the mapping of event vectors from a continuous model to the corresponding sampled-data model. These expressions were used in the implementation of the discrete time detection filters. The problem of designing detection filters for stochastic systems was shown to be essentially equivalent to the problem of choosing a gain that would yield desirable error dynamics, and yet maintain the failure detection properties. A solution was provided by making use of the eigenvalues provided by the Kalman filter. It was noted that since the system being observed has dynamics described by an M-matrix, that the Kalman filter provides error dynamics that are exponentially stable. Hence, the time-varying error dynamics have real, negative eigenvalues at each instant in time. This property allowed us to directly use the eigenvalues of the error dynamics provided by the gain to assign the eigenvalues of the detection filter error dynamics. The eigenvectors of the detection filter error dynamics were chosen to point in the direction of the desired error vectors. Although this method does not satisfy any optimality conditions, it provides a time-varying way of assigning eigenvalues for the detection filter, and most importantly in our case, it seems to work well as supported by simulations. Using

some results presented in Appendix A it can be shown that the detection filter designed in this way is exponentially stable.

A detection law based on the estimation error covariances generated by the Kalman filter was established to quantify the way in which failures are to be declared. This detection law is described in terms of a moving window that travels forward in time with incoming data points. The window is rectangular and contains information regarding the confidence region of the estimation errors in each error channel. The length of the window defines the degree of smoothing desired on the estimation errors and is inversely proportional to the probability of declaring a false alarm, while the height of the window describes the confidence region in which the estimation error should lie in the absence of failures and it is also inversely proportional to the probability of declaring a false alarm. Through simulations, the detection law is shown to be an effective way of deciding whether a failure has occurred or not.

5. In Chapter 6, results of physical experiments were presented to show that the concepts developed in Chapters 2 through 5 are effective in practice. It was shown that it is possible to estimate the average winding resistance accurately enough for the purpose of estimating temperature rises in the windings, using line current and voltage measurements only. Hence, temperature rises in the motor can be estimated noninvasively. The estimated values of R are usually biased so given the parameter estimation methods presented in this thesis, one can not reliably update a closed-loop controller for the motor using the estimated parameters. However, if the ambient temperature is known accurately, and is maintained fixed, the bias in these estimates may be removed by converting R into temperature rises, then calibrating these temperature rises to the ambient temperature, and solving back to find the actual, unbiased values of R.

The Kalman filter structure designed to track the temperature rises in the motor is shown to function effectively under both constant operating conditions and transient behavior of the thermal dynamics. The failure detection system based on this observer design is shown to effectively detect a cooling failure induced in the motor. It was shown that the average temperature rise in the windings can be tracked to within 2 °C, while the average temperature rise in the case can be tracked to within 0.5 °C. Using a 20-point median filtre, the failure detection

148

system was shown to successfully detect a cooling failure in the motor within 15 minutes of the start of the failure. This is sufficiently faster than the dynamics of the failure so that the failure can be declared before serious damage is done to the motor.

6. It is important to underscore the importance of the techniques developed in this thesis from the viewpoint of safety. The failure detection system not only serves to prevent and detect physical failures in the motor, but also serves as an indicator of the safe operating limits of the motor. In addition, the limits of stability of the dynamic thermal model indicate the largest currents under which the motor can operate safely, while the steady-state thermal model yields temperature dependent torque-speed curves that determine the safe operating limits of the motor.

7.3 Recommendations for Further Research

Several paths exists for further exploration of the concepts studied in this thesis. The first of these concerns parameter estimation. As we showed in Chapter 2, the parameter estimation problem studied here differs from a standard linear least-squares error problem in that in our framework, the relation $Ax = B$ involves noise in both matrices A and B. A standard linear least-square error problem assumes noise only in the matrix B. There exists a technique for dealing with the general case when there is noise in both A and B. This technique is known as *Total Least Squares* (TLS) and is described in [36, 9]. This technique could be potentially used to produced better estimates of the desired parameters. The method is basically based on the singular value decomposition of the block matrix $[A|B]$, and is hence numerically efficient. However, there is no recursive formulation for this method. Only batch estimation has been studied to this. TLS is a fairly recent discovery, and therefore the statistical properties of an estimator using this technique have not been characterized. It is, however, known that in the presence of noise in both A and B, TLS works better than ordinary least squares in solving overdetermined sets of linear equations.

The second recommendation for further work involves more detailed modeling of the thermal system of the motor. Our model is built upon average temperature rises in the motor. Since sensors buried within the core of the motor are not available, this model does not include phenomena such as hot spots in the windings. A more accurate representation of the thermal system would include such phenomena, leading to a more detailed model of the thermal behavior of the motor that could, in turn, serve as a basis for detecting a wider class of thermally induced failures.

The effect of significant changes in the magnet strength K deserves further attention. This effect couples the inputs to the thermal system to the states in a nonlinear fashion. Hence, if K is sufficiently sensitive to temperature, contrary to the case studied here, the effect of this change on the model can not be ignored.

Insofar as the observer design problem is concerned, the algorithms presented in this thesis can be modified to include more complicated models of the measurement process. What we have termed "direct measurement" of the average winding temperature is actually obtained through estimation of the average winding resistance R. The dynamics of the estimation process may be included in the description of the output equation that relates the states to the outputs of the thermal system. In our treatment, this mapping was simply taken to be the identity matrix. The outputs

and the states were the same. More accurate modeling of the statistical properties of the noise processes in the measurements and the effect of the dq-transformations on these also deserve further attention.

The failure detection schemes presented in this thesis may be extended in several different directions. To begin, a careful treatment of the geometric detection problem for time-varying systems can be pursued. In light of the fact that powerful statistically based methods are available for failure detection in these systems [40], the practical value of developing geometric approaches to the problem remains questionable since output-decoupling for a time-varying system is an extremely complex problem. A second extension to the ideas presented here maybe a more careful look at the failure detection problem for sampled-data, and discrete-time systems. The approach in this work as in [13] has been to study the problem as a corollary of the detection problem for continuous-time systems. However, it seems reasonable that one may be able to develop techniques that are specialized to the discrete-time case and provide more direct and accurate treatment of the problem.

It also appears useful to compile a catalog of all possible failures of a motor and their associated event vectors. In this way, one can easily decide which are mutually detectable, and hence the detection filter design problem is considerably simplified. Given this catalog, an efficient, comprehensive failure detection system may be designed to monitor every aspect of the operation of the motor.

Appendix A

Some Theoretical Results

Some results presented in this appendix rely on facts as presented in [42, 15, 26, 33, 18, 6, 25, 2, 21, 14, 38, 29]. The references are of a general nature and they have not been specifically cited elsewhere in this thesis.

A.1 Approximation Lemmas

The following lemmas prove the validity of the approximations used in Chapter 4 and 5.

Lemma 1 *Given an $n \times n$ real matrix A, for sufficiently small perturbations E, and a sufficiently fast sampling period t_0, we have:*

$$e^{(A+E)t_0} \approx e^{At_0} + Et_0 \tag{A.1}$$

Proof: We can write

$$
\begin{aligned}
e^{(A+E)t_0} &= I + (A + E)t_0 + o(t_0) \\
e^{At_0} &= I + At_0 + o(t_0)
\end{aligned}
$$

which yields

$$e^{(A+E)t_0} = e^{At_0} + Et_0 + o(t_0) - o(t_0) \tag{A.2}$$

Hence, for sufficiently small t_0, the result follows asymptotically.

Lemma 2 *The following gives a bound on the above approximation*

$$\|e^{At_0} + Et_0 - e^{(A+E)t_0}\| \leq \|E\|t_0(1 + M^2(t_0)e^{M(t_0)\|E\|t_0}\|e^{At_0}\|) \qquad (A.3)$$

where $M(t_0) = \sum_{k=0}^{n-1} \frac{\|Nt_0\|^k}{k!}$ *and* $Q'AQ = \Sigma + N$ *defines the Schur decomposition of* A *by* Q.

Proof: From the triangle inequality we have:

$$\|e^{At_0} + Et_0 - e^{(A+E)t_0}\| \leq \|e^{(A+E)t_0} - e^{At_0}\| + \|Et_0\| \qquad (A.4)$$

While from [9, 36] we have

$$\|e^{At_0} - e^{(A+E)t_0}\| \leq \|E\|t_0 M^2(t_0)e^{M(t_0)\|E\|t_0}\|e^{At_0}\| \qquad (A.5)$$

substituting this last relation into (A.4) gives the result immediately.

It is worth noting that the above bound is improved as N becomes closer to the zero matrix ($M(t_0) \to 1$), that is, as A is more like a symmetric matrix. This may mean that this approximation works best when A is symmetric. Figure A.1 shows the percentage error in the proposed approximation versus the norm of the disturbance E when $E = J_k$. The range of J_k shown represents square-sum currents between 0 and 300 amps^2. Here, a typical value of $t_o = 60$ seconds is used.
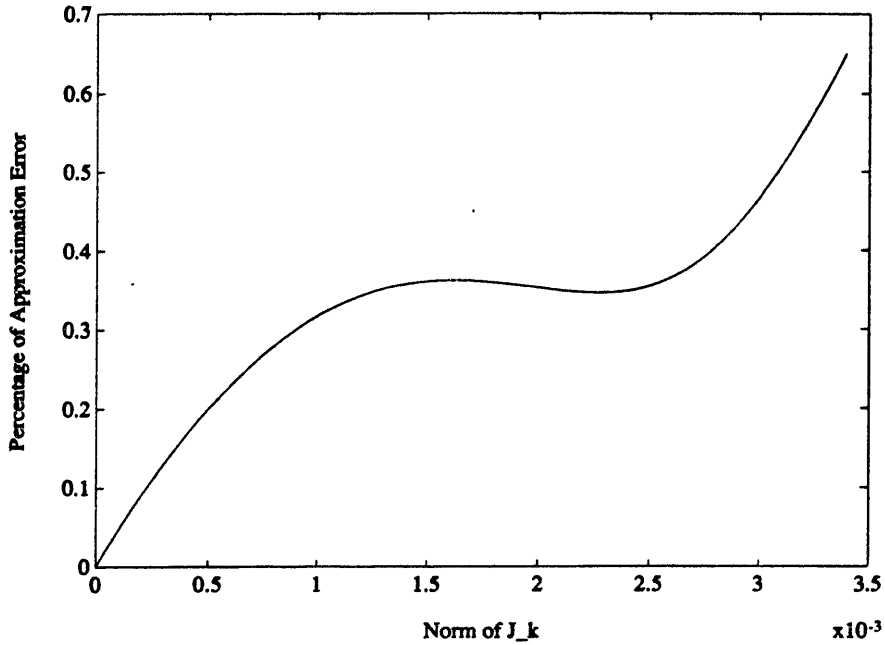
Figure A.1: Percent of norm error in approximation vs. $\|J_k\|$

A.2   Derivation of Kalman Filter Equations

The equations used in Chapter 4 and Chapter 5 for the Kalman filter implementations are derived below.

Consider the update equation for the observer

$$\hat{T}_k^+ = \hat{T}_k^- + H_k(Y_k - \hat{T}_k^-) \tag{A.6}$$

Given the measurement error n_k, this yields the following error update equation.

$$e_k^+ = (I - H_k)e_k^- + H_k n_k \tag{A.7}$$

Using this equation, we can find the expression for the change in the error covariance matrix, P_k, when a measurement is taken. We have

$$P_k^+ = E[e_k^+ e_k^{+'}] \tag{A.8}$$

Inserting A.7 in this expression and noting that

$$
\begin{aligned}
E[\epsilon_k^- \epsilon_k^{-\prime}] &= P_k^-, \\
E[n_k n_k'] &= S, \\
E[\epsilon_k^- n_k] &= 0.
\end{aligned}
$$

we obtain

$$
P_k^+ = (I - H_k)P_k^-(I - H_k)' + H_k S H_k' \tag{A.9}
$$

The criterion for choosing H_k is to minimize the variance of the norm of ϵ_k^+ at each k. Hence, the appropriate cost function to be minimized is

$$
C_k = E[\epsilon_k^{+\prime} \epsilon_k^+] = Trace(P_k^+)
$$

Differentiating this cost function with respect to the gain H_k and equating the result to zero gives

$$
-2(I - H_k)P_k^- + 2H_k S = 0 \tag{A.10}
$$

We can now solve this equation for H_k, obtaining

$$
H_k = P_k^-(P_k + S)^{-1} \tag{A.11}
$$

The covariance extrapolation equations may be derived according to

$$
P_{k+1}^- = E[\epsilon_{k+1}^- \epsilon_{k+1}^{-\prime}] \tag{A.12}
$$

Applying the definition of ϵ_{k+1}^- yields

$$
P_{k+1}^- = \Phi_k P_k \Phi_k' + Q_k \tag{A.13}
$$

Naturally, between measurements, the observer is simulated forward as

$$
\hat{T}_{k+1}^- = \Phi_k \hat{T}_k^+ + \Gamma_k u_k \tag{A.14}
$$

A.3   Stable Observers For Time-Varying Systems

The problem of designing a stable observer for time-varying systems is a nontrivial one. In the results derived below, a novel approach is presented to thedesign of stable

155

observers for time-varying systems that lead to time-invariant error dynamics. We used the approach presented below in Chapter 4 where Observer II was designed. This observer used the technique presented here to cancel the effect of the time-varying part of the dynamics on the error equations for the thermal observer.

Suppose we wish to design a state observer for the following m-input, l-output nonlinear dynamic system

$$\dot{x} = f(u,t)x + B(t)g(u,t) \tag{A.15}$$

$$y(t) = C(t)x(t) \tag{A.16}$$

where A is an $n \times n$ real matrix, $f(u,t)$ is a smooth mapping from R^{m+1} to R^{n^2}, x is an $n \times 1$ state vector, $B(t)$ is a smooth function from the set of real numbers into R^{nq}, $g(u,t)$ is a smooth function from R^{m+1} to R^q, and $C(t)$ is a smooth function from R into R^{ln}. For example, one may choose to design a time-varying identity observer for this system. Such an observer takes the form

$$\dot{\hat{x}} = f(u,t)\hat{x} + B(t)g(u,t) + H(t)(y - \hat{y}) \tag{A.17}$$

$$\hat{y}(t) = C(t)\hat{x}(t) \tag{A.18}$$

Define the observer error to be $\epsilon = \hat{x} - x$. Hence, this identity observer yields the following error dynamics

$$\dot{\epsilon} = (f(u,t) - D(t)C(t))\epsilon = G(u,t)\epsilon \tag{A.19}$$

In order to obtain error dynamics that converge to zero, we must pick $D(t)$ such that (A.19) is strictly stable. Given that (A.19) is a time-varying system, the choice of $D(t)$ may (and in most cases will) not be trivial. Here, we present an approach that is useful if the plant (A.15-16) satisfies certain conditions.

Theorem 4 *Let Ω denote an open set in the space of all allowable inputs u, and R the set of positive real numbers representing time. Now pick an $n \times n$ real matrix M, with stable eigenvalues such that for all $(u,t) \in \Omega \times R$, the rows of $f(u,t) - M$ are in the row-space of $C(t)$. Then the equation (A.20) can be solved for D with the solution given by (A.21).*

$$D(t)C(t) = f(u,t) - M \tag{A.20}$$

$$D(t) = (f(u,t) - M)C(t)'(C(t)C(t)')^{-1} \tag{A.21}$$

Proof: The solution is easily obtained by multiplying both sides of (A.20) by the left-inverse of $C(t)$.

Given this result, if the hypotheses of this theorem hold true, we may pick the gain $D(t)$ according to (A.21). This choice of gain yields the following error dynamics for the observer

$$\dot{e} = Me \qquad (A.22)$$

This is, by construction, a strictly stable system. Hence we can be assured that the observer error will decay to zero. Under certain circumstances, given a nonlinear system of the above type, several values for M may exist that will satisfy the premises of the theorem, and we may then choose the M that yields the most desirable error dynamics.

Example Consider the following nonlinear, time-varying dynamic system

$$\dot{x} = \begin{bmatrix} -1 & u_1(t)t^2 sin(t) \\ 0 & -1 + u_2(t)(sin(t) + cos(t)) \end{bmatrix} x + \begin{bmatrix} u_1(t) \\ u_2(t) \end{bmatrix}$$

$$y = [0 \quad 1.5 + cos(2t) + t^2]x$$

where the inputs are given by

$$u_1 = 2cos(5t)$$
$$u_2 = 2e^{-t/5} sin(3t)$$

Suppose that we are asked to build an observer with stable error dynamics for the above system. It is clear that due to the time-varying nature of the system, a stable observer is not easy to find. We will show that our method provides a simple solution. Let us write the above system as

$$\dot{x} = f(u,t)x + B(t)u(t) \qquad (A.23)$$
$$y = C(t)x \qquad (A.24)$$

An identity observer with a possibly time-varying gain $D(t)$ gives rise to the following error dynamics.

$$\dot{e} = (f(u,t) - D(t)C(t))e \qquad (A.25)$$

We wish to find a gain $D(t)$ such that

$$f(u,t) - D(t)C(t) = M = \begin{bmatrix} m_1 & 0 \\ 0 & m_2 \end{bmatrix} \qquad \text{(A.26)}$$

where m_1 and m_2 are negative, real numbers. According to our theorem, the above equation can be solved if the rows of $f(u,t) - M$ are in the row-space of $C(t)$ for all time. Given that $C(t) = [0 \quad 1.5 + cos(2t) + t^2]$, we see that we must have

$$m_1 = -1 = f_{11} \qquad , \qquad \text{(A.27)}$$

If this is acceptable, we may continue with our design, finding that

$$D(t) = \frac{1}{1.5 + cos(2t) + t^2} \begin{bmatrix} u_1 t^2 sin(t) \\ -1 + u_2(sin(t) + cos(t)) - m_2 \end{bmatrix} \qquad \text{(A.28)}$$

yields the desired error dynamics as

$$\dot{e} = \begin{bmatrix} -1 & 0 \\ 0 & m_2 \end{bmatrix} e \qquad \text{(A.29)}$$

Figures A.2-8 illustrate the response of the system and the performance of the observer for $m_2 = -1$ and the initial conditions shown on Figures A.3-4. In the remainder of this subsection we seek to identify a class of time-varying gains that lead to asymptotically stable error dynamics of an identity observer for a time-varying system.

The following lemma is well known in the literature on time-varying systems [5, 34].

Lemma 3 *The time-varying plant $\dot{x} = A(t)x$ is asymptotically stable if the symmetric matrix $A(t) + A^T(t)$ is strictly negative definite for all time.*

The proof makes straight-forward use of a Lyapunov function to prove stability. Using the above lemma, the following result characterizes the class of all time-varying gains that produce identity observers with asymptotically stable error dynamics for a class of nonlinear systems.

Theorem 5 *Consider the time-varying dynamic system given by*

$$\dot{x} = f(u,t)x + B(t)u(t) \qquad \text{(A.30)}$$

158
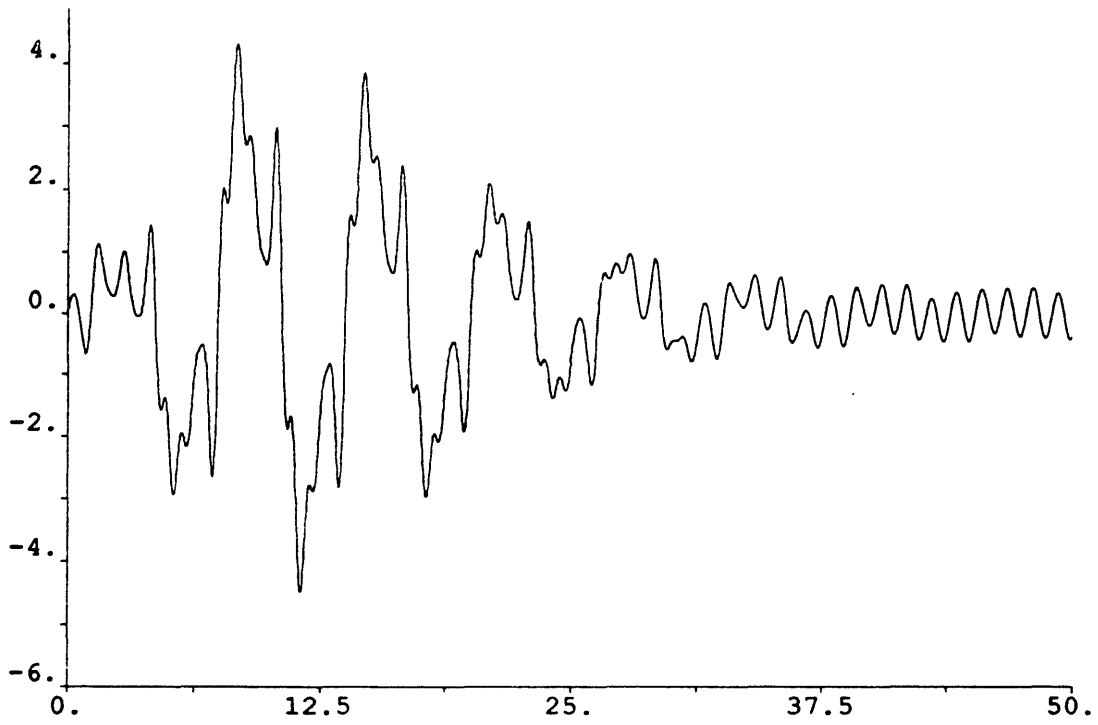
Figure A.2: The State x_1 vs Time
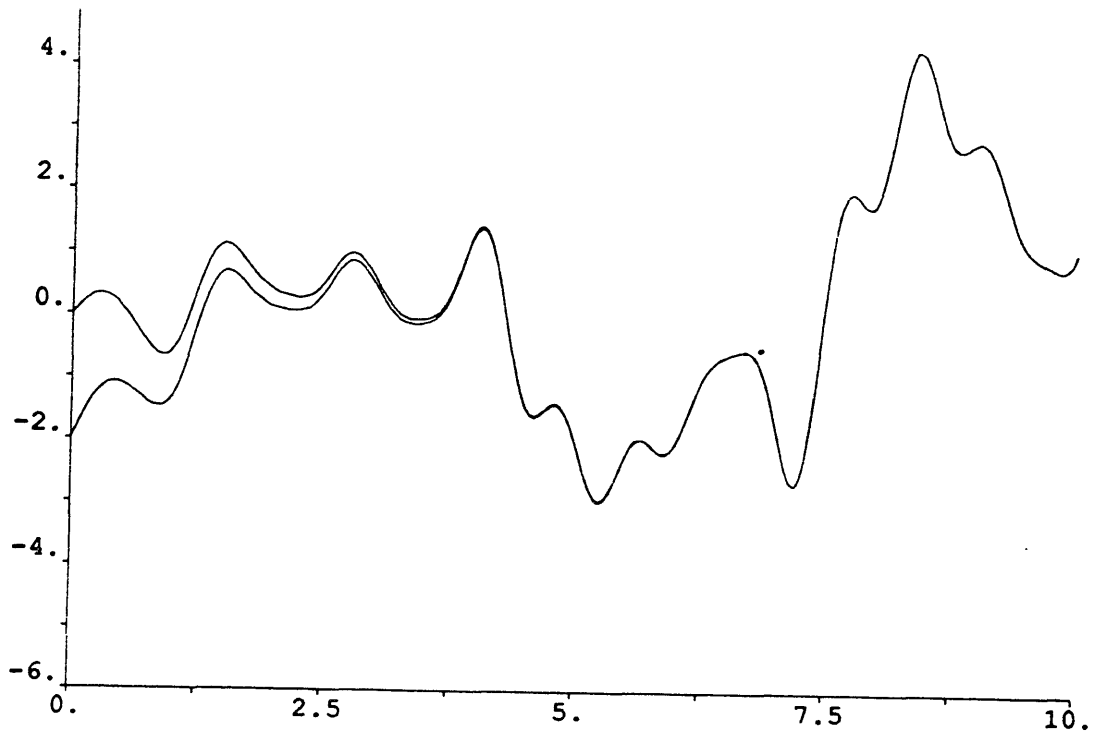
Figure A.3: The State x_1 and its Estimate $\hat{x}_1$ vs Time

159
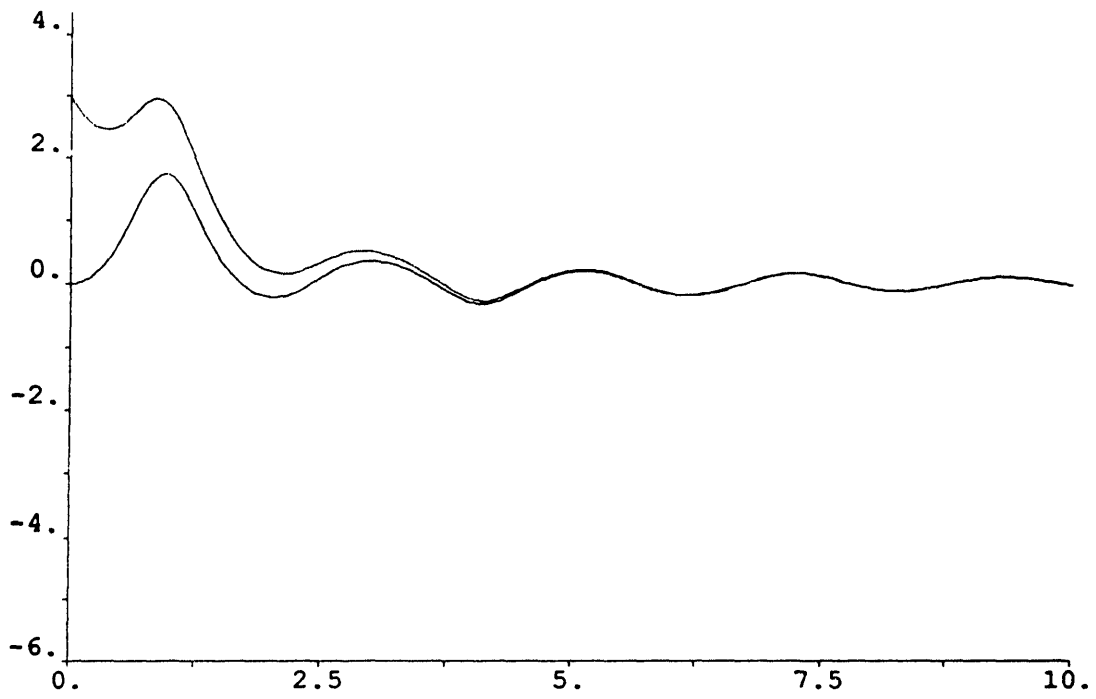
Figure A.4: The State x_2 and its Estimate $\hat{x}_2$ vs Time
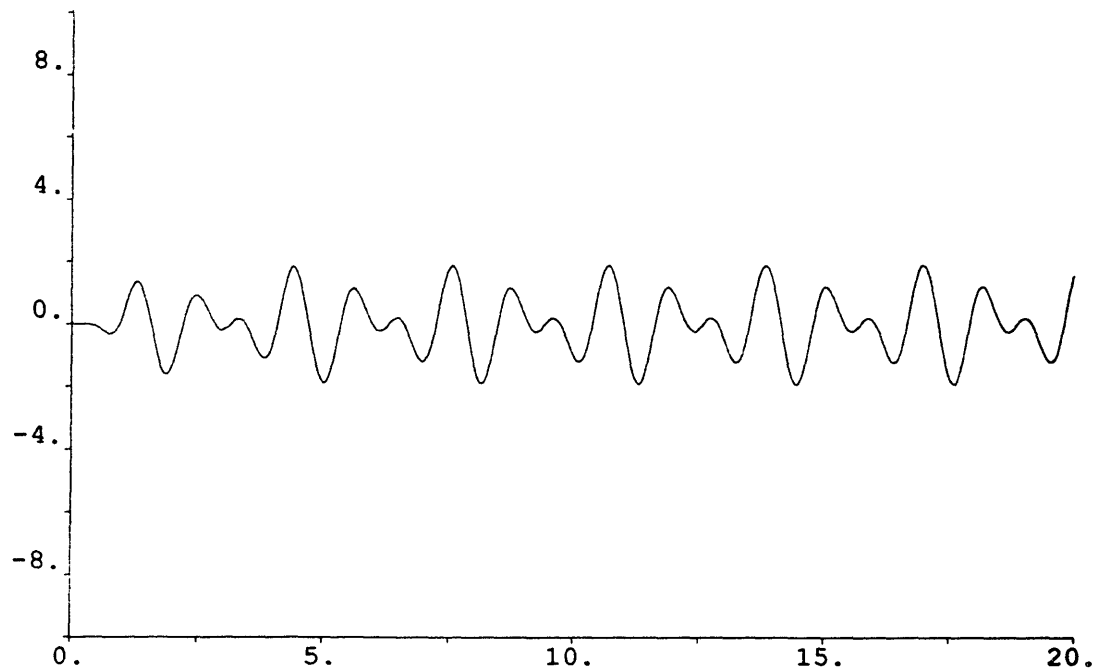
Figure A.5: The Gain $d_1(t)$ vs Time

160
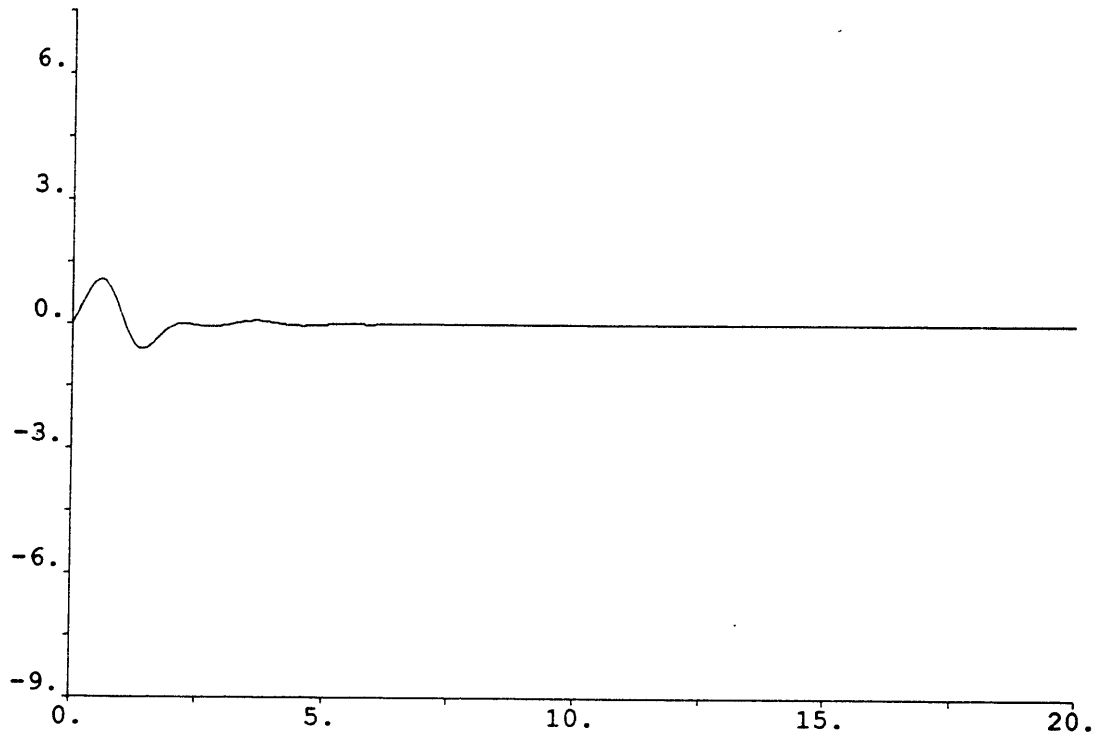
Figure A.6: The Gain $d_2(t)$ vs Time
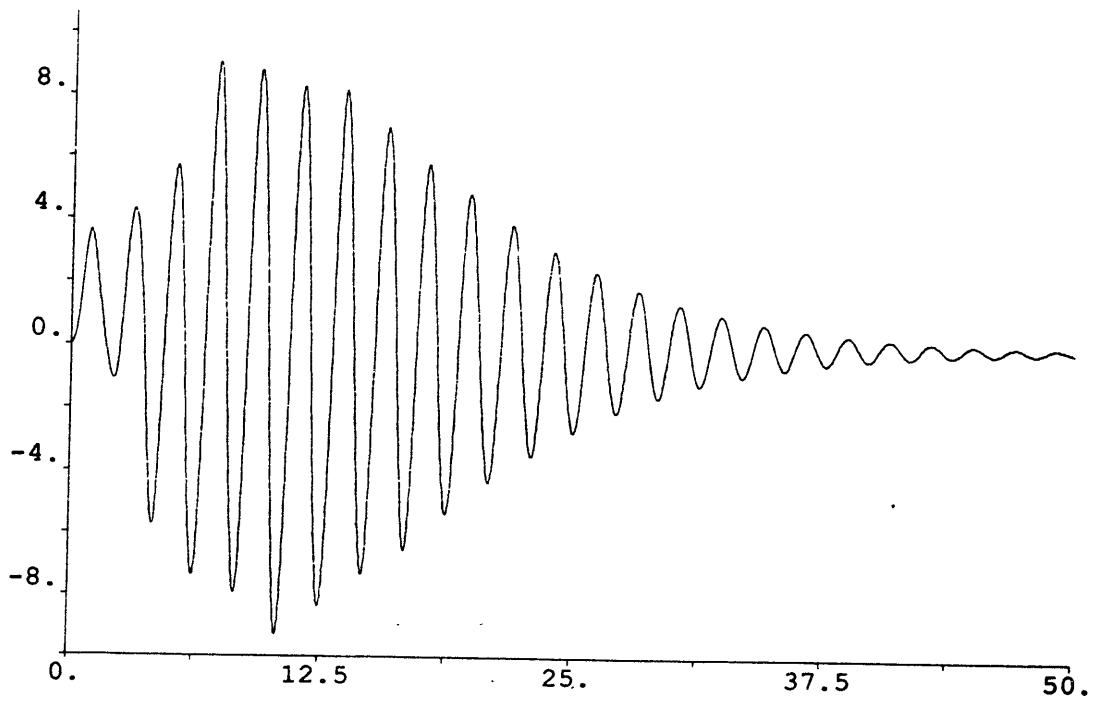
Figure A.7: The Output $y(t)$ vs Time

161
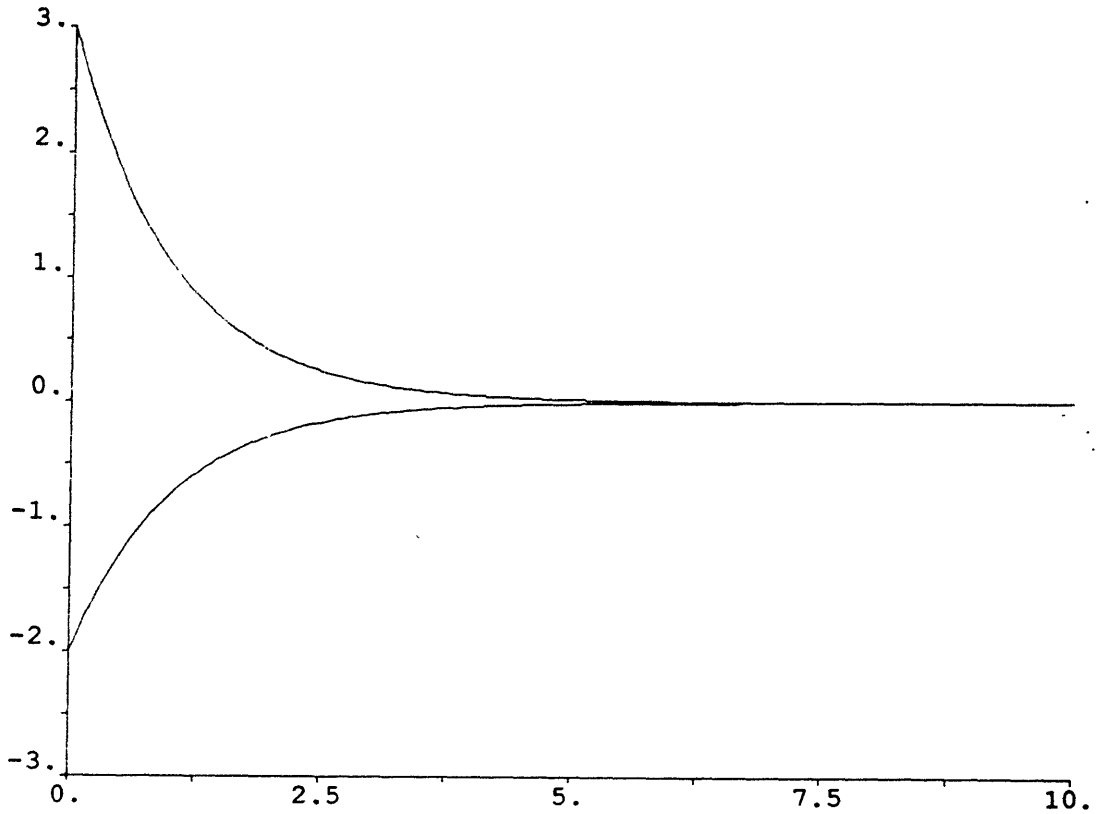
Figure A.8: The Error Dynamics vs Time

$$y(t) = C(t)x(t). \tag{A.31}$$

Assume that the symmetric matrix $f(u,t) + f(u,t)^T$ is strictly negative-definite for all time t, and all inputs $u \in \Omega^*$, where Ω^* is some open subset in the space of all allowable inputs to the plant. Then the identity observer

$$\dot{\hat{x}} = f(u,t)\hat{x} + B(t)u(t) + D(u,t)(y(t) - \hat{y}(t)) \tag{A.32}$$

$$\hat{y}(t) = C(t)\hat{x}(t) \tag{A.33}$$

gives rise to asymptotically stable error dynamics if the observer gain $D(u,t)$ satisfies

$$v^T D(u,t)C(t)v \geq 0 \quad \forall t, \quad \forall u \in \Omega^*, \quad \forall v \in R^n. \tag{A.34}$$

This is to say that the matrix $D(u,t)C(t)$ is positive semidefinite for all time t and all inputs u in Ω^*.

Proof: We have

$$v^T D(u,t)C(t)v \geq 0 \quad \forall t, \quad \forall u \in \Omega^*, \quad \forall v \in R^n \tag{A.35}$$

162

Hence, we can write

$$v^T C^T(t) D^T(u,t) v \geq 0 \quad \forall t, \quad \forall u \in \Omega^*, \quad \forall v \in R^n. \tag{A.36}$$

Therefore we can write

$$v^T (D(u,t)C(t) + C^T(t)D^T(u,t)) v \geq 0 \quad \forall t, \quad \forall u \in \Omega^*, \quad \forall v \in R^n. \tag{A.37}$$

Now the error dynamics for the identity observer are

$$\dot{e} = G(u,t)e, \tag{A.38}$$

where

$$G(u,t) = f(u,t) - D(u,t)C(t). \tag{A.39}$$

Using the hypothesis and the relation A.37 it is easy to see that the matrix $G(u,t) + G(u,t)^T$ is negative definite for all time t and all inputs $u \in \Omega^*$. Hence by the Lemma 3, the error dynamics are asymptotically stable and converge to zero, as desired.

A.3.1 A Linear Stable Observer

For the sake of completeness, we present a result regarding the stability of identity observers for a class of linear systems with nonlinear output functions. The theorem relies on the result due to Gronwall [5] which is as follows.

Theorem 6 *Let $f(t)$ be a positive scalar function defined over the real line. If*

$$f(t) \leq b + \int_0^t a f(\tau) d\tau \quad (a, b > 0) \tag{A.40}$$

Then,

$$f(t) \leq b e^{at} \tag{A.41}$$

for all real numbers t.

This key result is used to prove the following theorem.

Theorem 7 *Given the plant*

$$\dot{x} = Ax + Bu \tag{A.42}$$

$$y = Cx + f(x) \tag{A.43}$$

163

and assuming the following are true

$$\|f(x) - f(\hat{x})\| \leq \alpha \|x - \hat{x}\| \qquad \text{(A.44)}$$

and the pair (A, C) is detectable via a gain K such that

$$\|e^{(A-KC)t}\| \leq Me^{-\sigma t}, \quad \sigma > 0, \quad t \geq 0 \qquad \text{(A.45)}$$

$$\alpha < \frac{\sigma}{M\|K\|} \qquad \text{(A.46)}$$

then, the identity observer given by

$$\dot{\hat{x}} = A\hat{x} + Bu \qquad \text{(A.47)}$$
$$\hat{y} = C\hat{x} + f(\hat{x}) \qquad \text{(A.48)}$$

yields error dynamics which converge to zero exponentially at the rate $\tilde{\sigma} = \sigma - M\|K\|\alpha$.

The first condition in the hypothesis is one which states that the function f is to be *Lipschitz*. The second condition is a restatement of the observability condition for the nonlinear system, while the third condition relates the size of the gain matrix K and the eigenvalues of $A - KC$ to "how Lipschitz" f is. This condition is necessary to assure the convergence of the error dynamics. The proof of the result makes frequent use of Schwarz's inequality and the key point in the proof is the use of Gronwall's inequality.

A.4   Stability of Time-Varying Systems

In this section of the appendix, we present some results regarding the stability of time-varying linear systems. These results prove helpful in solving the geometric failure detection problem for time-varying systems as alluded to in Chapter 5. In particular, they provide the basis necessary to prove that the error dynamics of an identity observer/detection filter for a time-varying linear system have the origin as a global, asymptotically stable equilibrium point.

Theorem 8 *Given the n-dimensional, time-varying dynamic system $\dot{x} = A(t)x$, assume that $A(t)$ can be decomposed as*

$$A(t) = W\Sigma(t)W^{-1} \tag{A.49}$$

where W is a constant, invertible matrix, and $\Sigma(t)$ is the diagonal matrix of eigenvalues of $A(t)$. Then the dynamic system $\dot{x} = A(t)x$ is exponentially stable if for each eigenvalue $\lambda_i(t)$ of $A(t)$, the following relation holds

$$\int_0^t Re(\lambda_i(\tau))d\tau \leq -\epsilon\phi(t) \tag{A.50}$$

where $Re(z)$ denotes the real part of the complex number z, ϵ is a positive real number, and $\phi(t)$ is a positive, <u>unbounded</u>, real-valued function of t. (i.e. $\lim_{t\to\infty}\phi(t) = \infty$)

Proof: The dynamic system can be rewritten in terms of the state transition matrix as follows

$$x(t) = \Omega(t)x_o \tag{A.51}$$

since $\Sigma(t)$ and its integral $\int_0^t \Sigma(\tau)d\tau$ commute, the state transition matrix $\Omega(t)$ is given by

$$\Omega(t) = e^{\int_0^t W\Sigma(\tau)W^{-1}d\tau} \tag{A.52}$$

See [3]. Hence, we have

$$\|\Omega(t)\| = \|e^{\int_0^t W\Sigma(\tau)W^{-1}d\tau}\| \tag{A.53}$$

$$= \|W exp(\int_0^t \Sigma(\tau)d\tau)W^{-1}\| \tag{A.54}$$

$$\leq \kappa(W)\|exp(\int_0^t \Sigma(\tau)d\tau)\| \tag{A.55}$$

where all the above norms are the Frobenius norm, and $\kappa(W)$ denotes the condition number of the matrix W in this norm. Recall that $\kappa(W) = \|W\|\|W^{-1}\|$. Since Σ is diagonal, A.45 can be written as

$$\|\Omega(t)\| \leq \kappa(W)(\sum_{i=0}^n |exp(\int_0^t \lambda_i(\tau)d\tau)|^2)^{1/2} \tag{A.56}$$

$$\leq \kappa(W)(\sum_{i=0}^n |exp(\int_0^t Re(\lambda_i(\tau))d\tau)|^2)^{1/2} \tag{A.57}$$

165

$$\leq \quad \kappa(W)(\sum_{i=0}^{n} exp(-\epsilon\phi(t)))^{1/2} \tag{A.58}$$

$$= \quad \sqrt{n}\kappa(W)e^{-\epsilon\phi(t)} \tag{A.59}$$

This proves that the dynamics system is exponentially stable. A simpler proof that leads to a different bound on the norm of the state transition matrix may be obtained by considering the dynamic system $\dot{z} = \Sigma(t)z$ where $z = W^{-1}x$. This dynamic system can now be thought of as a set of n decoupled linear, scalar, time-varying systems. The stability of each of these scalar systems may then be proved by bounding the size of their corresponding states using the corollary of Theorem 9.

As a corollary to Theorem 8, we can see the following result

Corollary 1 *Given the n-dimensional, time-varying dynamic system $\dot{x} = A(t)x$, assume that $A(t)$ can be decomposed as*

$$A(t) = W\Sigma(t)W^{-1} \tag{A.60}$$

where W is a constant, invertible matrix, and $\Sigma(t)$ is the diagonal matrix of eigenvalues of $A(t)$. Then the dynamic system $\dot{x} = A(t)x$ is exponentially stable if all eigenvalue $\lambda_i(t)$ of $A(t)$ remain in the open left half of the complex plane for all time.

In this case, the function $\phi(t)$ becomes simply $\phi(t) = t$.

The following result gives a bound on the total variation of the eigenvalues for a stable time-varying system.

Theorem 9 *If the n-dimensional dynamic system $\dot{x} = A(t)x$ is stable in the sense of Lyapunov, then the real-valued function $V(t)$ given by*

$$V(t) = \sum_{i=0}^{n}(\int_{0}^{t} Re(\lambda_i(\tau))d\tau) \tag{A.61}$$

is bounded from above.

Proof: If the given dynamic system is stable in the sense of Lyapunov, then we have

$$\|\Omega(t)\| \leq \psi(t) \leq M \tag{A.62}$$

where M is a finite, positive real number, and the norm is the Frobenius norm. From [3] we know that the determinant $det(\Omega(t))$ is always positive. Furthermore, [20]

166

states

$$det(\Omega) \leq (\frac{1}{n}\|\Omega\|^2)^{n/2} \tag{A.63}$$

We also know [3] that

$$det(\Omega(t)) = exp(\int_0^t Trace(A(\tau))d\tau) \tag{A.64}$$

Combining relations A.53 and A.54 with the definition of stability, we obtain

$$exp(\int_0^t Trace(A(\tau))d\tau) \leq \frac{1}{n^{n/2}}\psi(t)^n \tag{A.65}$$

Since

$$Trace(A(t)) = \sum_{i=0}^n Re(\lambda_i(t)), \tag{A.66}$$

Taking logs of both sides of inequality A.55 we obtain

$$V(t) = \sum_{i=0}^n (\int_0^t Re(\lambda_i(\tau))d\tau) \leq nlog(\frac{\psi(t)}{\sqrt{n}}) \tag{A.67}$$

which proves the result. A simple corollary of this result is that the scalar system $\dot{x} = a(t)x$ is stable in the sense of Lyapunov if and only if the function $v(t)$ given by

$$v(t) = \int_0^t a(\tau)d\tau \tag{A.68}$$

is bounded from above.

Appendix B

Listings of Computer Programs

B.1 Matlab Listings

The following programs were written for Matlab to perform a variety of simulations of the parameter estimation, Kalman filtering, and failure detection in the permanent-magnet, synchronous motor.

```
function [olsest1,olsest2,olsest3]=estimator(plt,skip)
%
% [olsest1,olsest2,olsest3]=estimator(plt,skip)
%
% plt : If plt=1 plots are done. Optional: default=0
%        skip : Skip Factor
%                 : The Skip Factor 'skip' will show
%                 : the parameter estimates at every
%                 :'skip-th' point in time.


%     This routine simulates the Omron motor in electromechanical
%     steady-state given desired operating conditions. This
%     simulation includes the injection of gaussian noise at line
%     measurements. These noisy measurements are then used to estimate
%     R and K, the winding resistance and the magnet constant, respectively.
%     Two estimation schemes are done in parallel. Namely those described in
%     Chapter 2 of the thesis.
%
%                                        (C)  6/89 Peyman Milanfar.
```

```
rand('normal');

if nargin<1; % Set default plotting toggle
plt=0;
end;


        %Input Operating Conditions and Noise Characteristics.

w=(pi/30)*3000;  % The speed
tau=.636;        % The torque in N-m
id=1; % id in Amps
R=1.7479; % R in ohms
K=.0917;  % K in V-s/rad
sig1sq=4e-5;  % The variance of the current measurement errors
sig2sq=4e-5;  % The variance of the voltage measurement errors
sig3sq=4e-5;  % The variance of the speed measurement errors
sig4sq=4e-6;  % The variance of the angle measurement errors
sig1=sqrt(sig1sq);
sig2=sqrt(sig2sq);
sig3=sqrt(sig3sq);
sig4=sqrt(sig4sq);


        %Set Motor Constants.

B=5.8e-4;
C=1.91e-2;
N=3;
P=0.00039;
Lq=0.0084;
Ld=0.00917;


        %Begin Simulation of Motor.

iq=(B*w+C+tau)/(2*N*P*id+N*K);
vd=R*id-N*Lq*w*iq;
vq=N*Ld*w*id+R*iq+N*K*w;
t=[0:.3:60];  % Time steps
theta=3*w*t;
va=vd*cos(theta)-vq*sin(theta);
vb=vd*sin(theta)+vq*cos(theta);
ia=id*cos(theta)-iq*sin(theta);
ib=id*sin(theta)+iq*cos(theta);
```

```
v1=sqrt(2/3)*va;
v2=-sqrt(1/6)*va+sqrt(1/2)*vb;
v3=-sqrt(1/6)*va-sqrt(1/2)*vb;
i1=sqrt(2/3)*ia;
i2=-sqrt(1/6)*ia+sqrt(1/2)*ib;
i3=-sqrt(1/6)*ia-sqrt(1/2)*ib;

% Assign Measurement Noise

v1n=v1+sig2*rand(1,length(v1));
v2n=v2+sig2*rand(1,length(v2));
v3n=v3+sig2*rand(1,length(v3));
i1n=i1+sig1*rand(1,length(i1));
i2n=i2+sig1*rand(1,length(i2));
i3n=i3+sig1*rand(1,length(i3));
wn=w*ones(1,length(t))+sig3*rand(1,length(t));
thetan=theta+sig4*rand(1,length(theta));

        % Forward Blondel-Park Transformations

van=sqrt(2/3)*v1n-sqrt(1/6)*v2n-sqrt(1/6)*v3n;
vbn=sqrt(1/2)*v2n-sqrt(1/2)*v3n;
ian=sqrt(2/3)*i1n-sqrt(1/6)*i2n-sqrt(1/6)*i3n;
ibn=sqrt(1/2)*i2n-sqrt(1/2)*i3n;
vdn=van.*cos(thetan)+vbn.*sin(thetan);
vqn=-van.*sin(thetan)+vbn.*cos(thetan);
idn=ian.*cos(thetan)+ibn.*sin(thetan);
iqn=-ian.*sin(thetan)+ibn.*cos(thetan);

%Low-Pass Filtering if Needed
%%%%%%%%%%%%%%%%%%%%%%%%%%%%%%%
%[B,A]=butter(6,.1);          %
%iqns=filtfilt(B,A,iqn);      %
%idns=filtfilt(B,A,idn);      %
%vqns=filtfilt(B,A,vqn);      %
%vdns=filtfilt(B,A,vdn);      %
%wns=filtfilt(B,A,wn);        %
%%%%%%%%%%%%%%%%%%%%%%%%%%%%%%%

iqns=iqn;
idns=idn;
vqns=vqn;
```

```
vdns=vdn;
wns=wn;


% Generate A,B Matrices for Estimation



niqn=length(iqn);                       % Find length of iqn vector

A=zeros(2*niqn,2);              % Initialize A, B to zero matrix
B0=zeros(2*niqn,1);    % (don't have to change zero entries)



A(1:2:2*niqn-1,1)=idns'; % Assign 1,1 entries of the A sub-blocks
A(2:2:2*niqn,1)=iqns';           % Assign 2,1 entries of the A sub-blocks
A(2:2:2*niqn,2)=3*wns'; % Assign 2,2 entries of the A sub-blocks

B0(1:2:2*niqn-1,1)=3*Lq*wns'.*iqns'+vdns'; % Assign 1,1 entries of B sub-blocks
B0(2:2:2*niqn,1)=-3*Ld*wns'.*idns'+vqns';   %Assign 2,1 entries of B sub-blocks

A2(1:2:2*niqn-1,1)=idns';
A2(2:2:2*niqn,1)=iqns';

B02(1:2:2*niqn-1,1)=3*Lq*wns'.*iqns'+vdns';
B02(2:2:2*niqn,1)=-3*Ld*wns'.*idns'+vqns'-3*wns'*K;


        % Estimation Algorithms



olsest1=[];
olsest2=[];


for l=1:skip:niqn;


    % Ordinary Least Squares (OLS) estimation algorithms.

D2=A(1:2*l,:)\B0(1:2*l,:);
olsest1=[olsest1,D2];           %Estimator I
```

```
        D23=A2(1:1,:)\B02(1:1);
        olsest2=[olsest2,D22];         %Estimator II

clc
disp(['Percent completed : ',num2str(100*l/niqn)])
end;


if plt==1,

clg

subplot(221)
plot(olsest1(1,:)-R*ones(olsest1(1,:)));
title('Estimator I Error in R');

subplot(222)
plot(olsest1(2,:)-K*ones(olsest1(2,:)));
title('Estimator I Error in K');

subplot(223)
plot(olsest2(1,:)-R*ones(olsest2(1,:)));
title('Estimator II Error in R');

subplot(224)
plot(olsest2(2,:)-K*ones(olsest2(2,:)));
title('Estimator II Error in K');

pause

clg

plot(olsest3-R*ones(olsest3));
title('Estimator III Error in R')

end;
```

```
%       OBS1.m
%  This program Simulates the exact Kalman filter used to track
%  temperatures in the motor. That is the matrix of estimated temperatures.
% Calls are made to the following routines:
%
% Motor.m : This programs simulates the Omron motor in
%   electromechanical steady-state, and provides noisy
%   values of the dq-frame variables.
% bEstim.m: Computes batch Estimates of R and K
%
% These two are essentially the program Estimator.m split apart.

wk=(pi/30)*[1000*ones(1,25) 1000*ones(1,25) 1000*ones(1,50) 1000*ones(1,50)];
tauk=[.212*ones(1,50) .212*ones(1,50) .212*ones(1,50)];

%Load seed from it.mat. It is the seed for the random number generator.

rand('normal')
rand('seed',it)

%Observer Initial Conditions...
%%%%%%%%%%%%%%%%%%%%%%%%%%%%%%%%%

Thatold0=[1 2];
Tnew0=[0 0];
T=[];
That=[];

    %Load System Dynamics
load Aans
load Bans


%--------------------------------------------------------------------------

%Inputs to the motor program
%%%%%%%%%%%%%%%%%%%%%%%%%%%%%%%%

%Input Definitions

I=eye(2);
```

```
%w:=(pi/30)Speed in RPM
%tau:=Torque in N-m
%id:=id in Amps
%Tamb:=Ambient T in degrees C
%sig1sq:=Variance of the current measurement errors
%sig2sq:=Variance of the voltage measurement errors
%sig3sq:=Variance of the speed measurement errors
%sig4sq:=Variance of the angle measurement errors
%t:=[Start time: Time step: End time]


%Input Values

tf=60;
t=[0.01:.4:tf];
id=1;
Tamb=24;
R=(1.8517/258.5)*(Tamb+234.5);
K=(8.204e-2)*sqrt(1.5)*(Tamb^(-2.965e-2));
sig1sq=0.00004;
sig2sq=0.00004;
sig3sq=0.00004;
sig4sq=0.000004;
sig1=sqrt(sig1sq);
sig2=sqrt(sig2sq);
sig3=sqrt(sig3sq);
sig4=sqrt(sig4sq);

%Set Motor Constants
%%%%%%%%%%%%%%%%%%%%%%

B=5.8e-4;
C=1.91e-2;
N=3;
P=0.00039;
Lq=0.0084;
Ld=0.00917;


%Variance of measurement errors (Tc and Tr)
std=0.1;
std2=1;
beta=1/139.6;
```

```matlab
SS0=diag([std  std2]);
SS=SS0;


%---------------------------------------------------------------


%%%%%%%%%%%%%%
%INITIALIZING Gain, Covarianve, count...
%%%%%%%%%%%%%%%%

PP=[.5 0;0 .75]
H=PP*inv(PP+SS0);

err=[];

m=50;
count=1;

Y=[sqrt(PP(1,1))*3 sqrt(PP(2,2))*3];

ev=[];

total=150;


%---------------------------------------------------------------


%Begin loops...
%%%%%%%%%%%%%%%


w=wk(1);   %Speed
tau=tauk(1); %Torque
motor
bEstim
makeu

[phi,gamma]=c2d(Aans+J,Bans,tf);

vars=((Bans*beta*mean(u11)*[70 0 0]'));
Q=diag((vars)); %Process Noise Covariance Matrix

Thatnew=Thatold0+(Tnew0-Thatold0)*H';
```

```
PP=(I-H)*PP*(I-H)'+H*SS*H';

Thatold=Thatnew*phi'+U*gamma';

PP=phi*PP*phi'+Q

Tnew=Tnew0*phi'+U*gamma'+rand(1,2)*sqrt(Q');

H=PP*inv(PP+SS);

T=[Tnew0;Tnew];

That=[Thatold0;Thatold];

%%%%%%%%%%%%%%%%%%%%%%%%%%%%%%%%%%%%%%%%%%%%%

for i=2:m

w=wk(i);
tau=tauk(i);
motor
bEstim
makeu

[phi,gamma]=c2d(Aans+J,Bans,tf);

vars=((Bans*beta*mean(u11)*[70 0 0]'));
Q=diag((vars));

Thatnew=Thatold+(Tnew-Thatold+rand(1,2)*sqrt(SS'))*H';

PP=(I-H)*PP*(I-H)'+H*SS*H';

Thatold=Thatnew*phi'+U*gamma';

PP=phi*PP*phi'+Q

Yk=[sqrt(PP(1,1))*3 sqrt(PP(2,2))*3];
Y=[Y;Yk];

Tnew=Tnew*phi'+U*gamma'+rand(1,2)*sqrt(Q');
```

```
H=PP*inv(PP+SS);

T=[T;Tnew];

That=[That;Thatold];

count=count+1;
percent=(count/total)*100

end

%%%%%%%%%%%%%%%%%%%%%%%%%%%%%%%%%%%%%%%%%%%%

for i=m+1:2*m

w=wk(i);
tau=tauk(i);
motor
bEstim
makeu

[phi,gamma]=c2d(Aans+J,Bans,tf);

vars=((Bans*beta*mean(u11)*[70 0 0]'));
Q=diag((vars));

Thatnew=Thatold+(Tnew-Thatold+rand(1,2)*sqrt(SS'))*H';

PP=(I-H)*PP*(I-H)'+H*SS*H';

Thatold=Thatnew*phi'+U*gamma';

PP=phi*PP*phi'+Q

Yk=[sqrt(PP(1,1))*3 sqrt(PP(2,2))*3];
Y=[Y;Yk];

Tnew=Tnew*phi'+U*gamma'+rand(1,2)*sqrt(Q');

H=PP*inv(PP+SS);

T=[T;Tnew];
```

```
That=[That;Thatold];

count=count+1;
percent=(count/total)*100

end

%%%%%%%%%%%%%%%%%%%%%%%%%%%%%%%%%%%%%%%%%%%%

for i=2*m+1:3*m

w=wk(i);
tau=tauk(i);
motor
bEstim
makeu

[phi,gamma]=c2d(Aans+J,Bans,tf);

vars=((Bans*beta*mean(u11)*[70 0 0]'));
Q=diag((vars));

Thatnew=Thatold+(Tnew-Thatold+rand(1,2)*sqrt(SS'))*H';

PP=(I-H)*PP*(I-H)'+H*SS*H';

Thatold=Thatnew*phi'+U*gamma';

PP=phi*PP*phi'+Q

Yk=[sqrt(PP(1,1))*3 sqrt(PP(2,2))*3];
Y=[Y;Yk];

Tnew=Tnew*phi'+U*gamma'+rand(1,2)*sqrt(Q');

H=PP*inv(PP+SS);

T=[T;Tnew];

That=[That;Thatold];
```

```
count=count+1;
percent=(count/total)*100

end
```

```
%       MOTOR.M
%       This routine simulates the Omron motor in electromechanical.
%       steady-state given desired operating conditions. This
%       simulation includes the injection of gaussian noise at line
%       measurements. These noisy measurements are then used to estimate
%       R and K, the winding resistance and the magnet constant, in
%       the program bEstim.m.
%                                               (C)  6/89 Peyman Milanfar.
%

rand('normal');


%%%%%%%%Begin Simulation of Motor.

iq=(B*w+C+tau)./(2*N*P*id+N*K);
vd=R*id-N*Lq*w.*iq;
vq=N*Ld*w.*id+R*iq+N*K*w;
theta=3*w.*t;
va=vd.*cos(theta)-vq.*sin(theta);
vb=vd.*sin(theta)+vq.*cos(theta);
ia=id.*cos(theta)-iq.*sin(theta);
ib=id.*sin(theta)+iq.*cos(theta);
v1=sqrt(2/3)*va;
v2=-sqrt(1/6)*va+sqrt(1/2)*vb;
v3=-sqrt(1/6)*va-sqrt(1/2)*vb;
i1=sqrt(2/3)*ia;
i2=-sqrt(1/6)*ia+sqrt(1/2)*ib;
i3=-sqrt(1/6)*ia-sqrt(1/2)*ib;


%%%%%%%%% Assign Measurement Noise
wn=w.*ones(1,length(t))+sig3*rand(1,length(t));
thetan=theta+sig4*rand(1,length(theta));
v1n=v1+sig2*rand(1,length(v1));
v2n=v2+sig2*rand(1,length(v2));
v3n=v3+sig2*rand(1,length(v3));
i1n=i1+sig1*rand(1,length(i1));
i2n=i2+sig1*rand(1,length(i2));
i3n=i3+sig1*rand(1,length(i3));
van=sqrt(2/3)*v1n-sqrt(1/6)*v2n-sqrt(1/6)*v3n;
vbn=sqrt(1/2)*v2n-sqrt(1/2)*v3n;
ian=sqrt(2/3)*i1n-sqrt(1/6)*i2n-sqrt(1/6)*i3n;
ibn=sqrt(1/2)*i2n-sqrt(1/2)*i3n;
vdn=van.*cos(thetan)+vbn.*sin(thetan);
```

```
vqn=-van.*sin(thetan)+vbn.*cos(thetan);
idn=ian.*cos(thetan)+ibn.*sin(thetan);
iqn=-ian.*sin(thetan)+ibn.*cos(thetan);

%%%END%%%
```

```
%  obs1LTI.m
%  This program is identical to obs1.m except for the fact that
%   the matrix J is adaptively canceled from the error dynamics.

wk=(pi/30)*[1000*ones(1,25) 1000*ones(1,25) 1000*ones(1,50) 1000*ones(1,50)];
tauk=[.5*ones(1,50) .5*ones(1,50) .5*ones(1,50)];

rand('normal')
rand('seed',it)

%Observer Initial Conditions
%%%%%%%%%%%%%%%%%%%%%%%%%%%%%%

ThatoldO=[1 2];
TnewO=[0 0];
T=[];
That=[];

load Aans
load Bans


%----------------------------------------------------------------------------

%Inputs to the motor program
%%%%%%%%%%%%%%%%%%%%%%%%%%%%%%%%%%%%%%

%Input Definitions

I=eye(2);

%w=(pi/30)*input('Enter the speed in RPM: ');
%tau=input('Enter the torque in N-m: ');
%id=input('Enter id in Amps: ');
%Tamb=input('Enter ambient T in degrees C: ');
%sig1sq=input('Enter the variance of the current measurement errors: ');
%sig2sq=input('Enter the variance of the voltage measurement errors: ');
%sig3sq=input('Enter the variance of the speed measurement errors: ');
%sig4sq=input('Enter the variance of the angle measurement errors: ');
%t=[Start time: Time step: End time]

%Input Values
```

```
tf=60;
t=[0.01:.4:tf];
id=1;  % The smaller this number, the worse the estimate of R
Tamb=24;
R=(1.8517/258.5)*(Tamb+234.5);
K=(8.204e-2)*sqrt(1.5)*(Tamb^(-2.965e-2));
sig1sq=0.00004;
sig2sq=0.00004;
sig3sq=0.00004;
sig4sq=0.000004;
sig1=sqrt(sig1sq);
sig2=sqrt(sig2sq);
sig3=sqrt(sig3sq);
sig4=sqrt(sig4sq);

%%%%%%%%Set Motor Constants.
B=5.8e-4;
C=1.91e-2;
N=3;
P=0.00039;
Lq=0.0084;
Ld=0.00917;

%---------------------------------------------------------------------

%Inputs to the Estim program
%%%%%%%%%%%%%%%%%%%%%%%%%%%%%%%%%%%%%

%Skip is the skip factor. Parameters are estimated every skipth data point.

skip=1;

%Opt is the option to plot

opt=1;

%Plt is another option to plot

plt=1;

%---------------------------------------------------------------------
```

```
%Inputs to dObsever.m or dFailfilt.m
%%%%%%%%%%%%%%%%%%%%%%%%%%%%%%%%%%%%%
std=0.1;
std2=1;
beta=1/139.6;
SS0=diag([std  std2]);
SS=SS0;
E=.001*[.2 .15;0 0];


%----------------------------------------------------------------


%%%%%%%%%%%%%%%%
%INITIALIZING THE GAINS----->
%%%%%%%%%%%%%%%%%%%

PP=diag([.5,.75]) %[.0144 .0053;.0053 .0771];
h=PP*inv(PP+SS0);


%%%%%%%%%%%%%%%%%%


Y=[sqrt(PP(1,1))*3 sqrt(PP(2,2))*3];


total=150;

%----------------------------------------------------------------


%Begin loops...
%%%%%%%%%%%%%%%%
err=[];

m=50;
count=1;
Y=[];


w=wk(1);
tau=tauk(1);
motor
bEstim
```

```
makeu

H=H+J*tf;

M=(I+inv(H)*J*tf);
SS1=M*SS0*M';

[phi,gamma]=c2d(Aans+J,Bans,tf);

vars=((Bans*beta*mean(u11)*[70 0 0]'));
Q=diag((vars));

Thatnew=Thatold0+(Tnew0-Thatold0)*H';

PP=(I-H)*PP*(I-H)'+H*SS1*H';

Thatold=Thatnew*(phi)'+U*(gamma)';

PP=(phi)*PP*(phi)'+Q

Tnew=Tnew0*phi'+U*gamma'+rand(1,2)*sqrt(Q');

H=PP*inv(PP+SS1);

H=H+J*tf;

T=[Tnew0;Tnew];

That=[Thatold0;Thatold];

%%%%%%%%%%%%%%%%%%%%%%%%%%%%%%%%%%%%%%%%%%%%%

for i=2:m

w=wk(i);
tau=tauk(i);
motor
bEstim
makeu

M=(I+inv(H)*J*tf);
SS1=M*SS0*M';
```

```
[phi,gamma]=c2d(Aans+J,Bans,tf);

vars=((Bans*beta*mean(u11)*[70 0 0]'));
Q=diag((vars));

Thatnew=Thatold+(Tnew-Thatold+rand(1,2)*sqrtm(SS1'))*H';

PP=(I-H)*PP*(I-H)'+H*SS1*H';

Thatold=Thatnew*(phi)'+U*(gamma)';

PP=(phi)*PP*(phi)'+Q

Yk=[sqrt(PP(1,1))*3 sqrt(PP(2,2))*3];
Y=[Y;Yk];

Tnew=Tnew*phi'+U*gamma'+rand(1,2)*sqrt(Q');

H=PP*inv(PP+SS1);

H=H+J*tf;

T=[T;Tnew];

That=[That;Thatold];

count=count+1;
percent=(count/total)*100

end

%%%%%%%%%%%%%%%%%%%%%%%%%%%%%%%%%%%%%%%%%%%%%%

for i=m+1:2*m

w=wk(i);
tau=tauk(i);
motor
bEstim
makeu
```

186

```
M=(I+inv(H)*J*tf);
SS1=M*SS0*M';

[phi,gamma]=c2d(Aans+J,Bans,tf);

vars=((Bans*beta*mean(u11)*[70 0 0]'));
Q=diag((vars));

Thatnew=Thatold+(Tnew-Thatold+rand(1,2)*sqrtm(SS1'))*H';

PP=(I-H)*PP*(I-H)'+H*SS1*H';

Thatold=Thatnew*(phi)'+U*(gamma)';

PP=(phi)*PP*(phi)'+Q

Yk=[sqrt(PP(1,1))*3 sqrt(PP(2,2))*3];
Y=[Y;Yk];

Tnew=Tnew*phi'+U*gamma'+rand(1,2)*sqrt(Q');

H=PP*inv(PP+SS1);

H=H+J*tf;

T=[T;Tnew];

That=[That;Thatold];

count=count+1;
percent=(count/total)*100

end

%%%%%%%%%%%%%%%%%%%%%%%%%%%%%%%%%%%%%%%%%%%%%%

for i=2*m+1:3*m

w=wk(i);
tau=tauk(i);
motor
bEstim
```

```
makeu

M=(I+inv(H)*J*tf);
SS1=M*SS0*M';

[phi,gamma]=c2d(Aans+J,3ans,tf);

vars=((Bans*beta*mean(u11)*[70 0 0]'));
Q=diag((vars));

Thatnew=Thatold+(Tnew-Thatold+rand(1,2)*sqrtm(SS1'))*H';

PP=(I-H)*PP*(I-H)'+H*SS1*H';

Thatold=Thatnew*(phi)'+U*(gamma)';

PP=(phi)*PP*(phi)'+Q

Yk=[sqrt(PP(1,1))*3 sqrt(PP(2,2))*3];
Y=[Y;Yk];

Tnew=Tnew*phi'+U*gamma'+rand(1,2)*sqrt(Q');

H=PP*inv(PP+SS1);
H=H+J*tf;

T=[T;Tnew];

That=[That;Thatold];

count=count+1;
percent=(count/total)*100

end
```

```
%  detect1.m
%  This programs is based on the first observer structure
%     and simulates a failure at 50 cycles and a failure
%     detection filter that captures it. The main difference
%  between this and the observer code is the
%  recomputation of the gain.

wk=(pi/30)*[3000*ones(1,25) 3000*ones(1,25) 1000*ones(1,50) 3000*ones(1,50)];
tauk=[.636*ones(1,50) .212*ones(1,50) .636*ones(1,50)];

rand('normal')
rand('seed',it)

Thatold0=[1 2];
Tnew0=[0 0];
T=[];
That=[];

load Aans
load Bans

%------------------------------------------------------------------------

%Inputs to the motor program
%%%%%%%%%%%%%%%%%%%%%%%%%%%%%%%%%%%%%%

%Input Definitions

I=eye(2);

%w=(pi/30)*input('Enter the speed in RPM: ');
%tau=input('Enter the torque in N-m: ');
%id=input('Enter id in Amps: ');
%Tamb=input('Enter ambient T in degrees C: ');
%sig1sq=input('Enter the variance of the current measurement errors: ');
%sig2sq=input('Enter the variance of the voltage measurement errors: ');
%sig3sq=input('Enter the variance of the speed measurement errors: ');
%sig4sq=input('Enter the variance of the angle measurement errors: ');
%t=[Start time: Time step: End time]

%Input Values
```

```
tf=60;
t=[0.01:.4:tf];
id=1;   % The smaller this number, the worse the estimate of R
Tamb=24;
R=(1.8517/258.5)*(Tamb+234.5);
K=(8.204e-2)*sqrt(1.5)*(Tamb^(-2.965e-2));
sig1sq=0.00004;
sig2sq=0.00004;
sig3sq=0.00004;
sig4sq=0.000004;
sig1=sqrt(sig1sq);
sig2=sqrt(sig2sq);
sig3=sqrt(sig3sq);
sig4=sqrt(sig4sq);

%%%%%%%Set Motor Constants.
B=5.8e-4;
C=1.91e-2;
N=3;
P=0.00039;
Lq=0.0084;
Ld=0.00917;

%-------------------------------------------------------------------------

%Inputs to the Estim program
%%%%%%%%%%%%%%%%%%%%%%%%%%%%%%%%%%

%Skip is the skip factor. Parameters are estimated every skipth data point.

skip=1;

%Opt is the option to plot

opt=1;

%Plt is another option to plot

plt=1;

%-------------------------------------------------------------------------
```

```
%Inputs to dObsever.m or dFailfilt.m
%%%%%%%%%%%%%%%%%%%%%%%%%%%%%%%%%%%%
std=0.2;
std2=5;
beta=1/139.6;
SS0=diag([std  std2]);
SS=SS0;
E=.001*[0 0;.2 .15];


%-----------------------------------------------------------------


%%%%%%%%%%%%%%%%
%INITIALIZING THE GAINS----->
%%%%%%%%%%%%%%%%%%
%[phi,gamma]=c2d(Aans,Bans,tf);
PP=diag([.5,.75]) %[.0144 .0053;.0053 .0771];
H=PP*inv(PP+SS0);
%H=phi-diag(eig(phi-H));
%%%%%%%%%%%%%%%%%%


Y=[sqrt(PP(1,1))*3 sqrt(PP(2,2))*3];


total=150;

%-----------------------------------------------------------------


%Begin loops...
%%%%%%%%%%%%%%%%
err=[];

m=50;
count=1;


w=wk(1);
tau=tauk(1);
motor
bEstim
makeu
```

191

```
[phi,gamma]=c2d(Aans+J,Bans,tf);

vars=((Bans*beta*mean(u11)*[70 0 0]'));
Q=diag((vars));

Thatnew=Thatold0+(Tnew0-Thatold0)*H';

PP=(I-H)*PP*(I-H)'+H*SS*H';

Thatold=Thatnew*phi'+U*gamma';

PP=phi*PP*phi'+Q

Tnew=Tnew0*phi'+U*gamma'+rand(1,2)*sqrt(Q');

H=PP*inv(PP+SS);
H=phi-diag(eig(phi-H));

T=[Tnew0;Tnew];

That=[Thatold0;Thatold];

%%%%%%%%%%%%%%%%%%%%%%%%%%%%%%%%%%%%%%%%%%%

for i=2:m

w=wk(i);
tau=tauk(i);
motor
%bEstim
makeu

[phi,gamma]=c2d(Aans+J,Bans,tf);

vars=((Bans*beta*mean(u11)*[70 0 0]'));
Q=diag((vars));

Thatnew=Thatold+(Tnew-Thatold+rand(1,2)*sqrt(SS'))*H';

PP=(I-H)*PP*(I-H)'+H*SS*H';
```

```
Thatold=Thatnew*phi'+U*gamma';

PP=phi*PP*phi'+Q

Yk=[sqrt(PP(1,1))*3 sqrt(PP(2,2))*3];
Y=[Y;Yk];

Tnew=Tnew*phi'+U*gamma'+rand(1,2)*sqrt(Q');

H=PP*inv(PP+SS);
H=phi-diag(eig(phi-H));

T=[T;Tnew];

That=[That;Thatold];

count=count+1;
percent=(count/total)*100
clc

end

%%%%%%%%%%%%%%%%%%%%%%%%%%%%%%%%%%%%%%%%%%%%%%%

for i=m+1:2*m

w=wk(i);
tau=tauk(i);
motor
bEstim
makeu

[phi,gamma]=c2d(Aans+J,Bans,tf);

[phi1,gamma1]=c2d(Aans+J+E,Bans,tf);

vars=((Bans*beta*mean(u11)*[70 0 0]'));
Q=diag((vars));

Thatnew=Thatold+(Tnew-Thatold+rand(1,2)*sqrt(SS'))*H';

PP=(I-H)*PP*(I-H)'+H*SS*H';
```

```
Thatold=Thatnew*phi'+U*gamma';

PP=phi*PP*phi'+Q

Yk=[sqrt(PP(1,1))*3 sqrt(PP(2,2))*3];
Y=[Y;Yk];

Tnew=Tnew*phi1'+U*gamma1'+rand(1,2)*sqrt(Q');

H=PP*inv(PP+SS);
H=phi-diag(eig(phi-H));

T=[T;Tnew];

That=[That;Thatold];

count=count+1;
percent=(count/total)*100
clc

end

%%%%%%%%%%%%%%%%%%%%%%%%%%%%%%%%%%%%%%%%%%%%%

for i=2*m+1:3*m

w=wk(i);
tau=tauk(i);
motor
bEstim
makeu

[phi,gamma]=c2d(Aans+J,Bans,tf);

vars=((Bans*beta*mean(u11)*[70 0 0]'));
Q=diag((vars));

Thatnew=Thatold+(Tnew-Thatold+rand(1,2)*sqrt(SS'))*H';

PP=(I-H)*PP*(I-H)'+H*SS*H';
```

194

```
Thatold=Thatnew*phi'+U*gamma';

PP=phi*PP*phi'+Q

Yk=[sqrt(PP(1,1))*3 sqrt(PP(2,2))*3];
Y=[Y;Yk];

Tnew=Tnew*phi'+U*gamma'+rand(1,2)*sqrt(Q');

H=PP*inv(PP+SS);
H=phi-diag(eig(phi-H));

T=[T;Tnew];

That=[That;Thatold];

count=count+1;
percent=(count/total)*100
clc

end
```

B.2 Assembly Code Listings

The following programs in assembly language provide the data acquisition functions used to collect the data used in experiments described in Chapter 6.

```
%Program to acquire data on 6 channels synchronously. The channels are
%two line currents, two line voltages, one thermocouple, and a shaft
%encoder count reading. The motor is commanded to be spinning
%continuously, while 100 data points are acquired at the end of every
%1 minute for the length of .3 seconds at the rate of 3000
%micro-seconds. The experiment is run for 135 minutes, after which the
%motor is commanded to turn off. The first program is the assembled
%main program. The second is the link program.

%EXAMP.PRN
%%%%%%%%%%

0'000000              5.          section 0
```

```
                  --  --  --  --  --  --  --  --  --  --  --  --  --  --   .

0'000000                        7.  main.prog        proc
0'000000  13FC 0080             8.            move.b  #$80,$ff8011   ;clear hold,turn mot
          00FF8011
                                9.
0'000008  3C3C 0000            10.            move.w  #0,d6      ;initialize the counter
                               11.
0'00000C  383C 0010            12.            move.w  #$10,d4     ;allow motor to reach it
0'000010  3A3C EFFF            13.  dly1:     move.w  #$efff,d5
0'000014  5345                 14.  dly:      subq.w  #1,d5
0'000016  0C45 0000            15.            cmpi.w  #0,d5
0'00001A  66 F8                16.            bne     dly
0'00001C  5344                 17.            subq.w  #1,d4
0'00001E  0C44 0000            18.            cmpi.w  #0,d4
0'000022  66 EC                19.            bne     dly1
                               20.
0'000024  41F9'00000000        21.  strt:     lea shaft,a0      ;theta
0'00002A  43F9'00000000        22.            lea ch0,a1        ;i2
0'000030  45F9'00000000        23.            lea ch1,a2        ;i1
0'000036  47F9'00000000        24.            lea ch2,a3        ;v2
0'00003C  49F9'00000000        25.            lea ch3,a4        ;v1
0'000042  4BF9'00000000        26.            lea ch4,a5        ;Tc
                               27.
0'000048  363C 0087            28.            move.w  #135,d3       ;run the system 135 (
0'00004C  46FC 2300            29.            move.w  #$2300,sr
0'000050  13FC 00B4            30.            move.b  #$b4,$ff8007
          00FF8007
0'000058  13FC 00B8            31.            move.b  #$b8,$ff8005
          00FF8005
0'000060  13FC 000B            32.            move.b  #$0b,$ff8005
          00FF8005
0'000068  13FC 0080            33.            move.b  #$80,$ff8011
          00FF8011
0'000070  4E71                 34.  loop:     nop
0'000072  0C43 0000            35.            cmpi.w  #0,d3
0'000076  6F00 0006            36.            ble     done
                               37.
0'00007A  4EFA FFF4            38.            jmp     loop
                               39.
```

```
0'00007E   13FC 00B4        40.  done:    move.b   #$b4,$ff8007
           00FF8007
0'000086   13FC 0000        41.           move.b   #$0,$ff8011
           00FF8011
0'00008E   46FC 2700        42.           move.w   #$2700,sr
0'000092   4EFA FFFE        43.  here:    jmp      here
                            44.
0'000096                    45.  interrupt.prog proc
1'000000                    46.           section 1
                            47.
                            48.
                            49.
1'000000   0646 0001        50.           addi.w   #1,d6        ;update counter
1'000004   0C46 4E20        51.           cmpi.w   #20000,d6  ;Compare counter to 1 m
1'000008   6F00 0010        52.           ble      down
1'00000C   0C46 4E84        53.           cmpi.w   #20100,d6  ;Compare counter to 1 m
1'000010   6F00 000E        54.           ble      low        ;if less or equal to take
1'000014   3C3C 0000        55.           move.w   #0,d6
1'000018   5343             56.           subq.w   #1,d3
                            57.
1'00001A   4EF9'000000DA    58.  down:    jmp      cont
                            59.
1'000020   33FC 0000        60.  low:     move.w   #0,$fff000
           00FFF000
1'000028   3239 00FFF000    61.  test1:   move.w   $fff000,d1
1'00002E   E359             62.           rol.w    #1,d1
1'000030   64 F6            63.           bcc.b    test1
1'000032   3039 00FF8008    64.           move.w   $ff8008,d0
1'000038   E158             65.           rol.w    #8,d0
1'00003A   30C0             66.           move.w   d0,(a0)+
                            67.
1'00003C   3239 00FFF000    68.  test2:   move.w   $fff000,d1
1'000042   E359             69.           rol.w    #1,d1
1'000044   65 F6            70.           bcs.b    test2
1'000046   E241             71.           asr.w    #1,d1
1'000048   32C1             72.           move.w   d1,(a1)+
                            73.
1'00004A   33FC 0001        74.           move.w   #1,$fff000
           00FFF000
1'000052   3239 00FFF000    75.  test3:   move.w   $fff000,d1
1'000058   E359             76.           rol.w    #1,d1
1'00005A   64 F6            77.           bcc.b    test3
```

```
1'00005C   3239 00FFF000      78.   test4:    move.w    $fff000,d1
1'000062   E359               79.             rol.w     #1,d1
1'000064   65 F6              80.             bcs.b     test4
1'000066   E241               81.             asr.w     #1,d1
1'000068   34C1               82.             move.w    d1,(a2)+
                              83.
1'00006A   33FC 0002          84.             move.w    #2,$fff000
           00FFF000
1'000072   3239 00FFF000      85.   test5:    move.w    $fff000,d1
1'000078   E359               86.             rol.w     #1,d1
1'00007A   64 F6              87.             bcc.b     test5
1'00007C   3239 00FFF000      88.   test6:    move.w    $fff000,d1
1'000082   E359               89.             rol.w     #1,d1
1'000084   65 F6              90.             bcs.b     test6
1'000086   E241               91.             asr.w     #1,d1
1'000088   36C1               92.             move.w    d1,(a3)+
                              93.
1'00008A   33FC 0003          94.             move.w    #3,$fff000
           00FFF000
1'000092   3239 00FFF000      95.   test7:    move.w    $fff000,d1
1'000098   E359               96.             rol.w     #1,d1
1'00009A   64 F6              97.             bcc.b     test7
1'00009C   3239 00FFF000      98.   test8:    move.w    $fff000,d1
1'0000A2   E359               99.             rol.w     #1,d1
1'0000A4   65 F6             100.             bcs.b     test8
1'0000A6   E241             101.             asr.w     #1,d1
1'0000A8   38C1             102.             move.w    d1,(a4)+
                            103.
1'0000AA   33FC 0004         104.             move.w    #4,$fff000
           00FFF000
1'0000B2   3239 00FFF000     105.   test9:    move.w    $fff000,d1
1'0000B8   E359             106.             rol.w     #1,d1
1'0000BA   64 F6             107.             bcc.b     test9
1'0000BC   3239 00FFF000     108.   test10:   move.w    $fff000,d1
1'0000C2   E359             109.             rol.w     #1,d1
1'0000C4   65 F6             110.             bcs.b     test10
1'0000C6   E241             111.             asr.w     #1,d1
1'0000C8   3AC1             112.             move.w    d1,(a5)+
                            113.
                            114.
1'0000CA   13FC 0081         115.             move.b    #$81,$ff8011
           00FF8011
```

```
1'0000D2  13FC 0080     116.        move.b  #$80,$ff8011
          00FF8011
                        117.
                        118.
                        119.
1'0000DA  4E73           120. cont:  rte
                        121.
                        122.
2'000000                123.        section 2
2'000000  <1D4C0>        124. shaft: ds      60000
3'000000                125.        section 3
3'000000  <1D4C0>        126. ch0:   ds      60000
4'000000                127.        section 4
4'000000  <1D4C0>        128. ch1:   ds      60000
5'000000                129.        section 5
5'000000  <1D4C0>        130. ch2:   ds      60000
6'000000                131.        section 6
6'000000  <1D4C0>        132. ch3:   ds      60000
7'000000                133.        section 7
7'000000  <1D4C0>        134. ch4:   ds      60000
                        135.
                        136. *pointer to interrupt routine goes in address 80 l
                        137. *will use link file examp.lnk to place pointer a:l
                        138.
                        139.        end
```

```
%EXAMP.LNK
%%%%%%%%%
* Linker for sampling routine
* Location of program in memory is placed by this program

link examp

org $10000
section 0

org $10100
section 1

org $80

dc.w $0001
dc.w $0100

org $11000
section 2

org $1fa60
section 3

org $2e4c0
section 4

org $3cf20
section 5

org $4b980
section 6

org $5a3e0
section 7


end
```

Bibliography

[1] *Handbook of Chem. and Physics.* CRC Press, 56th edition, 1975-76.

[2] S. Beghelli. The frisch scheme in dynamic system identification. *Automatica*, 26(1), 1990.

[3] R. Brockett. *Finite Dymensional Linear Systems.* Wiley, 1970.

[4] Kyong Rae Cho. Detection of broken rotor bars in induction motors using parameter and state estimation. Master's thesis, MIT, Dept. of EECS, 1989.

[5] II. D'Angelo. *Linear Time-Varying Systems: Analysis and Synthesis.* Allyn and Bacon, 1977.

[6] C. A. Desoer. *Notes for a Second Course on Linear Systems.* Van Nostrand Reinhold Company, 1967.

[7] G. Franklin. *Feedback Control of Dynamic Systems.* Addison-Wesley, 1986.

[8] A. Gelb. *Applied Optimal Estimation.* The MIT Press, tenth edition, 1988.

[9] G. Golub and H. VanLaon. *Matrix Computations.* Johns Hopkins Univ. Press, second edition, 1989.

[10] J. P. Holman. *Heat Transfer.* McGraw-Hill Book Company, fifth edition, 1982.

[11] R. Isermann. Process fault detection based on modeling and estimation methods– a survey. *Automatica*, 20(4):387–404, 1984.

[12] T.M. Jahns. Flux weakening regime operation of an interior permanent-magnet synchronous motor drive. *IEEE Trans. Indus. Appli.*, 4, July/Aug. 1987.

[13] II. Jones. *Failure Detection in Linear Systems.* PhD thesis, MIT, Dept. of Aeronautics and Astronautics, Cambridge, MA, Sep. 1973.

[14] L. Jones and J. H. Lang. A state observer for the permanent magnet synchronous motor. In *IECON*, Cambridge, MA, Nov. 1987.

[15] B. Kågström. Bounds and perturbation bounds for the matrix exponential. *BIT*, 17:39–57, 1977.

[16] R. Kalman. New methods in wiener filtering theory. In *Proceedings of the First Symposium on Engineering Applications of Random Function Theory and Probability*, 1963.

[17] R. E. Kalman and R. S. Bucy. New results in linear filtering and prediction theory. *Journal of Basic Eng.*, page 95, Mar. 1961.

[18] W. C. Karl. Applications of a class of nonlinear filters to problems in power electronics. *IEEE Trans. Power Elec.*, 1990. to appear.

[19] P. Krause. *Analysis of Electric Machinery*. McGraw-Hill, 1986.

[20] P. Lancaster. *The Theory of Matrices with Applications*. Academic Press, 1985.

[21] J. H. Lang, G. C. Verghese, and Ilić. Opportunites in estimation and control of electrical machines. In *Proceedings of the 25th IEEE Conf. on Decision and Control*, Athens, Greece, Dec. 1986.

[22] X. Z. Liu. Extending the blandel-park transformation to generalized electrical machines. MIT Lab for Electromagnetic and Electronic Systems, 1988.

[23] D. G. Luenberger. *Introduction to Dynamic Systems*. John Wiley and Sons, 1979.

[24] M. Massoumnia. A geometric approach to the synthesis of failure detection filters. *IEEE Trans. Auto. Cont.*, AC-31(9), Sep. 1986.

[25] M. Massoumnia, G. Verghese, and A. Willsky. Failure detection and identification. *IEEE Trans. Auto. Cont.*, 34(3), Mar. 1989.

[26] R. K. Mehra and J. Peschon. An innovative approach to fault detection and diagosis in dynamic systems. *Automatica*, 7:637–640, 1971.

[27] E. A. Nesbitt and J. H. Wernick. Magnetic moments of alloys and compound of iron and cobalt with rare-earth metal additions. *Journal of Applied Physics*, 30(3), Mar. 1959.

[28] E. A. Nesbitt and J. H. Williams. Magnetic moments of compounds of cobalt with rare-earth elements having a cu_5ca structure. *Journal of Applied Physics*, 32(3), Mar. 1959. suppl. to.

[29] A. V. Oppenheim and R. W. Schafer. *Discrete-Time Signal Processing*. Prentice Hall, 1989.

[30] I. J. Perez and J. G. Kassakian. A stationary thermal model for smooth air-gap rotating electric machines. *Electric Machines and Electromechanics: An International Quarterly*, 3:285–303, 1979.

[31] R. J. Plemmons. M-matrix charcterizations I: Nonsigular M-Matrices. *Linear Algebra and Its Applications*, 18:175–188, 1977.

[32] G. Poole and T. Boullion. A survey on m-matrices. *SIAM Review*, 16(4), Oct. 1974.

[33] L. J. Scanlon. *The 68000: Principles and Programming*. Howard Sams and Co. Inc., 1985.

[34] J-J. Slotine. Advanced control: 2.152 course notes. MIT, Mechanical Engineering Dept., Spring 1989.

[35] G. Strang. *Linear Algebra and Its Applications*. Academic Press, 1988.

[36] C. VanLoan. The sensitivity of the matrix exponential. *SIAM J. Numer. Anal.*, 14(6), Dec. 1977.

[37] G. Verghese. Dynamic systems: 6.241 course notes. MIT, Electrical Engineering Dept., Fall 1990.

[38] G. C. Verghese, J. H. Lang, and L. Casey. Analysis of instability in electrial machines. *IEEE Trans. on Industry Appl.*, IA-22(5), Sep/Oct 1986.

[39] J. White and J. Speyer. Detection filter design: Spectral theory and algorithms. *IEEE Trans. Auto. Cont.*, AC-32(7), Jul. 1987.

[40] A. Willsky. A survey of design methods for failure detection in dynamic systems. *Automatica*, 12:601–611, 1976.

[41] J. L. Jr. Wyatt, C. A. Zukowski, and P. Penfield. Step response bounds for systems described by m-matrices, with applications to timing analysis of digital mos circuits. In *Proceedings of the 24th IEEE Conf. on Decision and Control*, Ft. Lauderdale, FL, Dec. 1985.

[42] L. Zadeh and C Desoer. *Linear System Theory*. McGraw-Hill Book Company, 1963.